Detection and imaging of pharmaceutical compounds in skin by MALDI-MS.

BUNCH, Josephine.

are charged at 50p per hour

REFERENCE

Detection and Imaging of Pharmaceutical Compounds in Skin by MALDI-MS

Josephine Bunch B.Sc. (Hons)

A thesis submitted in partial fulfilment of the requirements of
Sheffield Hallam University
for the degree of

Doctor of Philosophy

January 2005

This thesis is dedicated to my wonderful parents. I could not have done this without their fathomless love and support. Thank you so much.

Acknowledgements

I would like to take this opportunity to thank my supervisor at Sheffield Hallam University, Dr Malcolm Clench, for all his advice and support throughout this project.

I am grateful to Pfizer Global R&D, for sponsorship of this work, and thank my external advisor, Dr Don Richards, for all his assistance throughout this project.

Images presented in this thesis were constructed using beta test ion imaging software, kindly supplied by MDS Sciex, Ontario, Canada. I would like to thank Dr Julie Wingate at MDS Sciex for all her support in using this application.

Kind thanks are due to Stuart Creasey and Jonnie Plumb, at Sheffield Hallam University, for their assistance with the SEM and confocal microscopy work respectively.

I gratefully acknowledge financial support from the British Mass Spectrometry Society, enabling my attendance at the International Conference for Mass Spectrometry (IMSC), Edinburgh, 2003.

Special thanks to Sam Ramsay for all his help with the 'spot calculator and for all the Saturday mornings.

Thanks to Brendan, Karen, Sally, Paul and Jill for making life in the lab so much fun. And thanks to Alysia, Gerard, Sam, Tim, Gail, Scarlet, Kerry, Claire, Jane and Alice for making life outside the lab so much fun.

Finally, thank you Nikki, for putting up with so much, and making me so happy.

Abstract

Mass spectrometric techniques have been developed recently for the examination of biological tissue samples. Tandem mass spectrometry has been employed for the detection of pharmaceutical compounds and also mass spectrometric 'images' have been produced which show the spatial distribution of peptides, proteins and drugs in tissue.

In this thesis, a programme of method development for the detection and imaging of topically applied pharmaceutical compounds in porcine epidermal tissue by MALDI-TOF-MS is presented.

Direct analysis of fresh tissue sections was compared with the analysis of tissue imprints formed by blotting onto a variety of substrates. The samples were coated with matrix material by a prototype electrospray deposition device. Analyses were performed on a linear time-of-flight (LaserTOF 1500, SAI) mass spectrometer. Direct analysis of tissue and analysis of the C18 blots gave irreproducible data. Problems with matrix layer in-homogeneity were experienced with nitrocellulose and polyvinyl difluoride (PVDF) membranes. Reproducible data were obtained by analysis of tissue imprints created on carbon and cellulose membranes.

All subsequent work was conducted using an Applied Biosystem Qstar pulsar *i* hybrid quadrupole time-of-flight mass spectrometer fitted with an orthogonal MALDI ion source and ion imaging software. The advantages of superior mass accuracy and resolution with such an instrument configuration were investigated.

Electrospray and airspray methods were compared for analysis of tissue imprinted carbon and cellulose membranes. A novel method of precoating cellulose membranes in matrix by airspray prior to the blotting procedure was developed. The method was found to retain the expected distribution of the analyte.

Ion images demonstrating the permeation of the applied compound into the skin were achieved by imaging a cross sectional imprint of treated tissue on a cellulose membrane precoated in matrix material. A calibration graph for the determination of ketoconazole was prepared using the sodium adduct of the matrix ion as an internal standard. This enabled construction of a quantitative profile of drug in skin. Conventional haematoxylin and eosin staining and microscopy methods were employed to obtain a histological image of the porcine epidermal tissue. Superimposing the mass spectrometric and histological images revealed drug permeation into the dermal tissue layer.

A quantitative corneum tape stripping/HPLC method was developed for comparison. Useful data was acquired and further work suggested to facilitate a full validation of the methods presented in this thesis.

Contents

List of Figures

List of Tables

Chapter 1

Introduction

1.1 Mass spectrometry

Mass spectrometry is concerned with the separation of matter according to atomic and molecular mass. The technique may be described as the science of 'weighing' individual atoms and molecules. This is accomplished using instrumentation that generates gas-phase ions from the analyte that are then subjected to electrostatic and/or magnetic fields. The gas-phase ions are mass measured or discriminated based on their interaction and trajectories within these fields. Samples may be introduced in gas, liquid or solid states. In the latter two cases, volatilisation must be accomplished either prior to, or accompanying ionisation. Many ionisation techniques are available to produce charged molecules in the gas phase, ranging from simple electron (impact) ionisation (EI) and chemical ionisation (CI) to a variety of desorption ionisation (DI) methods.

1.1.1 Desorption ionisation

The inherent restrictions of electron ionisation and chemical ionisation that limited applications to volatile sample molecules were overcome with the introduction of desorption ionisation methods in which molecules are brought to the surface (desorbed) and ionised at the same time.

The development of these techniques over the past two decades has made it possible to produce intact, high molecular weight gas-phase ions of thermally labile or non-volatile compounds without derivatisation. This is generally referred to as *soft ionisation*, because of the (virtual) absence of fragmentation induced by the

desorption/ionisation process. The various soft ionisation techniques use different physical approaches to produce ions:

- A high electric field is applied to the sample in field desorption (FD) mass spectrometry [1];
- The sample is bombarded with highly energetic atoms or ions in fast atom bombardment (FAB) [2], ^{252}Cf plasma desorption (PD) [3] and secondary ion mass spectrometry [4];
- Short and intense pulses of laser light are used to induce the formation of ions in laser desorption (LD) [5] and matrix-assisted laser desorption/ionisation (MALDI) [6].

This thesis is concerned with the development of methods for the analysis and imaging of drugs in skin by MALDI-TOF-MS. Hence only the theoretical aspects of MALDI-TOF and mass spectrometric imaging are discussed in detail in this section.

Laser desorption and matrix–assisted laser desorption/ionisation mass spectrometry

The use of laser desorption (LD) for the analysis of non-volatile, organic molecules dates back to the 1960s when it was demonstrated that irradiation of low-mass organic samples with a high-intensity laser pulse produced ions that could be successfully mass analysed. These experiments, however, revealed an upper mass limit of $5 - 10\,\mathrm{kDa}$.

The mass limit probably arises because the energy required to cause the resonant excitation and successful energy transfer is greater than the dissociation energy of the analyte. Thus the analyte is not desorbed as the intact molecule ion in any significant amount resulting in a spectrum comprising only low-mass fragment ions.

Another major restriction of LD ionisation is the short duration of the ion burst following the laser pulse. A consequence is that the technique is unsuitable for scanning analysis on sector or quadropole instruments, but means that LD is particularly suited to time-of-flight mass spectrometry.

In 1987, *matrix-assisted laser desorption ionisation* (MALDI) was introduced by Hillenkamp and Karas—employing an organic matrix [6], and by Tanaka and

co-workers—who used an inorganic matrix [7]. The use of a matrix extended the analysable mass range up to about 350 kDa at fmol sensitivities, and thereby revolutionised the field of biological mass spectrometry.

1.1.2 Principles of MALDI

In MALDI, the laser is directed at an analyte embedded in an excess of matrix material. Optimal molar ratios are in the 1:1000–1:10000 (analyte:matrix) range. This results in the analyte molecules being singularised and fully surrounded (solvated) by matrix molecules. Thus laser photons have a high probability of encountering the matrix over the analyte molecules.

The laser energy is dispersed as vibrational energy within the sample. As the co-crystalline matrix/analyte structure becomes energised, the binding forces and crystal integrity are reduced. Resultant reactions in this energized state lead to ion formation (see page 12). The matrix molecules desorb (see page 16), leaving the ions. Some of the desorbed ions are still associated with the matrix molecules (Figure 1.1).

The ions are extracted from the MALDI plume by a strong electric field into the field-free drift tube of a time-of-flight (TOF) analyser. TOF analysis separates ions according to their mass-to-charge (m/z) ratio. A more detailed review of the TOF process is given on page 16.

Ions are converted into signals using ion-to-electron conversion detectors. These have a flat plate surface that is exposed to the incoming ions, which strike the surface (either a metal or metal oxide coating). The collision results in the emission of electrons and small negative ions, which are accelerated to another surface that produces only electrons which are amplified by conventional electron multipliers to yield a signal.

There are numerous experimental factors that affect the outcome of any MALDI experiment. The matrix, method of matrix/sample preparation, and the laser wavelength employed are generally accepted as the most influential parameters [8].

Lasers

A variety of lasers have shown success in MALDI-MS experiments, as summarised in Table 1.1. Nitrogen lasers are used most frequently due to their relatively low

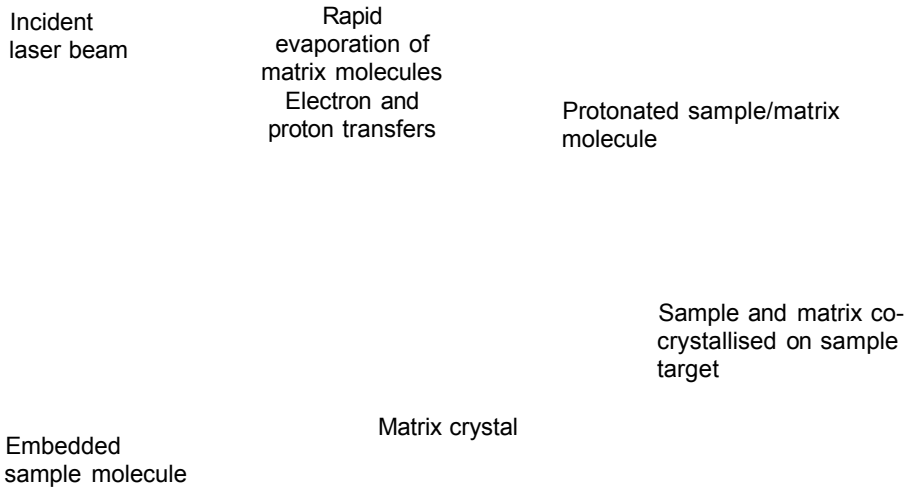

Figure 1.1: Energy absorption, ionisation and formation of molecular ion.

Ultraviolet (UV)	266 nm, frequency quadrupled Nd-YAG [9]
	337 nm, N_2 [6,7]
	355 nm, frequency tripled Nd-YAG [10]
Infrared (IR)	2.94 mm, Er-YAG [11]
	10 μm, CO_2 [12]
	Tuneable free electron laser (FEL) [13]
	Optical parametric oscillator (OPO) [14]
Visible	532 nm, frequency doubled Nd-YAG [15]

Table 1.1: Lasers employed in MALDI-MS

cost and good reliability.

The use of infrared (IR) lasers may however have some advantages over the more widely adopted ultraviolet (UV) approach. Liquid matrices in IR MALDI may yield more reproducible spectra than in UV MALDI as solid crystalline samples prepared with UV matrices demonstrate a high degree of heterogeneity Also, it has been reported that IR MALDI is a softer ionisation technique (yields less metastable fragmentation) than UV MALDI [16]. A disadvantage of IR MALDI is that much more sample is ablated in IR MALDI MS. MALDI spectra are generated from multiple laser shots. Typically, UV MALDI experiments average 100 laser shots and it has been observed that that ions in IR MALDI MS can only be generated from the first two or three laser shots [17]. Several papers compare the use of UV and IR MALDI MS [18–21].

The matrix

The matrix performs two important functions: (1) it absorbs photon energy from the laser beam and transfers it into excitation energy, and (2) it serves as a solvent for the analyte, so that the intermolecular forces are reduced and aggregation of the analyte molecules is held to a minimum. Some desirable characteristics of a typical MALDI matrix are:

- high molar absorptivity at the laser wavelength employed;
- solubility in the same solvent as the analyte material;

- unreactivity towards the analyte. (However, evidence suggests that proton transfer reactions of excited states of the matrix are involved in UV MALDI: see page 14);
- appropriate physical properties, such as lattice structure and heat of sublimation;
- ability to promote ionisation;
- vacuum stability

The matrix should provide maximum ion intensity and signal reproducibility, and should minimise fragmentation and adduct formation. The matrix material must not give rise to ions with m/z values that may coincide with those of the analyte ions. The ideal matrix produces strong symmetrical peaks showing a minimum of unimolecular decay (except when desired, as in *post-source decay,* PSD [22]).

Many different matrix materials and matrix mixtures have been used since the introduction of the MALDI technique. Unfortunately there is not enough information to date to permit an *a priori* prediction of suitable matrices for experiments, largely due to the fact that the full MALDI ionisation and desorption processes are not completely understood. Thus vast numbers of potential candidates have been tested, and a general trial and error approach is still adopted in many scenarios. The majority of successful matrices are low molecular weight organic acids prepared in a suitable solvent.

The matrices and applications discussed in this section refer to UV (nitrogen) MALDI unless otherwise specified. Structures of commonly-used matrix compounds are shown in Figure 1.2.

$\alpha-$cyano$-4-$hydroxycinnamic acid (α-CHCA) [23] has proved particularly useful for peptide analysis. This is commonly prepared at a concentration of 5-25 $mg{\cdot}ml^{-1}$ in methanol or acetonitrile, incorporating 0.1 % aqueous trifluroacetic acid (TFA). $2,5-$dihydroxybenzoic acid (DHB, also called gentisic acid) [24] has also been widely used for the analysis of peptides, either alone, or in conjunction with a co-matrix. A co-matrix is a compound that has no specific matrix activity, but when added to a matrix (as an additive), enhances the mass spectral quality, generally by reducing the extent of analyte fragmentation. Fructose has been demonstrated as a good

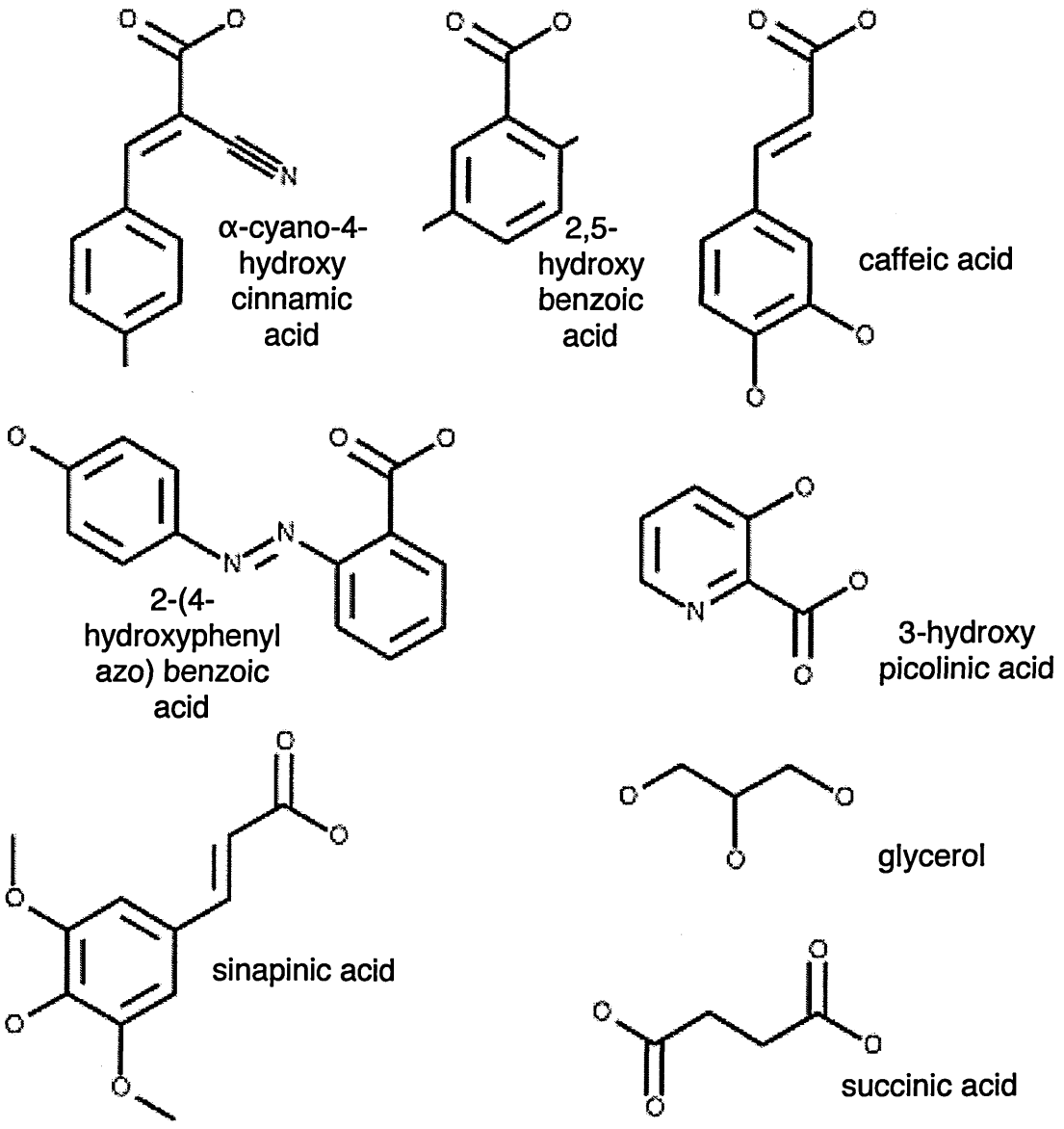

Figure 1.2: Chemical structures of some commonly-used MALDI matrices

co-matrix with DHB [25]. Super-DHB (sDHB, a 9:1 mixture of DHB and 2-hydroxy-5-methoxybenzoic acid (HMB)) [26], as well as DHB mixed with 5-methoxy-salicylic acid [27] have also shown excellent results. These may be described as binary matrix systems because both components of the mixture exhibit matrix activity.

The standard matrix for the analysis of proteins is $3,5-$dimethoxy$-4-$hydroxy-cinnamic acid (sinapinic acid [10]), most commonly prepared in 50:50 water:acetonitrile (0.1% TFA). This matrix typically requires more laser energy ($25\,\mu$J) than α-CHCA and DHB (around $5-15\,\mu$J).

$2-$(4$-$hydroxyphenylazo)-benzoic acid (HABA) has been used for the analysis of large proteins and glycoproteins, however, it has been shown to enhance formation of alkali metal adducts (though this is not particulary important at high mass ranges [28].

$3-$hydroxy-picolinic acid ($3-$HPA) has been used for the analysis of small proteins, but has demonstrated spot to spot variations and excessive adduct peaks [10].

Several authors have reported the use of binary matrix systems for protein analysis [27,29], For example, mixtures of matrices already mentioned as well as ferulic acid ($4-$hydroxy$-3-$methoxy-cinnamic acid) [30] and caffeic acid ($3,4-$dihydroxy-cinnamic acid).

The analysis of oligonucleotides has proved problematic, and the most useful matrix is probably $3-$HPA [31]. This may be substituted with (10%) diammonium tartrate or citrate (in order to remove alkali metal ions). $2,4,5-$trihydroxyacetophenone (THAP) with diammonium citrate or tartrate [32], $6-$aza$-2-$thiothymine [33] and quinaldic acid [34] have demonstrated good results for detection of nucleic acids. It should be noted that nucleic acid analyis is usually conducted in the negative ion mode.

Carbohydrate analysis is usually performed using either DHB or sDHB [35].

MALDI has also been used for the analysis of complex synthetic polymers, with a major problem being the solubility of the analyte and matrix in the same system. Water-soluble polymers have been successfully analysed with both sinapinic acid and DHB. Less polar polymers have proved more complicated, and some fairly uncommon matrices such as $7-$amino$-4-$carbostyril dissolved in tetrahydrofuran [36] have been described.

Recently a new matrix, 2,5−dihydroxybenzoic acid butylamine (DHBB) has shown improved results compared with α-CHCA for the analysis of oligosaccharides, glycoconjugates, polymers and gangliosides. However for peptide and protein analysis α-CHCA was found to be superior due to multiple alkali adducts observed with DHBB [37].

Ice [12], succinic acid [38], and glycerol [12] have all been identified as successful matrices for use with infrared MALDI.

Methods of matrix preparation/application

A variety of methods of matrix sample preparation have been developed. The most common method is the original dried-droplet method introduced by Hillenkamp and co-workers [24]. This method involves simple co-crystallisation of the matrix and analyte on a sample target. The surface of the droplet is the preferred site for crystallisaton: crystals form at the liquid/air interface and are carried into the rest of the solution by convection. A commonly observed problem with this technique is the aggregation of larger amounts of crystals around the edge of the dried spot. In addition, the overall sample surfaces obtained using the dried-droplet method are heterogeneous, with a crystal layer uneven both in size and number. Confocal fluorescence microscopy has been used to demonstrate that the analyte is not evenly distributed among or within the crystals, and that some matrix crystals contain no analyte at all [39]. Another limitation of the technique is segregation during crystallisaton: as the matrix forms crystals, the salts and some analyte molecules are excluded. Whilst this limits overall ionisation of the analyte, it is of particular consequence in situations where cationisation is preferred. The dried-droplet method often demonstrates both poor mass accuracy (particulatly on linear time-of-flight instruments) and poor spectral quality. Mass accuracy is the ability to measure or calibrate the instrument response against a known entity [40]. The measurement indicates the deviation of the instrument response from a known monoisotopic calculated mass.

Vacuum drying [41] has been developed to overcome some of the limitations associated with the dried-droplet method. The analyte/matrix drop on the target is rapidly dried in a vacuum chamber before MALDI analysis. This reduces crystal size, and increases crystal homogeneity by reducing the segregation effect. The

formation of smaller crystals offers the advantage of thinner samples and improved mass resolution and accuracy with certain instruments. (Mass resolution is the dimensionless ratio of the mass of the peak divided by its width. Usually, the peak width is taken as the full width at half maximum intensity. Resolution is a measure of the separating or resolving power of a mass spectromter, i.e. the ability to distinguish between two masses [40]).

A more uniform inclusion of the analyte into matrix crystals may be achieved by using the *crushed-crystal* technique [42]. Matrix-only solution is deposited onto the target and the resultant crystals are then crushed and spread by overlaying, pressing and twisting a glass slide upon them. Loose material is subsequently brushed away prior to the depostion of a mixture of analyte and matrix (prepared as in the dried-droplet method) onto the crushed crystals. In this method, crystallisation of the analyte and matrix onto the sample plate is facilitated by the nucleation sites of the crushed initial matrix layer. Crystal nucleation shifts from the liquid air interface to the surface of the substrate and microcrystals form within the solution. This results in a polycrystalline film of the matrix and analyte that is more uniform than in the dried-droplet method in terms of spot-to-spot reproducibility and ion production. This method has been claimed to be particularly useful in oligonuleotide and protein analysis [43].

An alternative method, fast-matrix-evaporation, was developed by Vorm *et al.* [44–46] with a view to improving mass accuracy and resolution. This involves application of the matrix layer in a highly volatile solvent (acetone) to create a thin film of matrix. The analyte is subsequently deposited onto the preformed matrix crystal layer. Confocal fluorescence microscopy [39] has been used to demonstrate that the crystals produced are more homogenous than those produced by the dried-droplet method.

The principles of the crushed-crystal and fast-evaporation methods were combined to develop the *overlayer* (also termed *seed-layer* and *two-layer*) method [39,45,47,48]. A layer of matrix crystals is created by fast evaporation, and onto this a mixture of the matrix and analyte is added (as in the crushed-crystal method). This has enhanced sensitivity and spot-to-spot reproducibility compared to fast evaporation, probably because of improved isolation of the analyte molecules on the crystal surfaces in the presence of extra matrix.

The *sandwich* method was derived from the fast-evaporation and overlayer methods. A droplet of analyte solution is applied to a thin thin film of matrix created by fast evaporation, followed by the depostion of a second layer of matrix so that the analyte is effectively sandwiched between two layers of matrix. This method was introduced by Li *et al.* for the analysis of single mammalian cell lysates [49], but has not been widely adopted by the mass spectrometric community.

Spin coating has proved useful for the analysis large biomolecules [50]. A relatively large volume (up to 10 ml) of matrix/analyte solution is deposited onto a plate, which is then spun at around 300 rpm to create a more homogeneous film than in the conventional dried-droplet method.

In cases where the analyte is insoluble, the pellet method may be useful [51]. A mixture of finely ground analyte and matrix is pressed together in a hydraulic press to give a combined pellet.

The use of matrix pre-coated targets and membranes has proved particularly useful when there is only a small amount of analyte available. A range of substrates including PVDF, nitrocellulose, cellulose, and nylon have all been tested. The use of such materials as a method of matrix support and also as tissue blotting substrates is reviewed more fully in Chapter 2.

Several research groups have investigated the use of *liquid matrices* as an alternative approach to the desorption of solid matrix-analye deposits. The major advantage of these methods is that the analyte is likely to be more evenly distributed throughout the matrix, as a function of simple molecular diffusion. Liquid matrices can be divided into three categories:

1. *Chemical liquid matrices* [52, 53]: the liquid matrix absorbs the laser energy (similarly to a solid matrix).

2. *Suspension or particle-doped liquid matrices* [7, 54–56]: fine graphite or metal particles are suspended in a liquid that does not absorb the laser energy (for example glycerol). The fine particles absorb the energy and facilitate desorption while the liquid molecules provide the charge for ionisation.

3. *Chemical-doped liquid matrices* [57]: an organic material that is highly absorbent at the laser wavelength employed is added to a liquid medium.

Alternative methods such as *electrospray* and *airspray* matrix depostion have been developed and show particular promise in investigations where the method of matrix application must offer a degree of matrix crystal homogeneity across the sample that would allow the full surface area to be scanned, and have spot-to-spot reproducibility.

Electrospray as a method of MALDI sample preparation was introduced by Owen [58,59] and independently by Axelsson [60]. In this technique a small amount of matrix-analyte mixture, or matrix alone, is elecrosprayed from a high voltage-biased (3-5 kV) stainless steel (or glass) capillary onto a grounded metal plate, mounted 0.5–3 cm away from the tip of the capillary. This method has superior crystal homogeneity, producing an even matrix layer across the sample surface. Quantitative analysis has been reported by Owen [58] with use of an internal standard.

The airspray method [61] uses a compressed airbrush device to spray matrix or a matrix/analyte mixture onto the sample plate. This is a very simple, inexpensive alernative to the electrospray method and has shown excellent reproducibility [61,62]

1.1.3 MALDI ion formation

Despite the widespread use and application of MALDI over the last twenty years, the process of ion formation remains poorly understood. MALDI has proved to be an extremely difficult process to characterise, and it is clear that even in a single experiment no one mechanism can explain all ions observed. It has also been calculated that while one laser pulse results in several thousands of ions, the overall ion:neutral ratio in UV MALDI is only about $1 : 10^4$. Thus we are trying to understand a mechanism that results in minority species. Several theories and mechanisms have been proposed, and are reviewed in an excellent article by Zenobi and Knochenmuss [8]. It is widely accepted that a variety of different pathways contribute to the ions observed in a MALDI spectrum, as summarised in Table 1.2.

MALDI ionisation mechanisms can be divided into primary and secondary ionisation steps [8]. *Primary ion formation* accounts for pathways in which neutral reactants are converted into charged products (gas phase ions) by action of the laser pulse on the sample. These conversions occur in the MALDI plume and usually result in the formation of matrix ions. *Secondary steps* are any subsequent ion-molecule reactions that convert the initial charged species into the ions that are

Primary ion formation	Desorption of preformed ions
	Multi-photon ionisation
	Energy pooling
	Excited-state proton transfer
	Disproportionation reactions
	Thermal ionisation
Secondary ion formation	Proton transfer
	Electron transfer
	Cationisation

Table 1.2: Possible pathways for MALDI ion formation (as reviewed by Zenobi and Knochenmuss [8])

observed at the detector. It is possible that primary ionisation may be partially or completely masked by secondary reactions [63]. While this complicates elucidation of the primary ionisation steps, it explains the similarity of MALDI spectra recorded under different conditions, and may be useful in predicting MALDI mass spectra [64].

Primary ion formation

An attractive mechanism is that ions observed in the spectrum may already be present in the solid sample and are liberated with the laser pulse *(desorption of pre-formed ions)* [65].

The formation of the cation radical of the matrix by *multi-photon ionisation* was considered by many as a likely model of primary ion formation [66]:

$$M \xrightarrow{h\nu} M^{+\bullet} + e^-$$

However, in theory the laser irradiances used in UV MALDI are too low to allow significant absorption of more than two photons by a matrix molecule. Since the ionisation energy of most matrices is estimated to be greater than the energy of two photons of a nitrogen laser, the two photon ionisation model cannot be assumed [67].

Nevertheless, two-photon excitation of a matrix molecule may still be an important step in the ionisation process. It has been observed that thermal energy from

the MALDI plume may make up the difference between a two-photon excitation and the ionisation potential, thus a *photothermal model* has been proposed [68]. Furthermore, energy pooling is considered as a likely mechanism [69]. In this model two or more matrix molecules pool their internal energy together while in an excited state (M^*M^*) to yield one matrix radical cation:

$$2M \xrightarrow{2h\nu} M^*M^* \longrightarrow M + M^{**} \longrightarrow M + M^{+\cdot} + e^-$$

Following photoionisation, *excited state proton transfer* (ESPT) is the most frequently proposed MALDI ionisation model, dating back to the origin of MALDI [9]. The acidic properties of many aromatic derivatives are enhanced when molecules are laser excited; thus a single excited matrix molecule (M^*) may transfer the labile proton to an analyte or matrix molecule in the ground state:

$$M \xrightarrow{h\nu} M^* \longrightarrow +A \longrightarrow [M+H]^- + [A+H]^+$$

or

$$M \xrightarrow{h\nu} M^* \longrightarrow +M \longrightarrow [M+H]^- + [M+H]^+$$

This is an attractive pathway as it only requires one photon, and also because it rationalises the formation of pseudomolecular ions. However, none of the popular matrices is known to be particularly ESPT-active in solution or gas phase, and also known ESPT compounds have been demonstrated to be poor MALDI matrices [70].

Disproportionation reactions have been proposed to explain the simultaneous formation of positive and negative ions [71,72]. Proton transfer of two coupled and excited matrix molecules is thought to give rise to positive and negative species as follows:

$$2M \xrightarrow{2h\nu} M + M^{**} \longrightarrow [M-H]^- + [M+H]^+$$

This reaction has been shown to be energetically possible with two nitrogen laser photons [71]. Despite this, there is still little evidence to support this mechanism [8].

Thermal ionisation has been demonstrated as a possible pathway of ion formation, and is particularly likely in scenarios employing particle suspension matrices [8]. In these cases, the laser energy is absorbed by particles suspended in a liquid that is transparent to the laser, and formation of ions from the excited particles is thus thought to occur via thermal routes.

Secondary ion formation

In cases where primary ions are radical cations, *gas phase proton transfer* reactions have been shown to occur with both neutral matrix and neutral analyte molecules [73].

Electron transfer has been shown to be a plausible pathway for MALDI analysis of compounds with low ionisation potential (IP) [74]. In this situation a matrix radical cation and an analyte molecule may react to produce an analyte radical cation:

$$M^{+\bullet} + A \longrightarrow M + A^{+}$$

Several studies of cationised molecules generated under MALDI conditions have shown that these ions often result from ion-molecule reactions in the gas phase. Thus the process of *cationisation* has been widely accepted as a pathway of secondary ion formation.

The fact that MALDI is generally characterised by the presence of only singly-charged molecules led to the development of the *lucky survivor model* [75]. This uniform model of the MALDI ionisation process proposes that multiply-charged clusters are desorbed, but are subsequently neutralised or have their charge reduced by proton transfers or electron captures with reactive matrix species. By this rationale, the only ions that will survive the process and reach the detector are those that are singularly charged.

Although all of these mechanisms are clearly important in MALDI, no definitive explanation of the process has been offered. A better understanding of MALDI ionisation could result in improved ion yields, control of fragmentation and ion charge states, permit access to new compounds by MALDI, provide a solid rationale for marix selection, and may also hi-light reasons for discrimination effects in quantitative UV MALDI [8].

1.1.4 Desorption mechansisms

Several theories have been developed to explain the desorption of molecules in the MALDI process.

The *thermal spike model* [76] proposes that the matrix molecules sublime from the surface as a result of local heating at low laser fluence, but above a certain laser intensity, a rapid increase in the desorption efficiency occurs. The ejection of intact molecules is attributed to poor vibrational couplng between the matrix and analyte which leads to a bottleneck in the energy transfer from the matrix to the vibrational mode of the analyte molecule.

The *pressure-pulse theory* [77] proposes that a pressure gradient is created normal to the surface, and that desorption of large molecules might be enhanced by momentum transfer from collisions with fast moving matrix molecules.

A more recent theory suggested by Hillenkamp *et al.* [78, 79], the *quasi-thermal model* is the most widely accepted scenario of desorption in MALDI. The primary step involves a pressure driven decomposition of the co-crystallised analyte/matrix material into smaller particles consisting of both clusters and single molecules. These are subsequently thermally desorbed in a second step to create the MALDI plume. High density and collision rates within the plume create an explosive phase transition that results in molecular gas phase species of both the matrix and analyte by expansion cooling.

1.1.5 Time-of-flight mass spectrometry

Time-of-flight (TOF) mass spectrometry was first successfully used as an ion analyser in the 1950's [80]. The principle of mass analysis in a time-of-flight analyser is based on the principle that ions of different m/z values have the same energy, but different velocities, after acceleration out of the ion source. Thus, the time required for each to traverse the flight tube is different: high mass ions take longer to reach the detector than low mass ions.

The kinetic energy given to an ion by the electric field is the product of the charge of the ion and the electrical field strength [81]. This is shown in Equation 1.

Equation 1: $$zeV = \frac{1}{2}mv^2$$

Where z = number of charges
e = charge of an electron
m = mass of ion
v = velocity of ion
V = electrical field strength

If the length of the source region is s, then the drift time, £1, through the source region is determined by Equation 2:

Equation 2: $$f_1 = \frac{2s}{v} = \frac{(2m)^{1/2}s}{(Zevy/2}$$

If the length of the drift tube is 1, then the time-of-flight, *t2,* of an ion through the drift tube is determined by Equation 3:

Equation 3: $$(2ZeV)^{1/2}$$

The time-of-flight for an ion can be determined by combining Equations 2 and 3:

Equation 4: $$t = \frac{}{(2ZeVy/2}$$

A schematic overview of MALDI-TOF-MS is illustrated in Figure 1.3.

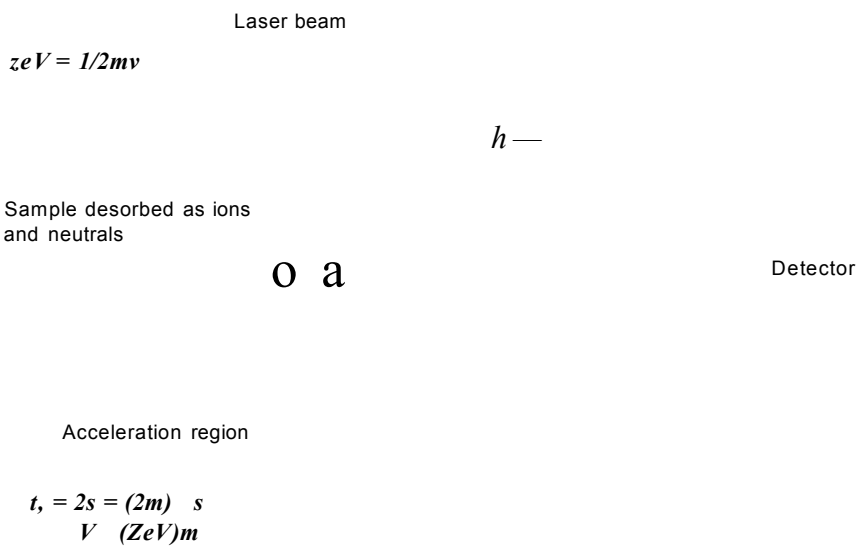

Figure 1.3: MALDI-TOF-MS (linear time-of-flight)

Thus the time taken for an ion to reach the detector is proportional to the square root of its *m/z* value. The larger the mass of a singly charged ion, the longer it takes to traverse the field free region.

The pulsed laser used for MALDI makes it an ideal technique for coupling with TOF mass spectrometry since there is a previously defined time of ion generation. Mass to charge ratios are determined by measuring the time that ions take to move through the drift tube between the source and the detector.

Today's linear TOF MS instruments are capable of attaining a resolution of 1 part per 1000. A major limitation in achieving high resolution is the consequence of the spread in time, space and kinetic energy of the initial ion packet. The time difference in formation of two ions of the same mass caused, for instance, by the length of a laser pulse, will remain the same during the flight to the detector. Ions that are not formed at the same location, due to the spread of the sample on the target or width of the ion beam, will be accelerated to different kinetic energies. Also, ions can be generated with different initial kinetic energy.

Reflectron TOF

This spread in kinetic energy can be partially compensated by using a device called a reflectron (Figure 1.4). Ions of higher energy will penetrate deeper into an electrostatic repeller field (ion mirror) and will be turned around and arrive at the detector at the same time as ions of lower initial energy that penetrate the field less. In a linear TOF, neutral and charged fragments generated through fragmentation of ions in the drift region cannot be distinguished from the original ion, because their velocity remains the same. Metastable ions generated prior to reflection have the same velocity as their precursor ion, but a reduced energy and hence can be distinguished when spectra acquired in linear and reflectron mode are compared, due to their time difference. Reflectron TOF instruments are capable of a resolving power of over 1:10,000.

Delayed extraction

Peak broadening can also be reduced by delayed ion extraction out of the ion source [82,83]. With delayed extraction (DE), the extraction voltage pulse is applied between 100 and 500 ns following the laser pulse. During this delay, ions are allowed to spread in the source and higher energy ions will move further away than lower energy ions with the same mass. The extraction voltage is applied as a potential gradient over the ion source. This compensates for the distribution of initial kinetic

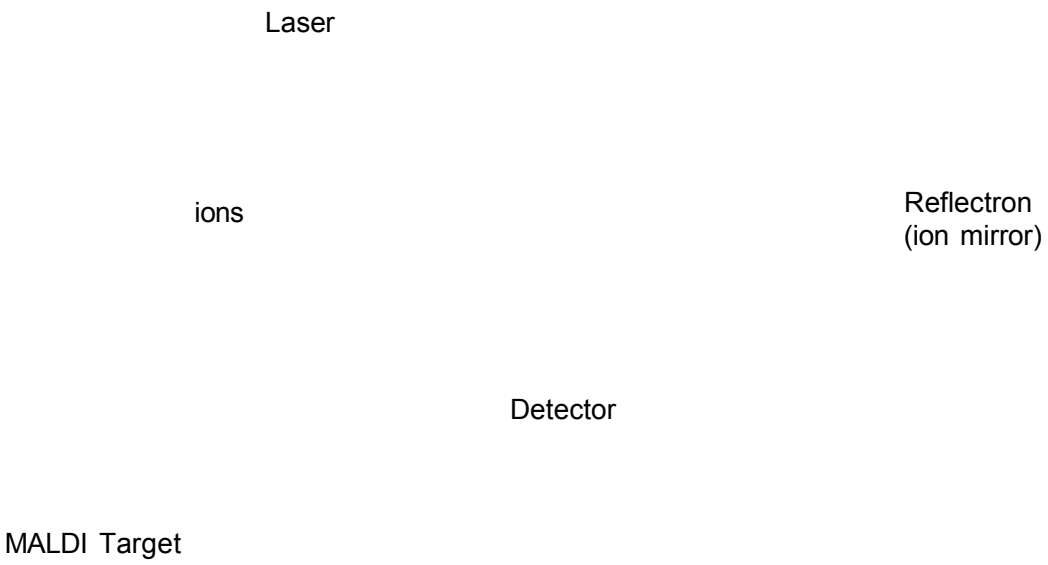

Figure 1.4: Reflectron TOF mass spectrometer.

energies, so that ions with identical m/z values will arrive at the same time at the detector.

Time-of-flight analysers have some special advantages. In contrast to sector instruments and quadropoles, all ions accelerated out of the ion source of the TOF instrument will reach the detector, giving it a relatively high sensitivity. Of course, the ions must be pulsed into the analyser, and so, some dead time exists when ions are not being analysed. Also, the mass range of TOF analysers is virtually unlimited and any practical upper limit is dictated by the ionisation process and by detector efficiency. The combinations of time-of-flight mass spectrometry with MALD, PD and ES have all been used extensively in biochemical research.

Latest instrument developments

A number of new instruments for MALDI-MS have been introduced over the last five years. These offer advantages such as enhanced sensitivity, improved mass resolution and accuracy, and the ability to perform tandem MS experiments. Thus the field of MALDI-MS continues to develop at an ever-increasing rate. These

novel instruments include a MALDI ion source coupled to a hybrid quadrupole-TOF (QTOF) [84]; tandem MALDI TOF-TOF [85]; and Fourier-transform ion cyclotron resonance (FT-ICR) MS [86,87].

The QTOF has already found widespread use in biomolecular analysis. Such instruments employ orthogonal ion acceleration (reviewed by Guilaus *et al.* [88]) which has a number of advantages over the more common axial-injection geometry. The hybrid mass analyser configuration permits compound identification either by analysis of the intact molecule or by spectral analysis of product ions produced by collisionally-induced dissociation of individual precursor ions in a collision cell. Both kinds of spectra can be acquired from a single sample in the same experiment. The use of collision-induced dissociation to yield sequence information circumvents the low product ion yields and problematic interpretation of product ion spectra acquired by the postsource decay technique. Collisional damping is used to cool the ions produced by MALDI before they enter the quadrupole. The time-of-flight measurement is thus decoupled from the MALDI process and provides high mass accuracy for both precursor and product ions, high resolution, simple selection of precursor ions and precise tuning of collision energies. MALDI-QTOF-MS with orthogonal ion injection has been evaluated for *in situ* analysis and imaging on skin in Chapters 3–6.

Finally, a range of separation techniques have been successfully interfaced with MALDI to improve the sensitivity further, e.g., scanning IEF gel separation coupled to MALDI-TOF mass spectrometry [89]; replacement of IEF with reversed phase (RP)-HPLC [90]; and nonporous RP-HPLC [91].

This ever-expanding range of new mass analysis and sample interface configurations is opening access to a range of new compounds for MALDI analysis, and is increasing the spectral quality of existing procedures.

1.2 Imaging mass spectrometry

The use of mass spectrometry (MS) to obtain spatially resolved information commenced 30 years ago with the advent of *secondary ion mass spectrometry* (SIMS).

In SIMS, the surface of the sample is subjected to bombardment by high energy ions — this leads to the ejection (or sputtering) of both neutral and charged (+/−)

species from the surface. The ejected species may include atoms, clusters of atoms and molecular fragments. In traditional SIMS, it is only the positive ions that are analysed. Since the technique uses a beam of atomic ions (i.e., charged particles) as the probe, it is a relatively easy matter to focus the incident beam and then to scan it across the surface. Thus the detector response for a selected mass at each raster spot becomes a pixel in the image. SIMS is particularly appropriate for the determination of the inorganic fraction and the elemental composition of the sample surface, whereas non-specific ions are usually generated from the organic fraction.

Secondary ion mass spectrometric imaging has been widely used and developed by both the chemical and biomedical communities. The technique has been applied to the analysis of biological samples in a range of applications, e.g., to monitor pharmaceuticals at the cellular and subcellular level; to study ion transport in organisms by isotopic labelling; to map the distribution of ions in hard tissue such as bone and teeth and to study chromosomes [92]. In addition, there have been recent efforts to apply SIMS to organic compounds and metabolites of low mass (500 amu) in single cells [93].

For the study of organic solid compounds, *laser desorption mass spectrometry* (LDMS) is a promising technique. The use of lasers in imaging MS has several advantages over the use of ion-beams alone, for example high sensitivity, selective ionisation, and quantification. This technique is similar to SIMS and permits investigation of solid samples directly—without the need for extensive sample preparation/separation prior to analysis. UV laser spot sizes can be focused to under 5 μm and thus the technique is ideally suited to spatially-resolved analyses. The use of laser desorption mass spectrometry to obtain spatial information is often referred to as *laser microprobe mass spectrometry* (LMMS). This technique became widely available with the introduction of commercial instruments [94]. Several reviews discuss applications, fundamentals and limitations of LD and LMMS [5, 94–97].

A major limitation of this technique is the accessible mass range, as ionisation of intact biomolecules over around 1000 amu was impossible. This was overcome with the introduction of *matrix-assisted laser desorption ionisation MS* (MALDI-MS) [6, 7, 9]. A low concentration of analyte is embedded in a matrix consisting of species that highly absorb the applied laser light. The development of MALDI

exponentially increased the mass limits of laser desorption. The technique was reviewed in detail above (page 3).

Recently, imaging using MALDI has become a subject of interest and is demonstrating great potential. Practical aspects of both MALDI and SIMS imaging are discussed in an excellent article by Todd *et al.* [98]. A review of imaging mass spectrometry covering applications of SIMS, LD and the introduction of MALDI imaging has been published by Pachowlski and Winograd [92].

1.2.1 Imaging MALDI MS

A common initial step in MALDI imaging involves the application of a thin layer of matrix to the sample. The chemistry of the sample can then be imaged by holding the laser, moving the sample and acquiring mass spectra from each point. Three-dimensional images may be obtained by plotting the spatial dimensions of x and y versus absolute ion intensity, which gives a semi-quantitative indication of analyte concentration at a given location.

MALDI has been used for the imaging of both biological samples [99–113] and thin layer chromatography (TLC) plates [114–118], with the method of matrix application to such samples requiring that the spatial distribution of the analyte in the sample be maintained. Conventional MALDI sample preparation is known to depend upon formation of a homogeneous liquid phase mixture of matrix and analyte before crystallisation. However, for spatially resolved analyses, it is essential that redistribution or migration of the analyte from its original location is avoided. Thus in imaging MALDI there should be no laterally-extended liquid phase mixing of the matrix and analyte. A number of methods of matrix application have been developed and assessed to meet this requirement, including indirect matrix deposition [115], brushing the sample with a supersaturated matrix solution [116], spreading a loaded matrix drop [103], electrospraying [101,116], airspraying [100,118,119], and robotic deposition of small (picolitre) volumes of matrix [113,120].

Imaging thin-layer chromatography (TLC) plates

The imaging of TLC plates by MALDI-MS was introduced by Gusev *et al.* [114], who were able to detect nanogram quantities of bradykinin, angiotensin and enkaphalin derivatives. The analyte molecules were brought to the surface of the TLC plate by

solvent extraction, and matrix material was dropped onto the plate with a syringe or pipette. The degree of analyte spreading was found to be around 1.5 mm. In addition, the surface heterogeneity of the sample resulted in signal intensities being averaged for five successive laser spots, so that the effective spatial resolution was estimated at 1 mm.

Further methods were developed for imaging compounds in the molecular weight region of $400 - 1100$ Da, for example bradykinin, angiotensin, rhodamine B and guinea green B [115]. Both direct and indirect methods of matrix deposition onto TLC plates were evaluated in these experiments.

The direct method involved gently spraying a matrix solution onto TLC plates with a glass reagent sprayer. However, this approach induced analyte spreading and so was considered unsuccessful. The indirect matrix deposition technique entailed initial crystallisation of the matrix solution on a stainless steel plate. The matrix was then transferred onto the TLC plate by pressing the steel plate matrix side down into the TLC plate. This method successfully restricted analyte spreading.

Images were obtained for all analytes at nanogram concentrations. Efforts were made to improve the spatial resolution by modification of the laser beam lens arrangement. However, focusing the beam to achieve a laser spot of under $30\,\mu$m resulted in signal degradation and poor signal reproducibility. This is a known limitation. Furthermore, matrix heterogeneity was estimated at $10 - 20\,\mu$m and so use of a laser spot size of $30\,\mu$m resulted in an ultimate resolution of around $50\,\mu$m.

Mowthorpe and colleagues [116] investigated the effectiveness of different matrix deposition methods onto TLC sample surfaces, extending the work of Gusev *et al.* [114,115]. They presented a method for analysing pharmaceutical compounds of $\sim 400 - 500$ Da separated by TLC with use of a linear time-of-flight instrument.

A method for brushing a supersaturated matrix solution onto a TLC plate was developed. The investigation concluded that matrix deposition by electrospray (using a purpose built device) was superior to the other methods, and indicated that this method should be used where spatial resolution of the analyte is desired. (Electrospray as a method of matrix application is discussed on page 12, and investigated in Chapters 2–4.)

By modification of a commercial MALDI-TOF mass spectrometer and software they succeeded in obtaining chromatographic data from replicate spots of tetracyc-

line at the 1 mg level, showing successful acquisition of chromatographic data from a TLC plate by MALDI-MS. A nitrogen laser was employed offering a spot size of $\sim 200\,\mu$m. In further work, methods for the quantitative determination of piroxicam by TLC MALDI were tested and developed. This work is discussed more fully in Chapter 5 of this thesis. A novel method of predeveloping TLC plates in an internal standard prior to drug separation and MALDI analysis was presented, in which linearity was observed over the range 400–800 ng of drug [118].

It has been shown that signal intensities may be improved by blotting the TLC plate onto a membrane by heat transfer [117]. Extraction solvent is applied to the chromatographic spots, and the analytes are then transferred to a membrane by pressing the plate onto the membrane with a hot iron. In this work matrix solution was applied by pipetting, and thus the problematic issues of analyte spreading resulted in a poor spatial resolution.

Imaging biological samples

Caprioli and co-workers (1997) developed MALDI imaging techniques to identify and profile peptides and proteins in biological tissue [101]. They presented successful localisation of hormone peptides in a tissue section taken from rat pituitary, and succeeded in mapping insulin within a section of rat pancreas. In addition, human buccal mucosa (cheek) cells were dried, sprayed with MALDI matrix, and then imaged. A protein involved in the prevention of tooth decay was identified. Methods of direct tissue analysis and indirect analysis (blotting onto a layer of C18 beads or a cellulose membrane) were compared. Analysis of C18 blots was found to be the superior method. Optimum results were achieved by electrospraying the matrix onto the C18 blots: this minimised analyte spreading and allowed mapping and localisation of specific compounds within tissue sections.

In a subsequent study, Caprioli investigated the use of a carbon-filled polyethylene membrane as a blotting substrate, selected because of its electrical conductivity and protein adhesion properties [102] . Analysis of such membranes yielded unique protein profiles [102]. The former facilitates matrix application by electrospray and the latter enables effective purification of proteins from intact tissue. A further study using improved instrumentation achieved faster image acquisition [103], lending itself to automation and use as a routine high throughput method.

The use of membranes for matrix support has been investigated for a variety of substrates e.g., nylon [121], poly(vinylidine difluoride) [122], nitrocellulose [123] and polyethylene [124]. The use of these membranes to enhance the mass spectrometric analysis of proteins has been reviewed by Vestling *et al.* [125]. The use of membranes as tissue blotting substrates, and as a method of achieving enhanced mass spectral profiles is investigated and reviewed in Chapters 2 and 4.

Disease state profiling MALDI peptide and protein imaging has paved the way for the development of techniques for disease state profiling, which are now described.

Stoeckli and co-workers investigated the use of MALDI imaging as a method for identifying and mapping amyloid beta (Aβ) peptides in transgenic mice brains [104, 105]. The formation of plaques containing high levels of Aβ is thought to be a central process in Alzheimer's disease. 50 μl of matrix was applied directly to the tissue surface. Crystallisation was performed at 4^0 C: this slow drying method was selected in order to increase signal intensity by reducing salt contamination. Unfortunately, although signal intensity was enhanced, the method typically yielded large crystals of $\sim 200\,\mu$m. In addition, by filming the drying process, migration of individual matrix crystals by up to 400 μm was observed, with obvious implications for analyte spreading. Despite limitations of the spatial resolution due to the matrix application and crystallisation, the mass images correlated well to optical images of the plaques indicating the potential of the technique.

Another major neurological disorder, Parkinson's disease, is currently being investigated by imaging MALDI-MS [106,107]. Imaging analysis of experimental models of Parkinson's disease in mouse brain demonstrated a range of region-specific protein images in affected vs. control tissues. Matrix deposition by spotting small matrix volumes (as described later in this section) reduced protein migration within the tissue samples.

The identification of tumour-specific proteins has been achieved by the analysis of tissue blotted membranes [108] and by direct tissue analysis [109]. Healthy and cancerous tissue from mouse colon was blotted onto a polyethylene membrane, which was subsequently coated in matrix material by elecrospray. Tumour-specific biomarkers were identified by comparison of the mass spectral profiles obtained from the blots of healthy and diseased tissue [108]. The alternative approach of direct

tissue analysis for tumour typing human brain tissue has recently been presented. Unique tumour associated protein profiles were obtained, and examination of the mass spectral profiles permitted classification of tumour samples by histological grade [109].

The studies described thus far have involved analysis of single, two-dimensional sections of tissue. Recently, a three-dimensional model of myelin basic protein in mouse brain tissue by MALDI-MS was presented [110]. Optical images of successive sections of mouse brain were compiled to give a three-dimensional model of the brain tissue. Approximately 1 in 20 of the sections obtained were subjected to imaging MALDI-MS. Resultant mass images were incorporated into the model by computer-aided design, and mass spectrometric images were incorporated into MRI images of the same tissue, demonstrating good anatomical homology.

Single-cell analysis MALDI-TOF can also be used to study single cells and is becoming a popular method of cellular peptide profiling. Peptides in single neurons from invertebrate ganglia and atrial glands were imaged by MALDI-MS by Sweedler *et al.* [111]. Invertebrates possess relatively large central nervous system neurons ($15 - 500\,\mu$m) compared to mammalian tissue, and thus successful imaging of peptides within individual neurons in such systems is conceivable. Intact tissue sections were coated with matrix by electrospray. The authors describe that both matrix deposition and tissue freezing and sectioning protocols influence the spatial resolution in terms of peptide migration and signal intensity. Images depicting the distribution of a neuropeptide are displayed at a laser spot size of $100\,\mu$m. The image demonstrates areas of both analyte spreading and signal suppression. This highlights that while the instrumentation employed offered a spatial resoltion of $30\,\mu$m, the ultimate resolution was impaired by sample preparation.

Peptide profiling in cells has also been accomplished with the use of *laser capture microdissection* (LCM). In LCM, a thermoplastic membrane placed directly on a tissue section melts and adheres selectively to cells of interest after irradiation with a focused infared laser pulse. The thermoplastic film is then coated with matrix and analysed by MALDI-MS. Caprioli and co-workers describe coating the membrane using picolitre volumes of matrix deposited via a finely-pulled glass capillary [112]. The reduced volume of solvent applied in this method has been shown to minimise

analyte spreading and, with the advent of specifically-designed robots [113,120], the technique is likely to have widespread use for imaging applications. Such robots are capable of spotting matrix in volumes low enough to achieve minimal analyte spreading. Furthermore, analyte migration is confined within the picolitre spot, and is likely to be comparable for all spots. Samples are spotted on specialised targets, and an ASCII file is generated containing the xy co-ordinates of all spots. Thus mass spectral data can be acquired from the tissue according to the precise location of the deposited matrix spots.

Analysis of pharmaceutical compounds In addition to the successful detection and mapping of peptides and proteins in tissue and single cells, *in situ* analysis [99] and imaging [100] of pharmaceutical compounds in tissue has also been demonstrated.

In situ MALDI analysis of drugs was introduced by Troendle and colleagues [99]. Matrix was applied to the tissue surface by pipetting and electrospraying. In these experiments, a MALDI quadropole ion trap was employed to detect the anti-cancer drug paclitaxel in a human ovarian tumour. In other studies, the anti-psychotic drug spiperone has been detected in spiked sections of rat liver tissue [99].

The determination of two pharmaceutical compounds in rat brain tumour tissue was presented by Reyzer *et al.* [100]. Tissue sections were coated in sinapinic acid by airspray deposition. It was found that MALDI-TOF technology was unable to differentiate between the drug compound, matrix clusters, and endogenous tissue molecules in the majority of samples. In order to overcome this, MALDI-Qq-TOF using selected reaction monitoring was evaluated. Unambiguous determination of the drug by dissociation of the protonated molecule to its predominant fragment was achieved. Thus the spatial location of the drug molecule in brain tumour tissue was shown as a map of the fragment ion by tandem MS. Ultimate spatial resolution in these experiments is not discussed, but is likely to be in the region of 50 μm—given the instrument employed (in the absence of excessive analyte spreading).

Other biological applications MALDI imaging has also been used to analyse plant tissues [119]. Successful localisation of a range of amino acids and primary

metabolites has been demonstrated by blotting potato tuber and leaf samples onto matrix coated membranes. This work is included in Appendix A of this thesis.

MALDI imaging has also been used as a method of assessing the homogeneity of matrix application methods. Electrospray was shown to be far superior to pipetted drops in terms of layer uniformity [126].

Recent developments Whilst MALDI imaging experiments have yielded better quality spectra, and can detect a superior mass and compound range compared with LDMS and SIMS, the lateral resolution is significantly less good than with laser microprobe or ion beam approaches. The quoted diameter of the laser spot size in most reports of MALDI imaging is between $50 - 200\,\mu$m, which may limit the usefulness of the technique for some applications. In view of this, efforts are being made to develop a microprobe MALDI approach: *scanning microprobe MALDI* (SMALDI) [127]. Sub-micron focusing of the laser beam is achieved by prefocusing outside the vacuum and final focusing directly above the sample. This permits a nitrogen laser to be focussed to approx $0.6\,\mu$m. Although this offers a 100-fold improvement in spatial resolution over the majority of MALDI imaging experiments, certain issues need to be addressed. First, smaller spot sizes have been associated with poor signal intensities [27] and, second, methods of matrix application that do not induce analyte spreading have only been reported for resolutions of $50\,\mu$m, and are yet to be demonstrated for the sub-micron range.

It is clear from the rapidly-emerging MALDI imaging literature that successful homogeneous coverage and formation of matrix crystals on the sample is key to the success of the technique. It has been demonstrated that there is no clear protocol for achieving the best results. Choice of matrix material and application method vary with respect to both the analyte (e.g., protein vs. drug), and the sample itself (e.g., intact tissue, cells, TLC plates, and membranes). Thus the various different approaches have shown success and failure in different applications. A recent article outlines optimal strategies for the direct analysis of proteins in tissue [113], and discusses aspects such as tissue handling & storage, as well as matrix application. However it is impossible as yet to make an *a priori* prediction of a successful protocol for new applications. Thus the majority of imaging experiments must start with

the trial, error, and evaluation of documented methods such as direct analysis vs. blotting, choice of matrix, and method of matrix application.

The detection and imaging of pharmaceutical compounds in tissue [99, 100], together with the imaging of drugs on TLC plates [114–118] and of proteins in tissue [101–113] by MALDI-MS shows that imaging with MALDI-MS has promise as a routine method for mapping drugs in tissues. This has widespread application in pharmaceutical and medical research.

The work described in this thesis concerns the development of optimal strategies for the analysis, imaging, and quantification of drugs in skin by MALDI-TOF-MS.

1.3 Dermal absorption

1.3.1 The structure of skin

The skin is a metabolically-active organ with vital functions such as thermoregulation, protection, metabolism, excretion, immunity and sensation. It consists of two distinct layers—the epidermis and the dermis—each with a distinct function. The dermis is attached to an underlying hypodermis, (subcutaneous tissue layer), consisting of adipose tissue and areolar connective tissue (Figure 1.5 [128]).

The stratified epidermis is the outermost layer of the skin ($100 - 150\,\mu$m thick) and is subdivided into five layers or strata (Figure 1.6): the stratum basale, the stratum spinosum, the stratum granulosum, the stratum lucidum, and the stratum corneum in which a keratinocyte (the principal cell type found in the epidermis) gradually migrates to the surface and is sloughed off in a process called desquamation. Keratinocytes comprise about 95% of the epidermis. The stratum basale is a single layer of columnar keratinocytes, attached to the basement membrane by hemidesmosomes—junctions that anchor the cell to a non-cellular substrate. After a mitotic division, newly formed cells will undergo a progressive maturation called keratinisation as they migrate to the surface. The stratum basale also contains melanocytes, Langerhans cells, and Merkel cells.(Figure 1.6 [129]).

The stratum spinosum consists of 8–10 layers of keratinocytes which accumulate many desmosomes (junctions that attach a cell to its neighbour) on their outer surface providing the characteristic 'prickles' of this stratum, which is often called the prickle-cell layer. Langerhans cells and melanocytes may also be present.

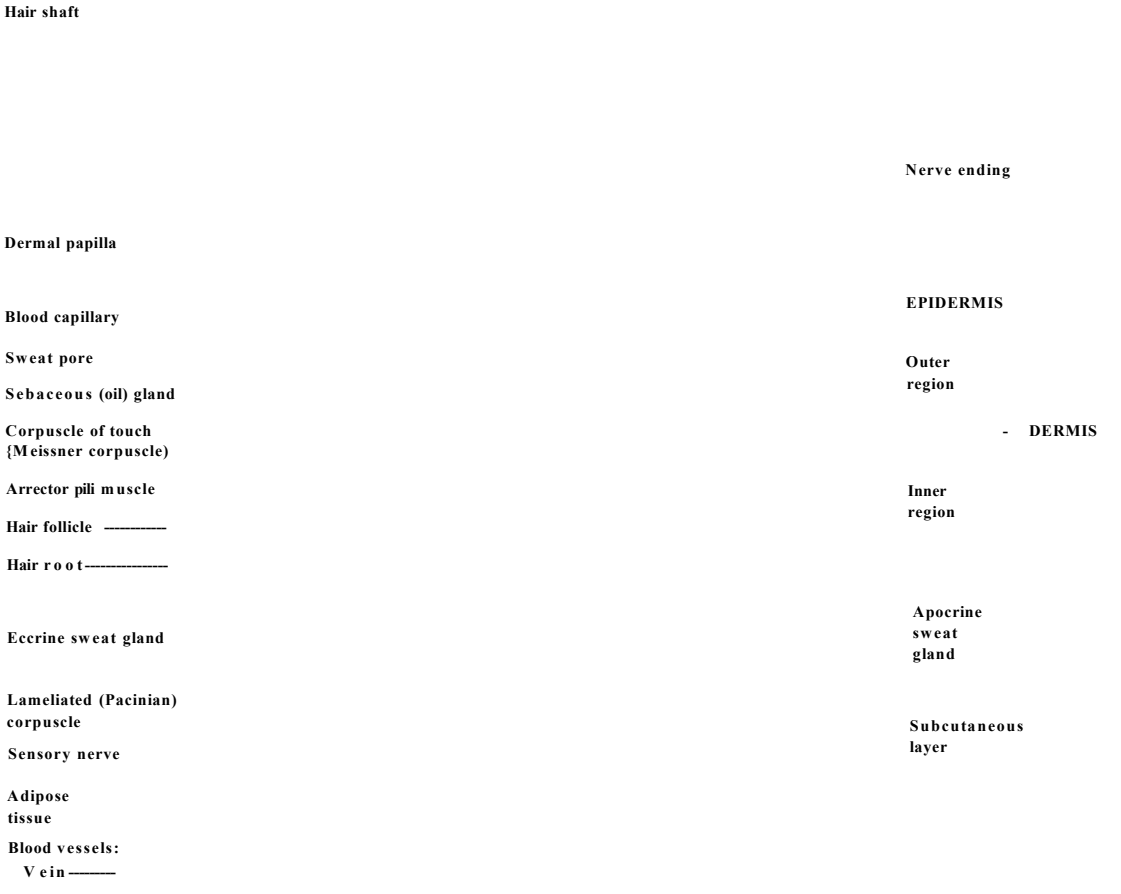

Figure 1.5: The integumentary system consists of skin, associated appendages, muscles and nerves (from [128]).

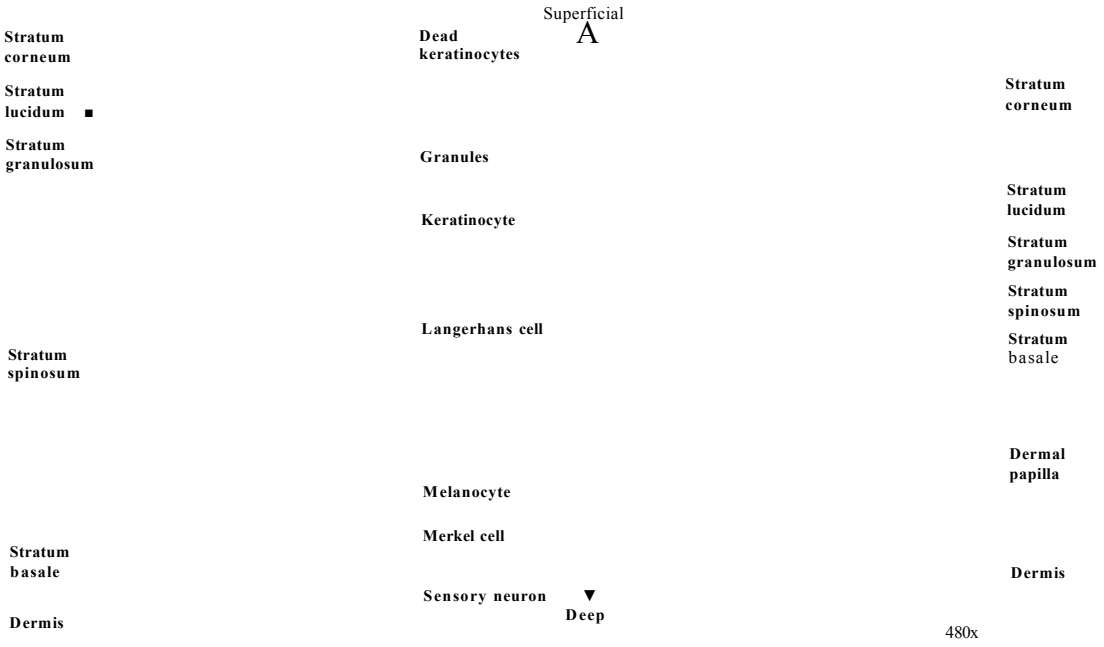

Figure 1.6: Layers of the epidermis (from [129]).

The stratum granulosum comprises around five layers of flattened keratinocytes. These cells accumulate dense basophilic keratohyaline granules, containing lipids, which along with the desmosomal connections, help to form a waterproof barrier that functions to prevent fluid loss from the body.

The stratum lucidum consists of about five layers of clear, flat, dead cells. This layer is normally only present in the thick skin of the palm and soles.

As a cell accumulates keratinohyaline granules, it is thought that rupture of lysosomal membranes release lysosomal enzymes that eventually cause cell death. The dead and dying cells filled with mature keratin form the stratum corneum. The deeper cells of the stratum corneum retain their desmosomal junctions, but as they are pushed to the surface by newly forming cells, the dead cells gradually desquamate.

The dermis assumes the important functions of thermoregulation and supports the vascular network to supply the avascular epidermis with nutrients. The dermis is typically subdivided into two zones, a papillary dermis and a reticular layer. The principal cell of the dermis is the fibroblast. Fibroblasts secrete collagen and elastin

that result in the support and elasticity of the skin. Also present are immune cells that are involved in defence against foreign bodies passing through the epidermis.

The papillary dermis contains vascular networks that have two important functions. The first being to support the avascular epidermis with vital nutrients and secondly to provide a network for thermoregulation. The papillary dermis also contains the free sensory nerve endings and structures called Meissners corpuscles in highly sensitive areas.

The reticular layer of the dermis consists of dense irregular connective tissue. This layer is responsible for the overall strength and elasticity of the skin, as well as housing other important epithelial derived appendages such as sebaceous glands and hair follicles.

1.3.2 The skin barrier

The barrier function of mammalian skin is principally attributed to the stratum corneum [130]. Barrier properties are based on the specific content and composition of the stratum corneum lipids [131] and in particular on the structural arrangement of the intercellular lipid matrix and the lipid envelope surrounding the cells [132].The lipids form bilayers surrounding the corneocytes, producing a brick and mortar model (proposed by Elias in 1983 [133–135]) with corneocytes as the bricks and the intercellular lipids forming the mortar. The intercellular lipids are primarily ceramides, cholesterol, cholesteryl esters, fatty acids, and a small fraction of cholesterol sulphate [136]. The protein enriched corneocyte bricks impart a high degree of tortuosity to water or any other molecule that traverses the stratum corneum, while the hydrophobic lipid mortar provides a water tight barrier property to the already tortuous route of permeation [137]. Gene gun studies have revealed that the corneocytes impart physical protection, in the form of impact resistance [138]. Extensive research has been performed to attempt to determine the composition and arrangement of the lipid mortar, and a detailed discussion is considered beyond the scope of this thesis. Current theories suggest that in fact the stratum corneum is not strictly a brick wall type barrier but instead a complex biopolymer with barrier and membrane properties [139].

1.3.3 Percutaneous absorption

A percutaneously-delivered therapeutic agent, whether directed at the systemic circulation or the local tissues, must traverse the stratum corneum. Despite an insufficient knowledge of the precise mechanism of skin penetration it is clear that both the physiochemical and structural properties of the penetrating molecules and the internal structure and composition of the skin membrane are involved in the process. The vitality of the skin determines the metabolism, distribution, and excretion of the compounds in the skin and body [140].

Absorption across the stratum corneum is a passive process of diffusion, with the stratum corneum behaving as a semi-permeable membrane. In principle, there are three routes of diffusion: intercellular diffusion through the lipid matrix; transcellular diffusion through the corneocytes; and pilosebaceous diffusion along the sweat pores and follicles that pierce the stratum corneum.

The route of pilosebaceous diffusion is considered to be insignificant because the orifices only account for 0.1% of the total skin surface area and because diffusion through sweat pores is against an aqueous flow [141]. Comparison of diffusion across skin and across a pore-free membrane showed little difference, suggesting that diffusion occurs without these aqueous channels.

Although recent mathematical modelling approaches suggest that permeation through the corneocytes should not be ignored [142], the majority of evidence suggests that the primary route of a drug through the skin is via the intercellular lipid matrices [143].

The thesis routes of permeation are illustrated in Figure 1.7 [144].

A variety of factors influence the absorption of compounds into the skin layers and these are summarised in Table 1.3.

1.3.4 Methods for the analysis of percutaneous absorption and quantification of drugs in skin

In vivo vs. *in vitro* methods

Percutaneous absorption studies are essential to the understanding of the dermatoxicity and pharmacological activity of substances that may come into contact with

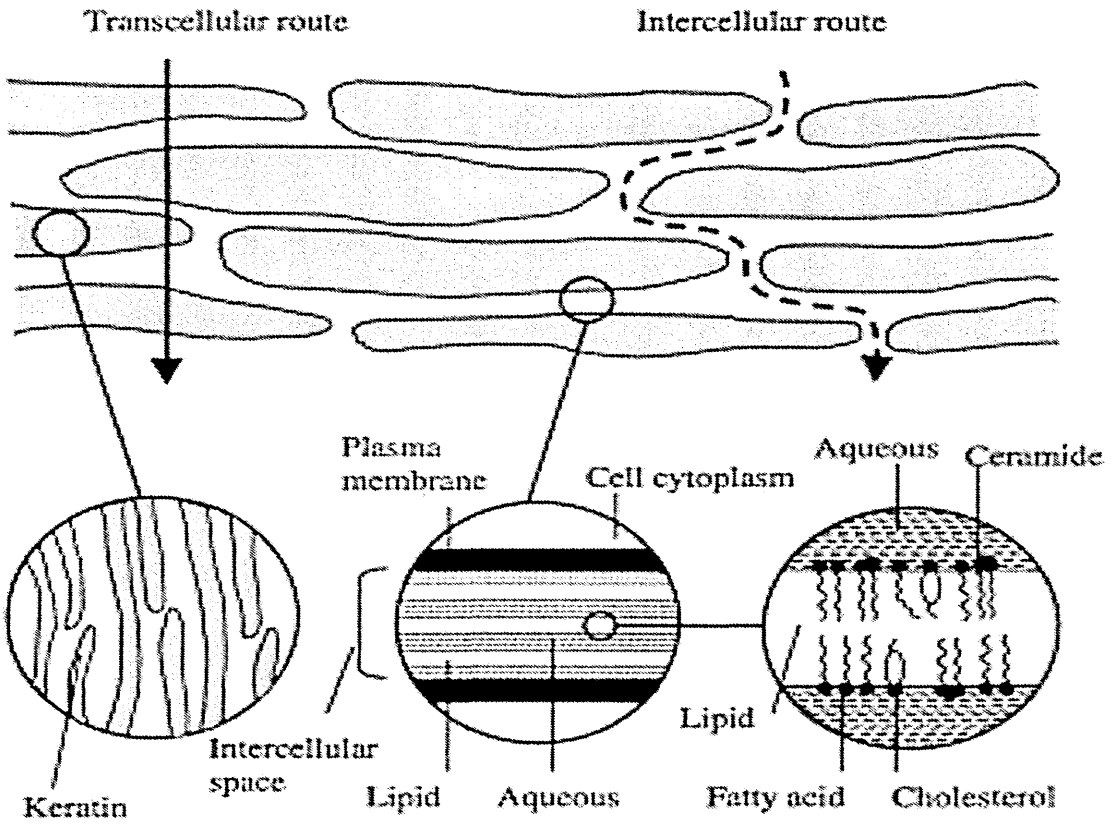

Figure 1.7: Permeation routes through the stratum corneum: (i) via the lipid matrix between the corneocytes (intercellular route) and (ii) across the corneocytes and the intercellular lipid matrix (transcellular route)[144].

Test compound	Molecular weight Water/lipid partition coefficient ionisation
Vehicle	Solubility/polarity Volatility Concentration Distribution in stratum corneum Penetration enhancer pH
Skin	Species Age, sex, race Anatomical site Temperature Hydration of stratum corneum Damage to stratum corneum Metabolism
Application	Skin area dose (e.g. film thickness, concentration) Total skin area in contact with vehicle Duration of exposure

Table 1.3: Factors affecting percutaneous absorption

the skin, e.g., an environmental hazard or drug intended for therapeutic use. Human *in vivo* studies are the most relevant and are obviously the preferred approach for obtaining data pertaining to man. However, human volunteer studies are often difficult to justify ethically, particularly if the dermal application has toxic or irritant properties, or if the methods involved areT invasive or painful to the subject. Therefore, *in vitro* techniques have also been used, and have good agreement with *in vivo* experiments [145–147]. Hence *in vitro* techniques are popular, especially in preliminary drug studies and method development.

In vivo assessment

It should be noted that some of these techniques may also be adopted in *in vitro* method but are included here because they can be performed in a safe, relatively non-invasive manner on living subjects.

Radioactivity in excreta Percutaneous absorption *in vivo* may be determined indirectly by measuring radioactivity in excreta or sometimes plasma after topical application of the radioactively-labelled compound. This approach is particularly useful when plasma levels of topically applied compounds are below assay detection level [148]. This method obviously offers no information about the location or quantity of drug in the skin layers but is used as a general measure of drug uptake through the skin.

Spectroscopic methods Attenuated total reflectance-Fourier transform infrared (ATR-FTIR) spectroscopy has been used to monitor the *in vivo* transport kinetics of drugs and other permeants within the stratum corneum [149]. IR spectroscopy records the molecular vibrations of an absorbing species, and consequently can either identify an unknown or track a known chemical entity. It is essential that the compound to be monitored possesses a uniquely identifiable IR absorbance distinct from those of the stratum corneum components. The IR absorbance is directly proportional to the amount of compound at the sample location. Profiles of the drug in skin can be compiled by repeated analysis of an area following sequential tape stripping and the data fitted to a Fick diffusion model [150]. This assumes that if the stratum corneum is the rate limiting step in dermal absorption, then

quantification of the drug within this layer must provide an estimate of the rate and extent of delivery to the underlying tissues. FTIR spectroscopy has also been used for biophysical examination of the skin barrier function [151].

Remittance spectroscopy involves the detection of backscattered light from the interior of the stratum corneum. Since the presence of additional light absorbing compounds in the skin will reduce backscattering, it is possible to quantify the compounds within the skin. This has been demonstrated to be highly sensitive and reproducible for analysis of compounds in skin [152].

Fluorescence spectroscopy has been successfully used for the quantification of drugs in skin, using a self fluorescent marker [153]. As in remittance this depends upon the analysis of remitted light, with measuring depth being dependent on beam wavelength. The light is detected after passing through a second monochromator, and so only a specific emission wavelength is detected [154].

Photothermal spectroscopy is based upon the projection of a modulated (chopped) monochromatic UV beam upon the skin followed by measurement of the subsequent periodic heating caused by light absorbance. The presence of a UV absorbing drug in the tissue will increase the oscillating surface temperature, resulting in pressure oscillations in the skin surface that can be detected with a microphone [155]. This technique is limited to the analysis of the drug in the stratum corneum [156].

Surface recovery This approach is based on loss of a material on the skin surface as it penetrates into the tissue. It is assumed that the difference in applied dose and residual dose is the amount of drug absorbed. A related technique, surface disappearance monitors the disappearance of ^{14}C from the skin surface as a ^{14}C–labelled compound is absorbed into the skin [157].

Autoradiography Autoradiography is a photographic technique used to detect the localisation of radioactive materials in specimens. Autoradiography for the examination of skin samples has been used at the tissue, cellular and sub-cellular levels [158]. The technique may be performed on small areas, or the whole body. Whole body auto-radiography provides an overall picture of the dermal absorption followed by the involvement of other body tissues [148]. Autoradiography is most

useful when used in conjunction with skin sectioning or stratum corneum tape stripping [157]. Semi-quantitative results may be obtained with the use imaging software. The autoradiograph is superimposed upon a histological image of the tissue and the computer system is used to quantify the drugs in all areas it is observed [154].

Tape stripping The tape-stripping technique is being increasingly used to measure a drug's concentration profile across the stratum corneum. The stratum corneum is progressively removed by serial adhesive tape-stripping (Figure 1.8 [159]), and the determination of (a) the drug amount in each tape and (b) the thickness of stratum corneum removed by each tape-strip, enable the diffusion capacity and solubility of the permeant within the stratum corneum to be calculated using Fick's second law of diffusion [150]. This predicts concentration of the drug (Cx) as a function of position (x) within the stratum corneum. The concentration of drug in the outermost layer of the stratum corneum ($Cx = 0$) divided by its concentration in the applied vehicle (Cv) gives the partition coefficient (k). Fitting experimental concentration profiles to the equation provides both k and $D/L2$.

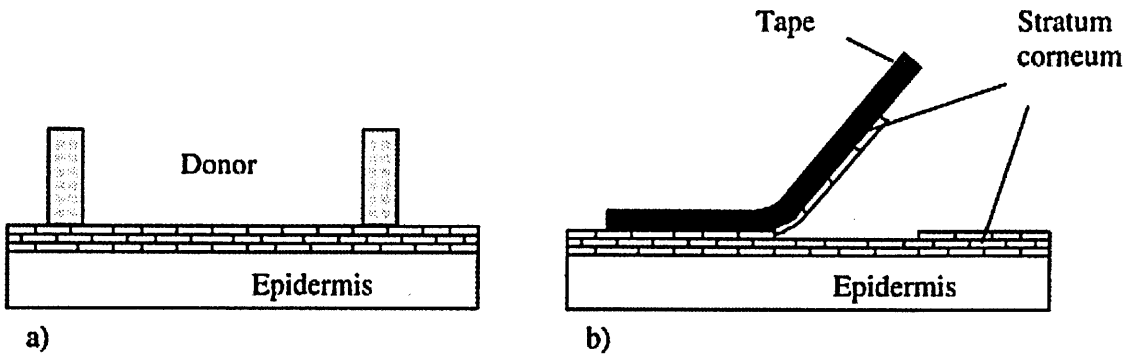

Figure 1.8: Schematic representation of the method of tape stripping for determination of the amount of drug penetrated into the skin. After application of the formulation at the donor site (a) and removal of the formulation, the stratum corneum is progressively removed by tape stripping (b) [159].

A major advantage of this technique is that 'unlabelled' compounds can be evaluated because the tape strippings contain adequate concentrations for non-labelled assay method. The two major disadvantages of the technique are: (a) unless sufficient data is available in the literature about the thickness of each skin layer at the

selected site, preliminary experiments are needed in order to assess this parameter and (b) the stratum corneum can not be removed entirely by stripping. Generally, about one third of the layer will remain attached as 'islets to the epidermal surface [146]. As a result of this the corneocytes collected on one tape strip may be derived from different depths. In addition any tape strip will remove different amount of stratum corneum at different depths and sites of the skin. This makes it necessary to estimate the body mass removed with each strip e.g., by weighing the pieces of sellotape before and after stripping. The experimental errors associated with these limitations may be large.

In vitro assessment

Skin source The most suitable source of skin is obviously human skin. However, availability is usually limited and ethical approval may be hard to obtain, and therefore animal tissue is often used. The most relevant animal model for human skin studies is the pig. Material is readily available from abattoirs and its histological and biochemical properties [160] have been shown to be similar to human skin. In addition, the permeability of drugs through pig skin is well documented as being similar to that in human skin [145, 161, 162]. Porcine ear is considered the best choice for permeation studies and has been shown to give comparable results to human skin [162–164]. While the act of freezing skin may affect its metabolic activity, permeation into the skin is a passive diffusion process, and it has been shown that freezing has little [164] or no [165] effect on skin permeability. It is therefore acceptable to use frozen tissue samples for *in vitro* measurement of drugs within skin.

Diffusion cell The classic diffusion cell consists of donor and receptor compartments separated by the skin sample. The permeation rate of the drug from the donor chamber through the skin and into the receptor is determined by measuring the amount of drug permeated over time e.g., with high-performance liquid chromatography (HPLC) as the analytical method.

Tape stripping *In vivo* studies can be hard to justify ethically and extremely expensive. In view of this *in vitro* tape stripping can be viewed as an alternative

option, and is particularly useful in initial studies of compounds traversing the stratum corneum [166]. (For methodological details see page 38).

Skin extraction measurements A biopsy of treated tissue is homogenised and the drug extracted in a suitable solvent. A sensitive analytical technique such as GLC, HPLC or scintillation counting is used to quantify the drug. This has the inherent disadvantage that destruction of the tissue structure in the drug extraction process rules out any information on the localisation of the drug being obtained [156].

Fluorescence microscopy Fluorescent or fluorescent-labelled substances can be localised in the skin strata with a fluorescent microscope. Some of the earliest fluorescent microscopy studies showed evidence that the shunt pathways of permeation through the pilosebaceous units are of relevance; wells of the applied compounds were demonstrated within the hair follicles [157].

In summary, a variety of techniques may be employed for the determination of drugs in skin. None of the methods discussed is capable of displaying quantitative information of the spatial location of an unlabelled drug in tissue.

Work presented in this thesis concerns the development of methods for the analysis of drugs in skin by imaging MALDI-MS. Direct tissue analysis is compared with the indirect analysis of a variety of tissue imprinted membranes. Methods of matrix application are evaluated with a view to creating a homogeneous matrix layer, without causing analyte spreading. Quantitative analysis of the drug by MALDI-TOF-MS is investigated. Finally, the methods developed are compared to corneum tape stripping/HPLC analysis.

Chapter 2

The Preparation of Tissue Samples for the Determination of Pharmaceutical Compounds by MALDI-TOF-MS

2.1 Introduction

The successful determination [99] and imaging [100] of pharmaceutical compounds and proteins [101–113] in tissue by MALDI-TOF-MS has been reported. In this chapter, methods for the analysis of drugs in porcine ear epidermal tissue by MALDI-TOF-MS are evaluated. Initial investigations were conducted with three test compounds to explore the feasibility of the technique as a method of profiling drugs in skin. Following the selection of a suitable test analyte, the methods of direct tissue analysis and the indirect analysis of tissue-imprinted membranes were compared and evaluated. Reyzer *et al.* [100] report successful localisation of a drug by direct analysis of matrix-coated brain tissue by MALDI-Qq-TOF-MS. The use of tissue blotting methods has been widely adopted for protein isolation and analysis [167]. Membranes have been used in mass spectrometry experiments as blotting substrates for the analysis of tissues by MALDI-MS, thereby as a means of spatially fixing proteins from tissues [102], and also as a method of matrix support and protein purification [125]. The indirect analysis of tissue-imprinted membranes for studying biological systems has shown promising results. Caprioli's group reported improved localisation of peptides and proteins when blotting onto C18 beads adherent to a MALDI target [101], or onto cellulose [101] or carbon conductive [102] membranes.

The use of poly(vinyl difluoride) (PVDF) and nitrocelluose membranes to improve ion intensities in protein analysis is well documented [122,123].

In the work described here, the utility of blotting drug treated skin samples onto substrates for MALDI-TOF-MS analysis was investigated. To enable a full comparison between blotting and direct tissue analysis, two different approaches to tissue treatment were adopted. For a technique to be useful in localising and profiling drugs in epidermal tissue, it must be able to show the correct spatial distribution of the analyte. Problems with analyte spreading by matrix application methods are well recognised [100–103, 113], and to assess the extent of this phenomenon in these experiments a method of confining the tissue area studied was devised. By fixing a plastic ring (with an internal diameter of 5 mm) onto the epidermal surface, and applying drug within the ring, it was anticipated that the drug should only be observed on the surface within this area.

2.2 Experimental

2.2.1 Materials

Ketoconazole (((±)−1−acetyl−4−[*p*−[[(2R,4S)−2−(2, 4−dichlorophenyl)−2−(imidazol−1−ylmethyl)−1, 3−dioxolan−4−yl]methoxy] phenyl] piperazine)), aciclovir (previously known as acyclovir, 2−amino−9− [(2−hydroxyethoxy) methyl]−1, 9−dihydro−6H−purin−6−one), and piroxicam (N−1(pyridyl)−4−hydroxy−2−methyl−2H−1, 2− benzothiazine−3−carboxamide 1, 1−dioxide), Sigma-Aldrich (Dorset, UK) were evaluated as potential test analytes. The structures of these compounds are shown in Figure 2.1.

The following MALDI matrices were investigated for *in situ* analysis of these compounds: α−cyano−4−hydroxycinnamic acid (α-CHCA), 2, 5−dihydroxbenzoic acid (DHB), 3, 4−dihydroxycinnamic acid (DHC), 2−aceto−2−hydroxybutyrate (AHB). All matrices and trifluoroacetic acid (AR grade) were purchased from Sigma-Aldrich (Dorset, UK). Methanol was HPLC grade, purchased from Fisher Scientific (Loughborough, UK). Nitrocellulose (0.2 μm pore size) membranes, C18 solid phase extraction discs (C18 Envidiscs), and PVDF (Immobilon P) transfer membranes (0.45 μm pore size) were purchased from Supelco/Sigma-Aldrich (Dorset, UK). Polyethylene-filled carbon conductive membranes (including their cellulose

Acyclovir FW: 225.21

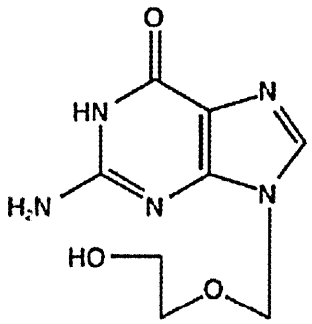

Piroxicam FW: 331.35

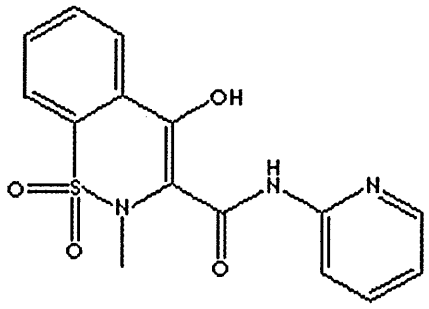

Ketoconazole FW: 531.44

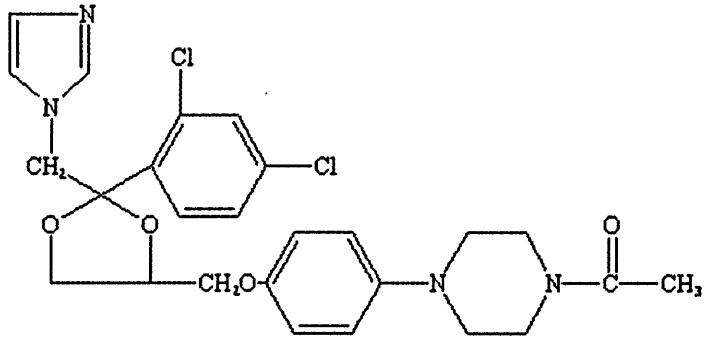

Figure 2.1: Structures and formula weights of the pharmaceutical analytes

membrane spacers) were obtained from Goodfellow (Huntingdon, UK). Double-sided sticky tape was obtained commercially (Sellotape). Fresh porcine ears were obtained from Doncaster abbatoir.

2.2.2 Instrumentation

The electrospray matrix deposition device developed at Sheffield Hallam University [110] was employed in all experiments. This comprises an in-house modified commercial robotic $x-y-z$-axis motion system (Figure 2.2, PROBOT, BAI, Germany). Modifications to the instrument were undertaken in order to use the apparatus as an electrospray deposition device. The alterations were as follows: a PTFE tube was used to transfer matrix solution from a 100 μl syringe to a Supelco coupling. The electrospray needle consisted of a 94 mm length of stainless steel capillary (0.5 mm OD, 0.11 mm ID, ASH Instruments, U.K.) and the seal to the PTFE tube was made within the Supelco coupling. The electrospray needle was threaded through a stainless steel Swagelock tee coupling (1/16 in OD) and through a piece of stainless steel tubing (38 mm length, 1/16 in OD, 0.75 mm ID, Jones Chromatography, U.K.). A gas line was attached to the tee to provide nitrogen (2 bar) coaxial to the spray to assist in gas nebulisation, if required.

The syringe pump (Harvard microliter syringe pump) set at a flow rate of 0.6 ml·hr^{-1} delivered the matrix solution to the tip of the stainless steel capillary. To obtain a fine spray of the matrix solution, ca. 2 kV was applied to the tee coupling using a high voltage supply. The metal plate (7×15 cm) was earthed and placed 2 mm from the end of the electrospray needle. The plate was then moved across in front of the spray at a rate of 25 mm·s^{-1}.

A modified LaserTOF 1500 (SAI, Manchester, UK) was employed in these investigations. This is a linear time-of-flight mass spectrometer, fitted with a 337 nm nitrogen laser and delayed ion extraction. Modified MALDI targets previously designed for the analysis of TLC plates [116] were used. These targets have a $64 \times 2 \times 0.2$ mm recess, into which a section of tissue or membrane was mounted with double-sided tape. Previous instrument modifications to the sample probe and software updates allowed free movement along the vertical (z) axis, and the construction of summed ion chromatograms. All samples were analysed in the positive ion mode.

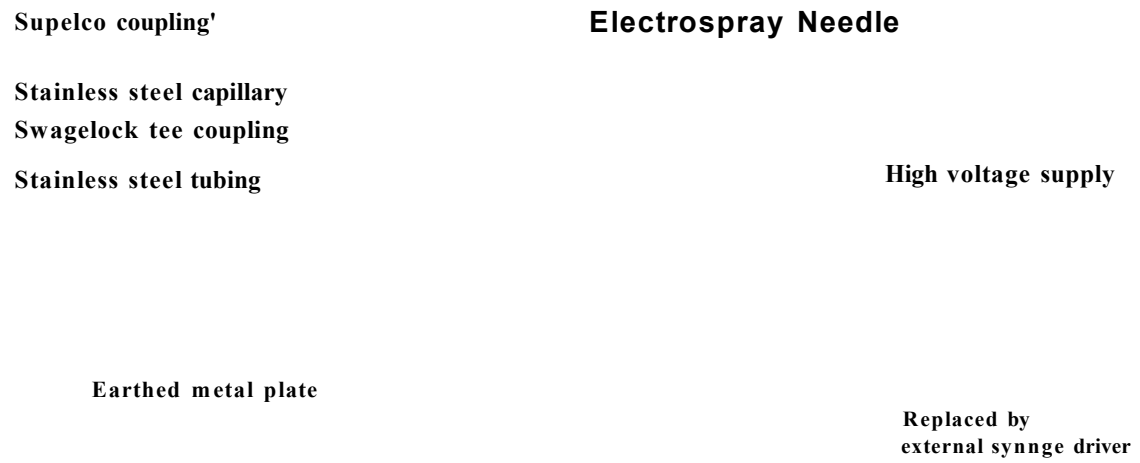

Figure 2.2: Electrospray deposition device employed in these investigations

Scanning electron microscopy was performed using a Phillips XL40 Scanning electron microscope, fitted with a tungsten wire filament. The working distance (from the bottom of the column to the sample surface) was 10 mm. An electron gun potential of 15 kV was employed in all experiments.

2.2.3 Methods

Porcine epidermal tissue was treated with 50 *A* 2 mg*ml_1 analyte solutions (prepared in methanol) by pipetting onto the tissue surface. Tissue was incubated at 37 °C for one hour. Following 'snap-freezing' in liquid nitrogen-cooled isopentane, the tissue was sectioned by microtoming in a cryostat. Surface sections of approximately 30 x 2 x 0.2 mm were mounted onto modified stainless steel MALDI targets using double-sided tape. The mounted tissue samples were left to dry under vacuum overnight. The matrix was then applied to the sample using the electrospray deposition device. Matrices were sprayed at concentrations between 10 and 25mg-ml_1 at a flow rate of 0.6mMir-1.

Following matrix deposition by electrospray, samples were dried under vacuum for one hour prior to analysis by MALDI-TOF-MS. Mass spectra were acquired

every 0.25 mm along the MALDI target.

Once a suitable test analyte and matrix had been selected, two different approaches for treatment were attempted in order to assess the potential of MALDI-TOF-MS for dermal permeation depth profiling: (1) *tissue spiking;* and (2) *confined tissue spiking* (spiking within a plastic ring). Direct analysis of a tissue section was compared with analysis of tissue imprints obtained by blotting onto a variety of substrates. Analyte solution (as described above) was pipetted either directly onto the surface, or in the centre of a plastic ring fixed to the tissue surface (confined tissue spiking) of a $30 \times 30 \times 5$ mm piece of porcine epidermal tissue.

The treated tissue was incubated at 37^0 C for 1 hour (and in confined tissue spiking experiments the ring removed), then rinsed in deionised water.

For direct analysis the sample was then frozen and a 15 μm surface section of tissue was obtained by microtoming. The resultant tissue slice was sectioned with a surgical scalpel within the frozen conditions of the cryostat to yield a strip of tissue 2 mm wide, which was then stuck onto the modified stainless steel TLC-MALDI target with double-sided tape.

For indirect analysis the tissue was blotted onto either PVDF, nitrocellulose, cellulose or carbon conducting membranes, or onto C18 beads directly adherent to the modified MALDI target. Sections of the membrane were prepared in the same dimensions as the tissue sections and mounted accordingly. All samples were then coated with matrix (as described above) and dried prior to MALDI analysis. Mass spectra were acquired every 0.25 mm along the MALDI target as previously described.

2.3 Results and discussion

Initial experiments were undertaken to assess the suitability of various matrices for the analysis of the potential test compounds.

In general, optimum results with MALDI-TOF-MS are achieved when a solvent is used in which both analyte and matrix are soluble. Matrix assessment was therefore based on solubility in methanol, and on the behaviour of a pre-mixed matrix/analyte solution during MALDI-TOF-MS analysis on a conventional 25 spot stainless steel target. Assessment was made according to the following criteria:

- the absence of interfering peaks in the spectral region of interest;
- the reproducibility of analyte signal intensity from laser spot to spot over the target;
- high analyte signal intensity for the pharmaceutical analyte.

Poor spectral results were obtained for all analytes using AHB and DHC matrices. These matrices were therefore not investigated further.

α-CHCA provided the best spectral results, analyte signal intensity and reproducibility for the detection of piroxicam and ketoconazole, while DHB was considered the optimum matrix for analysis of aciclovir. These matrices were therfore used in subsequent experiments, described below.

2.3.1 Evaluation of the suitability of different analytes

Aciclovir

The potassium adduct of α-CHCA (m/z 228) appeared to interfere with detection of the protonated molecule of aciclovir (m/z 226), and the best spectral results were observed using DHB as the matrix for analysis of this compound (Figure 2.3).

DHB could not be successfully electrosprayed at concentrations over 10 mg·ml^{-1} as at concentrations above this, matrix crystals appeared to block the capillary needle of the electrospray device, resulting in inefficient matrix coverage of the sample. However, α-CHCA could be successfully electrosprayed at concentrations up to 25 mg·ml^{-1}. In general, higher analyte intensities were observed using 25 mg·ml^{-1} α-CHCA compared to 10 mg·ml^{-1} DHB. α-CHCA was therefore chosen as the preferred matrix for further development of this method, and—in view of matrix-associated interference in the spatial region of interest when using α-CHCA—aciclovir was rejected as a poor choice of test compound for *in situ* MALDI-TOF-MS analysis with a linear TOF instrument.

Piroxicam

While mass spectra were obtained demonstrating the presence of piroxicam in the tissue section (Figure 2.4), results were not reproducible. This may have been due to poor ionisation of the drug in the tissue, and/or insufficient formation of matrix

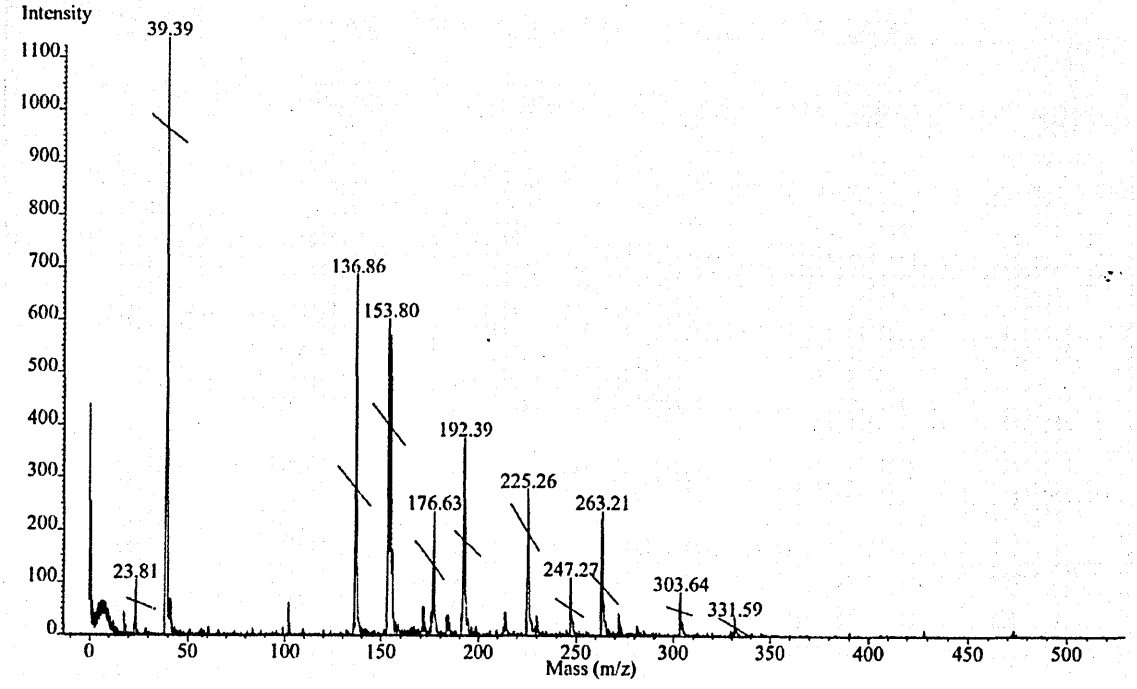

Figure 2.3: MALDI mass spectrum of aciclovir showing the protonated drug molecule $[M+H]^+$ at m/z 225, and the sodium and potassium drug adducts at m/z 247 and 263 respectively. DHB-associated peaks, $[Matrix+H]^+$ at m/z 154; $[Matrix+Na]^+$ at m/z 176; and $[Matrix+K]^+$ at m/z 192 are also seen.

crystals on the tissue surface. In the majority of spectra obtained, no compounds—including the matrix—were detected in the region where the tissue was mounted. Summed ion chromatograms for the range *m/z* 330-334 were inconclusive, and difficult to interpret (Figure 2.5): The majority of chromatograms indicated that piroxicam was not ionised in the tissue.

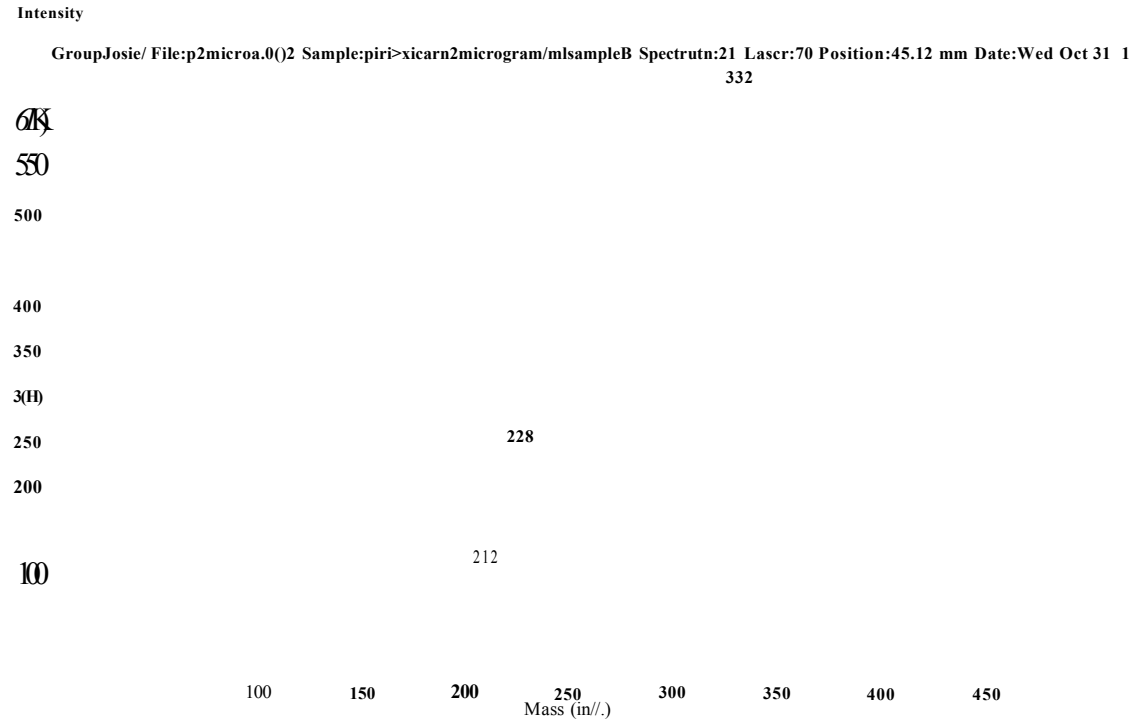

Figure 2.4: MALDI mass spectrum of piroxicam-treated tissue showing the protonated analyte ion [M+H]+ at *m/z* 332. Expected matrix peaks at *m/z* 191: [Matrix+H]+; *m/z* 212: [Matrix+Na]+; and *m/z* 228: [Matrix+K]+ are also observed. The matrix dimer ion is present at *m/z* 380. Drug-treated tissue was mounted from 3551 mm, and coated in a-CHCA by electrospray deposition.

Insufficient matrix coverage of the tissue samples resulted in chromatograms that initially implied the presence of piroxicam outside the region in which tissue was mounted. This may have been because, when there is little or no ionisation in the target region, noise either side may be mistaken for a significant signal. However, as well as this effect indicating the possible presence (in the chromatograms) of the compound outside the tissue area, spectra were acquired that demonstrated a compound at *m/z* 332 up to 1.5 cm either side of where the tissue was mounted.

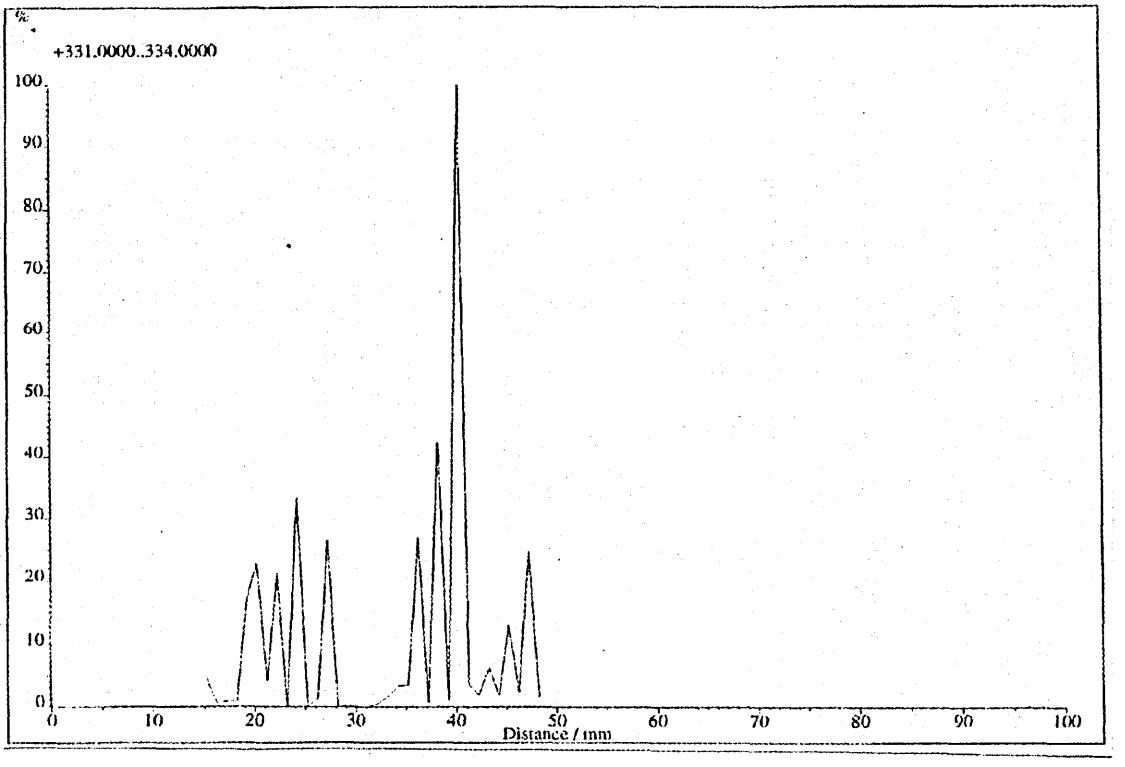

Figure 2.5: Summed ion chromatogram for the range m/z 330–334 demonstrating that compounds were detected from 15–28 mm and 32–48 mm. Treated tissue was mounted between 15–48 mm and coated in α-CHCA by electrospray deposition.

It was first considered that matrix application by electrospray was causing the analyte to be washed out of the tissue onto the target at either side. Though this may account for the detection of piroxicam a couple of millimetres either side of the mounted tissue section, electrospray matrix deposition is unlikely to cause such a high degree of analyte spreading.

Double-sided tape was used to mount the tissue sections onto the MALDI targets: a length of tape exceeding that of the tissue section ensured that either end of the section was fully stuck onto the target prior to MALDI analysis. The chromatograms and spectra clearly depicting a peak at *m/z* 332/333 either side of the tissue could therefore be considered to confirm detection of compounds present in the tape (Figures 2.5 and 2.6).

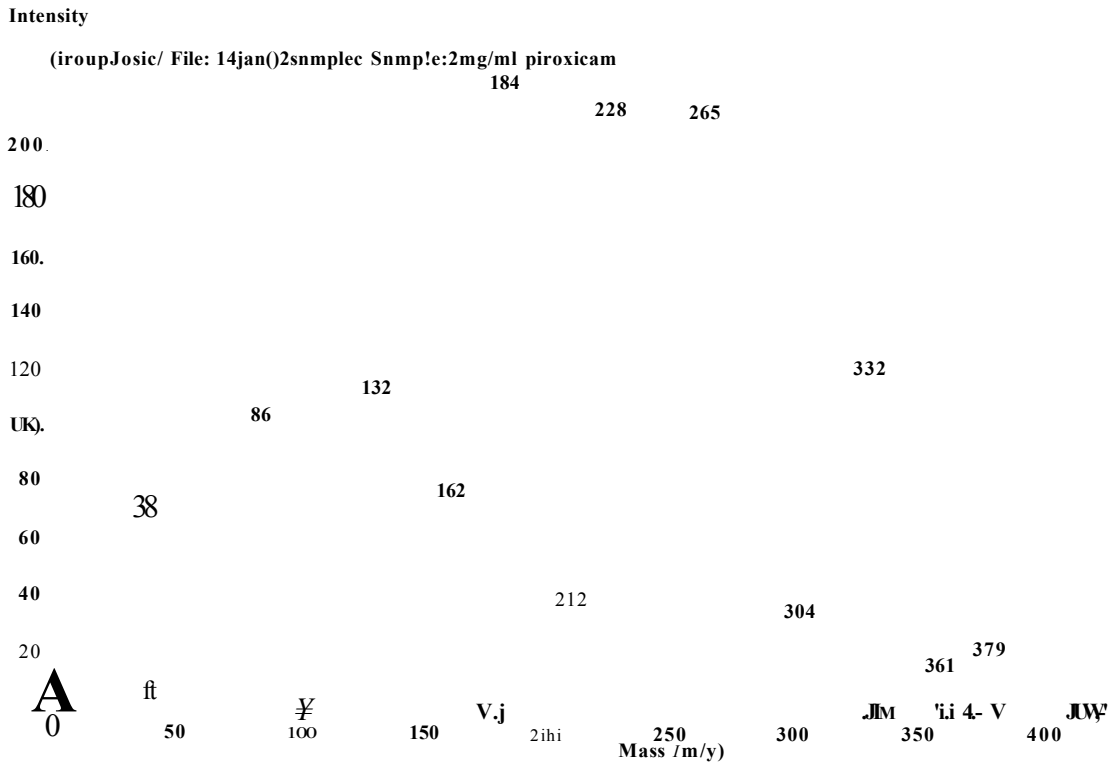

Figure 2.6: MALDI mass spectrum acquired at a position on the target where no tissue was present. A peak at *m/z* 332 can be seen with an ion intensity of approximately 120. Matrix associated peaks are observed at *m/z* 212: [M+Na]+; *m/z* 228: [M+K]+. The matrix dimer is present at *m/z* 379. Treated tissue was mounted onto a MALDI target and coated in a-CHCA by electrospray deposition.

Further experiments were performed to determine whether or not a compound with a molecular weight of 332 or 333 was present in the double-sided tape.

Tape was dissolved in THF and analysed by MALDI-TOF-MS following co-crystallisation with α-CHCA on a conventional 25 spot target. In a separate experiment tape was mounted onto a modified TLC target and α-CHCA was applied by electrospray.

Both experiments yielded spectra showing the presence of a peak at m/z 333, indicating that detection of a compound of molecular weight 332 either side of the mounted tissue sections could be as a direct result of analysing the tape itself.

Analysis of mounted, untreated tissue sections also yielded a peak at m/z 333. This indicated that either the tissue was absorbing compounds from the tape, or that the tissue itself contains a compound with a molecular weight of 332, observed at m/z 333. It was not possible to analyse sections of tissue on the modified TLC targets without the tape, and so tissue was homogenised, mixed with matrix and applied to a conventional 25 spot target. Spectra obtained showed the presence of a peak at m/z 333 (Figure 2.7). This suggested that a compound with molecular weight 332 was present in both tape and tissue, or was perhaps an instrument contaminant.

In order to ensure that peak m/z 333 was not associated with α-CHCA, some experiments were repeated using DHB as the matrix. In some cases with α-CHCA a peak occurs at m/z 334. This may be attributed to the matrix dimer ion undergoing a loss of the carboxylic acid group.

Results obtained for homogenised tissue, dissolved tape, mounted tape and mounted tissue using DHB as the matrix all clearly showed a peak with m/z 333. These results demonstrate that piroxicam is an unsuitable test compound for use by this method using this instrument.

Ketoconazole

Results obtained for the analysis of ketoconazole in tissue presented more promising results. Mass spectra were produced demonstrating detection of the protonated analyte in the tissue (Figure 2.8). No interfering compounds appeared to be present in either the tissue or the tape—no other peaks were observed in the region of m/z 530–535.

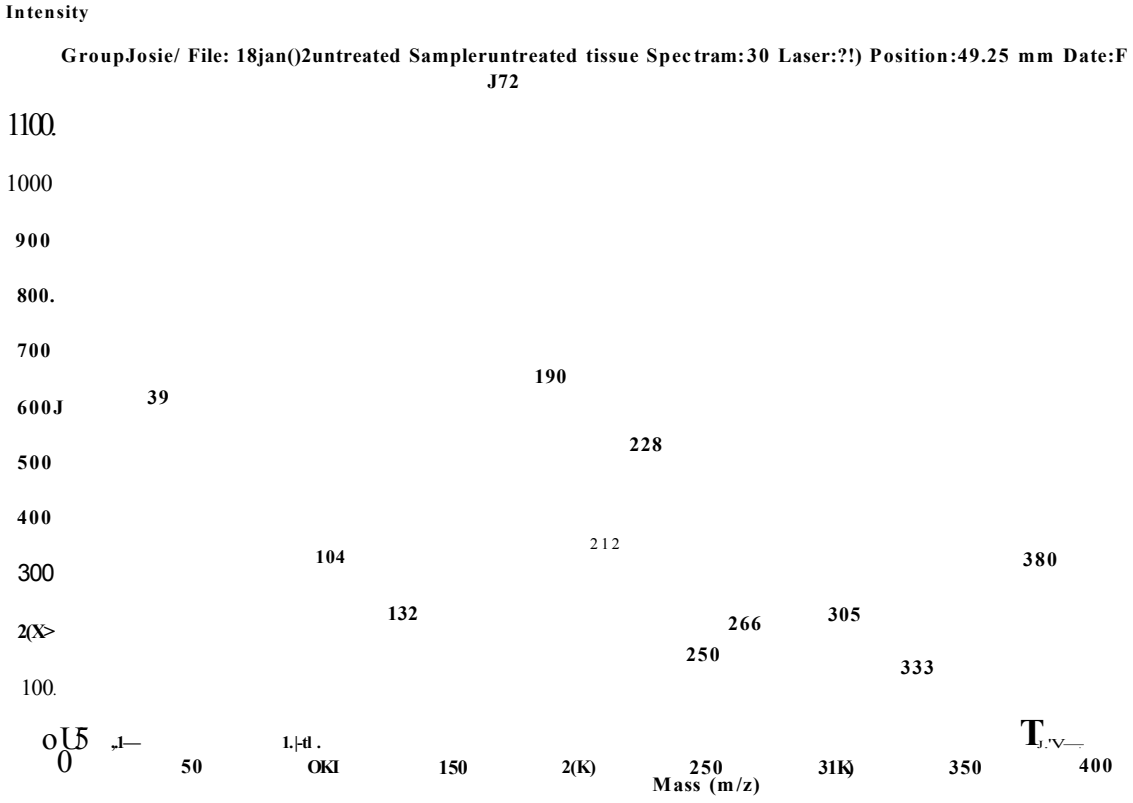

Figure 2.7: MALDI mass spectrum of untreated tissue, showing a peak at m/z 333. Tissue was coated in a-CHCA by electrospray deposition.

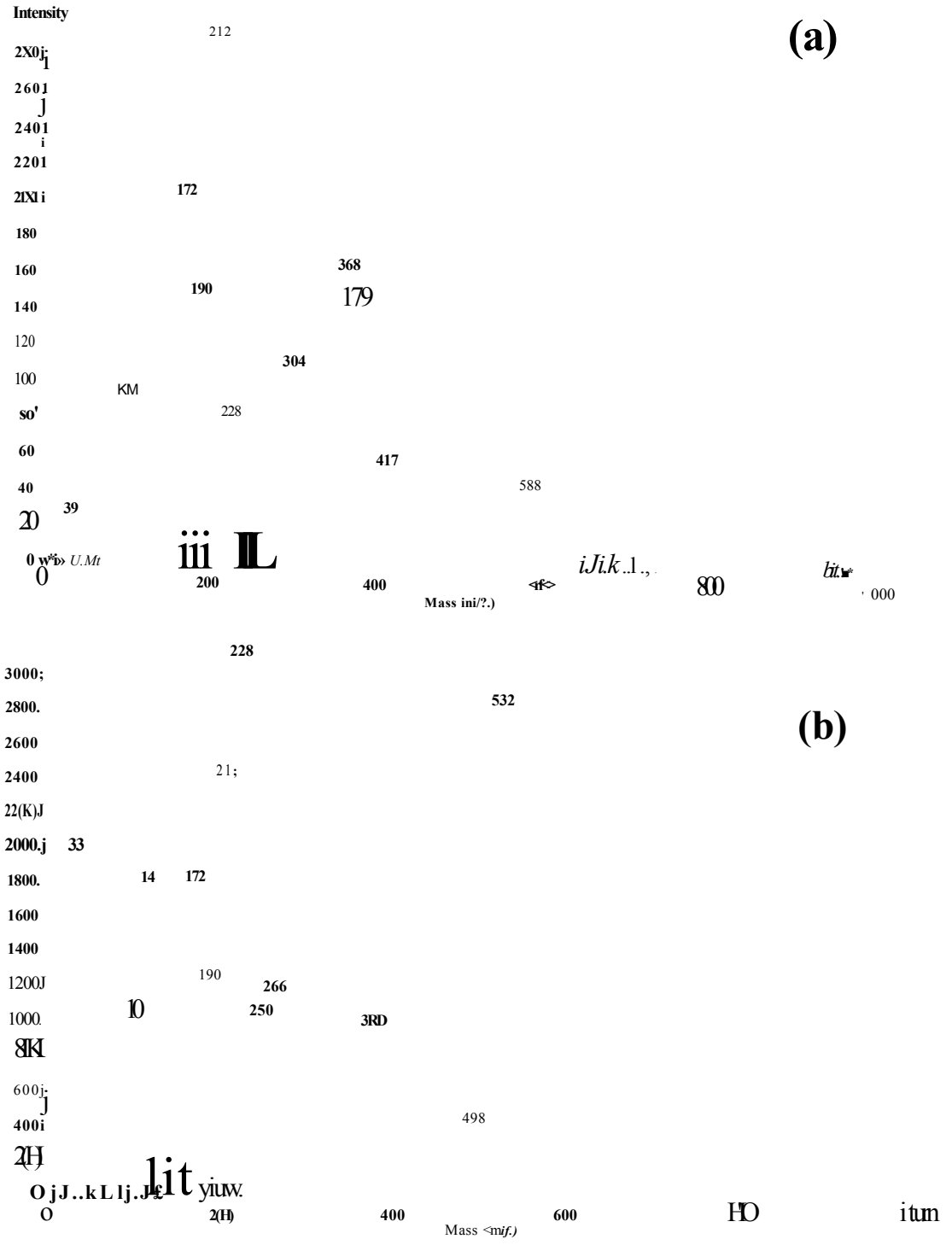

Figure 2.8: MALDI mass spectra for (a) untreated tissue, and (b) ketoconazole-treated tissue. Spectrum (a) clearly shows an absence of possibly-interfering peaks, while (b) clearly shows successful detection of the protonated analyte. Tissue was coated in a-CHCA by electrospray deposition.

However, results were not reproducible, and chromatograms were inconclusive (Figure 2.9), and again in the majority of cases no ions were detected within the tissue. This may have been attributed to poor matrix deposition by the electrospray device, or may have been associated with the sample itself. Varying the drying time of the tissue prior to both electrospray and MALDI analysis appeared to make no difference.

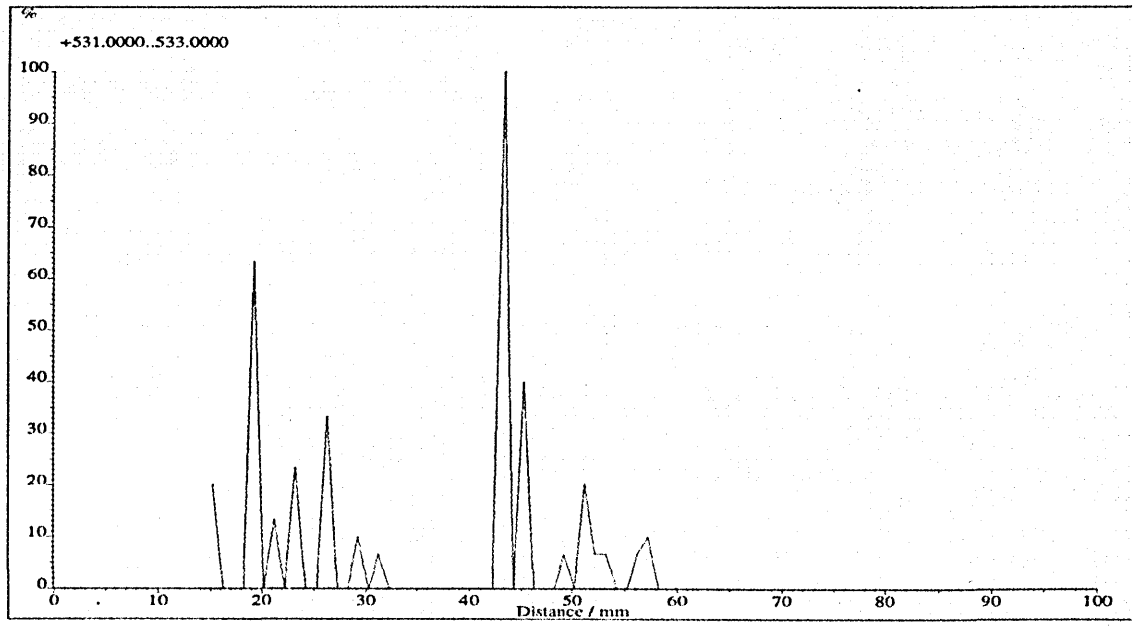

Figure 2.9: Summed ion chromatogram for the mass range m/z 531–533. No compounds in this range were detected between 32–42 mm. Treated tissue was mounted from 32–44 mm and coated in α-CHCA by electrospray.

These results suggest that the direct analysis of these test compounds (aciclovir, piroxicam and ketoconazole) in skin by MALDI-TOF-MS conducted on a linear TOF instrument is inconsistent and unreliable.

2.3.2 Comparison of direct tissue analysis vs. tissue blotting for the determination of ketoconazole in skin by MALDI-TOF-MS.

Direct analysis of drug treated tissue

As previously described, problems were encountered with direct analysis of tissue. The protonated analyte molecule could be detected, but not at every increment

along the target. In the majority of experiments, no ions were detected—indicating insufficient matrix crystal formation and sample coverage, or an inability to ionise compounds in (or on) the tissue.

C18 beads

Analysis of 'tissue-imprinted' C18 beads was also considered unsuccessful. Firstly it was extremely difficult to obtain an even layer of C18 beads on the MALDI target. Secondly it was observed that during the blotting procedure, the tissue surface became covered in the C18 beads, suggesting that they had in fact been removed from the target, and had become stuck to the tissue, rather than that a successful tissue imprint had been made upon 'anchored' beads. Thirdly it was observed that the electrospray procedure of matrix deposition displaced the 'loose' C18 covering. (This would obviously result in an inability to acquire useful information about the relative spatial distribution of the analyte). Some spectra depicting detection of the analyte were collected (Figure 2.10), but in the majority of experiments ion intensities were low, and in fact the analyte was detected at a location where it was not expected.

C18 Envidiscs

C18 Envidiscs could not be successfully analysed by this technique as it was discovered that these solid phase extraction discs were too thick to be mounted within the MALDI target recess. Because of this no mass spectrometry experiments were performed as it was thought that the extraction grid of the time-of-flight mass spectrometer would be damaged. In addition, preliminary blotting experiments revealed that this was unlikely to be a suitable blotting substrate: the blotting procedure resulted in the apparently 'loose' C18 covering ending up on the tissue surface, suggesting that an insufficient tissue imprint would have been made upon the substrate. Finally it was observed that following matrix deposition the membrane surface appeared to be 'cracked', presumably this occurred following drying/evaporation of the sprayed methanol. This is likely to have resulted in an un-even distribution of matrix crystals on the sample surface.

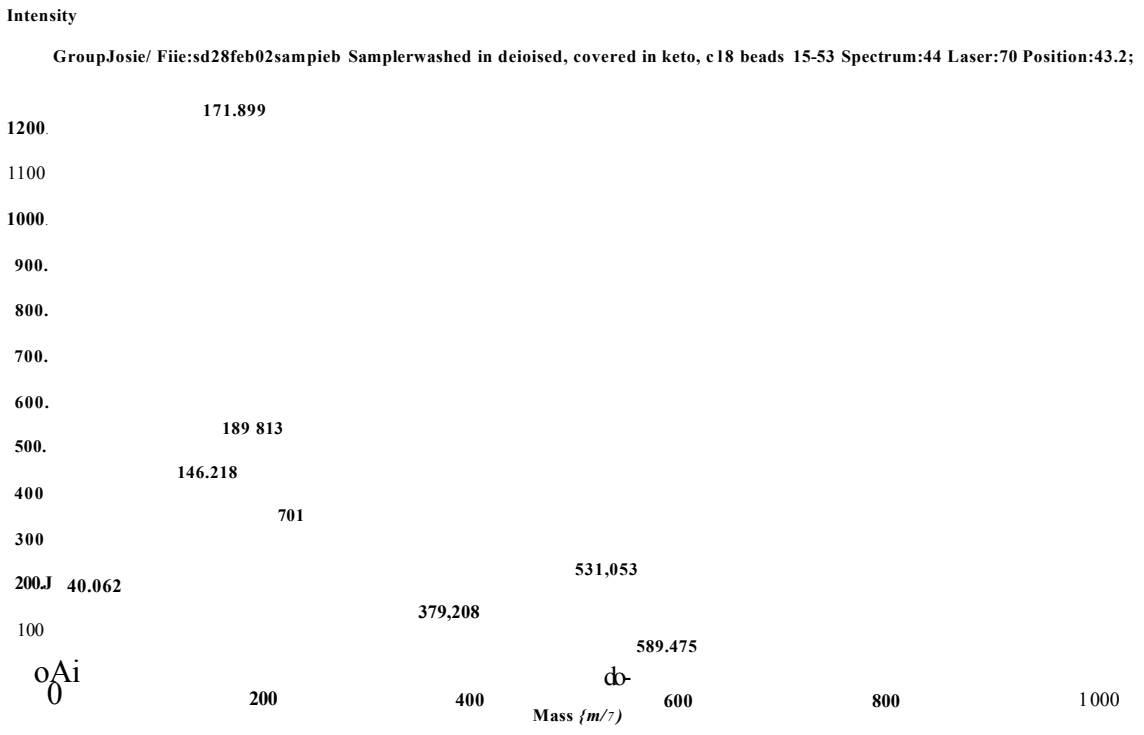

Figure 2.10: MALDI mass spectrum of a ketoconazole-treated tissue imprint on C18 beads. The analyte is detected at m/z 531 with a relative ion intensity of approximately 240. Matrix-associated peaks are observed at m/z 190: [Matrix+H]+; m/z 212: [Matrix+Na]+; and m/z 379 [Matrix-fMatrix]+. The sample was coated in a-CHCA by electrospray deposition.

Nitrocellulose membranes

Excellent mass spectra were acquired (Figure 2.11), demonstrating high ion intensities for the matrix ions and protonated analyte molecule.

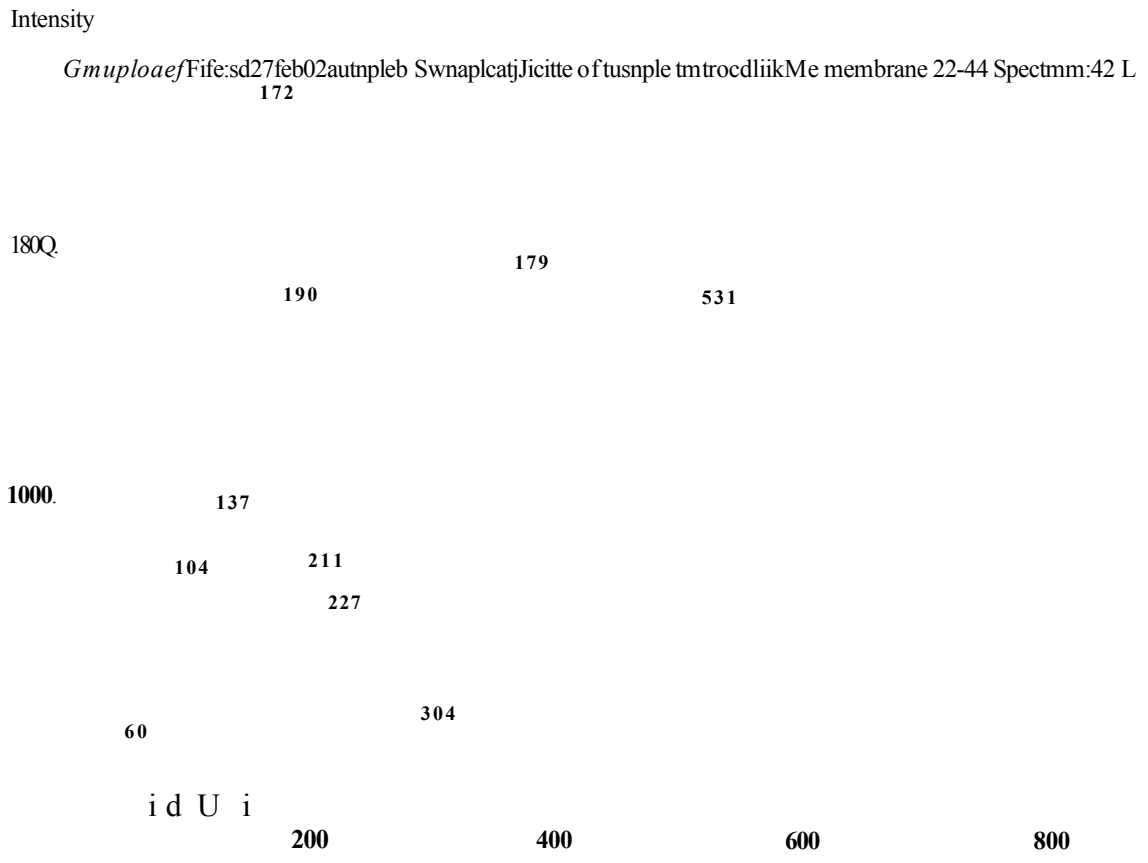

Figure 2.11: MALDI mass spectrum of a ketoconazole-treated tissue imprint on a nitrocellulose membrane. The analyte is detected at m/z 530 with a relative ion intensity of approximately 1600. Matrix-associated peaks are observed at m/z 190: [Matrix+H]+; m/z 211: [Matrix-f-Na]+; m/z 226.8: [Matrix+K]+; and m/z 379 [Matrix-f-Matrix]+. The sample was coated in a-CHCA by electrospray deposition.

Some promising summed ion chromatograms were constructed (Figure 2.12), illustrating that in the confined tissue treatment experiments, the analyte was predominantly observed within the diameter of the plastic treatment ring. However, it can be seen that it was also present in other areas, where perhaps no treated tissue was even blotted.

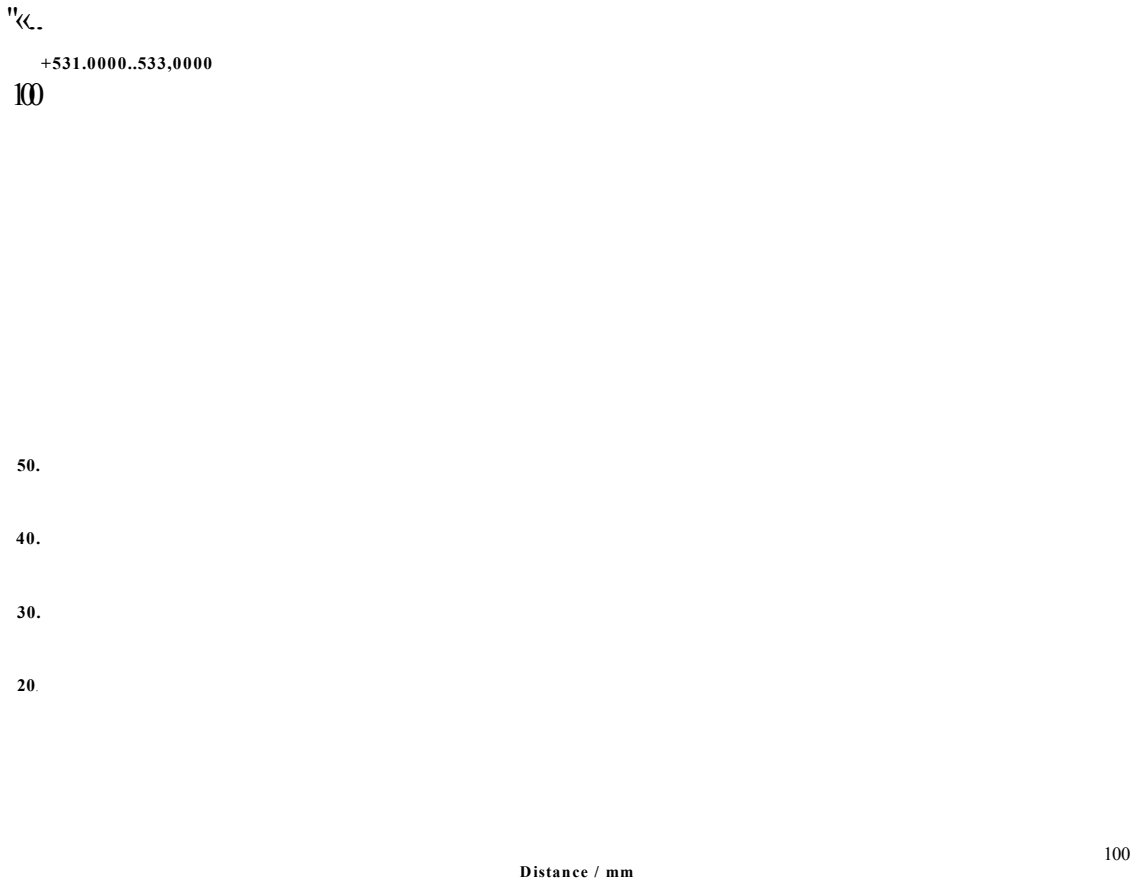

Figure 2.12: Summed ion chromatogram for the range *m/z* 531-533. Greatest ion intensities were observed between 41-43 mm. Tissue was treated with ketoconazole and blotted onto a nitrocellulose membrane coated with o-CHCA by electrospray. The original treatment area corresponded to between 38 and 43 mm.

However, this did not prove to be reproducible: in the majority of experiments the chromatograms did not demonstrate the expected distribution of the analyte, and at some points on the target, no ions were detected (as in the direct tissue analysis experiments). This is may be due to the nature of the membrane. The surfaces of the membranes were 'waxy' and because of this the matrix did not dry as a uniform layer, but instead formed 'beads'. As a result it could be seen that there were areas on the membrane where there were abundant crystals, and others where there were few or no crystals. This may account for the misleading chromatograms, and also for the spectra obtained that showed no ions (presumably because no matrix was present at these locations). So despite some good results, this was also found to be an unsuitable substrate for this application.

Polyvinyl difluoride (Immobilon P PVDF) membranes

Mass spectra showing relatively high analyte ion intensities were obtained (Figure 2.13). Some mass chromatograms were constructed demonstrating that the relative intensity of the analyte was greatest within the diameter of the plastic ring (confined tissue treatment experiments) (Figure 2.14).

However, in other experiments similar problems to those encountered in direct tissue analysis and whilst using nitrocellulose membranes were observed. Once again there appeared to be areas where no ionisation was achieved, and as with the nitrocellulose membranes this is thought to be attributed to the membrane itself. This substrate also possesses a 'waxy' surface which resulted in insufficient and non-homogeneous matrix coverage. Given that an even matrix layer is essential to the success of this technique, this limitation led to the conclusion that these were inappropriate substrates.

Cellulose membranes

Cellulose membranes proved to be suitable blotting substrates for this application. Mass spectra obtained exhibited good analyte intensities, and summed ion chromatograms from both the confined tissue treatment experiments and the standard treatment experiments identified the analyte only within the areas it was expected. In the confined tissue treatment experiments, the analyte was observed only within the diameter of the treatment ring (Figure 2.15), and in standard tissue treatment

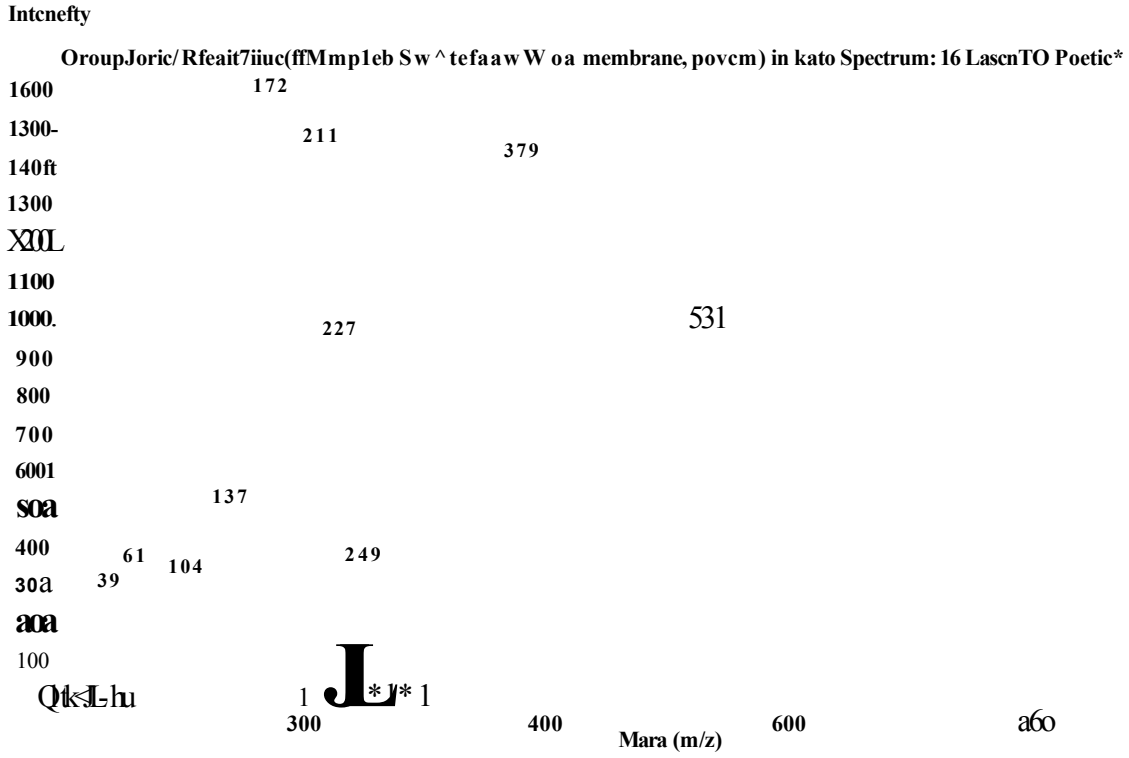

Figure 2.13: MALDI mass spectrum of a ketoconazole-treated tissue imprint on a PVDF membrane. The analyte is detected at m/2 530 with a relative ion intensity of 1000. Matrix-associated peaks are observed at *m/z* 211: [Matrix+Na]+; *m/z* 227: [Matrix+K]+; and *m/z* 379: [Matrix+Matrix]+. The sample was coated in a-CHCA by electrospray deposition.

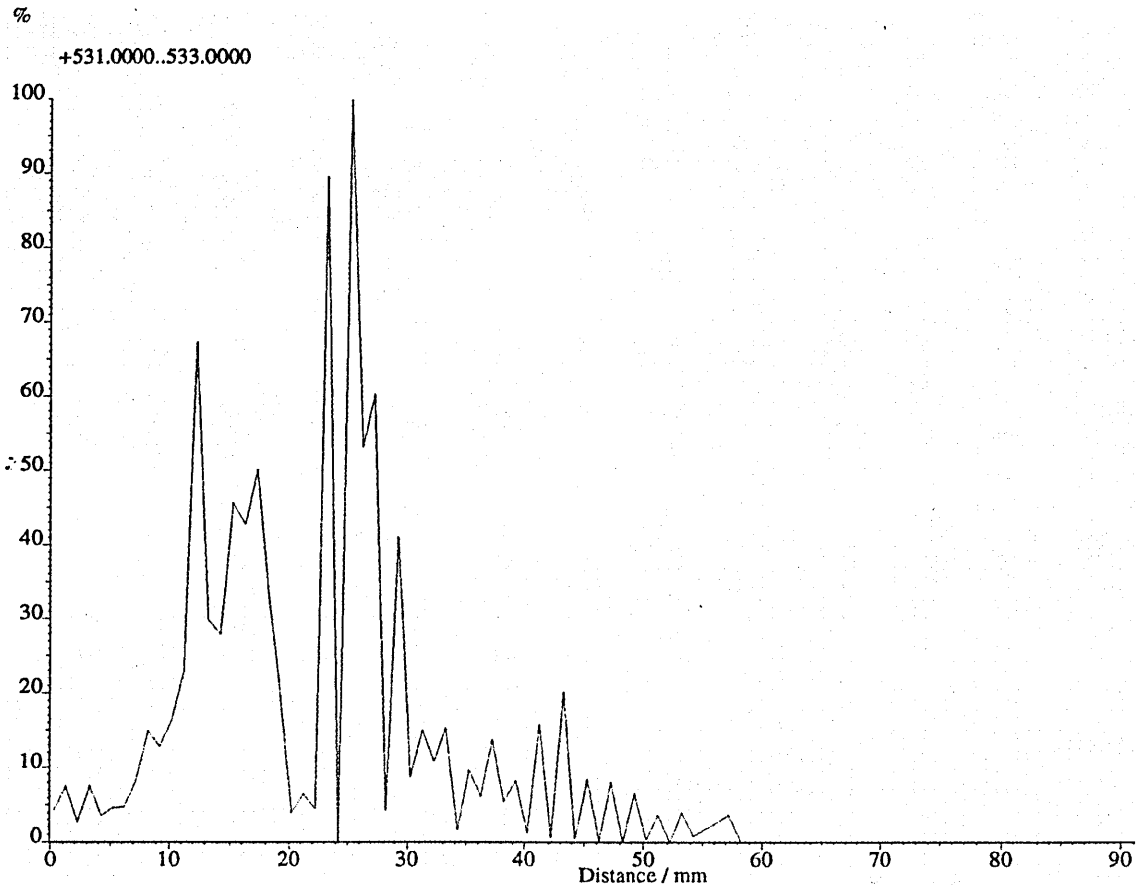

Figure 2.14: Summed ion chromatogram for the range m/z 530–533. Tissue was mounted from 21–42 mm. Ketoconazole was pipetted onto the surface of the tissue within the diameter of a plastic ring corresponding to 24–28 mm and subsequently blotted onto a PVDF membrane and coated with α-CHCA by electrospray.

experiments the analyte was detected across a larger area of the tissue surface (Figure 2.16), indicating that it had diffused through the tissue.

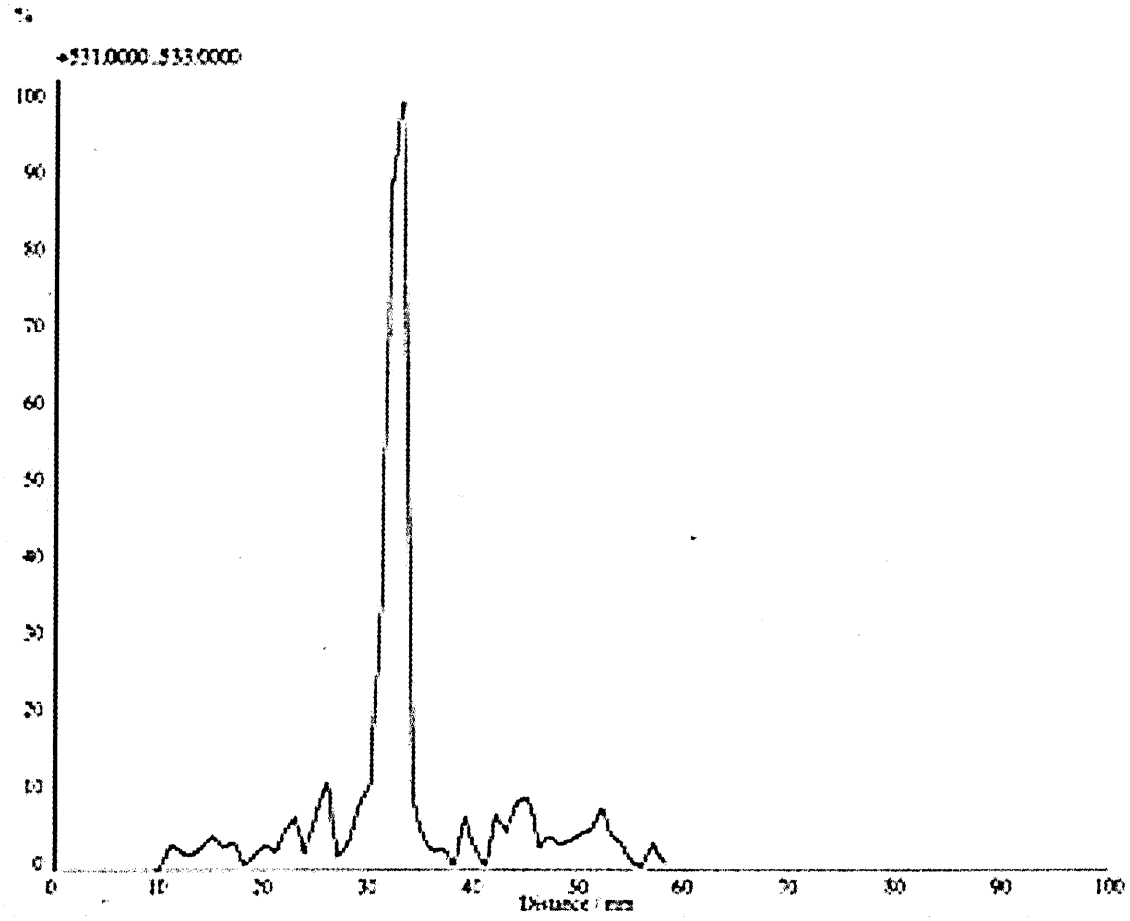

Figure 2.15: Summed ion chromatogram (from m/z 531–533) and mass spectra from a confined tissue treatment tissue blotting experiment, on a cellulose membrane. The diameter of the plastic ring corresponded to 30–35 mm. The protonated analyte molecule is detected between 30.5 and 35 mm. The sample was coated in α-CHCA by electrospray deposition.

These experiments showed good reproducibility, and no problems were incurred during matrix application. Mass spectra showing matrix ions and (when expected) the analyte were acquired at every position on the target. This was not achieved using the other substrates.

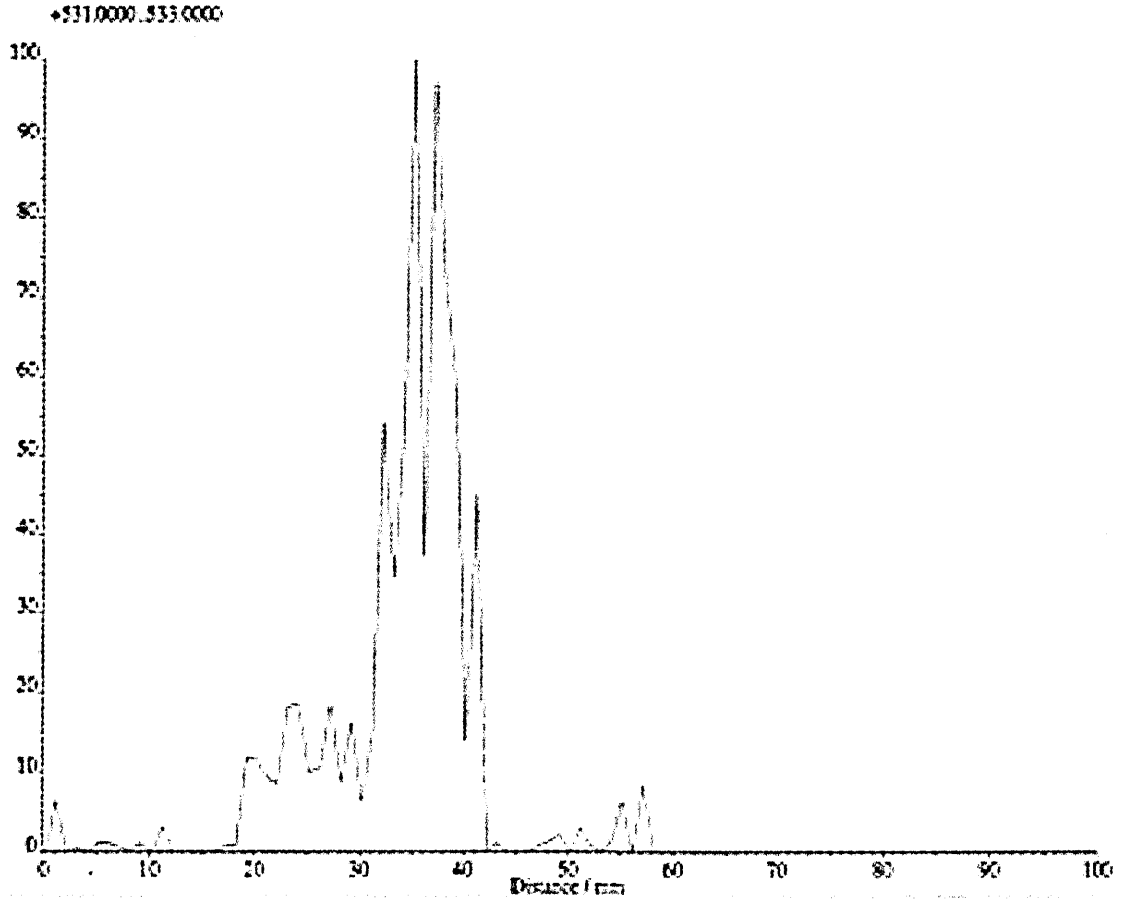

Figure 2.16: Summed ion chromatogram (from m/z 531–533 from a standard tissue spiking experiment. Treated tissue was blotted onto a cellulose membrane, and coated with α-CHCA by electrospray. The original treatment location corresponds to 32 mm.

Polyethylene-filled carbon conductive membrane

Mass spectra were acquired demonstrating successful determination of the protonated molecule of ketoconazole (Figure 2.17). Matrix ions were detected at all locations across the membrane, which was not achieved with any other substrate except cellulose. Unfortunately mass chromatograms obtained showed presence of the analyte at locations it was not expected, indicating evidence of analyte spreading, presumably by matrix application. The mass chromatogram presented in Figure 2.18 demonstrates that while analyte intensities were greatest at the original treatment location, the analyte was also evident at areas on the membrane outside the expected region corresponding to the confined treatment area. The results obtained indicate that if analyte spreading could be avoided, carbon conductive membranes may prove to be useful tissue blotting substrates for imaging MALDI-MS.

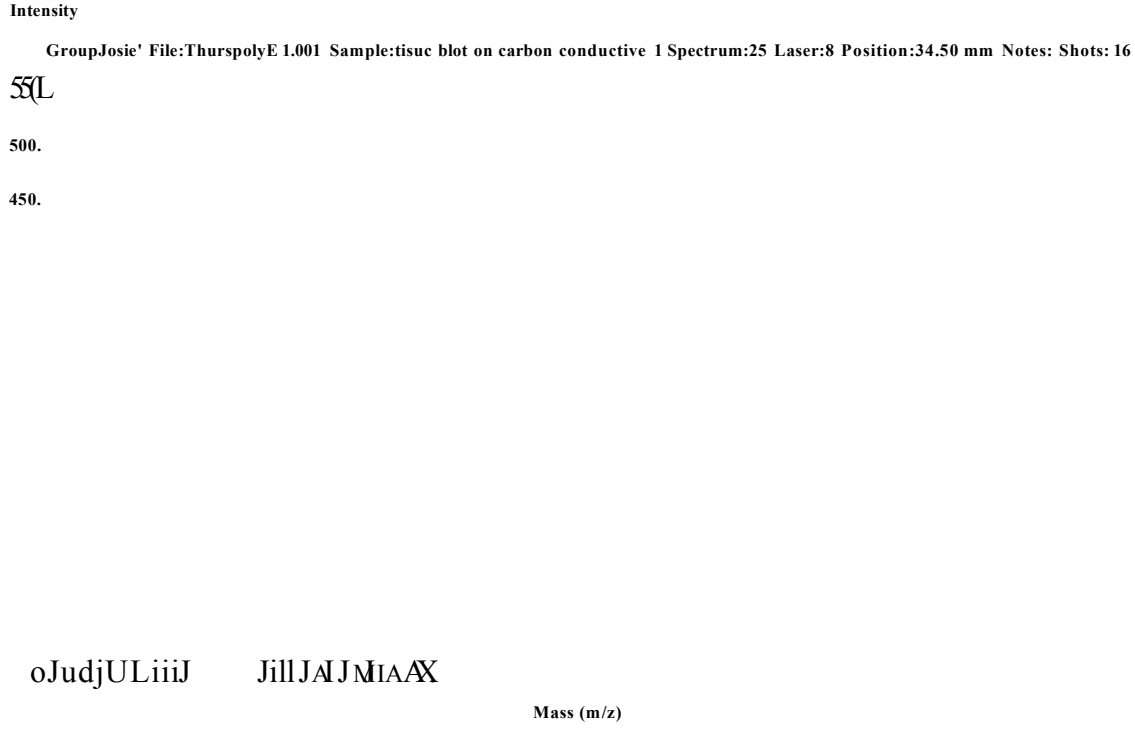

Figure 2.17: MALDI mass spectrum of a ketoconazole-treated tissue imprint on a carbon membrane. The analyte is detected at m/z 532 with a relative ion intensity of 170. The most abundant matrix-associated peak was observed at m/z 212: [Matrix+Na]+. The sample was coated in a-CHCA by electrospray deposition.

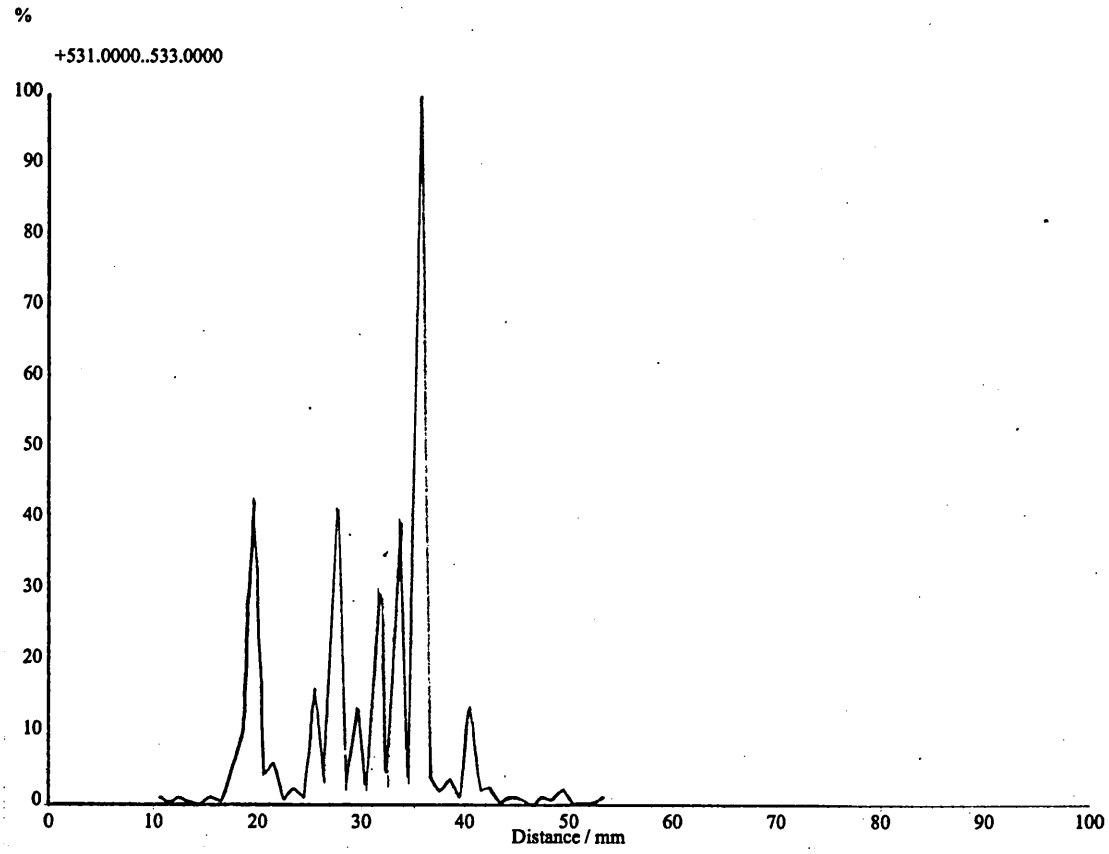

Figure 2.18: Summed ion chromatogram (from m/z 531–533) from a confined tissue treatment tissue blotting experiment. The tissue was treated with ketoconazole and blotted onto a carbon membrane. The membrane was coated with α-CHCA by electrospray. The original treatment area corresponded to 34-39 mm.

2.3.3 Assessment of matrix coverage

It is suggested here that there are two major factors that influence whether or not blotting onto a substrate is likely to be successful for the analysis of drugs in tissue by MALDI-TOF-MS: first, the efficiency of the blotting procedure itself, and the quality of the tissue imprint achieved and second, the ability to coat the sample with an even layer of matrix.

The matrix coverage is thought to have been at least partially responsible for the poor results observed with direct tissue analysis, and with analysis of C18 beads, nitrocellulose and PVDF membranes. As previously described, analysis of C18 beads was also problematic because of the feasibility of the actual blotting procedure, and the C18 Envidiscs were rejected as they were too thick.

Some spectra obtained from the PVDF and nitrocellulose experiments indicate that these were ideal blotting substrates, but the fact that these spectra were not acquired at all points along the target, and the chromatograms were often non-conclusive indicated that poor matrix coverage was achieved. Conversely results obtained from the carbon conductive membranes indicate that a relatively homogeneous matrix layer was deposited on the substrate, but that application of the matrix appeared to induce analyte spreading. Mass spectra and chromatograms obtained from analysis of tissue-imprinted cellulose membranes indicated that a sufficient and homogeneous layer of matrix was created upon the substrate, and that this did not induce analyte spreading.

In order to evaluate whether or not matrix coverage was truly the reason for success or failure of these experiments, matrix-covered membranes were examined by scanning electron microscopy. Images at a range of magnifications 200–6000× were obtained for the C18 Envidiscs, PVDF, nitrocellulose, and carbon conductive membranes. Images at 500× (Figures 2.19, 2.20, 2.21, 2.23 and 2.22) and 3000× (Figures 2.24, 2.25, 2.26, 2.28 and 2.27) magnifications are presented for these five membranes. The most abundant and superior matrix crystals were observed on the carbon conductive (Figure 2.23 and 2.28 and cellulose membranes (Figure 2.22 and 2.27. The C18 Envidisc surface morphology was very different to the other substrates and, as could be seen by eye, the surface appeared to be 'cracked'. Matrix crystals observed were sparse (Figure 2.19) and 2.24). The nitrocellulose (Figure 2.21) and

2.26)and PVDF membranes (Figure 2.20 and 2.25) appeared to be very similar. In both cases, areas of small and abundant crystals were observed, and there were also areas where no matrix crystals were seen. The SEM images indicate that the matrix coverage was the predominant factor in the quality of mass spectra and summed ion intensities acquired.

Figure 2.19: SEM images of Envidisc membrane coated with 15mg-ml 1 a-CHCA by electrospray deposition. Image acquired at 500 x magnification.

The presence or absence of a homogeneous matrix layer on the substrates may be attributed to a number of different factors. The poor matrix coverage observed with the PVDF and nitrocellulose membranes is believed to be due to the substrate's waxy surface nature. This resulted in the matrix drying in 'beads' or droplets, and not as a uniform layer. The success of the cellulose membranes may also be attributed to the polarity of the sample surface, and the drying 'pattern' of the matrix. The membranes were similar to a piece of filter paper, and appeared highly

Figure 2.20: SEM images of pvdf membrane coated with 15mg-ml 1 a-CHCA by electrospray deposition. Image acquired at 500 x magnification.

Figure 2.21: SEM images of nitrocellulose membrane coated with 15mg-ml 1 *a*-CHCA by electrospray deposition. Image acquired at 500 x magnification.

Figure 2.22: SEM images of cellulose membrane coated with 15 mg-ml 1 a-CHCA by electrospray deposition. Image acquired at 500 x magnification.

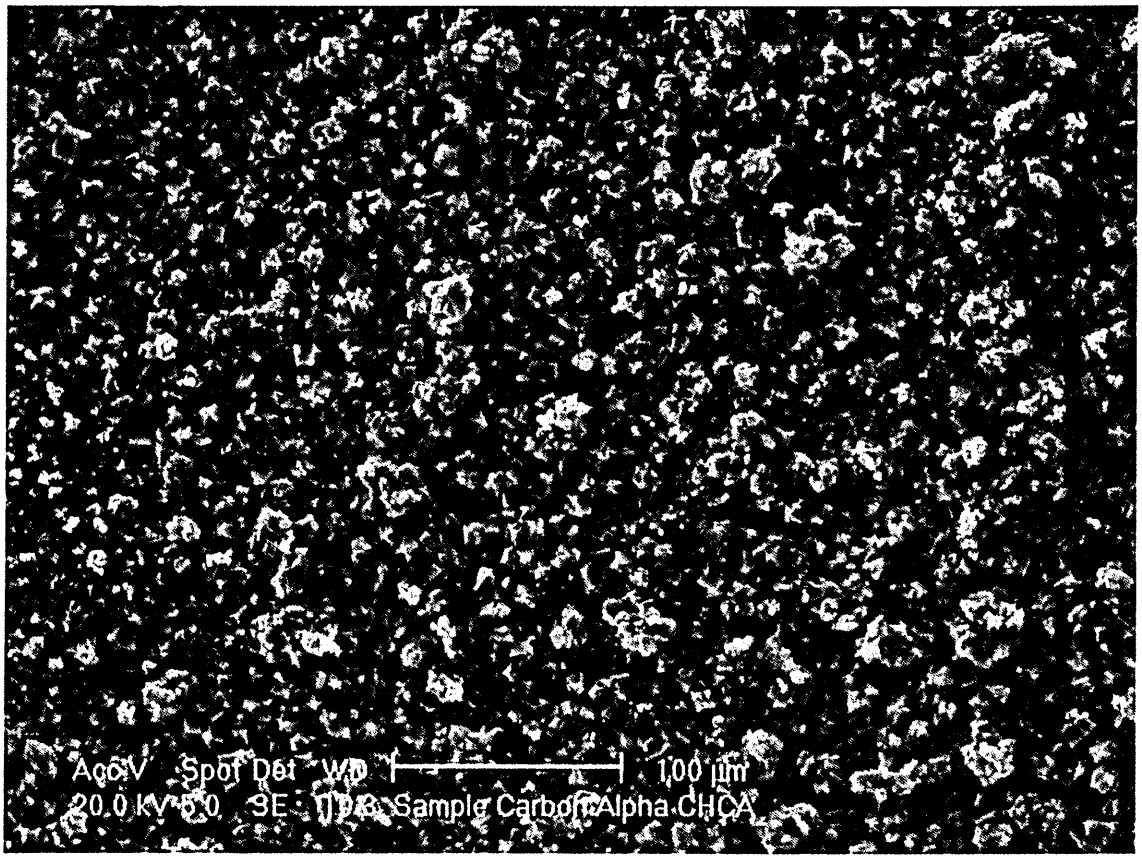

Figure 2.23: SEM images of carbon membrane coated with 15 mg·ml^{-1} α-CHCA by electrospray deposition. Image acquired at 500× magnification.

Figure 2.24: SEM images of Envidisc membrane coated with 15mg-ml 1 a-CHCA by electrospray deposition. Image acquired at 3000 x magnification.

Figure 2.25: SEM images of pvdf membrane coated with 15mg-ml 1 a-CHCA by electrospray deposition. Image acquired at 3000 x magnification.

Figure 2.26: SEM images of nitrocellulose membrane coated with 15mg-ml 1 *a*-CHCA by electrospray deposition. Image acquired at 3000 x magnification.

Figure 2.27: SEM images of cellulose membrane coated with 15mg-ml 1 a-CHCA by electrospray deposition. Image acquired at 3000 x magnification.

Figure 2.28: SEM images of carbon membrane coated with 15mg-ml 1 a-CHCA by electrospray deposition. Image acquired at 3000 x magnification.

absorbent. This may be the reason for the superior matrix layer observed using this membrane.

Another possible factor that may dictate whether or not matrix deposition by electrospray results in an even layer upon the membranes could be the conductive nature of the substrate. The principle of electrospray is that there is an applied potential between the end of the capillary needle and the grounded metal plate (upon which the sample is placed). If the sample is conductive (e.g., the carbon membrane) it will effectively become analogous to the sample plate, and the applied potential between needle and plate is maintained. If however the sample is non-conductive, this is not achieved and may perhaps result in charging, larger droplet formation, or a total cessation of matrix spraying. It is proposed here that a combination of the electrical conductivity and polar nature of the blotting substrates dictates whether or not a membrane is likely to be appropriate for use in this application, in terms of the ability to achieve a uniform layer of matrix upon the sample.

2.4 Conclusions

Preliminary investigations to select a test compound found both aciclovir and piroxicam to be unsuitable, because of the presence of interfering peaks in the spectral region of interest from the matrix (aciclovir), or compounds present in either the tissue or tape (piroxicam). Similar problems were encountered by Reyzer *et al.* [100], who were unable to differentiate between a pharmaceutical analyte and matrix clusters or endogenous biomolecules using conventional MALDI-TOF-MS technology. They overcame this by use of selected ion monitoring using MALDI-Qq-TOF-MS. This was not possible using the linear TOF instrument employed in this chapter. As a similar hybrid q-TOF instrument was used for the work described in the subsequent chapters of this thesis, and because (a) unambiguous determination of the protonated molecule of ketoconazole was achieved by MALDI-TOF-MS, and (b) a topical formulation of the drug is commercially available, ketoconazole was chosen for all subsequent work. However it should be noted that problems encountered with aciclovir and piroxicam could well be overcome by analysis with a hybrid qTOF instrument, partly because of its superior mass accuracy and resolution, and because

if interference continues, tandem mass spectrometry could be employed to map the analyte.

In some of the spectra presented in this chapter, there appears to be an apparent 'shift' in the expected masses for analyte and matrix ions e.g., ketoconazole was detected at m/z 530 and not at m/z 531. This is thought to be partially due to the poor mass accuracy and resolution of the linear TOF analyser. In addition, it is likely that none of the tissue samples or substrates were entirely 'even'. This will have resulted in erroneous mass values as mass analysis is based on flight times, and if the flight distances are different, the masses will appear distorted. This may be entirely overcome with the use of an orthogonal ion source, as discussed and evaluated in Chapter 3.

Uneven sample surfaces also lead to changes in the efficiency of the electrospray deposition: at different points along the surface the capillary needle will be at different distances from the sample surface. Thus the formation of crystals across the sample is likely to be different at different points. This has obvious implications in imaging experiments, where matrix layer homogeneity is key to the success of the technique.

As previously discussed, direct analysis of tissues was not reproducible and spectra and chromatograms show that this may have been attributed to poor matrix formation and coverage. Recent reports [100, 113, 168] demonstrate that crystal formation directly on a tissue sample is more readily achieved using sinapinic acid. This matrix has been found to be far more tolerant of salt content, which is likely to be the major factor in poor crystallisation of α-CHCA on tissue samples. Zhao *et al.* [168] compared the crystallisation of α-CHCA and sinapinc acid on tissue samples, and found sinapinic acid to be the matrix of choice for such investigations. However it was also commented that this matrix is far more suitable for protein analysis than for determination of small molecules, such as pharmaceutical compounds. The use of sinapinic acid for the direct examination of skin samples by MALDI-TOF-MS is investigated in Chapter 4.

Analysis of C18 Envidiscs was not possible due to the thickness of the substrates. Analysis of C18 beads was considered to be inferior to direct analysis of tissue sections, and provided the poorest results of all the tested substrates. This differs from the findings of Caprioli *et al.* [102], who reported success with this technique

and concluded that it was superior to direct tissue analysis and analysis of cellulose-imprinted membranes. However, their work concerned determination of peptides and proteins, and not drugs.

Mass spectra were acquired demonstrating that both the PVDF and nitrocellulose membranes were in fact good blotting substrates, though not for this application. Impressive ion intensities were observed, but due to the problems encountered with uniform matrix deposition, they failed to provide useful information about the spatial distribution of the analyte. This is of course key to the success of this technique. Both of these substrates have proved to be extremely useful in standard protein analysis, presumably where the degree of matrix homogeneity over a relatively large area is not essential.

Impressive spectral results were obtained using the polyethylene-filled carbon conductive membranes. This concurs with the findings of Caprioli's group that this substrate produced "unique protein profiles" [103]. For the analysis of ketoconazole, however, matrix application onto such membranes induced analyte spreading. This membrane was selected for peptide analysis by Caprioli *et al.* because of its electrostatic and protein adhesion properties. In their experiments, the peptide and protein analytes are likely to have been anchored to the substrate, and so matrix application by electrospray did not result in a loss of the expected spatial distribution. Unfortunately, the membrane appeared to have no binding specificity for ketoconazole. Results presented in this chapter demonstrate good spectral results, and SEM images indicate good formation and coverage of matrix crystals, but chromatograms show a lack of spatial information. This is believed to be due to analyte spreading by matrix application.

Cellulose membranes were found to be the best blotting substrate for the analysis of drugs in skin by MALDI-TOF-MS. This also differs from Caprioli's findings that this substrate was inferior to both analysis of tissue-imprinted C18 beads and direct tissue analysis [102]. This is unsuprising, however, as proteins and drugs are likely to behave differently. For the analysis of ketoconazole, spectra and chromatograms were obtained demonstrating the expected distribution of the analyte. Mass spectra reveal good analyte intensities and detection of the analyte only in areas it was expected. SEM images reveal excellent matrix crystal formation and coverage. Electrospray matrix deposition onto this substrate did not appear to induce analyte

spreading. It is proposed that the absorbant nature of this substrate resulted in the membrane being fully impregnated with matrix following the electrospraying procedure. Thus the matrix material was not left to run freely across the membrane surfaces until it dried, as was observed with the nitrocellulose, PVDF and carbon membranes. This is thought to have reduced analyte spreading.

The SEM images collated indicate that matrix coverage was the predominant factor in whether or not a substrate lent itself to this application. Mass spectrometric imaging is used in Chapter 4 to investigate matrix application for direct tissue analysis, and the use of cellulose and carbon membranes for the analysis of drugs in skin. No other substrates were investigated further.

Chapter 3

Imaging Tissue Imprints by MALDI-Q-TOF-MS

3.1 Introduction

The tissue blotting experiments showed that analysis of tissue imprints on cellulose membranes by MALDI-TOF-MS was capable of both detecting, and spatially resolving the test analyte, ketoconazole, in epidermal tissue. While these results were extremely promising, the instrument capabilities did not permit analysis of a larger area of membrane, or of obtaining information that could be considered 'biologically useful' in terms of drug mapping. Recent work by Caprioli and co-workers [100,102,103,113] has demonstrated that imaging of proteins, peptides and drugs in tissue could be achieved using a quadrupole time-of-flight instrument.

Such a hybrid instrument offers the capabilities of obtaining mass spectra from a range of x and y co-ordinates over a larger rectangular area, by moving the sample plate under the laser.

Furthermore, the hybrid instrumentation offers superior mass accuracy, resolution and sensitivity compared with conventional TOF analysis. Additional advantages are offered by an orthogonal ion source arrangement. It was observed in the data presented in Chapter 2 that mass values were distorted. This was partially attributed to the inherent mass accuracy, limitations of the linear mass analyser, and also to the sample topography of the tissue and membrane sections. As described in Chapter 2, irregularities of the sample surface may have resulted in erroneous mass determination.

This is a common problem with conventional linear MALDI-TOF arrangements, which are based on what is referred to as an 'axial' design. This axial geometry necessitates that the MALDI source is coupled by a direct flight path to the TOF mass analyser. In doing this, any variations associated with the ionisation of the sample and/or the sample surface are carried out to the detector. Deviations in sample topography which shift the relative position of the plate to the detector result in an effective shift of flight time, which in turn will be manifested as a mass shift. Despite the use of delayed extraction in the work described in Chapter 2, peak broadening was still evident. This is partly due to the wide energy distribution of the initial ion packet. Another limitation of axial systems is the fact that a large number of ions are produced per pulse and all must be measured because the detector is in-line with the target. Thus analog detection must be used. This requires careful matching of the detector gain to the laser fluence to avoid saturating the analog-to-digital converter on intense peaks, and to avoid detector shadowing problems produced by intense low-mass signals.

In an orthogonal arrangement, the MALDI source is decoupled from the TOF, which eliminates any effects associated with ionisation or sample topography. The relative position of the pulser to the detector is always constant, regardless of sample surface irregularities. This provides higher mass accuracy and stability, and better resolution over a wider mass range. Figure 3.1 illustrates the advantages of an orthogonal arrangement compared to the previously used axial geometry for surface analysis by MALDI-TOF-MS.

A hybrid quadrupole time-of-flight instrument fitted with an orthogonal MALDI ion source (Qstar pulsar i, Applied Biosystems, Foster City, US) and beta-test ion imaging software (MDS Sciex, Ontario, Canada) was employed in the work presented in this chapter. Whole membranes were analysed and ion images were created using the test software. The aim of this phase of work was firstly to determine whether or not images could be obtained by use of this instrument and software, and secondly to evaluate improvements in mass resolution and accuracy as compared to conventional MALDI-TOF-MS on a linear instrument. Parameters such as matrix coverage that had proved essential to success of earlier experiments were also investigated. The laser spot size of this instrument was also evaluated.

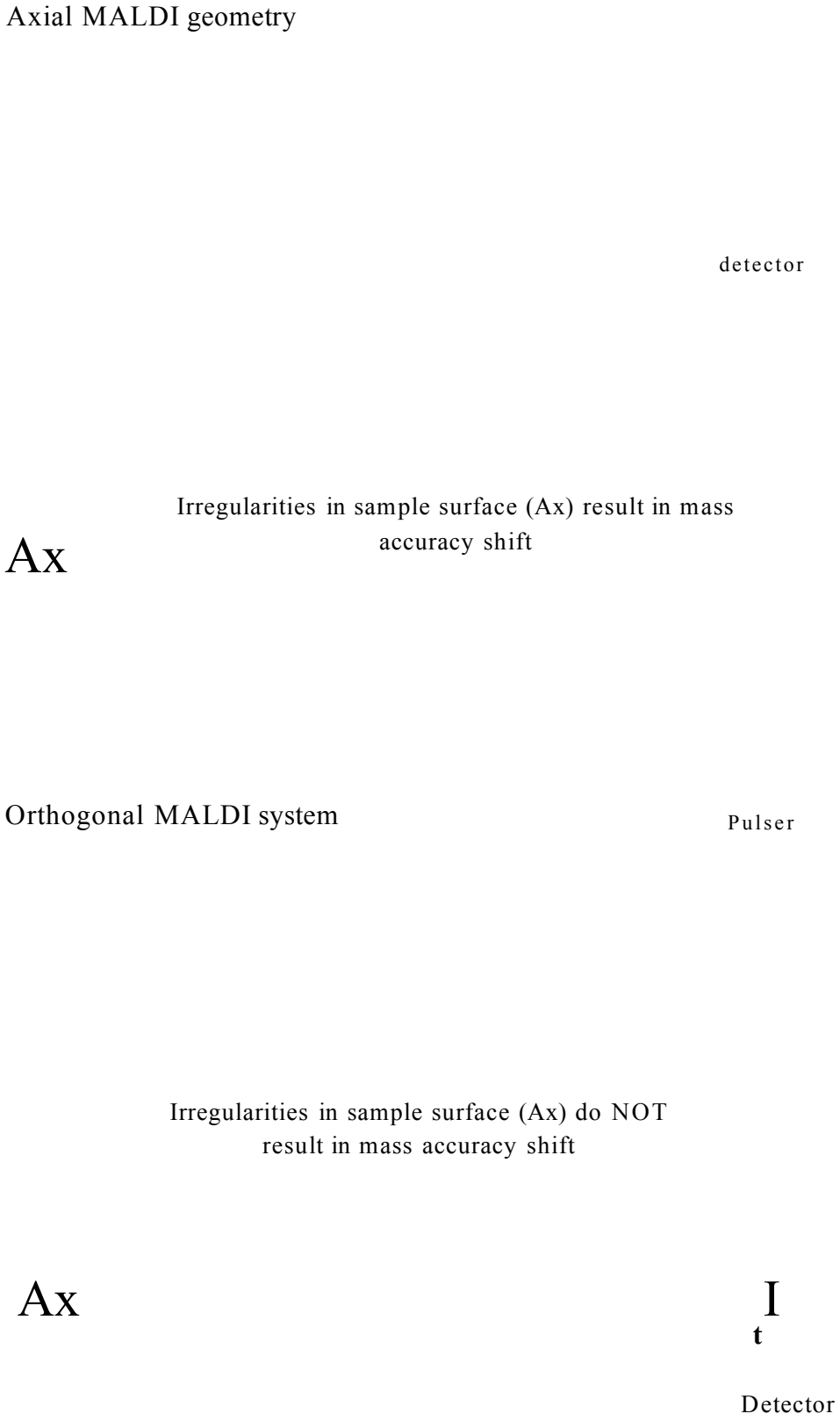

Figure 3.1: Use of an orthogonal MALDI ion source eliminates mass shifts that arise from irregular sample surfaces.

3.2 Experimental

3.2.1 Materials

Trifluoroacetic acid (AR grade) and α-CHCA were purchased from Sigma-Aldrich (Dorset, UK). Methanol was HPLC grade, purchased from Fisher Scientific (Loughborough, UK). Cellulose membrane spacers (as previously) were obtained from Goodfellow (Huntingdon, UK). Porcine ears were obtained from Doncaster abbatoir. Nizoral shampoo (2% ketoconazole) was obtained commercially.

3.2.2 Instrumentation

The electrospray deposition device developed at Sheffield Hallam University (as previously described in Chapter 2) was employed in these experiments. Mass spectrometric analysis was performed on an Applied Biosystems Qstar pulsar *i* hybrid quadropole time of flight mass spectrometer, fitted with an orthogonal MALDI source and beta test ion imaging software. A schematic of the Qstar pulsar i is shown in Figure 3.2

3.2.3 Methods

Porcine ear epidermal tissue was covered with $50\,\mu$l Nizoral shampoo (2% ketoconazole) and incubated at 37^0C for one hour. The tissue surface was rinsed in deionsised water to ensure removal of excess drug formulation on the skin surface. The tissue was then blotted onto a cellulose membrane. The membrane was fixed onto an aluminium backed TLC plate and coated in α-CHCA ($15\,\mathrm{mg{\cdot}ml^{-1}}$) by electrospray deposition. The sample was then mounted within the square recess of a specialised MALDI membrane target. Standard MALDI analysis and imaging of the membrane was performed on the Q-Star in the positive ion mode.

3.3 Results and discussion

3.3.1 MALDI-Q-TOF analysis of aciclovir and piroxicam

It was concluded in Chapter 2 that limitations in mass accuracy and resolution associated with the linear TOF instrument resulted in the unsuccessful determination of

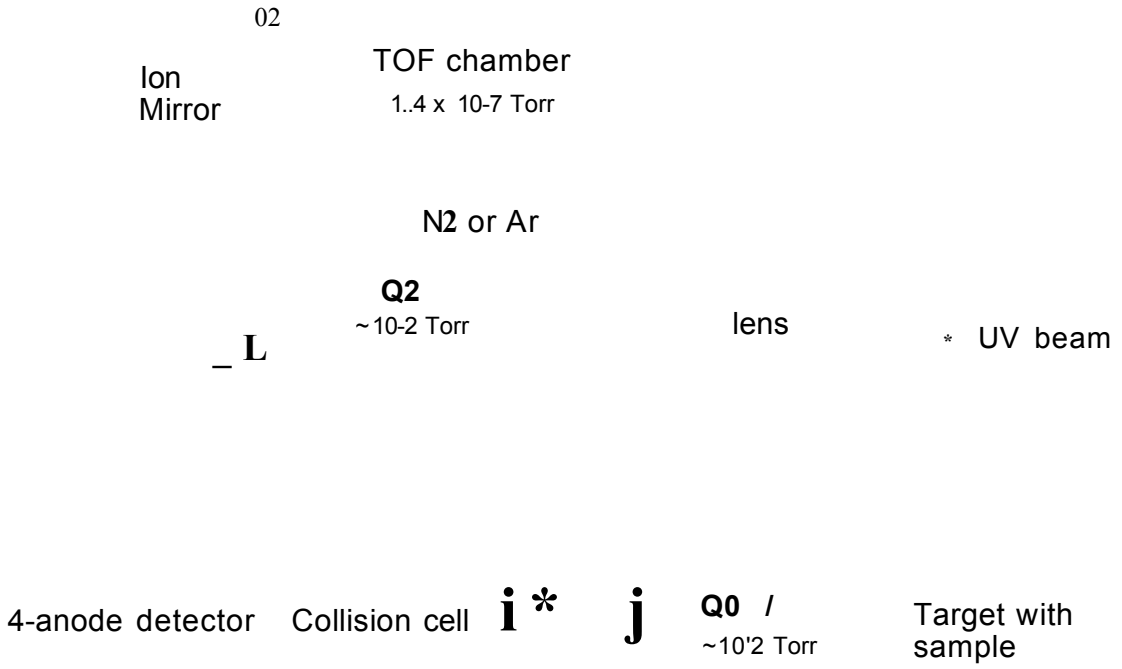

Figure 3.2: Schematic diagram of the hybrid quadrupole-time of flight mass spectrometer (Qstar pulsar i), fitted with an orthogonal MALDI ion source, as used in these investigations. Reprinted with kind permission from the oMALDI Server Users Manual, MDS Sciex, 2003.

acyclovir and piroxicam by MALDI-MS. Interfering peaks were observed in the spectral region of interest from the matrix (acyclovir) and endogenous/tape/instrument species (piroxicam). It was postulated that the superior mass resolution and accuracy of the hybrid QTOF instrument, together with the orthogonal ion source arrangement might permit successful MALDI-MS determination of these drugs. The following experiments were conducted in order to assess the suitability of this technology for the analysis of these drugs.

Double sided tape was mounted in the recess of a specialised MALDI target. 1 μl of an equal volumetric mixture of 1 mg·ml^{-1} drug and 25mg mg·ml^{-1} α-CHCA was spotted onto the tape. MALDI-Q-TOF analysis was performed on an Applied Biosystems Qstar Pulsar *i* in the positive ion mode.

Figures 3.3 and 3.4 demonstrate that the protonated molecule of acyclovir is clearly resolved from the potassium adduct of α-CHCA. This was not observed on the Linear TOF instrument, as presented in Chapter 2.

Figure 3.5 shows a cluster of peaks around m/z 332. Enlarging the spectral region of interest (Figure 3.6) reveals that the protonated molecule of piroxicam (m/z 332.13) is distinguishable from potentially interfering compounds detected at m/z 332.40, 333.14, and 334.13. All of these compounds are likely to have caused ambiguous determination of the drug molecule using a linear TOF instrument.

It is concluded from these experiments that both acyclovir and piroxicam can be successfully detected by MALDI-Q-TOF analysis. Spectra presented demonstrate the resolution of the protonated drug molecules from previously interfering compounds.

These drugs are not discussed further in this thesis as all subsequent imaging method development was conducted with a topical formulation of ketoconazole (Nizoral shampoo). However, these experiments show the potential of MALDI-MS for the *in situ* analysis of acyclovir and piroxicam, and again illustrate the advantages of the hybrid mass analyser.

Mass determination of ketoconazole by MALDI-Q-TOF MS

It was observed in spectra presented in Chapter 2 that ketoconazole was detected between m/z 530–533. There are three possible theories for these discrepancies in the

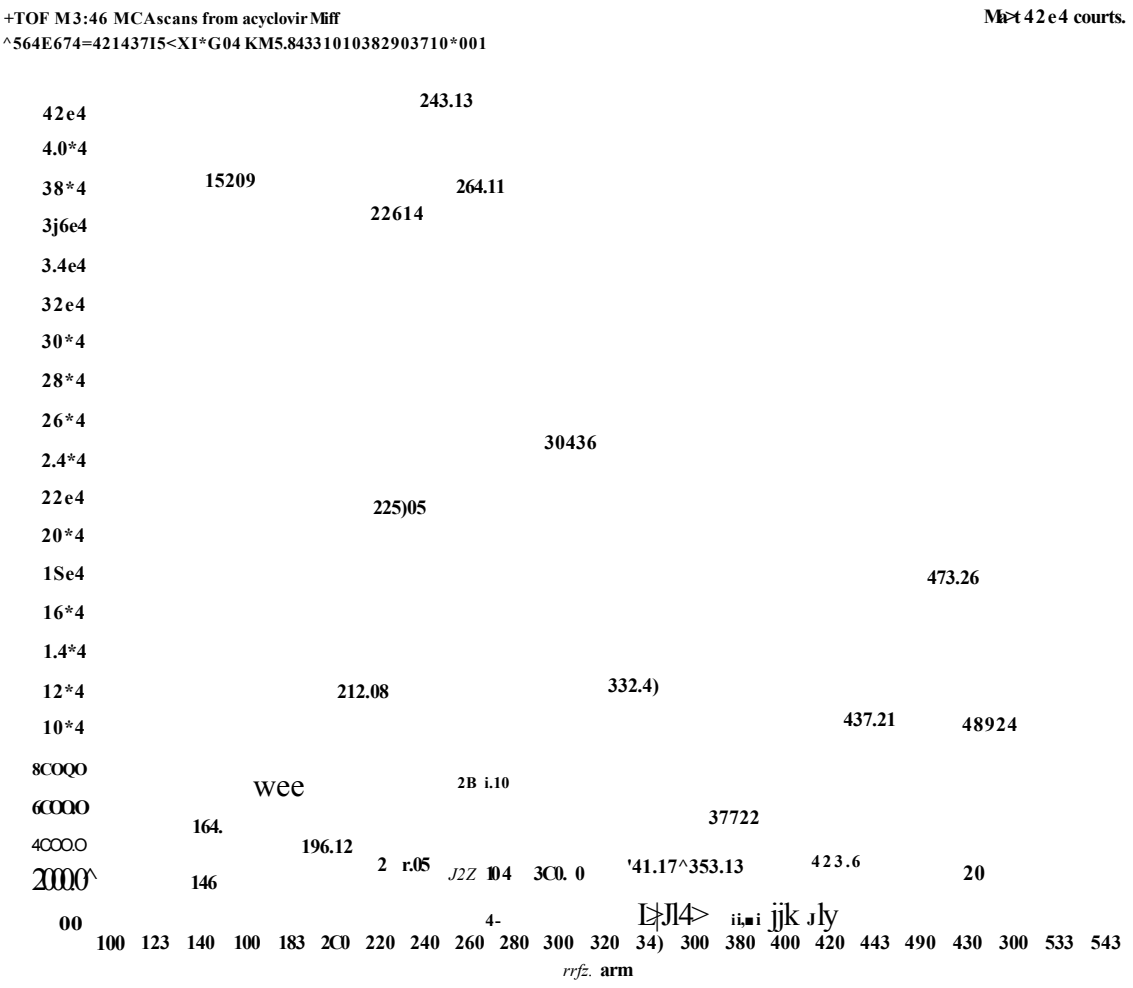

Figure 3.3: MALDI mass spectrum of acyclovir acquired using the Qstar Pulsar *i. a*-CHCA was employed as the matrix material. The protonated drug molecule *(m/z* 226) and the potassium adduct matrix ion *(m/z* 228) are clearly resolved as two separate peaks. Matrix-associated peaks are also observed at *m/z* 172 ([Matrix-H20+HJ+), *m/z* 190 ([Matrix-|-H]+), and *m/z* 228 ([Matrix+K]+).

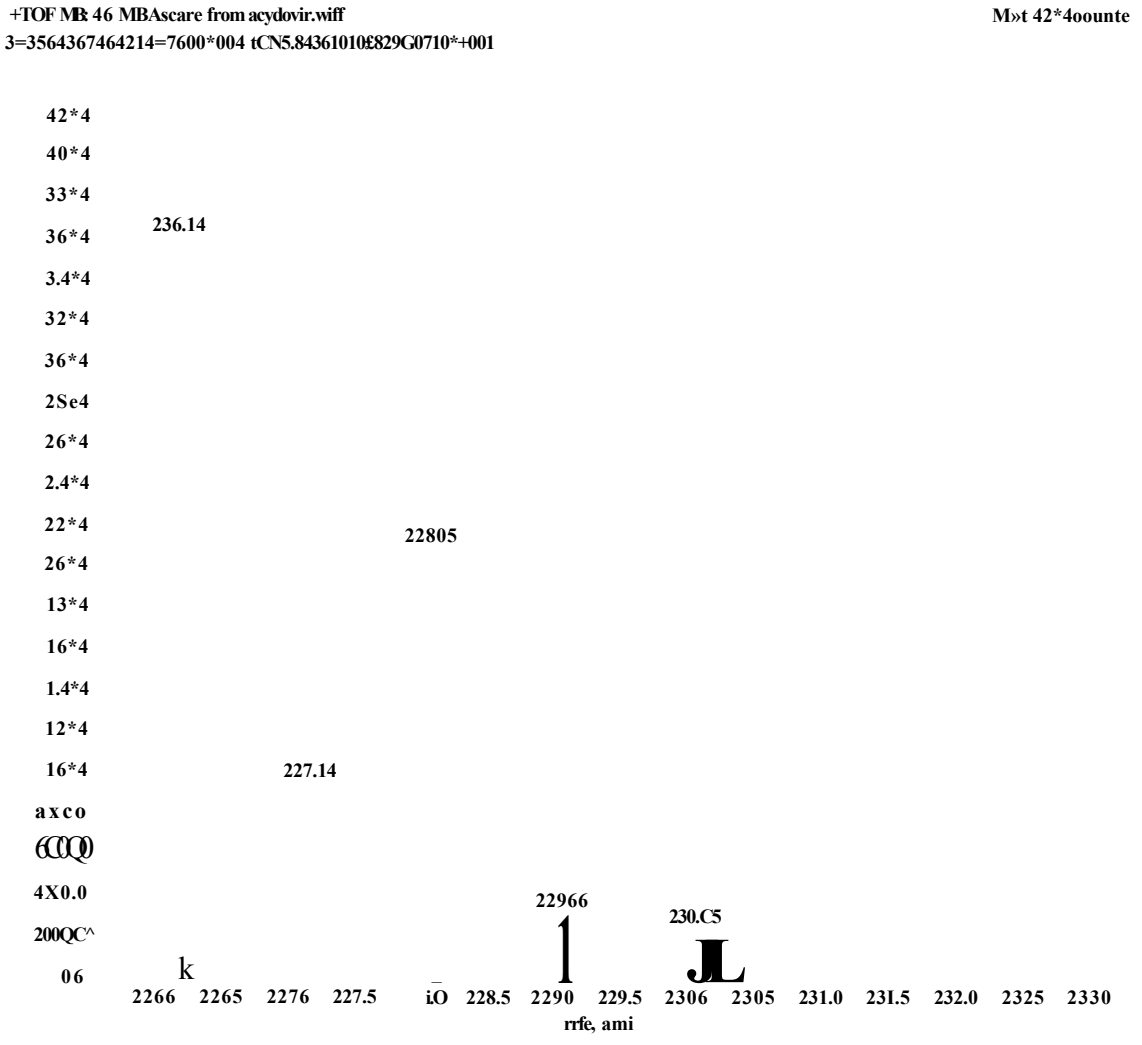

Figure 3.4: MALDI mass spectrum of acyclovir acquired using the Qstar Pulsar *i* a-CHCA was employed as the matrix material. The spectral region of interest *(m/z* 225-230) from Figure 3.3 is enlarged to reveal good resolution of drug and matrix peaks. The protonated drug molecule *(m/z* 226) and the potassium adduct matrix ion *(m/z* 228) are clearly resolved as two separate peaks.

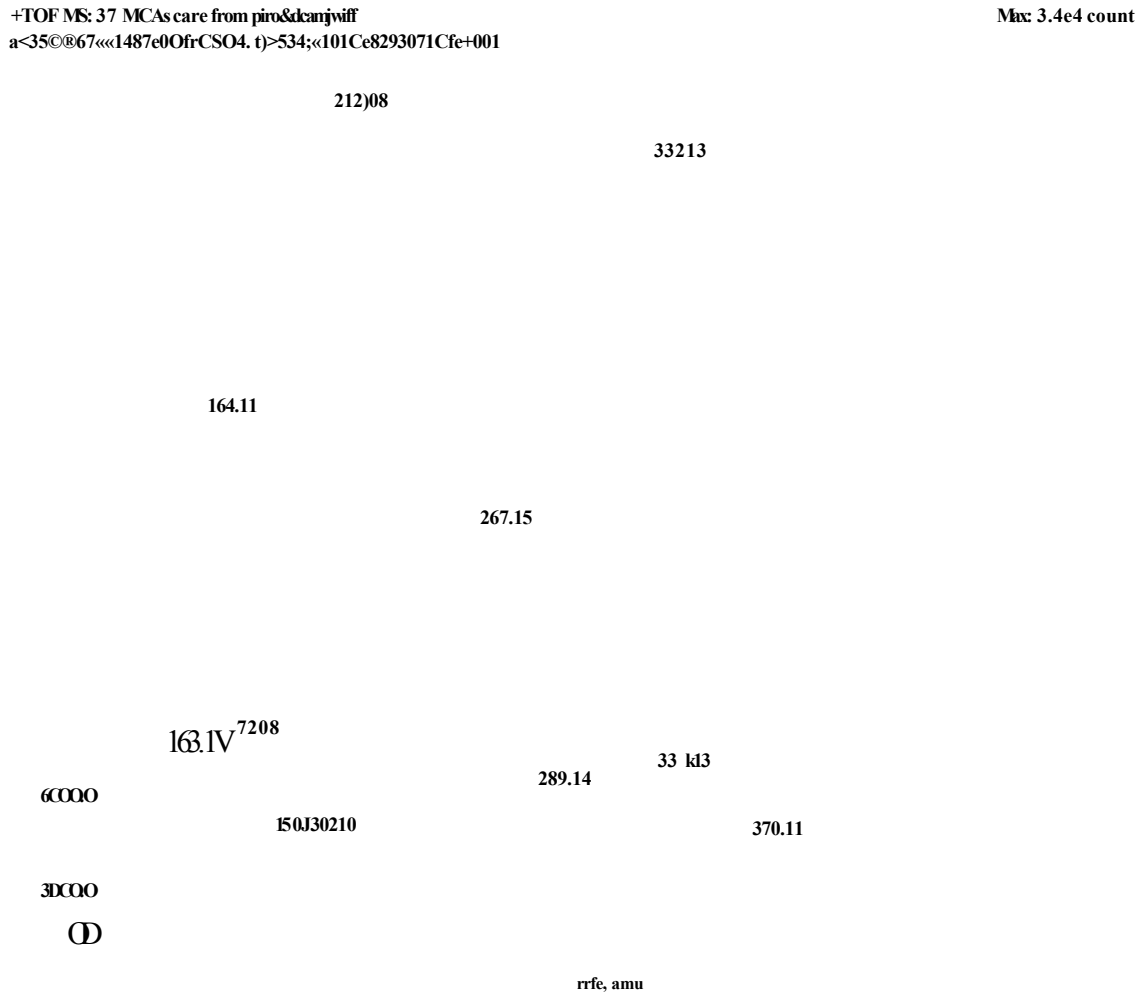

Figure 3.5: MALDI mass spectrum of piroxicam acquired using the Qstar Pulsar *i* o-CHCA was employed as the matrix material. A cluster of peaks with similar *m/z* values is evident around the protonated drug molecule (*m/z* 332). Matrix-associated peaks are observed at *m/z* 172 ([Matrix— *m/z* 190 ([Matrix+H]+), *m/z* 212 ([Matrix+Na]+) and *m/z* 228 ([Matrix+K]+).

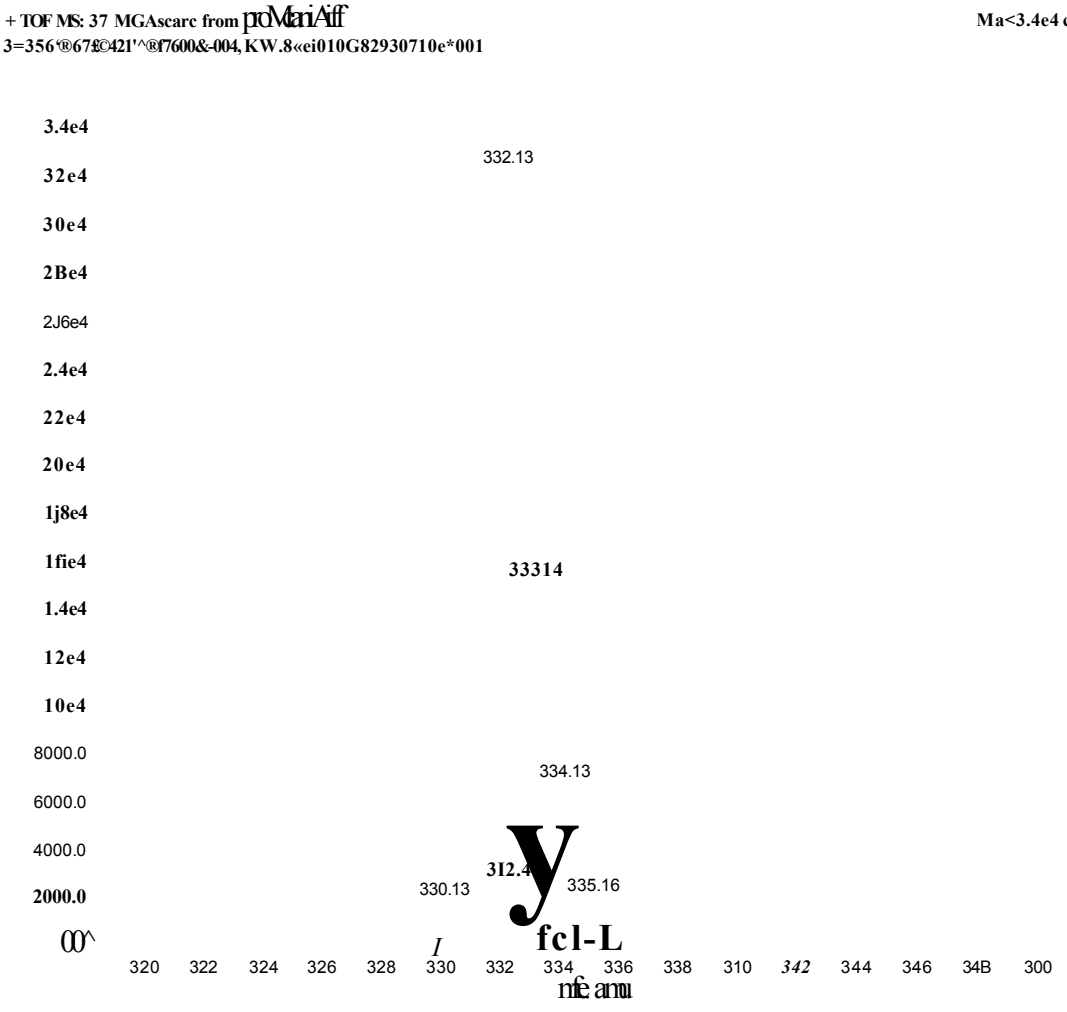

Figure 3.6: MALDI mass spectrum of piroxicam acquired using the Qstar Pulsar *i* a-CHCA was employed as the matrix material. Enlarging the cluster of peaks around *m/z* 332 shown in Figure 3.5 reveals that the protonated drug molecule is successfully resolved from other possibly interfering peaks. This illustrates the benefits of the hybrid mass analysis instrument compared to the linear TOF instrument employed in Chapter 2.

mass value: (1) Surface charging was observed; (2) Sample topography resulted in erroneous mass values; (3) Poor instrument mass accuracy or instrument calibration.

It was predicted that use of an orthogonal MALDI ion source would result in surface charging and sample irregularities having little effect on mass determination, and that QTOF analysis would offer exponential improvements in mass accuracy as compared to analysis with a linear TOF. Thus the mass determination of ketoconazole by oMALDI-Q-TOF MS was evaluated.

The m/z value of the protonated molecule of ketoconazole (m/z 531.1566) at 20 points across a 130 minute imaging run (analysis of a tissue imprinted cellulose membrane) were recorded, as presented in Figure 3.7 . An average error of 1.6 mmu was obtained, and mass values ranged from m/z 531.1529 to m/z 531.1616, demonstrating the superior mass accuracy of the hybrid instrumentation. It is clear that mass accuracy is maintained across the sample surface, thus sample topography has little effect on mass values in an orthogonal MALDI arrangement. In addition the random scatter of mass values indicates that mass measurements are not affected by surface sample charging with this instrument configuration.

These results illustrate the suitability of this instrument for imaging experiments (where a molecule is mapped across a relatively large and irregular area), and show the superior mass accuracy of the instrument as compared to the linear TOF instrument employed in Chapter 2.

MALDI-Q-TOF analysis of membranes

Mass spectra were acquired from a variety of positions on the membrane. Areas corresponding to regions outside the treated tissue imprint showed an absence of interfering peaks in the mass region of interest (Figure 3.8). Mass spectra acquired within the region of the tissue imprint showed detection of the analyte with good ion intensities (Figure 3.9). 'Background' spectra (obtained from a co-ordinate where no drug was present; Figure 3.8) were subtracted from the sample spectra (obtained from a co-ordinate where treated tissue was blotted), (Figure 3.9) and the resulting spectra created (Figure 3.10) could be considered to show drug associated peaks in better detail.

Spectra collected on the Qstar demonstrated significant improvements in terms of both mass resolution and mass accuracy, as expected. It was also noted that the

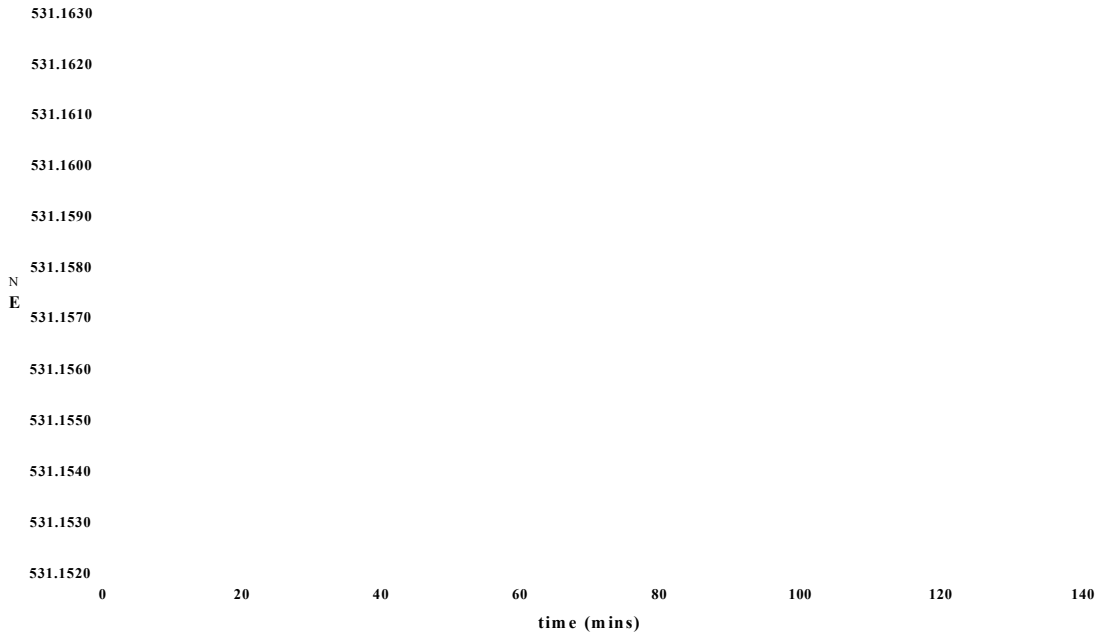

Figure 3.7: Mass measurement of the protonated molecule of ketoconazole at *m/z* 531.1566 across a 130 minute imaging run. Treated tissue was blotted onto a cellulose membrane. An average error of 1.6 mmu was obtained, demonstrating the superior mass accuracy of the hybrid instrumentation. It is clear that mass accuracy is maintained across the sample surface, thus sample topography has little effect on mass values in an orthogonal MALDI arrangement. In addition the random scatter of mass values indicates that mass measurements are not affected by surface sample charging, as is often noted with axial geometry.

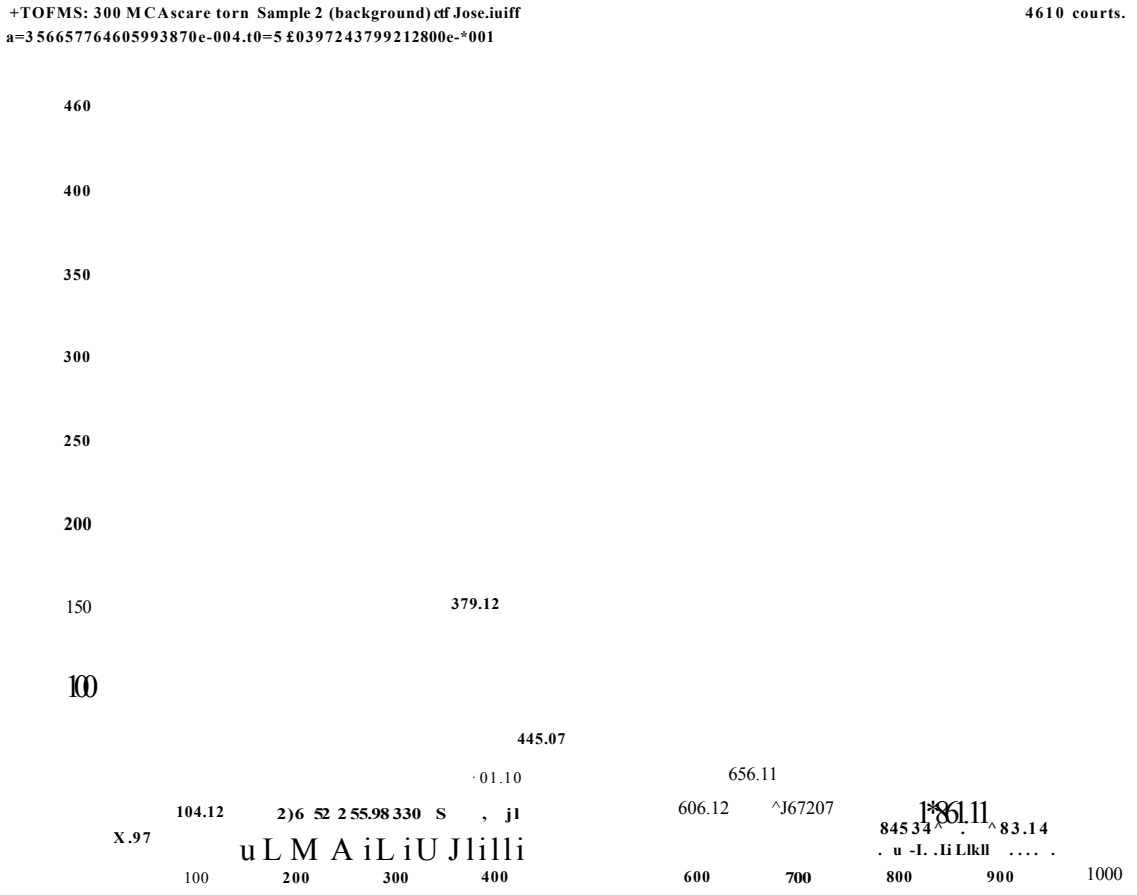

Figure 3.8: MALDI mass spectrum acquired at a position on the membrane where no drug was blotted. No possibly interfering peaks were observed in the region m/z 530-535.

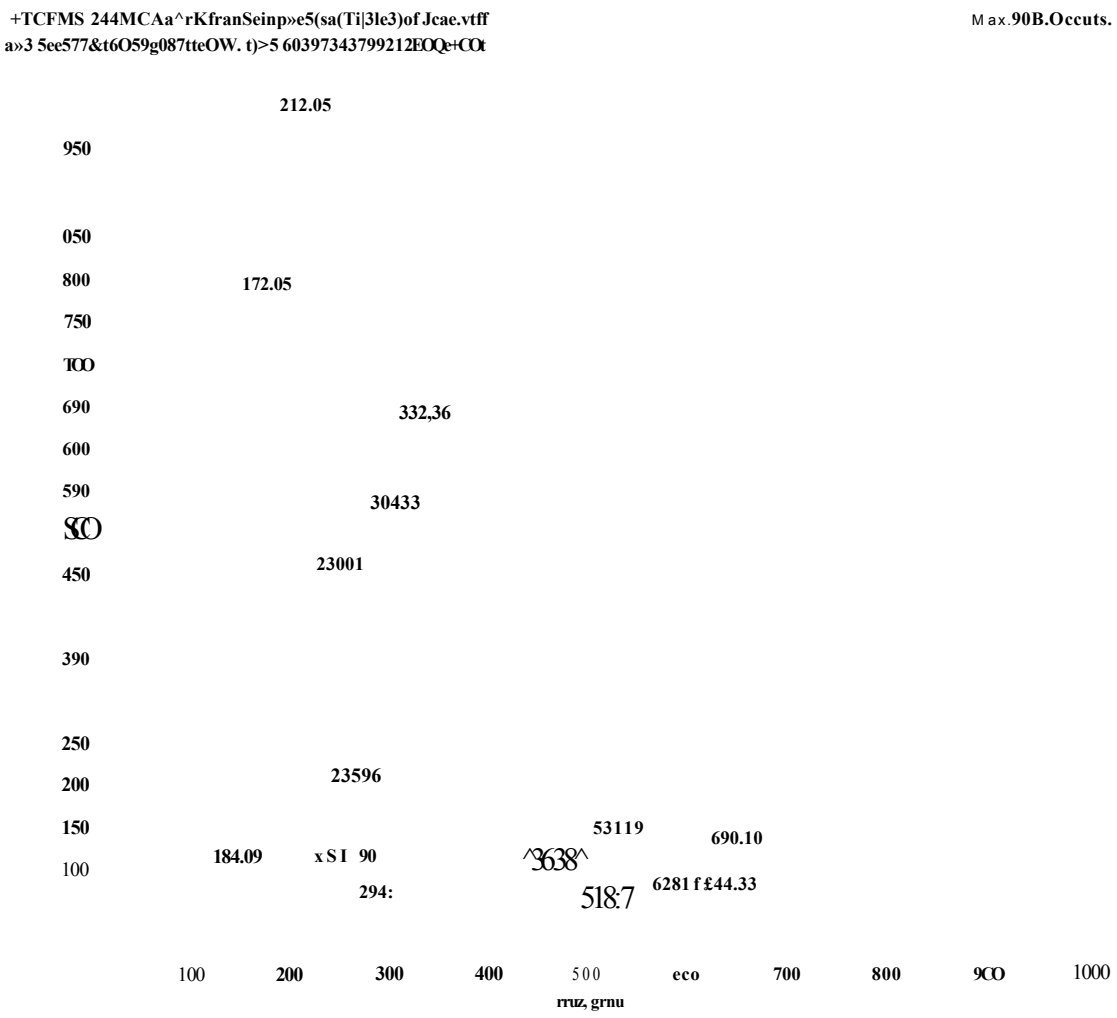

Figure 3.9: MALDI mass spectrum acquired at a position on the membrane where drug treated tissue was blotted. Ketoconazole was detected at m/z 531.19.

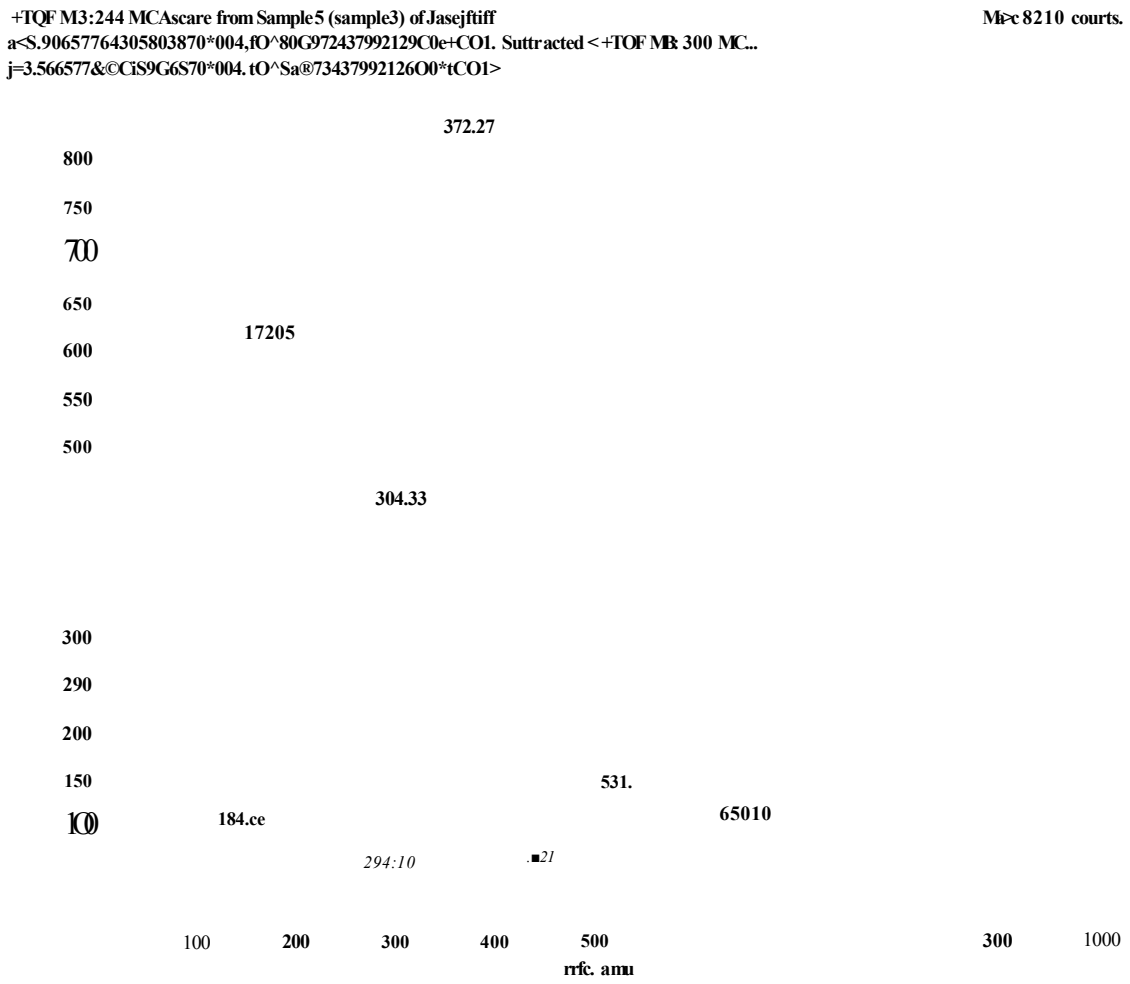

Figure 3.10: The background spectra can be subtracted from the sample spectra to emphasise the presence of the drug.

mass values for detected ions did not fluctuate across the sample surface, illustrating the advantage of the orthogonal arrangement. Improvements in mass resolution are best illustrated by comparison of the isotopic pattern of the protonated ketoconazole molecule as measured by the Linear TOF and the hybrid qTOF (Qstar) instruments, as shown in Figure 3.11.

Imaging the membrane

These preliminary imaging studies were conducted using novel beta test ion imaging software, supplied by MDS Sciex. This software had not been commercially released at the time of this work. The imaging facility is incorporated into the main data acquisition software (oMALDI server), which allows plate positioning and full design of data acquisition methods based on conventional experimental paprameters, such as ion mode, mass range, and laser power etc. oMALDI is designed as a Windows-based platform in order to permit theoretically simple integration of data and spectra into widely-used Microsoft applications. The imaging software permits selection of a rectangular region of interest on the specialised recessed targets, construction of a data acquisition pattern, mass spectral data collection from each location within the defined area, and finally construction of ion images.

The area on the target where the membrane was mounted was imaged by moving the sample stage under the nitrogen laser in the x and y dimensions (optimum results were achieved by firing the laser for 2 seconds at every location, at 25% laser threshold power ($14\,\mu$J)). Mass spectra were acquired at sequential increments over a 'snake like' pattern over the entire two-dimensional area. This created a data set of several thousand mass spectra. Software capabilities enabled ion images to be created by selecting peak mass ranges (e.g., m/z 531-533 for the isotopic envelope of the protonated drug molecule). The distribution, and relative ion intensities were displayed as two dimensional pixel images, with the colour of each pixel representing the intensity of ions at that location, thereby creating an xyz plot of location vs. intensity of the selected ion/ions.

Unfortunately, it proved impossible to manipulate directly the processed images with this version of the software. Although images were successfully generated, they could only be saved as a file type (.wiff) that was unreadable by other software applications. Furthemore, the graphical capabilities of the software did not permit

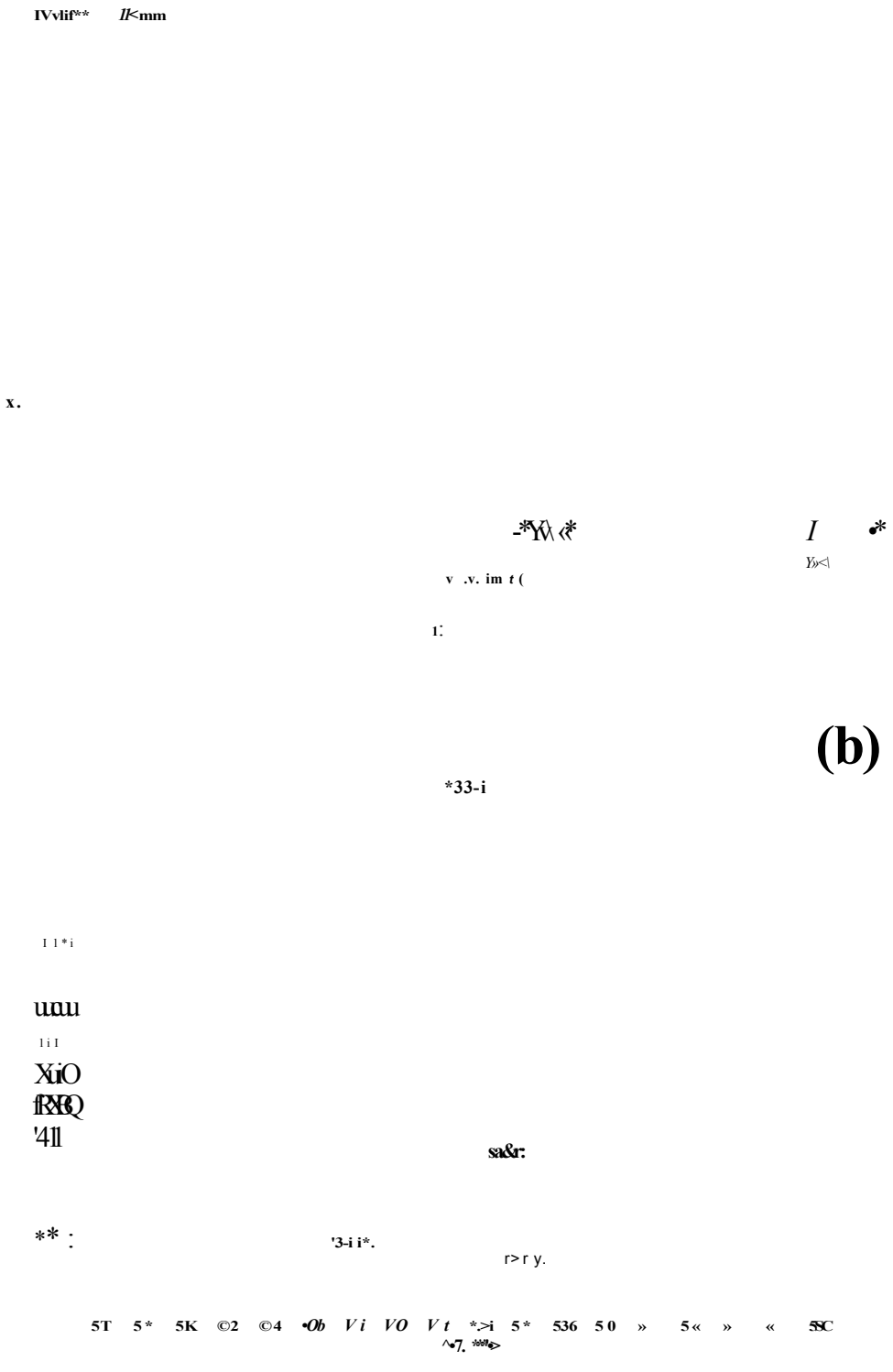

Figure 3.11: Mass spectra demonstrating the chlorine isotope pattern of ketoconazole acquired with (a) an SAI LinearTOF 1500, and (b) an Applied Biosystems Qstar pulsar*. This highlights the superior mass resolution of the Q-TOF mass spectrometer.

manipulation of the image. Thus in order to manipulate and present the images, they had to be generated by alternative software.

The mass spectrometric data acquired during an imaging run yields a total ion chromatogram (TIC) file of all ions detected at all locations. Information about relative ions intensities for selected mass ranges can be extracted from this 'master' data file, generating a table of ion intensity for the selected ion/ions at each spot acquired, i.e., a list of spot numbers and corresponding ion intensities. Calculation of the xy co-ordinate (relative position on the sample plate or membrane) of every 'spot number' would therefore enable images to be created in alternative graphics software.

Knowledge of the image search pattern, e.g., a "snake" rastering pattern, the start and end points as xy co-ordinates, and the increment size (vertical and horizontal spacing) can be obtained from the original data file.

An algorithm was therefore developed to convert spot number to an xy co-ordinate in the original area of interest, based the parameters described above. The mathematical reasoning is as follows:

Knowledge of the start and end co-ordinates of the imaging run gives information of the minimum and maximum x and y values, this enables calculation of the image area (Figure 3.12).

In all cases in this thesis the image search pattern (pattern of data acquisuition) was set as demonstrated in Figure 3.13. In this illustration z denotes the increment size (the degree of vertical and horizontal spacing between spots). This parameter is set by the user, and is thus known for all images.

Understanding of the image area (Figure 3.12) and increment size (Figure 3.13) permits simple calculation of both the number of spots in a row (x_{diff}), and the number of rows in the area (y_{diff}):

$$x_{diff} = (x_{max} - x_{min})/z \text{ =number of spots in a row.}$$

$$y_{diff} = (y_{max} - y_{min})/z \text{ =number of rows in the image area.}$$

The algorithm then calculates the xy co-ordinates for spots in the grid area in a mathematical loop until the co-ordinates of every spot have been generated (Algorithm 1).

An online resource was created (http://www.pugwash-uk.co.uk/spotcalc.php) to perform this calculation.

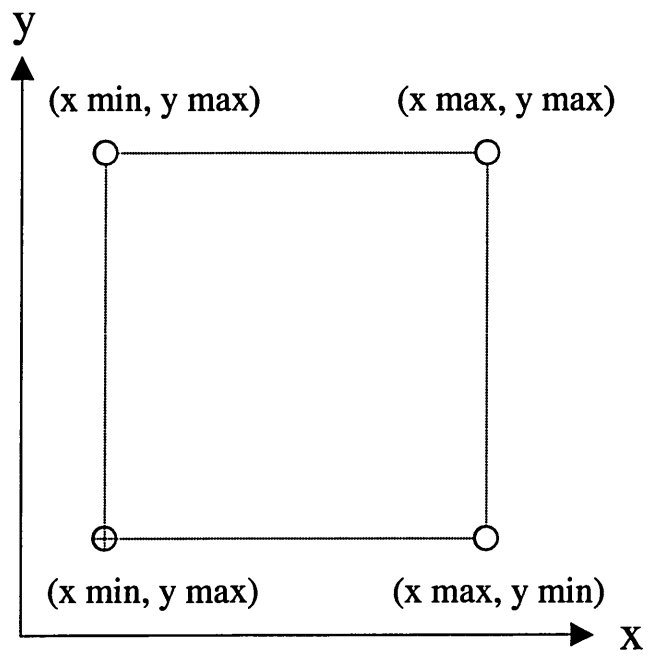

Figure 3.12: The start and end co-ordinates of an imaging run provide detail about the minimum and maximum x and y values of the area, thus defining the image area.

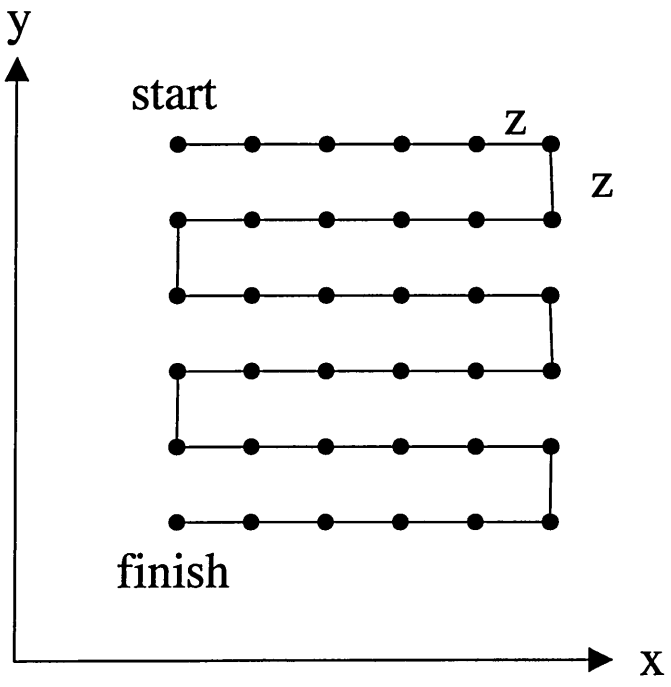

Figure 3.13: The image data acquisition search pattern, as defined within the imaging software application.

Algorithm 1: An algorithm to compute the xy co-ordinates of spots in the image area

given: x_{max}, x_{min}, y_{max}, y_{min}, z
$x_{diff} \leftarrow (x_{max} - x_{min})/z$
$y_{diff} \leftarrow (y_{max} - y_{min})/z$
$y \leftarrow y_{max}$
for $i \leftarrow 0; i \leq x_{diff}; i++$ **do**
  if $(i \bmod 2) == 0$ **then**
    $x \leftarrow x_{min}$
  else
    $x \leftarrow x_{max}$
  end if
  for $j \leftarrow 0; j \leq x_{diff}; j++$ **do**
    print x, y
    if $(i \bmod 2) == 0$ **then**
      $x \leftarrow x + z$
    else
      $x \leftarrow x - z$
    end if
  end for
  $y \leftarrow y - z$
end for

These *xy* values, plotted against the ion intensity *(z)* (extracted from the original .wiff file) for each spot number, may then be used to generate an image. The images presented here have been produced using a charting and graphing software package for Apple Macintosh, Delta Graph 4.5.

An imaging run was performed over the entire membrane (drug treated tissue imprint) area. The laser was fired for 2 seconds at 25% threshold power at each location. Data was collected for the mass range 0-1000 amu, in the positive ion mode. Horizontal and vertical spacing between spots (increment size, *z)* was set at 0.75 mm The area imaged had the following dimensions: *xmin*= 7.545 mm, *xmax*= 48.795 mm, *ymin*= 9.337 mm, *ymax*= 37.087 mm. Mass spectrometric data was thereby acquired at 2128 positions. The ions corresponding to the protonated drug molecule *(m/z* 531) and sodium adduct of the matrix *(m/z* 212) were extracted from the data file.

Spot numbers for all ions were converted to an *xy* co-ordinate using the algorithm to produce the following mass spectrometric images (Figures 3.14, 3.15 and 3.16) .

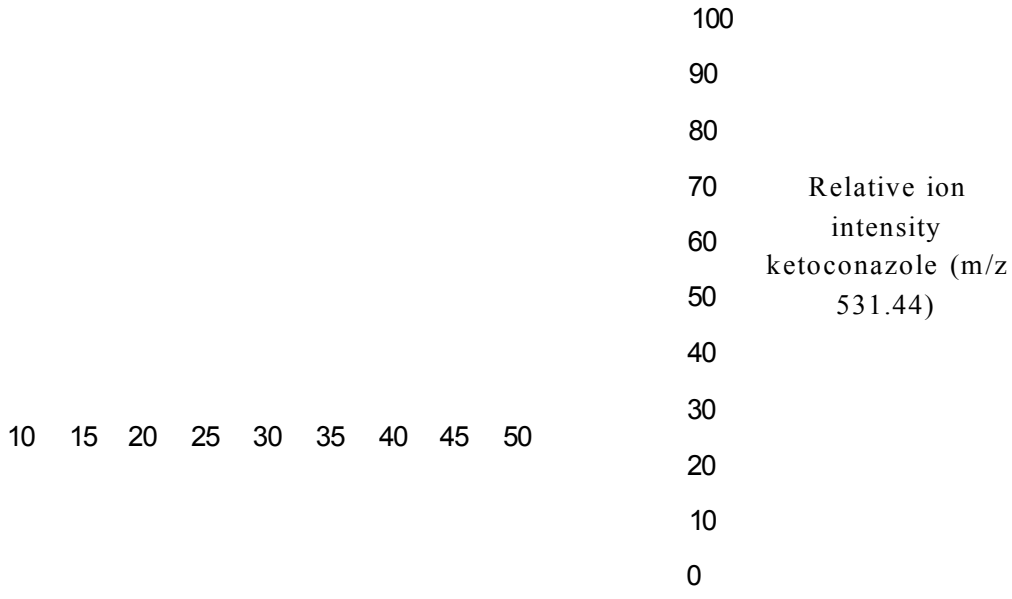

Figure 3.14: MALDI-TOF-MS image of the protonated molecule of ketoconazole on a tissue imprinted cellulose membrane.

It can be seen from these images that drug was detected at nearly all positions

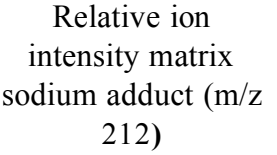

Figure 3.15: MALDI-TOF-MS image of the sodium adduct of a-CHCA coating the membrane.

on the membrane. There appears to be a 'cross' in the centre of the tissue where either no drug is present, or no drug is detected (Figure 3.14). Examination of coverage of the sodium adduct of o-CHCA reveals the same pattern (Figure 3.15). This indicates that the regions where no drug is detected is probably due to the absence of sufficient matrix crystals, limiting successful ionisation. This once again highlights the importance of a homogeneous matrix layer in imaging MALDI-MS. The pattern observed where neither the matrix or sample is detected is thought to have been attributed to the electrospraying procedure. After completion of 60 'rows', the spraying was stopped and the syringe refilled with matrix. It is thought that the areas where no drug, and no matrix were observed reflect a mis-calculation of the restart location of the spraying, resulting in a row being missed.

Figure 3.16 demonstrates how the images may be manipulated to show different information by altering the scale range of the axis. It effectively becomes a trade-off between qualitative and quantitiative information. This is because the range of intensities is so large (0 —2000), and so it is difficult to compare all intensities on the same scale.

The superiority of electrospray, compared to pipetting matrix solution onto a

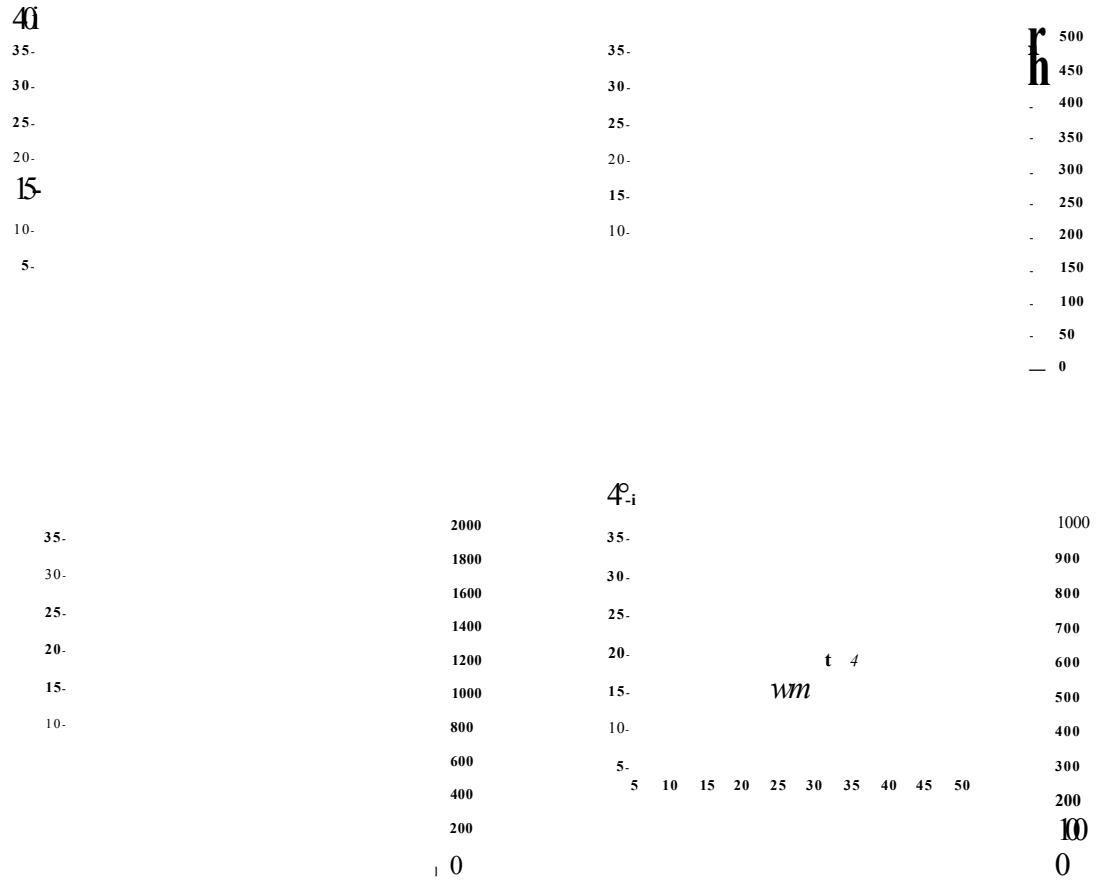

Figure 3.16: The effect of altering the *z* (ion intensity) scale on image presentation. All four images were created from the same data file: by altering the scale of ion intensity *(z* axis), very different images are produced.

membrane surface is demonstrated in Figure 3.17. In this experiment, two deposits of ketoconazole mixed with a-CHCA were applied to the membrane in the areas highlighted. The protonated ketoconazole molecule is only observed in a fraction of the expected area. This is thought to be attributed to the absence of a uniform layer of matrix. Spot samples are generally associated with achieving poor matrix homogeneity, and poor inclusion of the analyte molecule within the matrix crystals. Thus for this application matrix deposition by electrospray has clear advantages.

Airspray matrix deposition has been used previously for coating TLC plates at Sheffield Hallam University, and is considerably simpler and quicker than electrospraying matrix material onto samples. It is therefore evaluated in the next chapter.

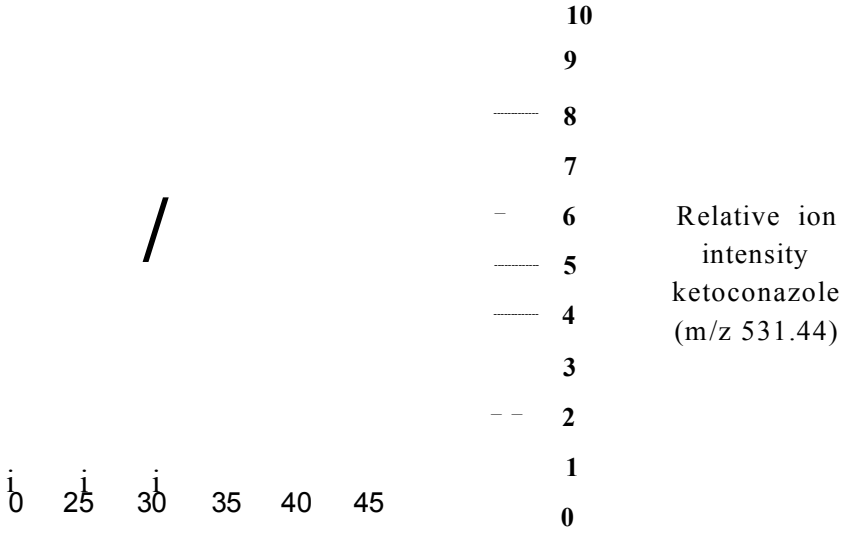

Figure 3.17: Imaging a spot sample: an indication of the superiority of matrix deposition by electrospray.

Another important experimental parameter in imaging investigations is the laser spot size. In order to estimate the dimensions of the Qstar pulsar i N2 laser spot size, an 'imaging run' was performed on heat sensitive paper. As before the laser was fired

for 2 seconds at 25% threshold energy (in order to mimic real imaging conditions). The heat sensitive paper was then viewed with a confocal microscope (Zeiss 510 CSLM, equipped with an argon laser), and a phase-contrast image was obtained. The laser spot size dimensions were measured using the confocal microscopy imaging software, and calculated as 150 x 200 /im (Figure 3.18). The spot size is elliptical, as would be expected.

Figure 3.18: Confocal microscopy image of the MALDI laser spot size obtained by analysis of heat-sensitive paper.

3.4 Conclusions

Superior mass spectra in terms of mass accuracy and resolution, as compared to those acquired with the linear TOF, were obtained. Spectra demonstrate excellent resolution of the isotopic peaks of the protonated analyte, highlighting its superiority to the instrument employed in Chapter 2. Use of the orthogonal ion source proved successful in maintaining mass accuracy across an uneven sample surface. This is essential in imaging applications. The ability to analyse larger areas has proved particulary useful, and beta test software provided permitted construction of ion images. Unfortunately, software limitations resulted in the need to construct an algorithm to enable construction of data images in an alternative software package, so that they may be presented in reports such as this. The algorithm created

has permitted images to be prepared in external graphical software. Images were created depicting the presence of the drug on/in the skin surface, by analysis of tissue imprinted, matrix-coated membranes.

Ion images depicting matrix coverage were created by selection of data pertaining to the presence of the sodium adduct of α-CHCA. This highlights that while in general the electrospray procedure resulted in a relatively homogeneous matrix layer, errors such as missed rows have profound effects on the relative display of the analyte location. Matrix coverage was once again found to be the predominant factor in successful detection of the drug, and while it appeared that problems had occurred during the spraying procedure, it was shown to produce a superior layer to simple pipetting. Images reveal superior crystal formation and more efficient incorporation of the analyte into crystals, as compared with spotted samples. This is concurrent with the findings of Garden *et al.* [126], who reported similar results by MALDI imaging.

The images presented in this chapter confirm the findings of Chapter 2, where cellulose membranes were found to be suitable blotting substrates for imaging MALDI-MS. This can be seen by both the successful imprint of drug onto the membrane, and secondly the presence of matrix crystals at nearly all locations.

Further manipulation of the images with the graphical software showed both a semi-quantitative and qualitative presentation of the acquired data. Changing the detail of the intensity range significantly altered the images produced. Thus it is important that a scale that offers both detection of the ions, as well as some semi-quantitative information is selected. It should be noted that incorporation of an internal standard or some form of data normalisation is necessary for true quantification of the drug in skin. This is investigated in Chapter 5 of this thesis.

The laser spot size was found to have elliptical dimensions of $150 \times 200\,\mu$m. This may in the future be a limiting factor, but with the current methods is not thought to be a major problem, especially when relatively large increment sizes are used. It does however imply that increment sizes should not be reduced beyond $200\,\mu$m, as this would result in overlapping spots, and ambiguous data. The majority of MALDI imaging literature reports use of similar spot size dimensions. The advent of lasers with smaller spot sizes was discussed in the Introduction (Chapter 1).

In conclusion, these initial imaging experiments demonstrated great promise for the application of imaging MALDI-MS as a method of profiling and quantifying drugs in epidermal tissue.

Chapter 4

Optimisation of methods of matrix application for analysis of treated tissue

4.1 Introduction

The success of an imaging experiment is highly dependent upon the formation of a homogeneous crystal layer upon the sample. Matrix application must not give rise to analyte spreading which will result in an incorrect impression of the spatial location of compounds of interest. Experiments presented in Chapter 2 indicated that both carbon and cellulose membranes could be successfully coated in matrix by electrospray deposition.

It is essential that matrix application is optimised so that a successful image depicting the true distribution of the drug may be acquired. In this chapter the considerably simpler approach of airspraying (as previously demonstrated for TLC-MALDI analysis [116] was compared to electrospray deposition for the coating of carbon and cellulose membranes.

The novel technique of precoating membranes prior to the tissue blotting process was also investigated.

Direct tissue analysis was revisited in this programme of work, given that the Qstar targets permitted analysis of an entire tissue section.

Ion imaging software updates (MDS Sciex, October 2003) permitted images acquired to be edited with the software provided (image rotation, selection of plot style) and saved as graphic files in .bmp format. These graphics were subsequently

imported into Adobe Photoshop to enhance the definition of the axis and label information and to convert to portable document format (.pdf) for incorporation into this thesis. The algorithm and graphical methods of data presentation employed in Chapter 3 were therefore not required, and all images presented in this chapter were created within the ion imaging software.

4.2 Experimental

4.2.1 Materials

Trifluoroacetic acid (AR grade). α-CHCA and sinapinic acid were purchased from Sigma-Aldrich (Dorset, UK). Methanol was HPLC grade, purchased from Fisher Scientific (Loughborough, UK). Polyethylene filled carbon conductive membranes and their cellulose membrane spacers (as previously) were obtained from Goodfellow (Huntingdon, UK). Porcine ears were obtained from Doncaster abattoir. Nizoral shampoo (2% ketoconazole) was obtained commercially.

4.2.2 Instrumentation

The electrospray deposition device developed at Sheffield Hallam University was employed in these investigations and is described in Chapter 2. Matrix application was alternatively conducted using a suction feed airspray device (Badger 150 Suction Feed air brush: The Air Brush Company, Lancing, West Sussex, UK). Mass spectrometric analyses were performed on an Applied Biosystems Qstar pulsar *i* hybrid quadropole time of flight mass spectrometer, fitted with an orthogonal MALDI source and ion imaging software, as discussed in Chapter 3.

4.2.3 Methods

Comparison of electrospray and airspray matrix deposition on carbon and cellulose membranes

$2 \times 2\,\text{cm}$ pieces of carbon and cellulose membranes were coated in $15\,\text{mg}\cdot\text{ml}^{-1}$ or $25\,\text{mg}\cdot\text{ml}^{-1}$ α-CHCA by electrospray (as described in Chapter 2) and airspray deposition respectively. All matrix solutions were prepared in methanol containing 0.1% trifluoroacetic acid. The airspray method involved the application of matrix

($25\,\mathrm{mg{\cdot}ml^{-1}}$) to the membrane using 5 cycles of the air brush, where one cycle comprises five passes of the air brush over the sample, giving an estimated total matrix usage of approximately 375 mg per sample. The membranes were dried under a heat lamp for 5 minutes between each cycle.

Treatment

A 'confined treatment area' was created on the tissue surface by protecting the skin around the application site with adhesive tape sealed with barrier cream to give a 'triangular' treatment area. The tissue was treated with 500 μl Nizoral shampoo (2% ketoconazole) inside the area of the former and incubated for one hour at 37^0 C. These experiments were used to assess the success of the matrix application methods in retaining spatially relevant information.

After incubation the tissue surface was rinsed with deionised water to remove any excess formulation.

Membrane preparation and tissue blotting

The epidermal surface of the treated tissue was blotted (pressed) onto either cellulose or carbon membranes and subsequently coated in α-CHCA ($25\,\mathrm{mg{\cdot}ml^{-1}}$) by airspray deposition (as above).

In separate experiments, membranes were coated in matrix prior to the tissue blotting procedure.

All membranes were mounted in the square recess of a specialised MALDI target (VoyagerDE, MDS Sciex, Canada) prior to mass spectral analysis.

Direct tissue analysis

Porcine epidermal tissue was snap frozen in liquid nitrogen cooled isopentane and sectioned by microtoming to achieve 15 μm surface sections. The sections were thaw-mounted in the recess of a specialised MALDI target and dried prior to coating with α-CHCA or sinapinic acid by airspray deposition.

Standard MALDI analysis and imaging of the membranes and tissue sections was performed on the Q-Star in the positive ion mode. In all images presented in this chapter, the increment size (degree of horizontal and vertical spacing) was set at

0.25 mm. The laser was fired for 2 seconds, with an energy of 14 μJ and a repetition rate of 20 Hz at all spots.

4.3 Results and discussion

Airspray and electrospray methods were evaluated with respect to the formation of an abundant and homogeneous matrix layer upon cellulose and carbon membranes. MALDI imaging was used to determine the extent of matrix coverage on both membranes by both methods.

4.3.1 Electrospray matrix deposition

Images of the sodium adduct of α-CHCA (Figures 4.1 and 4.2) reveal that similar patterns of matrix coverage are observed on both carbon and cellulose membranes. While in general the crystal coverage is dense, there are areas on both substrates where no matrix material is detected. This is thought to be attributed to capillary needle blockages resulting in a loss of spraying. This is consistent with the findings presented in Chapter 2. Higher matrix ion intensities are observed with the carbon membrane than with cellulose: this may be explained by the electrical conductivity of the substrate. The electrospraying procedure is optimised by an applied potential being maintained between the end of the capillary needle and the grounded sample stage; carbon membranes are therefore ideal for coating by electrospray. Several groups report matrix application by electrospray, and successful coating of carbon membranes with α-CHCA by electrospray for MALDI imaging of tissue blots for protein analysis has been carried out by Caprioli *et al.* [102,103].

4.3.2 Airspray deposition

Images of the sodium adduct of α-CHCA deposited by airspray deposition onto a carbon membrane (Figure 4.3) demonstrate complete coverage. It is clear however that there are variations in the matrix intensities observed. This matrix layer inhomogeneity may be problematic in an imaging experiment. However, providing that data collated is purely qualitative, and that at all areas on the membrane there is sufficient matrix for analyte ionisation, the extent of matrix coverage may overcome limitations of uniformity, and this may therefore be a suitable approach.

Figure 4.1: MALDI image of the sodium adduct of a-CHCA. Carbon membrane was coated in 15mg-ml_1 a-CHCA by electrospray deposition. Image demonstrates areas of dense matrix coverage, but also areas where the electrospray procedure failed.

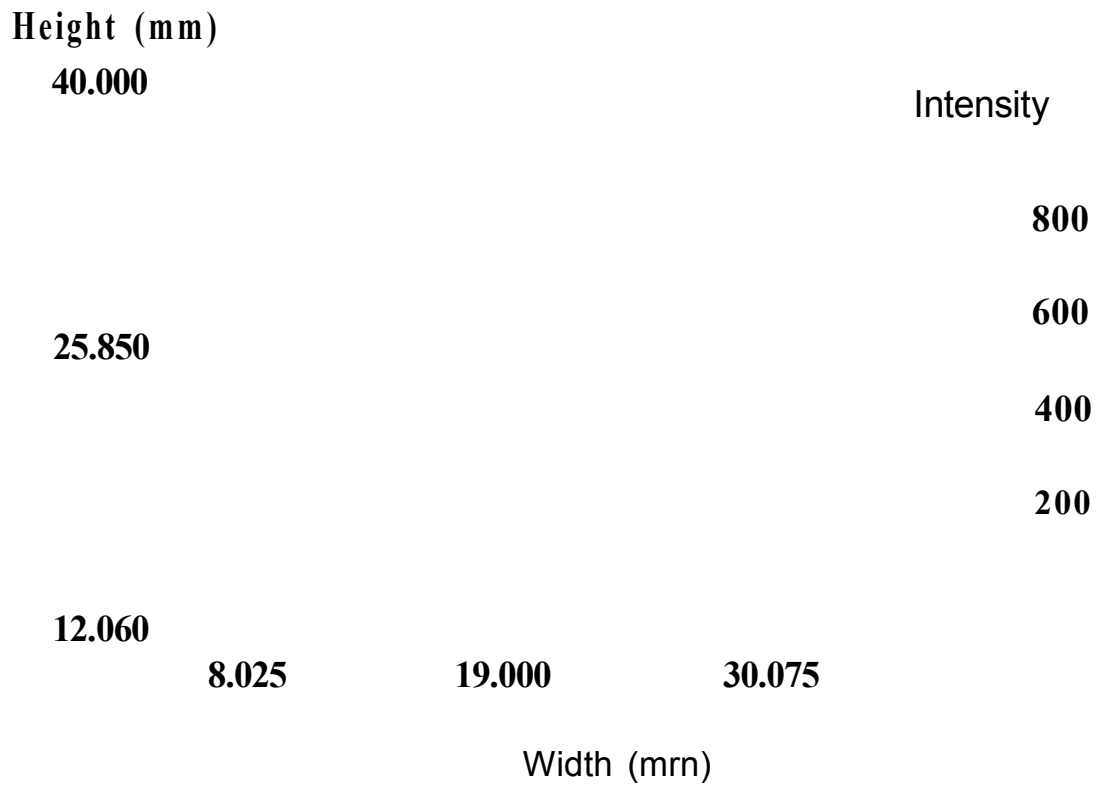

Figure 4.2: MALDI image of the sodium adduct of a-CHCA. Cellulose membrane was coated in 15mg-ml_1 a-CHCA by electrospray deposition. Image demonstrates areas of dense matrix coverage, but also areas where the electrospray procedure failed.

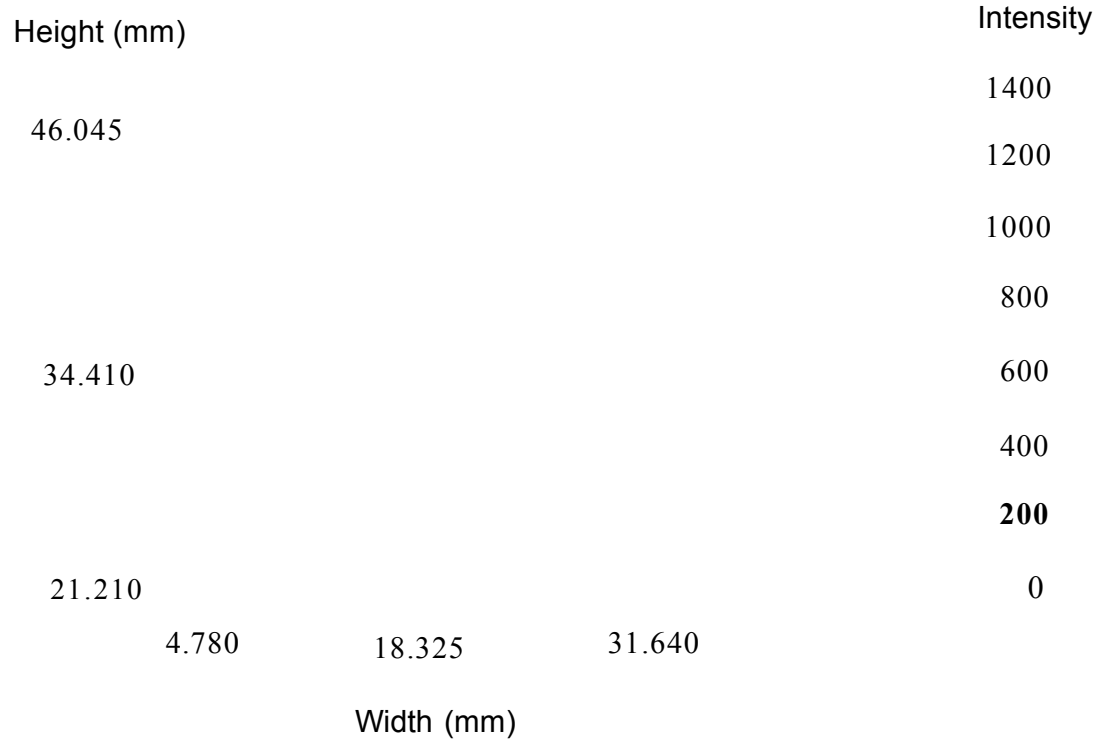

Figure 4.3: MALDI image of the sodium adduct of a-CHCA. Carbon membrane was coated in 25mg-ml_1 a-CHCA by airspray deposition. Image demonstrates good area coverage of the membrane, but indicates that the matrix layer is inhomogeneous.

Figure 4.4 shows an image of the sodium adduct of a-CHCA on a cellulose membrane. As observed with the carbon substrate, the entire membrane area is coated with matrix material. The matrix coating appears more uniform than with the carbon membrane, which may be due to the absorbent nature of the material. As discussed in Chapter 2, the absorbent quality results in matrix being drawn into the membrane, rather than running freely over a hydrophobic surface until it dries. Areas of relative matrix abundance in Figure 4.3 may therefore represent areas where the matrix 'pooled' prior to solvent evaporation.

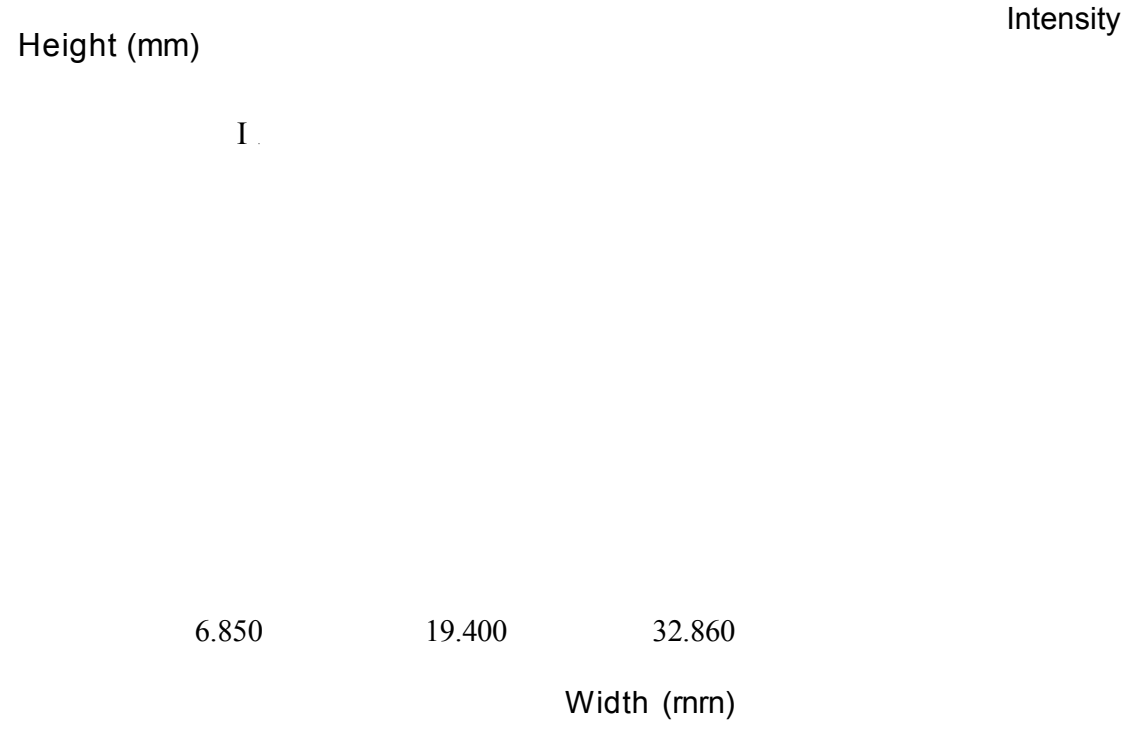

Figure 4.4: MALDI image of the sodium adduct of a-CHCA. Cellulose membrane was coated in 25mg-ml_1 a-CHCA by airspray deposition. Image demonstrates a relatively homogeneous matrix coverage.

These results indicate that matrix application by airspray deposition offers a more uniform and 'reliable' matrix coverage than electrospray.

Over the last year, several reports of airspray deposition as a method of coating tissue samples in imaging MALDI-MS experiments have been published [100, 113,168]. The technique offers enormous advantages of speed, and simplicity, as compared to electrospray.

In Chapter 2, analyte spreading by matrix application was observed on all substrates except cellulose. It is essential that matrix application does not result in analyte migration, as this would give rise to an incorrect display of the analyte's spatial location. Thus a method of pre-coating membranes in matrix material prior to the blotting procedure was investigated. This strategy would negate the possibility of matrix deposition causing the analyte to be 'washed' to new areas. For this to be a viable approach, successful inclusion of the blotted analyte into predried matrix crystals must be observed, and the expected distribution of the analyte must also be evident.

The following phase of work was conducted in order to assess the suitability of carbon and cellulose membranes as tissue blotting substrates in imaging MALDI-MS. Membranes were coated in matrix material by airspray deposition, either before or after the blotting procedure. The methods were assessed by the degree of matrix layer homogeneity on the substrates, as well as the distribution and successful detection of the analyte molecule. Tissue treatment was performed within a triangular former, and thus the successful method was predicted to demonstrate a triangular distribution of the protonated molecule of ketoconazole.

Analysis of tissue-imprinted carbon membranes: matrix applied after the blotting procedure

The image presented in Figure 4.5 shows the distribution of the isotopic envelope of the protonated drug molecule. It is evident that a high degree of analyte spreading occurred. Similar findings were presented in Chapter 2, where electrospray deposition resulted in analyte spreading on carbon membranes. The airspray method uses a considerably higher volume of matrix—and therefore solvent—than electrospray, and thus this is likely to result in extensive analyte migration. There appears to be an area in the centre of the image where no drug is observed. This is in fact the area where drug was expected. The image of the distribution of the sodium adduct matrix ion (presented in Figure 4.6) illustrates that matrix coverage shows a similar pattern. It is proposed that shampoo formulation blotted in this area has resulted in inferior matrix crystal formation. There is clearly an area of no crystals or ion suppression in the area where drug was expected. These results show that

the method of coating carbon membranes in matrix after the blotting procedure is unsuitable for this application.

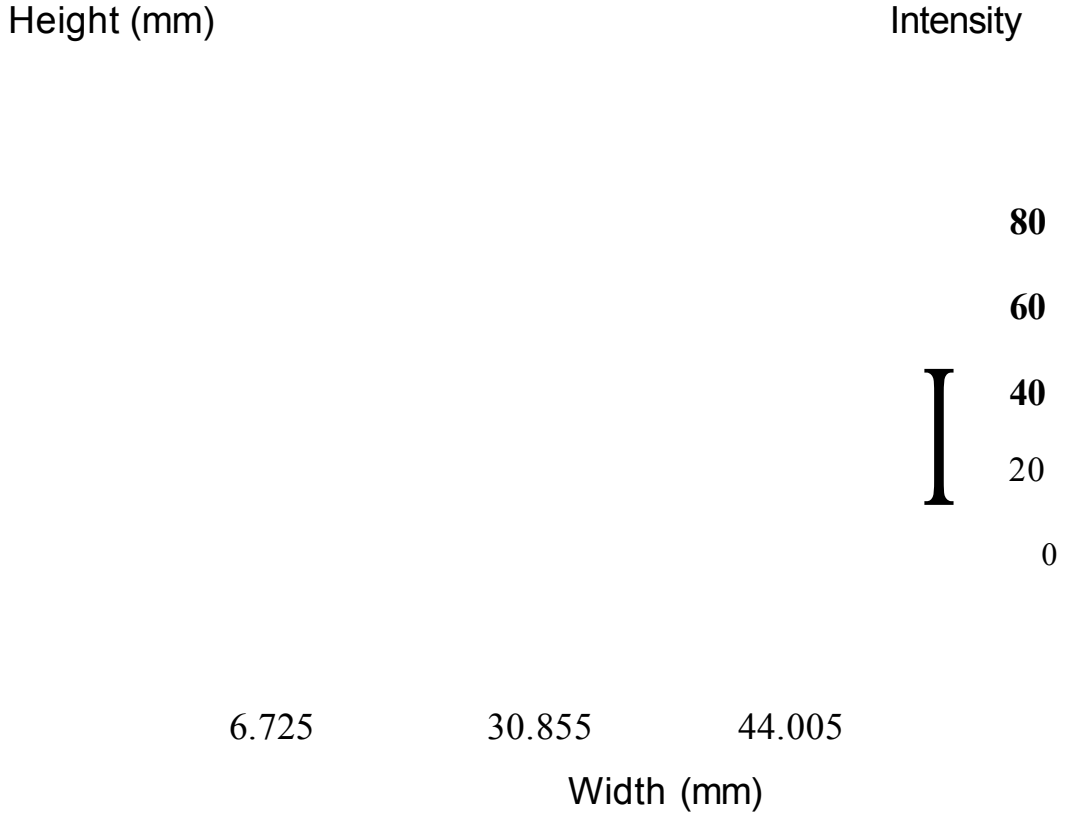

Figure 4.5: MALDI Image of the distribution of the isotopic envelope of the protonated molecule [M-f-H]+ *(m/z* 531-533) of ketoconazole. Tissue was treated with Nizoral within a triangular former. The skin was blotted onto a carbon membrane, and subsequently coated in a-CHCA by airspray deposition. The image demonstrates an unsuccessful triangular imprint, indicating analyte spreading by matrix application. Ketoconazole is detected across the majority of the membrane area.

Analyte spreading on a carbon membrane does not concur with the findings of Caprioli *et al.* [103]. However, as discussed in Chapter 2, they describe an analysis of proteins, which are likely to be bound to such a substrate by electrostatic attraction.

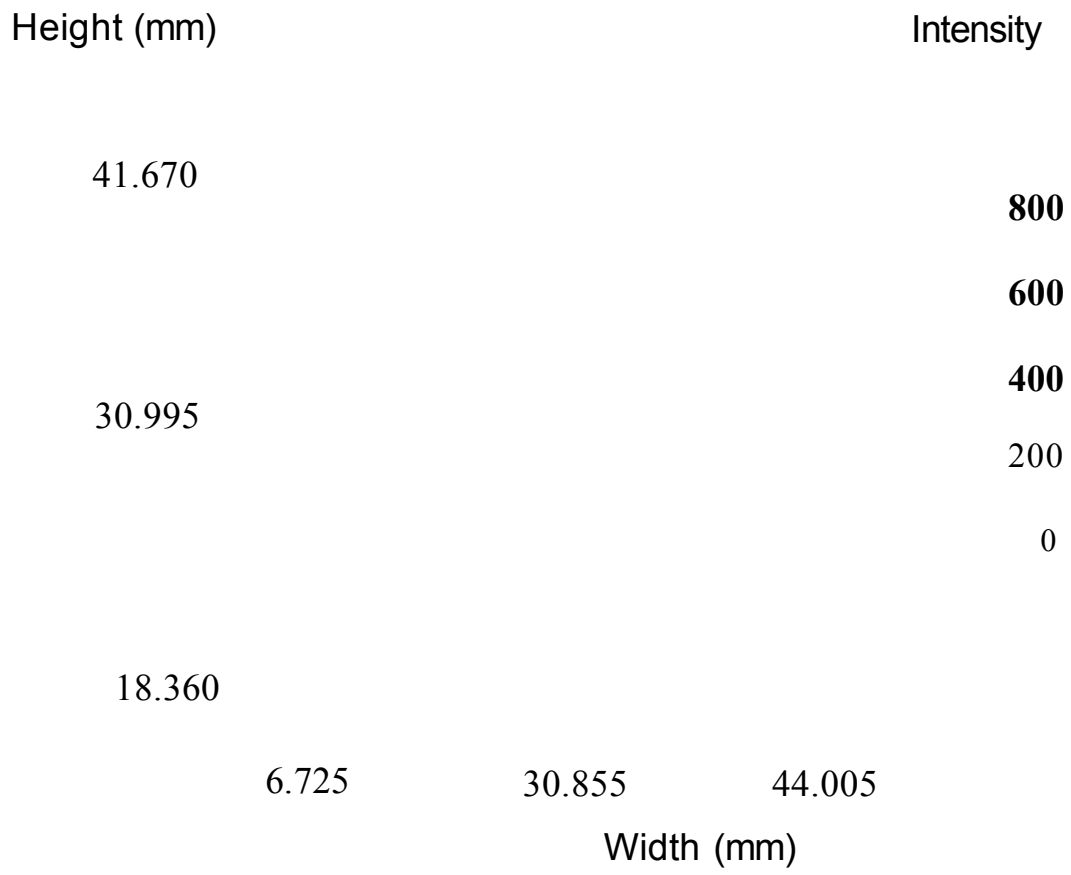

Figure 4.6: MALDI Image of the sodium adduct matrix ion [Matrix+Na]+ *(m/z* 211.5-212.5). Tissue was treated with Nizoral within a triangular former. The skin was blotted onto a carbon membrane, and subsequently coated in o-CHCA by airspray deposition. Image demonstrates relatively dense and homogeneous matrix coverage, but reveals a triangular area of matrix suppression.

Analysis of tissue-imprinted cellulose membranes: matrix applied after the blotting procedure

It can be seen from the image representing the distribution of the isotopic envelope of the protonated molecule of ketoconazole (Figure 4.7) that the analyte was detected across the majority of the membrane surface. This high degree of analyte spreading was not expected. It was postulated in Chapter 2 that the absorbent nature of the cellulose substrate reduced effects of analyte spreading. However, as discussed above the airspray method uses a much larger volume of solvent, and this is thought to have attributed to the analyte distribution observed. In addition, experiments presented in this chapter entailed analysis of a much larger membrane area than investigated in Chapter 2. It is likely that results presented in Chapter 2 did not fully demonstrate the extent of lateral migration, which can only be appreciated by imaging a larger square, as presented here.

The image of the distribution of the sodium adduct matrix ion (Figure 4.8) shows that matrix coverage in this experiment was surprisingly poor compared to all other airspray experiments. Given that there was clear analyte spreading, the method of airspraying matrix onto a tissue imprinted cellulose membrane was rejected as being unsuitable for this application. The poor matrix coverage is thought to be an anomaly, given the success of airspray deposition in all other experiments.

Analysis of tissue imprinted carbon membranes: matrix applied prior to the blotting procedure

The image presented in Figure 4.9 shows the distribution of the isotopic envelope of the protonated molecule of ketoconazole. An outline of the expected triangular distribution of the drug was observed. However the imprint appeared to be incomplete. It was observed during sample preparation of these membranes that there were loose or residual matrix crystals on the membrane following the airspraying procedure. This is thought to be due to the un-absorbent nature of the substrate. Thus it was observed that the tissue became covered in matrix within the triangular treatment area (due to wet formulation) after the blotting procedure. This resulted in an insufficient tissue imprint being made upon the membrane. This is similar to problems incurred in Chapter 2 while blotting tissue onto C18 beads.

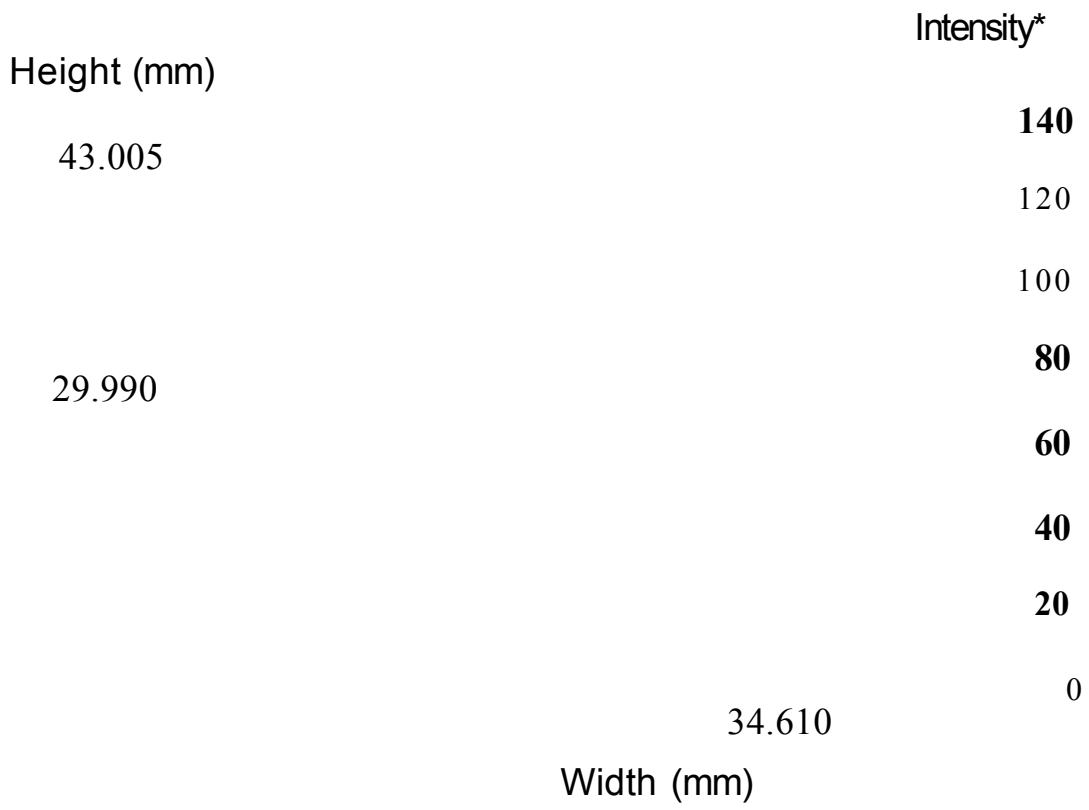

Figure 4.7: MALDI Image of the distribution of the isotopic envelope of the protonated molecule [M+H]+ *(m/z* 531-533) of ketoconazole. Tissue was treated with Nizoral within a triangular former. The skin was blotted onto a cellulose membrane, and subsequently coated in a-CHCA by airspray deposition. Image demonstrates an unsuccessful triangular imprint, indicating analyte spreading by matrix application. Ketoconazole is detected across the majority of the membrane area

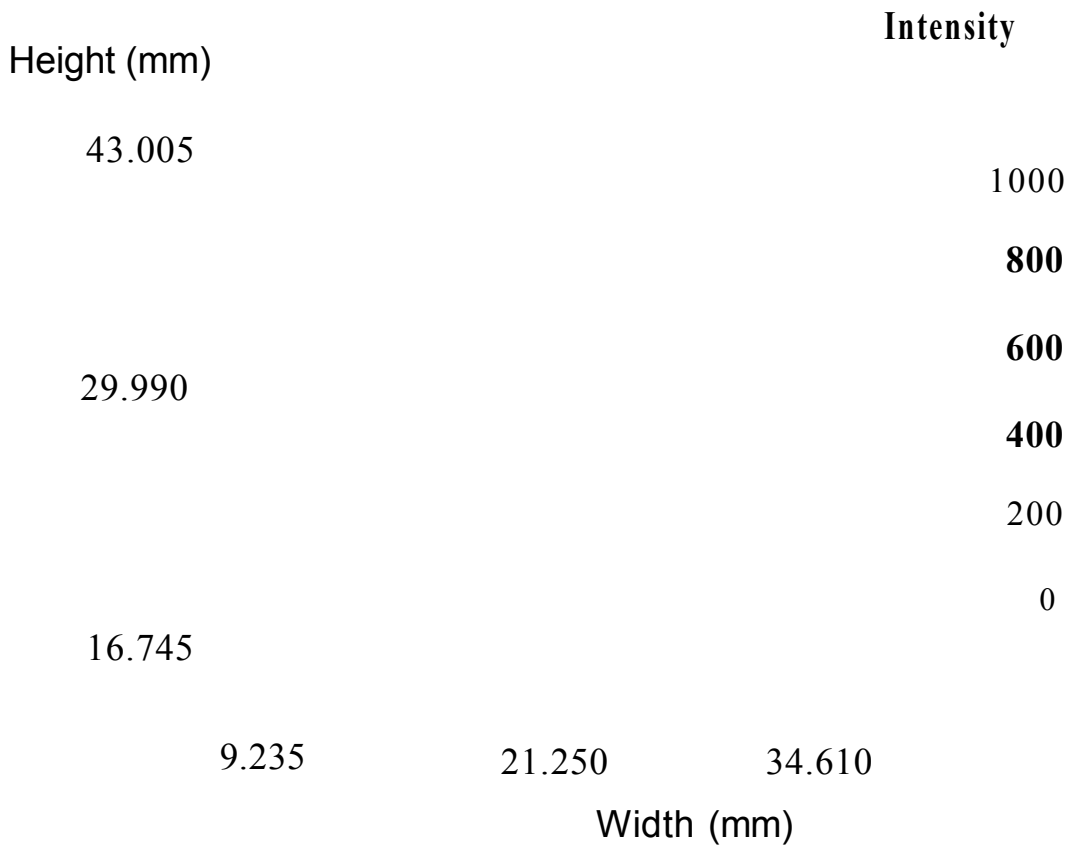

Figure 4.8: MALDI image of the sodium adduct matrix ion [Matrix+Na]+ *(m/z* 211.5-212.5). Tissue was treated with Nizoral within a triangular former. The skin was blotted onto a cellulose membrane, and subsequently coated in a-CHCA by airspray deposition. Image demonstrates poor matrix homogeneity as compared with the other airspray experiments.

While there appears to be no analyte spreading, the method was not found to be suitable given the poor quality of tissue imprint.

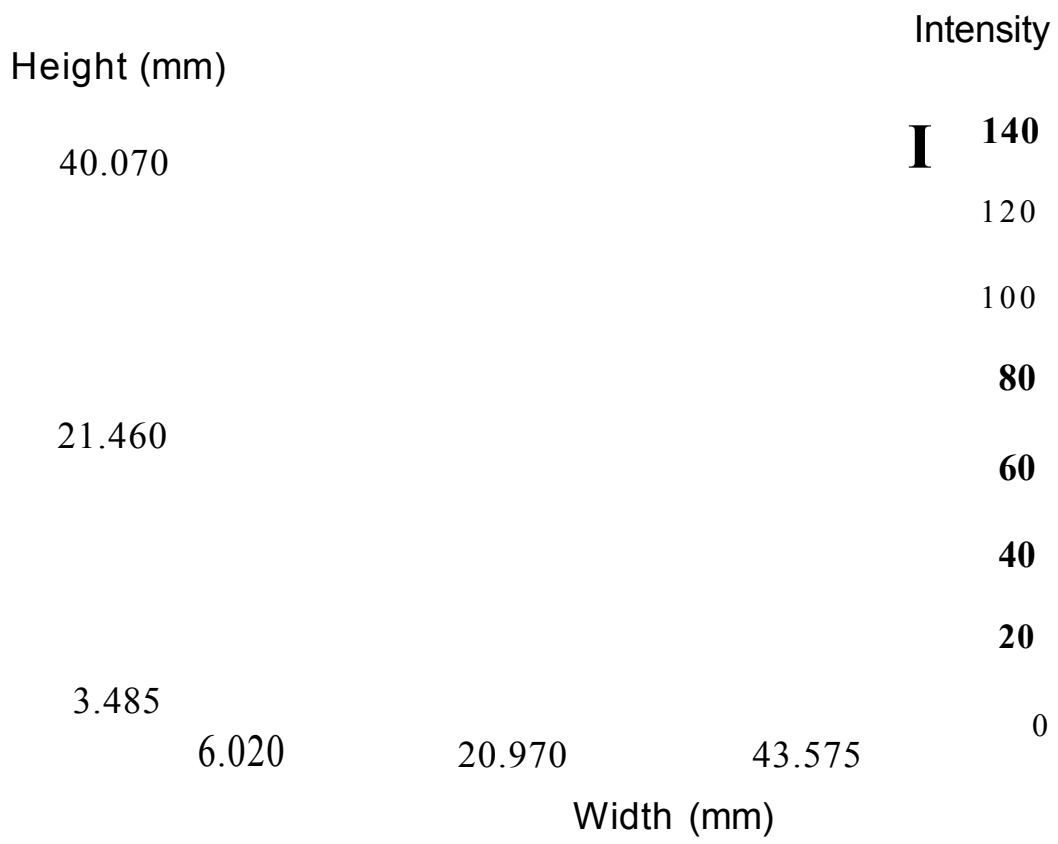

Figure 4.9: MALDI Image of the distribution of the isotopic envelope of the protonated molecule [M+H]+ *(m/z* 531-533) of ketoconazole. Tissue was treated with Nizoral within a triangular former. The skin was blotted onto a carbon membrane, precoated in a-CHCA by airspray deposition. Image demonstrates an incomplete triangular imprint.

The image of the distribution of the matrix (Figure 4.10) does not show a triangular area of missing matrix material. The matrix coverage appears to be relatively abundant and homogeneous. Despite some matrix material being removed by the blotting process there is still an impressive matrix layer. The experiment was repeated using 3 instead of 5 cycles of airspray deposition. No drug was detected and matrix appeared sparse.

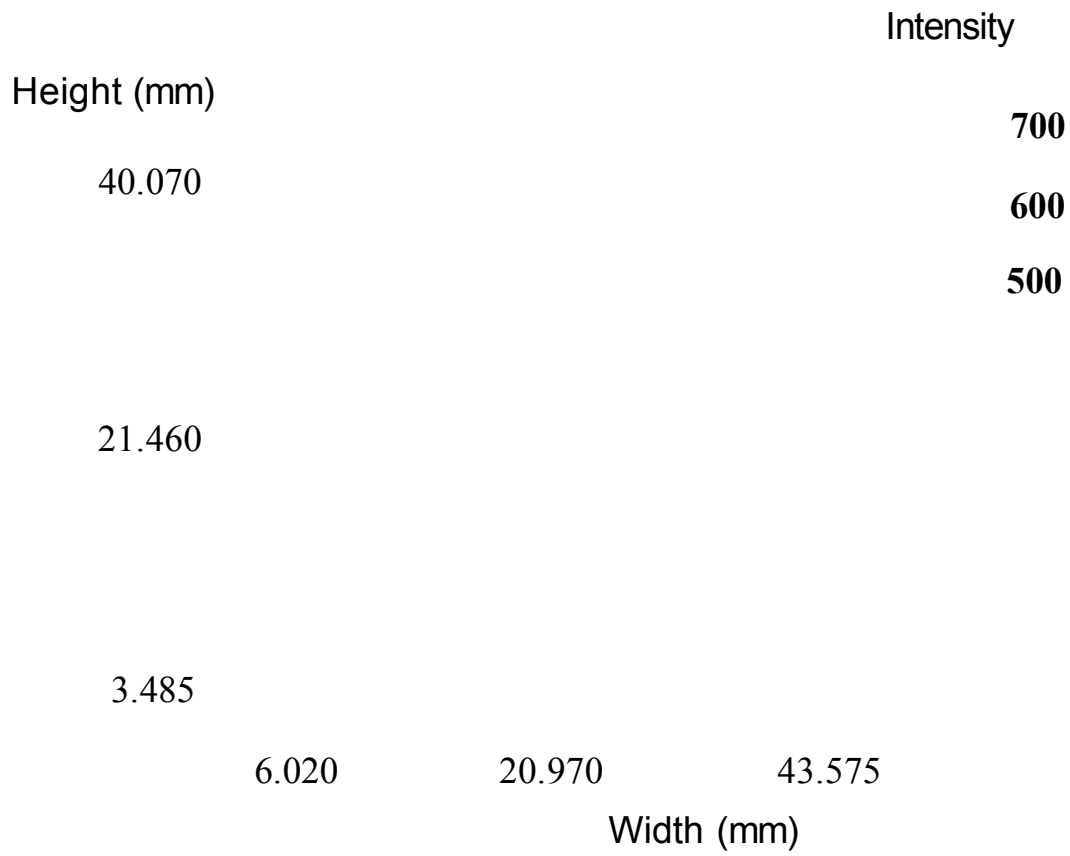

Figure 4.10: MALDI Image of the sodium adduct matrix ion [Matrix+Na]+ (*m/z* 211.5-212.5). Tissue was treated with Nizoral within a triangular former. The skin was blotted onto a carbon membrane, precoated in a-CHCA by airspray deposition. Image demonstrates relatively abundant and homogeneous matrix coverage.

Analysis of tissue imprinted cellulose membranes: matrix applied prior to the blotting procedure

This method was found to be superior to all other methods investigated. A dense and uniform triangle of ketoconazole can be seen from the image of the distribution of the isotopic envelope of the protonated drug molecule (Figure 4.11). This triangular distribution shows that successful tissue imprints may be made upon matrix coated cellulose membranes. There were no problems encountered during the sample preparation. The membranes were found to become fully impregnated with matrix material, and the absence of excess surface matrix material enabled the creation of an impressive tissue imprint. Matrix application prior to the blotting process prevented matrix associated analyte migration.

Figure 4.12 shows a relatively dense and even matrix coverage. However, as was observed with carbon membranes, there appears to be an area of matrix suppression in the presence of excess drug. The determination of ketoconazole throughout the triangular area implies that matrix crystals were formed, and so the absence of matrix ions detected in this region is thought to be attributed to the matrix suppression effect.

4.3.3 Direct tissue analysis

Poor results were obtained for direct tissue analysis in Chapter 2. Given that entire tissue sections could be mounted in the recess of Qstar targets, direct tissue analysis was re-evaluated in this phase of work. It was felt that analysis of a larger area might offer more promising results. However, as presented in Figures 4.13 and 4.14, similarly disappointing results were obtained. No drug was detected in the area where the tissue sample was mounted (Figure 4.13). Figure 4.14 reveals that this is likely to have been because no matrix material was detected on the tissue surface. Both the drug and matrix compounds were detected around the edge of the skin section, indicating analyte spreading. It is thought that the high salt content of skin is likely to have prevented the formation of viable matrix crystals.

Recent reports have shown that sinapinic acid, which is generally used for the analysis of high molecular weight proteins, may be useful as a matrix material for direct tissue analysis [100, 113, 168]. Sinapinic acid has a much higher salt tolerance

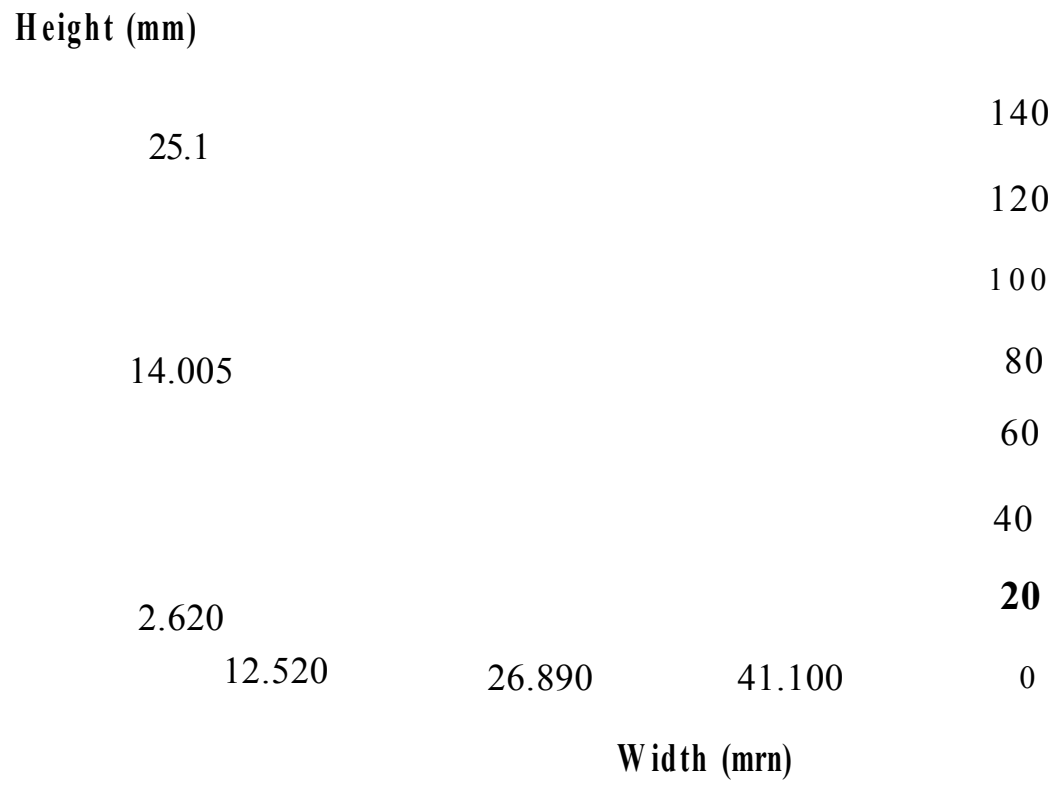

Figure 4.11: MALDI Image of the distribution of the isotopic envelope of the protonated molecule [M+H]+ *(m/z* 531-533) of ketoconazole. Tissue was treated with Nizoral within a triangular former. The skin was blotted onto a cellulose membrane, precoated in <a-CHCA by airspray deposition. A triangular distribution of the drug is observed. Image demonstrates retention of spatial information when the blotting technique is employed.

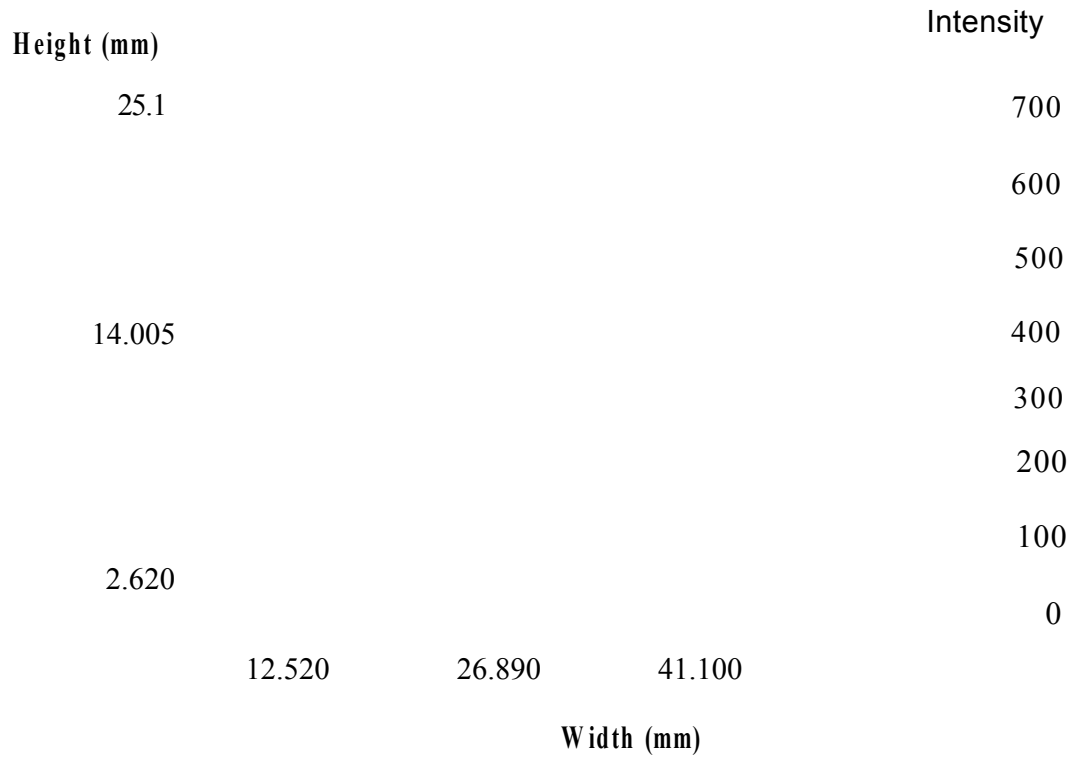

Figure 4.12: MALDI Image of the sodium adduct matrix ion [Matrix+Na]+ *(m/z* 211.5-212.5). Tissue was treated with Nizoral within a triangular former. The skin was blotted onto a cellulose membrane, precoated in a-CHCA by airspray deposition. Image demonstrates a triangular area of matrix suppression.

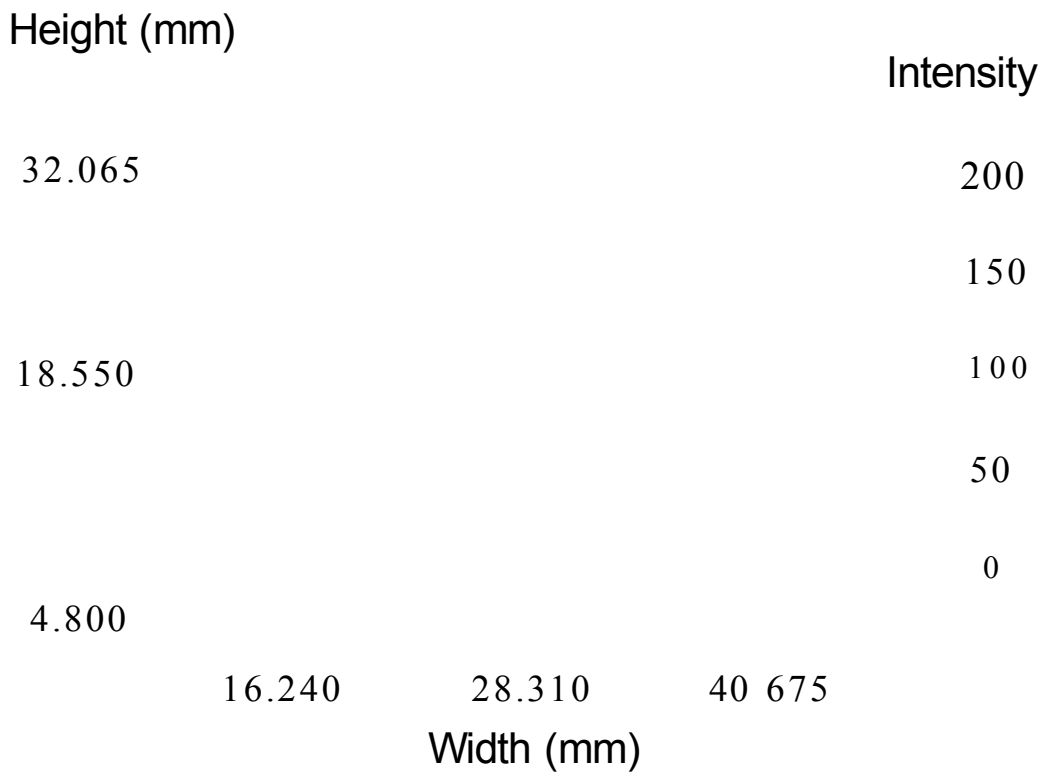

Figure 4.13: Image of the distribution of the isotopic envelope of the protonated molecule [M+H]+ *(m/z* 531-533) of ketoconazole. Porcine epidermal tissue was treated with 500*fi*\ Nizoral shampoo. A 15*/im* surface section was obtained by microtoming and coated in 25 mg*ml' 1 *a*-CHCA by airspray deposition (while mounted on the MALDI target). Image demonstrates unsuccessful ionisation of drug within the area where tissue was mounted, and analyte spreading from the tissue onto the target.

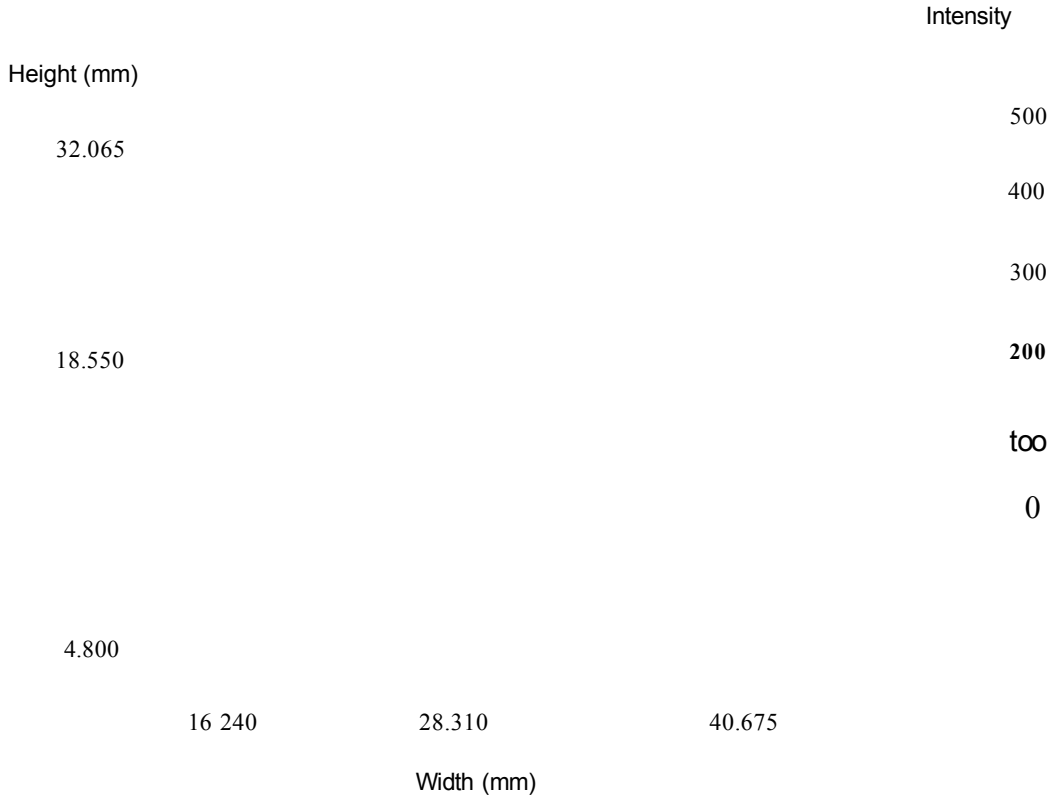

Figure 4.14: MALDI Image of the sodium adduct matrix ion [Matrix+Na]+ (m/z 211.5-212.5). Porcine epidermal tissue was treated with 500*A* Nizoral shampoo. A 15 //m surface section was obtained by microtoming and coated in 25mg-ml-1 cc-CHCA by airspray deposition (while mounted on the MALDI target). Image demonstrates unsuccessful coverage or ionisation of matrix material within the area where tissue was mounted. Matrix is only detected outside the tissue region.

than o-CHCA, and so may form matrix crystals on the skin surface. Thus the experiment was repeated employing sinapinic acid as the matrix.

Unfortunately while spectra were acquired outside the area of drug treated skin showing successful determination of ketoconazole (Figure 4.15), no compounds, including the matrix were detected on or in the skin section. It is probable that matrix compounds behave differently on different tissue groups; while this matrix has been usefully employed in the in analysis of brain tissue [113,168], it was not found to be suitable for the examination of skin.

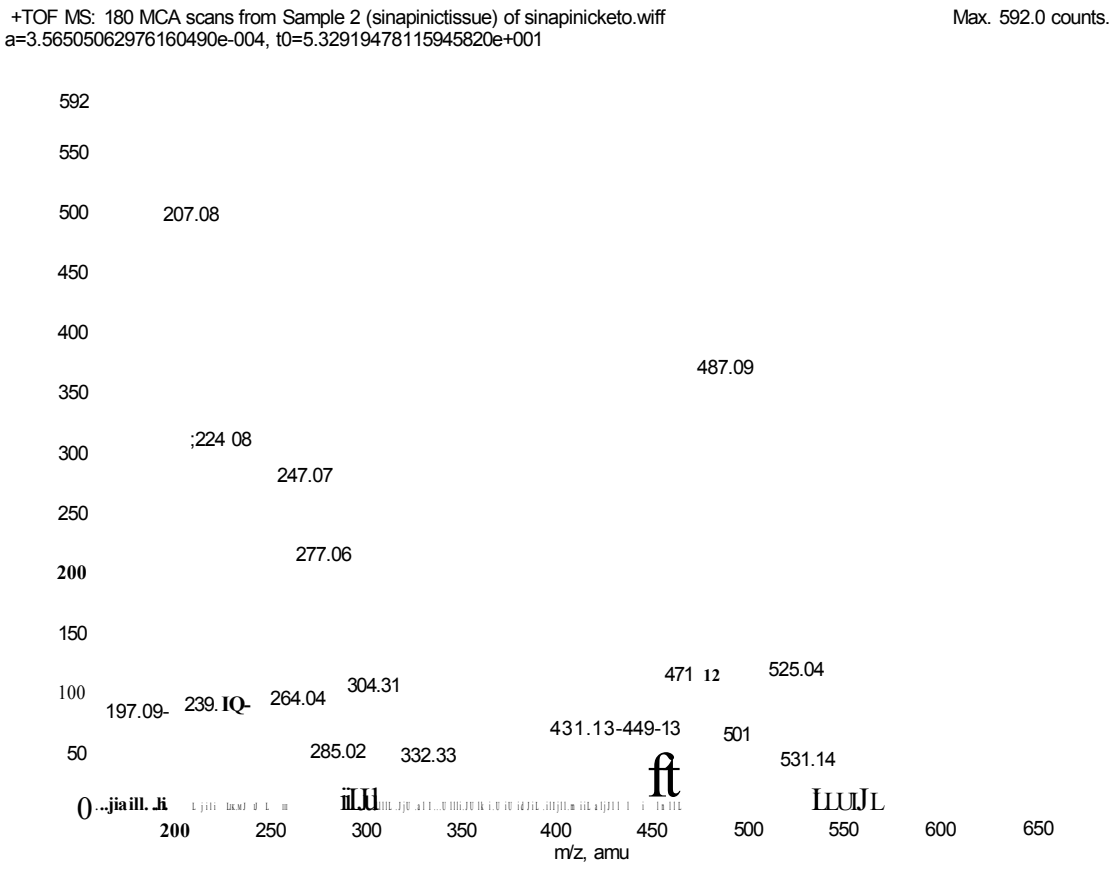

Figure 4.15: MALDI mass spectrum of ketoconazole acquired with sinapinic acid as the matrix material. The protonated drug molecule is detected at m/z 531. The protonated matrix molecule is detected at m/z 224.

Results from this chapter are in accordance with the findings presented in Chapter 2; the direct analysis of drug treated skin is inferior to the analysis of tissue imprinted

membranes.

4.4 Conclusions

Images of the sodium matrix adduct ion on carbon and cellulose membranes (Figures 4.1–4.4) indicate that airspray deposition is most reliable method. While there were areas on both cellulose and carbon membranes of abundant matrix material in electrospray experiments, the coverage over the entire membrane area is not as homogeneous as achieved by airspraying.

Regions in the images acquired from both substrates show areas where the electrospraying procedure failed (Figures 4.1 and 4.2). Ion images reveal that greater ion intensities were observed upon the carbon substrate (Figure 4.1), highlighting the advantages of a conductive sample for electrospray deposition. Conversely intensities may have been higher as all matrix material dries upon the surface, as opposed to being drawn into the absorbent cellulose membrane.

The technique of coating the membranes in matrix by airspray deposition (Figures 4.3 and 4.4) was found to give rise to complete coverage of both substrates. The layer achieved upon the cellulose membranes demonstrated a lower matrix ion intensity, but a more uniform coverage as compared to analysis of the carbon substrate. These results may also be attributed to the absorbent nature of cellulose.

In addition, as described in Chapter 2, concentrations above $15\,\mathrm{mg{\cdot}ml^{-1}}$ could not be sprayed using the electrospray device as this appeared to block the capillary needle, resulting in a loss of spraying. Samples were successfully coated with $25\,\mathrm{mg{\cdot}ml^{-1}}$ by airspray, resulting in a superior matrix layer.

Sample preparation times are another important factor. Electrospray deposition over a $2 \times 2\,\mathrm{cm}$ area took around 3 hours, as compared to airspraying, which took approximately 15 minutes. Shorter preparation times are thus a major advantage of the airspray method. In addition airspraying requires considerably simpler and cheaper 'instrumentation', as compared to the robotic electrospray device.

Given the superior uniform coverage, and faster preparation times, airspraying was considered the optimum method of matrix deposition.

Airspraying matrix onto both substrates after the blotting procedure (Figures 4.5 and 4.7) was found to cause extensive analyte spreading. This is because keto-

conazole is highly soluble in methanol. The procedure involves use of a relatively large volume of solvent and thus analyte on both substrates was washed to new locations. In the carbon membrane experiments insufficient matrix crystal formation was observed in areas of excess formulation, resulting in poor detection of both the drug and matrix material (Figure 4.5 and 4.6).

The technique of pre-coating carbon membranes with matrix prior to the blotting procedure was found to be unsuccessful. Excess matrix crystals were found to become stuck to the tissue surface during the blotting procedure resulting in an incomplete tissue imprint (Figure 4.9).

The approach of blotting treated tissue onto a cellulose membrane pre-coated in matrix material was found to be the optimum strategy. An impressive image demonstrating the triangular distribution of ketoconazole is presented in Figure 4.11. Matrix ions were suppressed in the presence of excess formulation (Figure 4.12), but ketoconazole was detected at all expected locations.

Direct tissue analysis was found to be unsuccessful with both α-CHCA and sinapinic acid. This is thought to have been attributed to poor matrix crystal formation upon the tissue surface.

Results presented in this chapter reveal that the novel method of blotting drug treated skin onto matrix coated cellulose membranes may be useful in permeation depth profiling of pharmaceutical compounds in skin.

Chapter 5

Analysis of a Vertical Imprint of Drug-treated Tissue with respect to the Quantification of Ketoconazole at Different Tissue Depths

5.1 Introduction

In Chapter 4 the method of blotting treated tissue onto cellulose membranes pre-coated in α-CHCA by airspray deposition was found to be successful in maintaining the expected analyte distribution. Therefore, given that the method does not show analyte spreading by matrix application, studying the relative location of the drug on a membrane surface may demonstrate potential as a method of permeation profiling.

The aim of work presented in this chapter was to estimate the extent of drug permeation by analysis of a cross sectional imprint of treated tissue. Histological examination of porcine ear epidermal tissue should enable the calculated depth profile to be related to the tissue structure.

To date there have been no reports of quantitative MALDI-MS images.

The main factor complicating the use of MALDI for quantitative analysis is the inhomogeneous distribution of matrix and analyte molecules in the crystalline sample [126], This results in poor shot to shot and spot to spot reproducibility. The need for matrix homogeneity across a sample surface in imaging experiments has been discussed in Chapters 1-4, and is essential if imaging MALDI is to be a

quantitative assessment. A range of techniques have been described to improve the homogeneity of matrix crystals [7,39,41–43,45–50,52–56,58–62,120], as discussed in sections 1.1.2 and 1.2.1 of the Introduction (Chapter 1). Investigations in Chapter 4 reveal that airspray deposition is the most suitable technique for this application.

As with many other mass spectrometric techniques, incorporation of an internal standard has resulted in successful quantification by standard MALDI-TOF. In such experiments the internal standard selected should possess high molecular identity with the analyte, and thus have similar crystallisation behaviour.

Internal standards have been used to quantify antibiotics [169], bile acids in urine [170], drugs from blood samples [171], [172], chlormequat [173], substrates or products from cultivations [174], enzyme kinetics [165, 175–177], peptides [178], neurotensin in brain tissue [167] and, alpha- and beta-myosin proteins in atrial tissue [179] by MALDI-TOF-MS.

While the use of internal standards in conventional MALDI analysis has proved successful, imaging experiments present a complicated issue: How should the internal standard be incorporated into the experiment?

Several strategies have been considered for quantitative TLC-MALDI analysis of drugs [118]:

1. Application of the internal standard to the TLC plate by electrospray before matrix deposition;

2. Application of internal standard to TLC plate after matrix deposition;

3. Spraying the matrix and internal standard concurrently as a mixture;

4. Pre-developing the TLC plate in internal standard prior to the TLC separation (matrix deposited as the final stage).

The technique of pre-developing the TLC plate in the internal standard was found to be the optimum method.

This is not predicted to be as useful for the indirect analysis of tissue imprints on membranes: While the membrane could be precoated in internal standard prior to matrix application, this is likely to favour the inclusion of the internal standard into

the matrix crystals as the solvents dry, over the inclusion of the analyte molecules that are blotted onto the preformed crystals. This is less than ideal.

There have been reports of MALDI quantification without the inclusion of an additional compound serving as an internal standard. Such methods may be useful in imaging experiments. Successful calibrations for the quantitative determination of lysophospholipids using the signal: noise ratio for analyte peaks was reported by Petkoviac *et al.* [180]. While this may help to reduce variations in analyte respnse due to laser fluence, it does not address issues of matrix heterogeneity which are likely to result in erroneous determinations in imaging experiments.

Dally *et al.* [181] reported quantification of underivatised free amino acids in mammalian cell culture media on spot targets by MALDI-TOF-MS. They present calibrations for 12 amino acids, using an airspray sample deposition method to improve spot homogeneity. The matrix (α-CHCA) served as an internal standard.

Using the matrix as an internal standard in an imaging experiment is an attractive possibility. Firstly there is no need to incorporate an additional and problematic stage in the sample preparation, and secondly, measuring the response of analyte: matrix at each location is likely to normalise any discrepancies in matrix coverage that might otherwise result in erroneous analyte intensities.

Thus in this phase off work the quantitative determination of ketoconazole at different tissue depths, using the matrix as an internal standard, is to be investigated

5.2 Experimental

5.2.1 Materials

Trifluoroacetic acid (AR grade) and $\alpha-$cyano$-4-$hydroxy cinnamic acid—α-CHCA) were purchased from Sigma-Aldrich (Dorset, UK). Methanol was HPLC grade, purchased from Fisher Scientific (Loughborough, UK). Nizoral shampoo ($20\,\mathrm{mg{\cdot}g^{-1}}$ ketoconazole ((($\pm$)$-1-$acetyl$-4-$[$p-$[[(2R,4S)$-2-(2,4-$dichlorophenyl)$-2-$(imidazol$-1-$ylmethyl)$-1,3-$dioxolan$-4-$yl]methoxy] phenyl] piperazine)), manufactured by Janssen Cilag, Buckinghamshire, UK, and cellulose membranes were obtained commercially. Porcine ears were obtained from Doncaster abbatoir.

5.2.2 Instrumentation

All mass spectrometric analysis was performed using an Applied Biosystems (Foster City, USA) hybrid quadrupole time-of-flight instrument (QStar) fitted with an orthogonal MALDI ion source and beta test imaging software supplied by MDS Sciex (Ontario, Canada). The nitrogen laser used has an elliptical spot size of $100 \times 150\,\mu$m and an available power range of $0 - 58.4\,\mu$J.

Confocal microscopy was performed on a Zeiss 510 CSLM, equipped with an argon laser. Phase contrast images were acquired with a $\times 20$ objective lens.

Sample preparation for optical microscopy

Samples for optical micrcoscopy were prepared by microtoming to an approximately $15\,\mu$m thick section. They were subsequently mounted onto a polylysine-coated microscope slide (BDH, Poole, UK) and stained using a conventional Harris haematoxylin and eosin (H&E) staining protocol.

Tissue treatment and membrane preparation

Cellulose membranes were coated in α-CHCA matrix material by airspray deposition, as described and presented in Chapter 4.

A 2×2 cm piece of porcine epidermal tissue was treated with $500\,\mu$l Nizoral shampoo, and incubated at 37^0 C for 1 hr. Following incubation any excess formulation present on the skin surface was washed away. Tissue samples were subsequently bisected and a cross sectional imprint was created on the matrix coated cellulose membrane.

Imaging the membrane

The area on the target where the membrane was mounted was selected within the software and then imaged as follows: the target was moved in x and y dimensions at set increments of 0.2 mm while firing the laser for 2 seconds at each location, at a laser repetition rate of 20 Hz.

5.3 Results and discussion

Figure 5.1 shows an image generated of ketoconazole distribution in a 'vertical' skin section following blotting of the bisected tissue cross-section onto a precoated cellulose membrane. The apparent localisation of the drug in the uppermost layers of the skin is clearly observable.

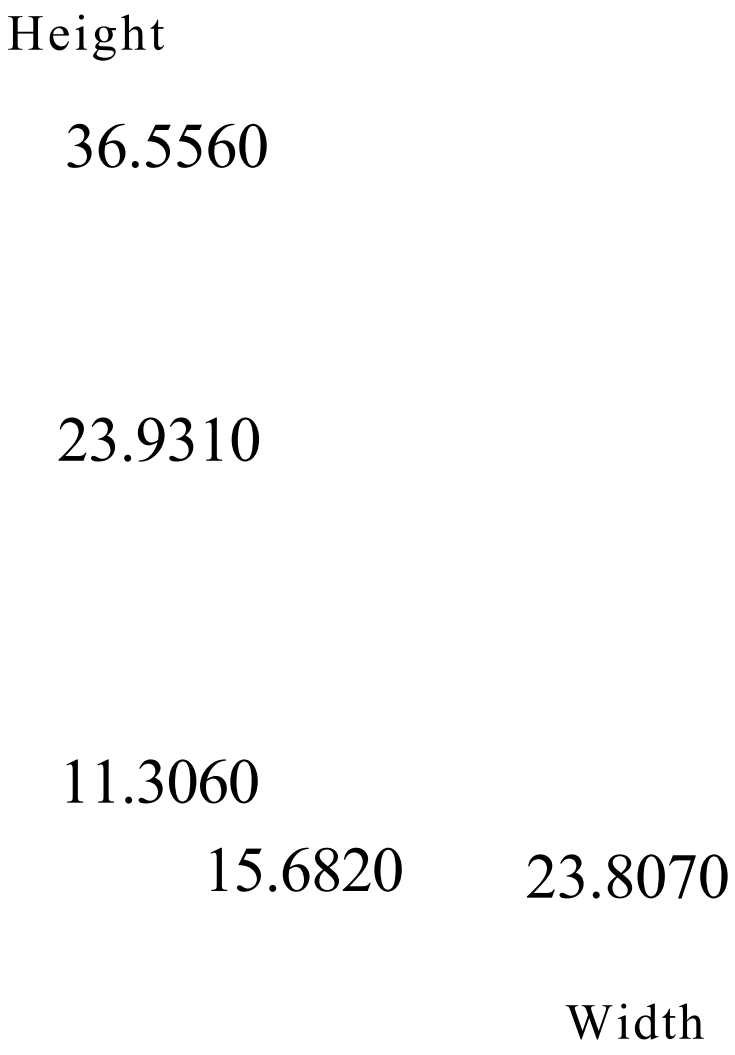

Figure 5.1: MALDI Image of the distribution of the isotopic envelope of the protonated molecule [M-f-H]+ *(m/z* 531-533) of ketoconazole in a vertical section of porcine epidermal tissue. Treated tissue was bisected and a cross section was blotted onto cellulose membrane, precoated in a-CHCA by airspray deposition. The image shows a 'vertical' distribution of the protonated drug molecule.

In order to clearly see the apparent depth of penetration the image shown in Figure 5.1 can be rotated via 90^0 using the supplied software. This is shown in Figure 5.2. This form of presentation allows a semi-quantitative assessment of the data.

5.3.1 Quantification of drugs in skin

The use of matrix peaks as an 'internal standard', for the normalisation of ketoconazole signals has been investigated. This procedure was used in order to compensate for variations in matrix coverage. Examination of spectra and images obtained from analysis of (pre-coated) tissue imprinted cellulose membranes reveals that the most abundant and consistent matrix peak observed is the sodium adduct of α-CHCA (m/z 212) (Figures 5.3 and 5.4).

An initial calibration graph for the concentration range 0.25–1.75 $mg{\cdot}ml^{-1}$ ketoconazole was prepared by plotting the ratio of m/z 531–533:212 against drug concentration (Figure 5.5). The calibration represents the mean value of 20 samples and their associated error. All analyses were performed using an automated search pattern to acquire data from within the sample spots.

The ratio of drug to matrix observed on tissue imprinted membranes is consistently under 0.5, indicating that a more effective calibration range would be 0–0.4 $mg{\cdot}ml^{-1}$. The calibration was repeated for this range to ensure a more accurate interpretation of results (Figure 5.6). Good linearity ($r^2 = 0.9686$) and precision (average standard deviation = 0.055 ($n = 20$)) were achieved.

The straight line equation from Figure 5.6 was then used to calculate the concentration of ketoconazole in a vertical profile as follows: the data set used to construct the 3D images was was displayed in two dimensions and magnified in the software in order to observe individual pixels. Each pixel in the image corresponds to a spectrum acquired in the imaging run. Thus the intensities of the protonated analyte and sodium matrix adduct peaks were extracted from spectra acquired in a sequential, vertical fashion—as illustrated in Figure 5.7. The ratio of the peaks was calculated and the straight line equation from the calibration was used to calculate the concentration of drug at each location.

Figure 5.2: MALDI Image of the distribution of the isotopic envelope of the protonated molecule [M+H]+ (*m/z* 531-533) of ketoconazole in a vertical section of porcine epidermal tissue. In this case the treated tissue was bisected and a cross section was blotted onto cellulose membrane, precoated in a-CHCA by airspray deposition. The image shows a 'vertical' distribution of the protonated drug molecule. This is the same data as shown in Figure 5.1 and has been rotated through 90°, giving a clear picture of the apparent change in drug concentration with depth.

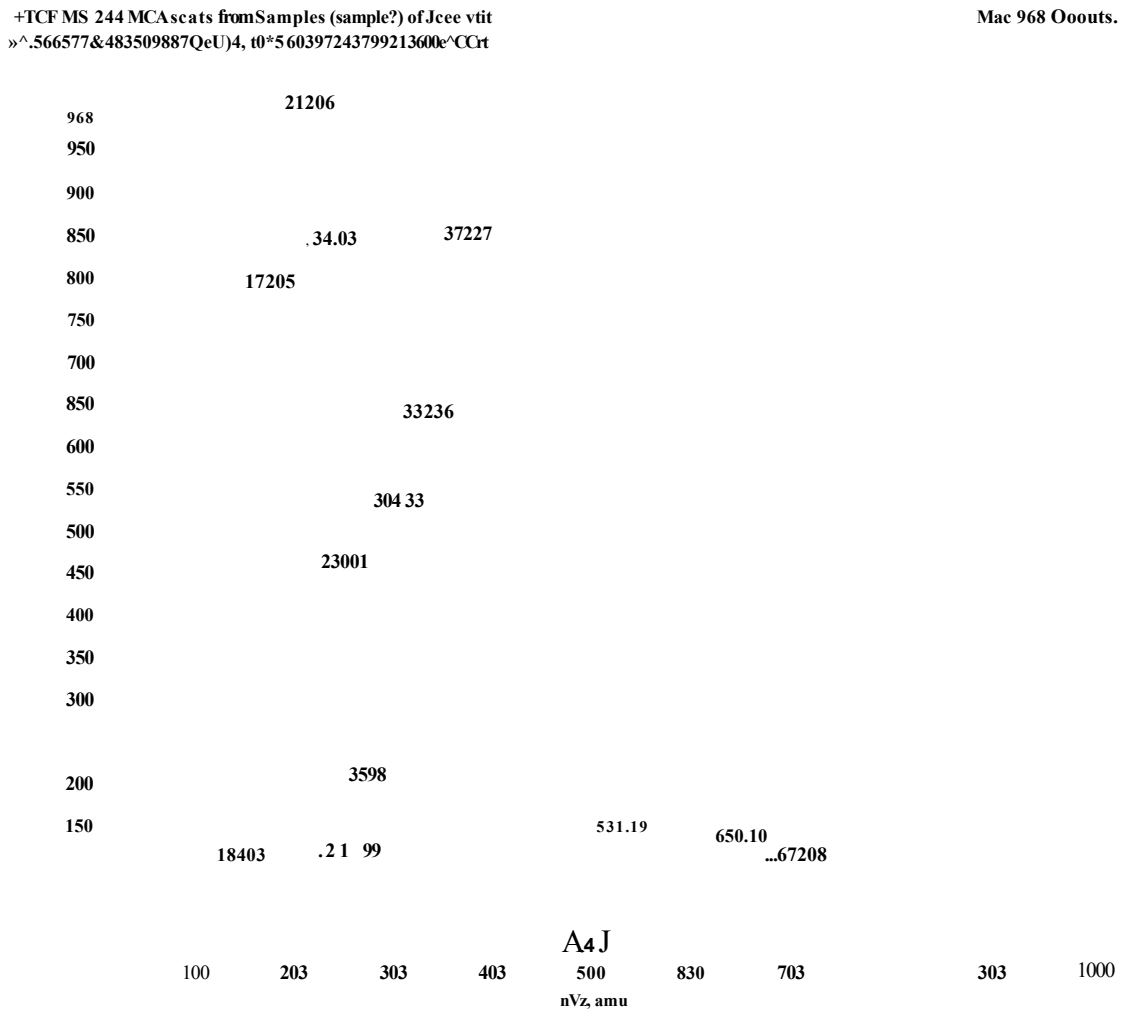

Figure 5.3: MALDI mass spectrum of ketoconazole treated tissue imprint on a cellulose membrane, precoated in a-CHCA by airspray deposition. The sodium matrix adduct ion is the most abundant matrix associated peak

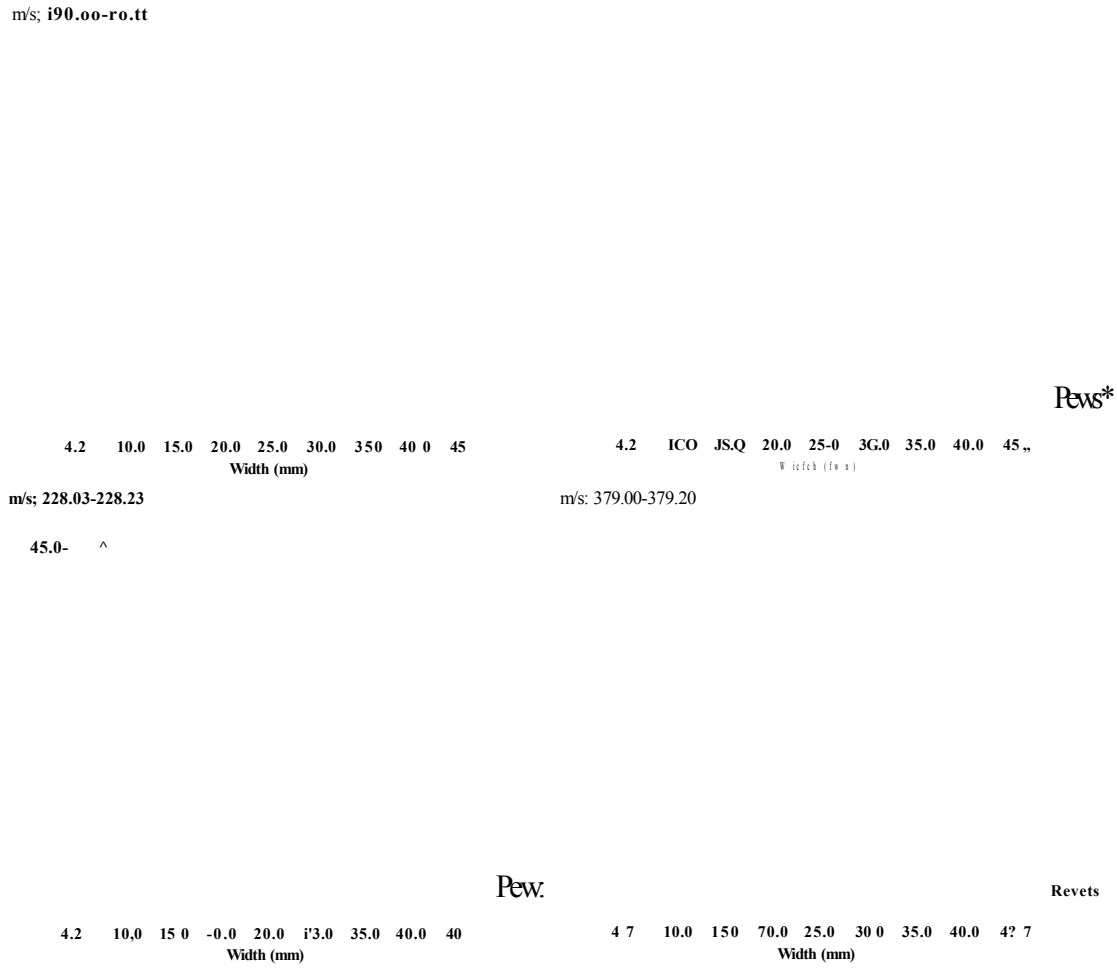

Figure 5.4: MALDI images of o-CHCA on cellulose membrane: (a) the protonated molecule *(m/z* 190), (b) the sodium adduct *(m/z* 212), (c) the potassium adduct *(m/z* 228), and (d) the matrix dimer *(m/z* 379).

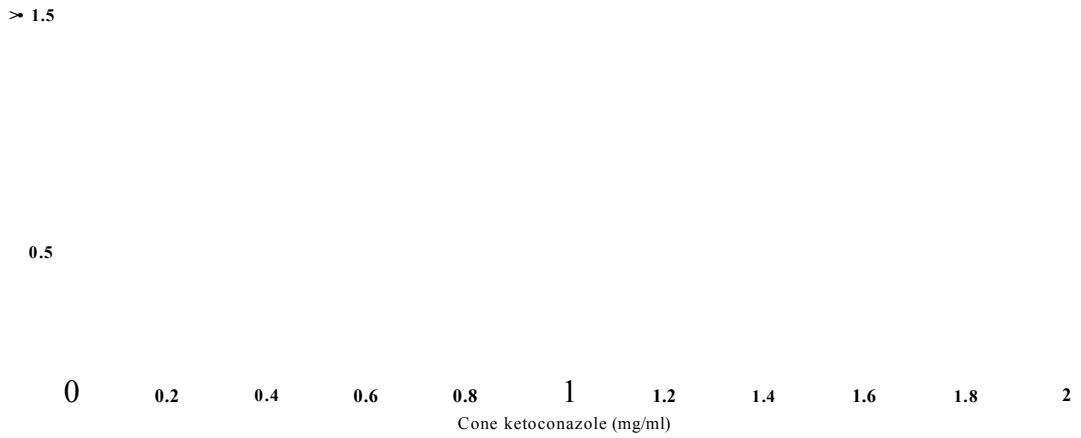

Figure 5.5: Calibration plot for the determination ketoconazole 0.25-1.75 mg constructed using the intensity of the Na adduct of o-CHCA ion at m/z 212 as an 'internal standard' (y = 1.0699a; + 0.3566, r 2 = 0.9224.)

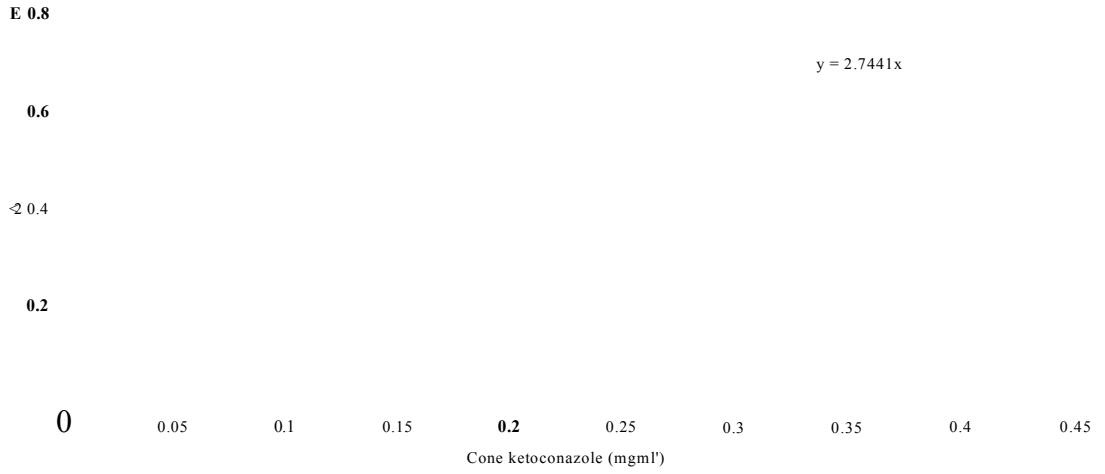

Figure 5.6: Calibration plot for the determination ketoconazole 0-0.4 mg-ml-1 constructed using the intensity of the Na adduct of a-CHCA ion at m/z 212 as an 'internal standard' (y = 2.7441a:, r2 = 0.9686)

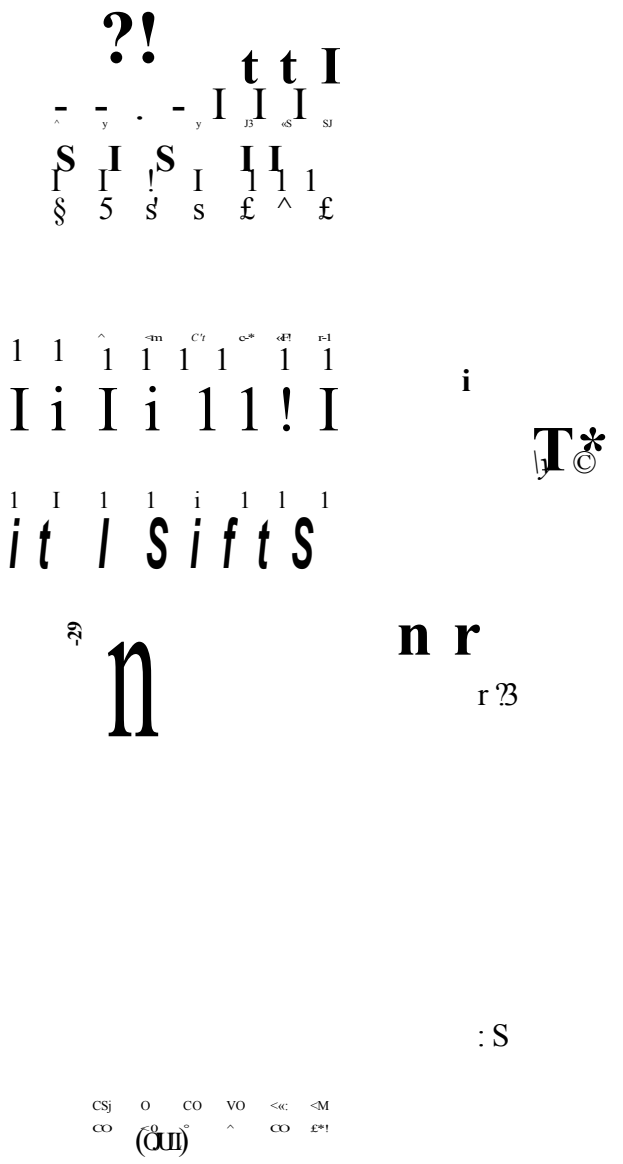

Figure 5.7: A 2D representation of the data presented in Figure 5.1 was enlarged within the software to reveal pixels. Each pixel within the image corresponds to an individual mass spectrum. The ratio of drug to matrix in these spectra was used to calculate the concentration of drug at each location by rearranging the straight line equation obtained from the calibration plot shown in Figure 5.6.

Knowledge of the degree of vertical spacing between spectra enables the data to be presented as a profile of drug concentration against increasing depth as shown in Figure 5.8. The drug is detected up to 0.8 mm into the skin.

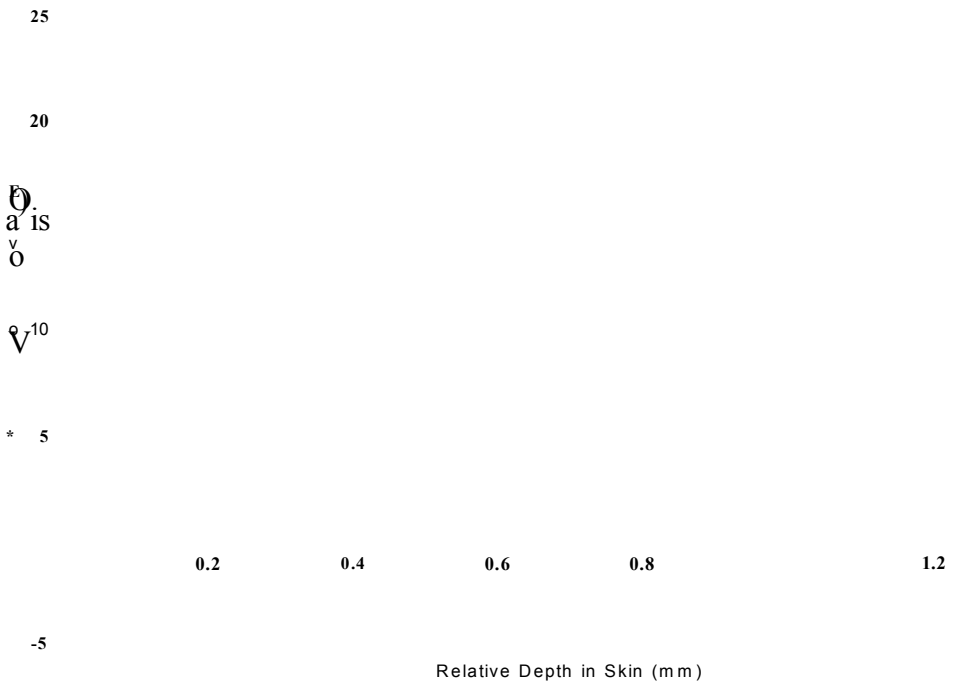

Figure 5.8: A quantitative profile of ketoconazole in porcine skin constructed from examination of selected spectra acquired during an imaging run.

In order to relate the profile to skin structure, conventional haemotoxylin and eosin staining was performed on a cross section of porcine epidermal tissue. The section was imaged by confocal microscopy and the histological image obtained is demonstrated in Figure 5.9. The original MALDI image (Figure 5.1) was enlarged to reveal individual pixels (each representing a 0.2 mm2 area) and this was superimposed upon the histological image, as shown in Figure 5.10. This demonstrates drug permeation up to and including the dermal skin layer. No drug is detected in the underlying connective tissue. All labelled concentrations are equivalent to the concentration of ketoconazole in solution. Thus further work will be necessary to calculate a true concentration in skin. This may be possible by preparing calibrations of different drug concentrations on cellulose membranes, calibrations of different

drug concentrations applied to the skin surface and blotted onto a membrane, and hence determining the blotting efficiency itself.

Figure 5.9: Confocal microscope image of a cross section of porcine skin. The sample was prepared by conventional haemotoxylin and eosin staining methods.

There may be concern over the possibility of smudging during the blotting procedure resulting in a loss in quality of spatial information. It is therefore essential to optimise methods for this blotting procedure, so that they are normalised or automated to ensure reproducibility. However the data shown here appear to confirm that at the current spatial resolution of 100/un, smudging is not significant.

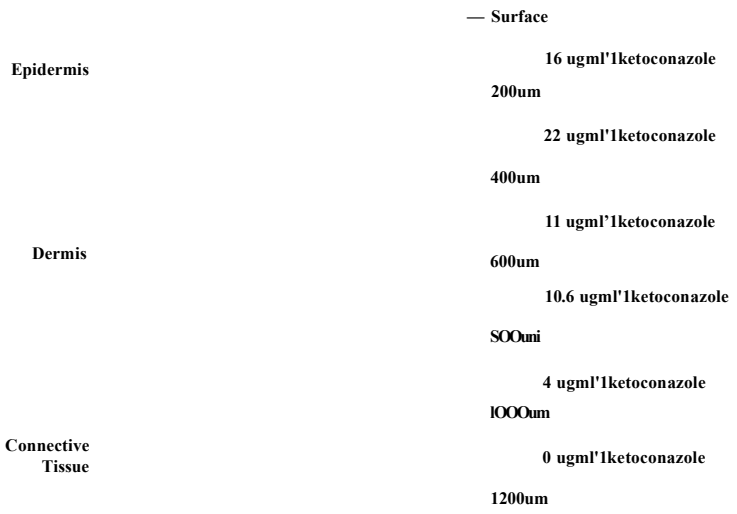

Figure 5.10: The mass spectrometric image is superimposed upon a histological image to reveal that the drug is absorbed into the dermal skin layer. All concentrations are equivalent to concentration in solution.

5.4 Conclusions

This programme of work has demonstrated that imaging MALDI-MS is a potentially powerful tool for studying pharmaceutical compounds in biological systems.

To date there has been limited exploration of the use of imaging MALDI in biomedical applications. Ion beam approaches such as SIMS have been used in similar applications, but suffer limitations such as mass range and sensitivity. Caprioli and co-workers have introduced the use of MALDI imaging for studying peptides, proteins, and drugs in tissues. The author is unaware of any other research that employs imaging MS in percutaneous depth profiling. The work presented in this chapter illustrates the possibilities of this technique in such an application.

The use of lasers in imaging MS has several advantages as compared to using ion-beams alone, such as high sensitivity, selective ionisation, and quantification. However, while MALDI imaging experiments have yielded better quality spectra and can detect a higher mass range than SIMS, the lateral resolution needs to be greatly improved.

Successful detection and imaging of drug compounds on and under the skin surface has been achieved by the indirect analysis of tissue imprinted cellulose mem-

branes by MALDI-TOF-MS. The methods developed have yielded high quality spectra and images of the drug molecule. The method of precoating celluose membranes in matrix by airspray deposition gives rise to a relatively abundant and homogeneous layer of matrix crystals as compared to other methods investigated. Treatment through a triangular former (presented in chapter 4) shows that the method is capable of maintaining the spatial distribution of the analyte. Images have been generated showing the dermal uptake of the drug molecule in skin, and show the expected trend of diminishing drug concentration with increasing depth.

Calibration graphs for the determination of ketoconazole have been prepared using the sodium matrix adduct as an internal standard. A relatively good degree of linearity and precision have been achieved. The linear relationship obtained has permitted calculation of the concentration of ketoconazole at different skin depths by examination of individual spectra acquired during an imaging run. Histological images reveal that this corresponds to drug permeation up to and including the dermal skin layer.

Chapter 6

Methods for the Quantification of Drug in Tissue by Imaging MALDI-TOF-MS and a Comparison with HPLC Corneum Tape Stripping

6.1 Introduction

The optimum method for the analysis of ketoconazole in porcine epidermal tissue by MALDI-TOF-MS was found to be the 'indirect analysis' of tissue imprints on cellulose membranes, precoated in α-CHCA by airspray deposition. This method was found to retain the expected distribution of the analyte molecule (as presented in Chapter 4 of this thesis). This approach was then employed for the analysis of a cross sectional tissue imprint, which permitted construction of a semi-quantitative profile of ketoconazole in skin (as presented in Chapter 5 of this thesis).

The percutaneous absorption of ketoconazole into porcine epidermal tissue should be assessed by an alternative method in order to validate the profile obtained by imaging MALDI-MS. Autoradiography would permit a comparison of images but is only semi-quantitative. In addition, labelled ketoconazole was not available, and thus this technique was not explored.

A widely used and well-documented technique for the determination of the permeation depth of drugs in skin is stratum corneum tape stripping, with analysis by high performance liquid chromatography (HPLC) [166]. In addition to permeation

profiling, tape stripping has also been used for the study of biophysical properties [162], and the examination of skin constituents [182]. The technique is simple to perform and is reviewed on page 38.

In this chapter, a method for the analysis of ketoconazole in skin by tape stripping/HPLC is presented. The analysis of ketoconazole at different skin depths by this method was then compared to tape stripping with analysis by tissue blotting and MALDI-MS.

6.2 Experimental

6.2.1 Materials

Ketoconazole, econazole, triethylamine, tetramethyl ammonium hydroxide, diisopropylamine, and tetrahydroxybenzophenone were all purchased from Sigma-Aldrich (Dorset, UK). All solvents were HPLC grade and obtained from Fisher Scientific (Loughborough, UK). Porcine ears were obtained from Doncaster abbatoir. Sellotape and Nizoral shampoo were obtained commercially.

6.2.2 Instrumentation

The chromatographic (HPLC) system comprised a Waters 600MS System controller, a Perkin Elmer ISS200 advanced LC sample processor, a Waters 490E programmable multiwavelength detector and a DP700 CE instruments integrator. The column employed in this work was a Supelcosil LC-18 (Supelco) 15 cm×2·1 mm with a 5 μm pore size.

All mass spectrometric analyses were performed on a Qstar pulsar *i* (Applied Biosystems, Foster City, USA) fitted with an orthogonal MALDI ion source and beta test ion imaging software (MDS Sciex, Ontario, Canada).

6.2.3 Methods

Optimisation of HPLC determination of ketoconazole in tape strippings

Methods were developed to determine concentrations of ketoconazole and an internal standard, without interference from either Sellotape components or matter

extracted from tissue. Ketoconazole was detected by UV detection at 232 nm. Initial HPLC conditions comprising a mobile phase of 60:40 acetonitrile and 0·02M disodium hydrogen orthophosphate buffer, pH 4·0, containing 0·2% diisopropylamine and a flow rate of 0·15 ml·min^{-1} [183] were considered unsuccessful. All matter extracted from tape was eluted between 8 and 12 minutes, with the drug eluted at 10 minutes. Introduction of a gradient method could not overcome this.

The instrument was refitted with stainless steel tubing and a mobile phase comprising acetonitrile, 1.59 mM tetramethyl ammonium hydroxide (TMAH) buffer, pH 7·8 and tetrahydrofuran (THF) was investigated [184]. Under these conditions, the drug was successfully separated from all other components, and the optimum mobile phase was determined as containing 55% acetonitrile, 14·3% THF and 31·7% TMAH buffer, set at a flow rate of 0·15 ml·min^{-1}. Under these conditions, ketoconazole was eluted at around 9·6 minutes.

In order to permit the quantitative determination of ketoconazole by HPLC, compounds were investigated for use as internal standards. The structural analogue, fluconazole, was the first choice of internal standard. Unfortunately this was not commercially available as an analytical reagent. An alternative azole anti-fungal agent, econazole, was subsequently evaluated. Despite showing good absorbance at 232 nm, econazole could not be detected by this method. Tetrahydroxybenzophenone was finally selected as the internal standard to be used in these experiments. Under the aforementioned conditions it was eluted at 4·6 minutes.

Topical treatments

A 'confined treatment area' of 2×2 cm was created on all tissue types by protecting the skin around the application site with adhesive tape (to ensure that the stripped area corresponded rigorously to the treated area).

Fresh porcine epidermal tissue was treated with 50 μl Nizoral shampoo (2% ketoconazole) and transferred to an incubator (37^0 C) for one hour. Following incubation, the excess formulation was blotted away, and the tissue surface was rinsed in deionised water, and allowed to dry for 30 minutes.

Tape stripping

The stratum corneum of the confined treatment area was sequentially stripped up to 20 times with a commercially available adhesive tape (Sellotape), which was pressed to the skin by rubbing it back and forth with a spatula.

Ketoconazole was extracted from the tape strips over 16 hours in 2 ml of an 80:20 mixture of acetonitrile and aqueous 0·72 mM TEA buffer, pH 2·5 [184] (containing 100 $\mu g \cdot ml^{-1}$ tetrahydroxybenzophenone as an internal standard). The solution was then passed through an Acrodisc syringe filter and transferred to HPLC vials for quantification.

HPLC analysis

The mobile phase was isocratic and comprised a volumetric mixture of 55% acetonitrile, 14·3% THF and 31·7% 1.59 mM tetramethyl ammonium hydroxide buffer, pH 7·8. The flow rate was set at 0·15 $ml \cdot min^{-1}$. Sample volumes of 5 μl of 'tape extract' solution were injected into the system. UV detection was performed at 232 nm.

Drug concentrations were determined from calibration plots generated with ketoconazole dissolved in the same mixture used for extraction.

Tissue blotting and corneum tape stripping

In separate experiments, tissue was treated with 500 μl Nizoral (2% ketoconazole) within a 2 × 2 cm treatment area, and incubated at 37^0 C for one hour. The tissue surface was subsequently blotted onto a 2.2 × 2.2 cm cellulose membrane that had been precoated in 25 $mg \cdot ml^{-1}$ α-CHCA (prepared in methanol (0·1% trifluoroacetic acid)) by airspray deposition.

The stratum corneum of the confined treatment area was then sequentially stripped as described above (page 152). The blotting procedure was repeated after every five tape strips.

MALDI-MS analysis of membranes

All membranes were analysed by MALDI-TOF-MS with the Qstar pulsar *i* in positive ion mode. Mass spectra were acquired every 0·5 mm by firing the laser for

two seconds at each location at an energy of 14 μJ and a repetition rate of 20 Hz. Relevant data was then extracted from the TIC file.

6.3 Results and discussion

6.3.1 Determination and quantification of ketoconazole in tape strip samples by HPLC

Examination of the chromatograms obtained by analysis of extracts from tapes used to strip treated and untreated tissue (presented in Figures 6.1 and 6.2 respectively) did not reveal any interfering peaks when compared to chromatograms obtained by analysis of ketoconazole standards (Figure 6.3). The chromatograms show that no interfering compounds were extracted from the tissue (analysis of a tape strip from untreated tissue shows no peak at 9·6 minutes (Figure 6.2), compared to analysis of a ketoconazole standard (Figure 6.3), and a tape strip from treated tissue (Figure 6.1), which both clearly show presence of a peak at 9·6 minutes. The experiments also demonstrate that the drug was successfully separated from Selloptape components in the chromatographic system. Chromatograms obtained from analysis of tape strip samples from treated (Figure 6.1) and untreated (Figure 6.2) tissue did not give rise to any possibly-interfering peaks in the chromatographic region of interest, when compared to analysis of a drug standard (Figure 6.3). The internal standard, tetrahydroxybenzophenone, was detected at around 4·6 minutes in all experiments. Ketoconazole was detected at around 9·6 minutes.

A calibration plot for the quantitative determination of ketoconazole (in concentrations from 0–100 μg·ml^{-1}) by HPLC was prepared, as presented in Figure 6.4. This permitted calculation of the concentration of ketoconazole obtained from tape strippings.

The recovery of ketoconazole from tape was determined by coating tape samples with 50 μl of a 10mg mg·ml^{-1} ketoconazole solution preprared in 60:40 acetonitrile:TEA buffer (corresponding to 500 μg per piece of tape used) and submitting them to the extraction protocol described on page 152 . The concentration of ketoconazole (μg·ml^{-1}) in the injected sample was calculated from the calibration graph. Thus the amount of ketoconazole extracted into 2 ml acetonitrile/TEA buffer was

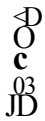

Time (min)

Figure 6.1: Chromatogram obtained from analysis of tape used to strip the surface of treated tissue. Porcine epidermal tissue was treated with 50 /d Nizoral shampoo. Following incubation the surface layer was removed by stripping with Sellotape. Ketoconazole was extracted from the tape over 16 hours in an 80:20 mixture of acetonitrile and TEA buffer, containing tetahydroxybenzophenone as internal standard. 5/il of the extracted mixture was injected into the chromatographic system. Separation was performed on a Supelco C18 column, the mobile phase (14-3% THF, 31-7% TMAH buffer, 55% acetonitrile) was set at a flow rate of0-15mhmin_1. UV detection was performed at 232 nm. Ketoconazole was detected at 9-65 minutes, the internal standard was detected at 4-66 minutes. The figure annotations refer to the elution times (in minutes) of detected compounds. Peak areas of the internal standard (eluted at 4.66 minutes) and ketoconazole (eluted at 9.65 minutes) were reported as 633608 and 559201 respectively.

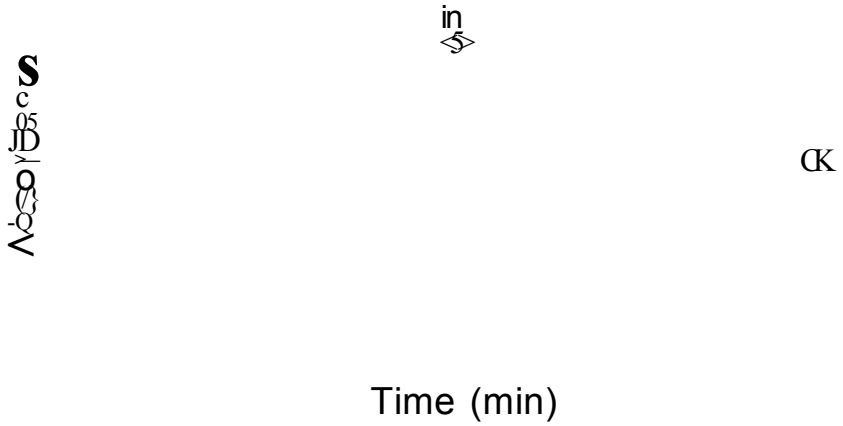

Figure 6.2: Chromatogram obtained from analysis of tape used to strip untreated tissue: The surface layer of porcine epidermal tissue was removed by stripping with sellotape. The tape was subsequently digested over 16 hours in an 80:20 mixture of acetonitrile and TEA buffer, containing tetahydroxybenzophenone as internal standard. 5/d of the digestion/extraction mixture was injected into the chromatographic system. Separation was performed on a Supelco C18 column, the mobile phase (14-3% THF, 31-7% TMAH buffer, 55% acetonitrile) was set at a flow rate ofO-15 ml-min-1. UV detection was performed at 232 nm The internal standard was detected at 4.66 minutes. No peaks were detected at around 9-6 minutes, indicating that no compounds were removed from the tissue or extracted from Sellotape that might have interfered with the determination of ketoconazole. The figure annotations refer to the elution times of detected compounds (in minutes). The peak area of the internal standard (eluted at 4.66 minutes) was reported as 604902.

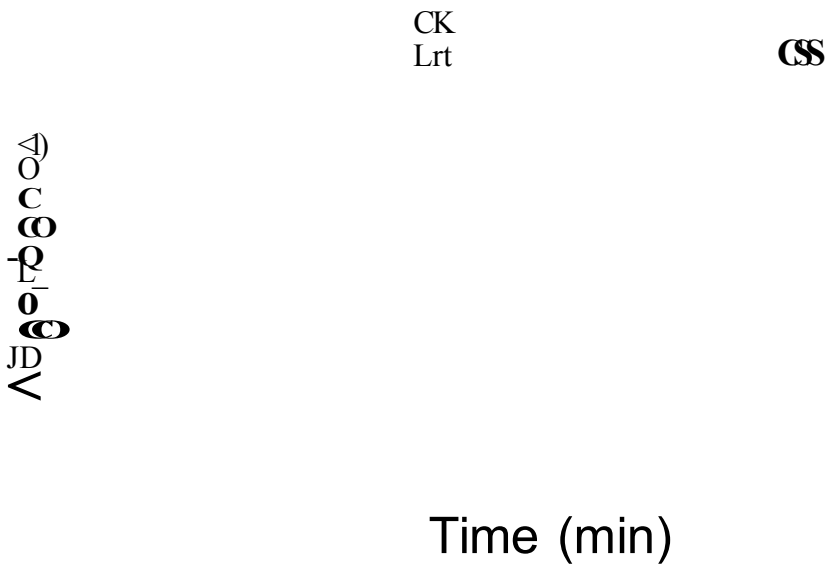

Figure 6.3: Chromatogram obtained from analysis of 100mg-ml-1 solution of keto-conazole (prepared in an 80:20 mixture of acetonitrile and TEA buffer, containing tetahydroxybenzophenone as internal standard). 5/d of the mixture was injected into the chromatographic system. Separation was performed on a Supelco C18 column, the mobile phase (14-3% THF, 31-7% TMAH buffer, 55% acetonitrile) was set at a flow rate of0*15ml*min_1. UV detection was performed at 232 nm, keto-conazole was detected at 9*50 minutes, the internal standard was detected at 4-59 minutes. The figure annotations refer to the elution times (in minutes) of detected compounds. Peak areas for the internal standard (eluted at 4.59 minutes) and keto-conazole (eluted at 9.50 minutes) were reported as 73081 and 478680 respectively.

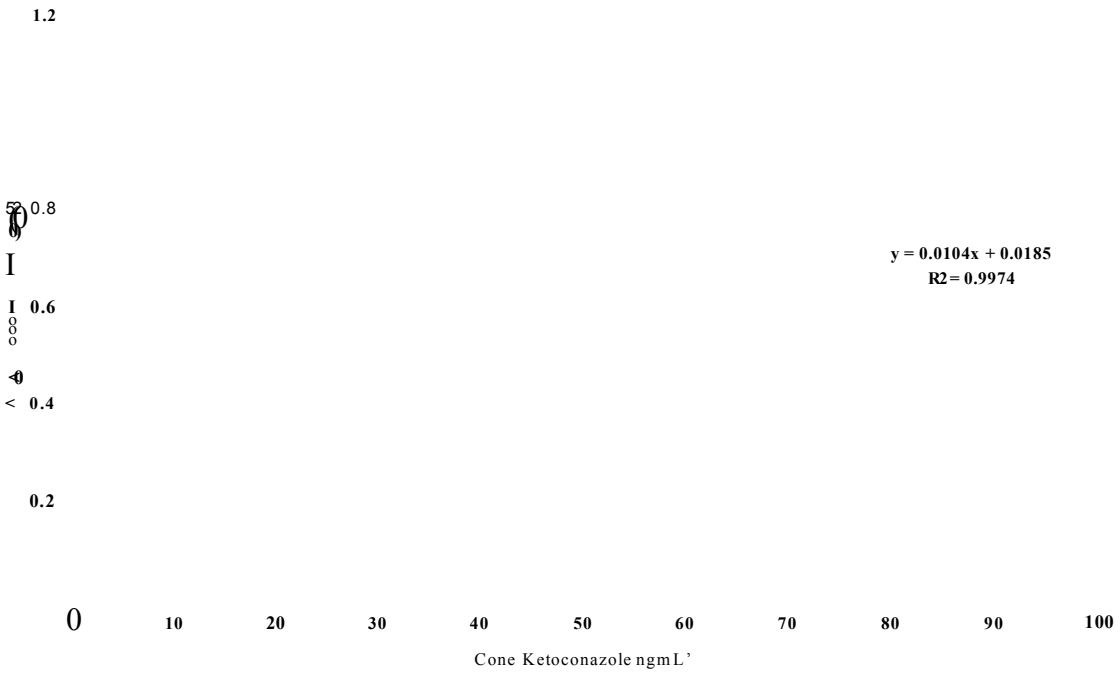

Figure 6.4: Calibration plot for the determination of ketoconazole (0—100//g-ml_1) by HPLC. Ketoconazole was prepared in an 80:20 mixture of acetonitrile and TEA buffer, containing lOO/rg-ml-1 tetrahydroxybenzophenone as an internal standard. Samples of 5*fi*\ were injected into the chromatographic system. Separation was performed on a Supelco C18 column, the mobile phase (14-3% THF, 31-7% TMAH buffer, 55% acetonitrile) was set at a flow rate of0-15 ml-min-1. UV detection was performed at 232 nm, ketoconazole was detected at 9-6 minutes, the internal standard was detected at 4*6 minutes. The ratio of peak areas of ketoconazole and the internal standard were plotted against concentration of ketoconazole *(y* —0.0104a; + 0.0185, r2 = 0 •9974).

calculated and compared to the expected value of 500 μg (100% extraction efficiency). The extraction efficiency of ketoconazole from tape was determined to be 65%. Concentrations presented in this chapter are adjusted to account for this efficiency, and thus all concentrations represent the theoretical value that would have been obtained given a 100% extraction efficiency.

In all cases within this chapter samples were injected in duplicate, and the mean value of the ratio of drug:internal standard in each solution was used in all subsequent calculations.

6.3.2 Determination of ketoconazole in porcine epidermal tissue by corneum tape stripping/HPLC

Analysis of previously-frozen porcine tissue was unsuccessful. No ketoconazole was detected in any of the tape strips. This is believed to be because freezing tissue alters the hydration properties of the skin surface [164], resulting in insufficient adherence of the tape to the tissue. Consequently, no stratum corneum was stripped from these samples. Thus in all experiments fresh porcine epidermal tissue was used for this phase of work.

A quantitative profile of ketoconazole in porcine epidermal tissue by corneum tape stripping/HPLC was prepared, as presented in Figure 6.5. The profile demonstrates the expected distribution of decreasing drug concentration with increasing strip number. The graph represents the mean of three experiments. All errors are presented on the graph.

6.3.3 Determination of ketoconazole in porcine epidermal tissue by corneum tape stripping/tissue blotting with analysis by MALDI-TOF-MS

Treated tissue was blotted onto matrix coated membranes following sequential tape stripping. For each imaged sample the total ion chromatogram (TIC) generated was summed to give a resultant 'averaged' spectra. Intensities of the protonated molecule of ketoconazole (m/z 531–533) and the sodium matrix adduct ion (m/z 212) were extracted. The calibration graph prepared previously for determination of ketoconazole (0-0·4 mg·ml^{-1}) by MALDI-TOF-MS (Figure 5.6, presented in Chapter 5) was used to relate the ratio of these two values to a concentration of ketoconazole.

Tape strip

Figure 6.5: A quantitative profile of ketoconazole in porcine epidermal tissue by tape stripping/HPLC analysis. Tetrahydroxybenzophenone was employed as the internal standard. The tape strip number provides a measure of relative depth within the skin.

Figure 6.6 shows a quantitative profile of ketoconazole in porcine epidermal tissue by corneum tape stripping/MALDI-TOF-MS. The profile represents the mean of three experiments. All errors are demonstrated on the graph. The profile shows the expected trend of diminishing concentration with increasing depth (strip number). However, there appears to be an increase in drug concentration between the surface blot, and the blot obtained after 5 strips. A similar fluctuation was observed in the quantitative profile obtained by MALDI imaging (Chapter 5, Figure 5.8). However, given that the data presented in this chapter does not give a measure of the true depth, it is not necessarily a comparable fluctuation.

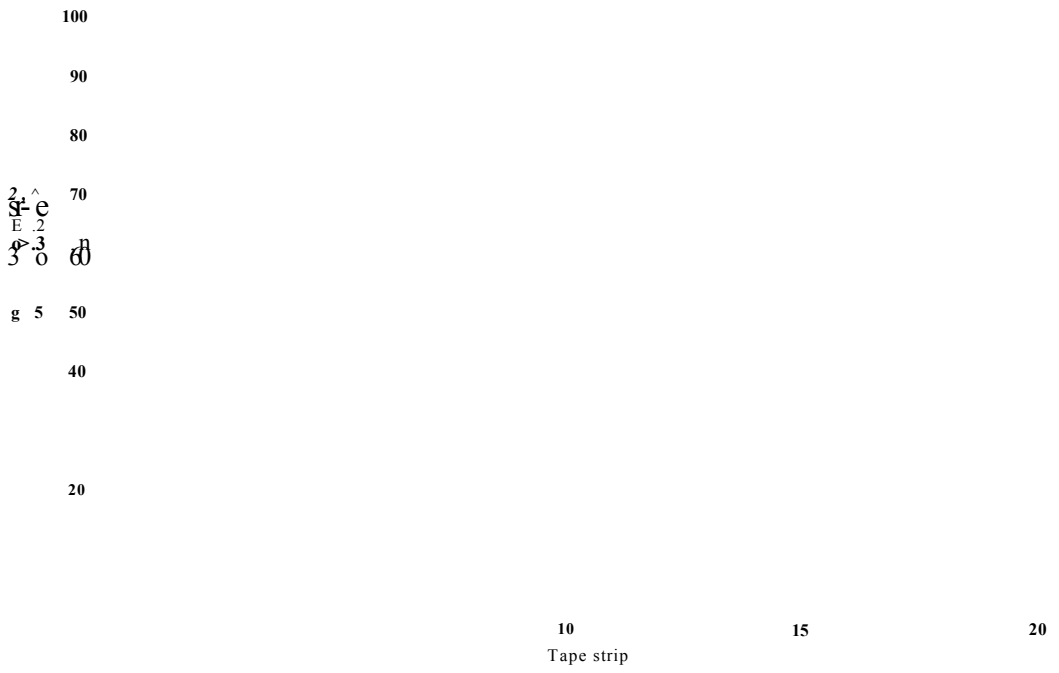

Figure 6.6: A quantitative profile of ketoconazole in porcine epidermal tissue by tape stripping/tissue blotting/ MALDI-MS analysis. Treated tissue was blotted onto matrix coated membranes following sequential tape stripping. Whole membranes were analysed by MALDI-MS. The ratio of drug:to matrix was calculated from the TIC file, and the calibration previously presented in Chapter 5 was used to relate this to an equivalent concentration of ketoconazole. Tape strip number provides a measure of relative depth within the skin.

Although both the HPLC and MALDI-TOF-MS tape stripping experiments show the expected trend of diminishing drug concentration with increasing depth and similar concentration ranges, the data has several limitations.

There are problems associated with the tape stripping technique itself. First, the stratum corneum can not be removed entirely by stripping; generally about one third of the layer will remain attached as 'islets' to the epidermal surface [146]. As a result, the corneocytes collected on one tape strip may have been derived from different depths, and may therefore have led to an ambiguous representation of drug concentration. Another major limitation of the technique is that any tape strip may remove different amounts of the stratum corneum at different depths and sites of the skin. To account for such variations, it is necessary to determine the tissue mass removed with each strip, for example by weighing the pieces of Sellotape before and after the stripping procedure. Evaluation of this parameter would also permit the relative depth associated with each tape strip to be calculated. Assuming that the stratum corneum density is constant ($1\,g/cm^3$) across its thickness, then these weights can be converted to volumes and, given that the area stripped is constant, to the stratum corneum thickness removed. This would enable a plot of concentration against relative depth.

It was found in this phase of work that limitations associated with balance sensitivity and issues due to static electricity prevented this assessment. However, given that the stripping procedure was normalised—and that the type and site of skin did not vary—the degrees of error are thought to be constant and therefore the strip number has been used as a measure of relative depth. In addition, all limitations associated with the tape stripping technique exist in both the HPLC and MALDI-MS experiments. Thus it was hoped that these experiments would have enabled a calculation of the efficiency of the tissue blotting procedure (efficiency of transfer of drug from tissue to membrane) presented throughout this thesis.

It is clear from observation of the two profiles that the MALDI-MS method (Figure 6.6) demonstrates considerably more error and variation than the HPLC method (Figure 6.5). Maximum errors observed in tape stripping/HPLC methods were about $\pm 5\%$ of the mean value, whereas errors of up to $\pm 18\%$ of the mean value are evident from the tape stripping-MALDI-MS experiments. However, this high degree of variation is only observed with the surface imprint and the imprint made after 5 tape strips. All other data points indicate errors comparable with the HPLC methods.

The source of this error in the MALDI-MS experiments is likely to be the blotting procedure, and these experiments highlight the need for this process to be standardised as this is likely to have enormous effect on the quantitative determination of drug from membranes. A form of mechanical 'press' that exerts a known pressure for a set length of time could be developed for further tissue blotting experiments. Significant errors observed from the surface imprint and that made after 5 tape strips may conversely be associated with erroneous MALDI determination of the drug in the presence of excess dosage. It was observed in Chapter 4 that, in some instances, suppression of matrix and analyte is observed in the presence of excess drug concentration or shampoo formulation. Repetition of the MALDI-MS experiments with a less concentrated tissue treatment would establish if this is a significant factor.

Although both methods demonstrated a similar range of ketoconazole concentration over 20 tape strips, the data collected did not permit a direct comparison of the methods. HPLC experiments involved a tissue treatment of 50 μl Nizoral (because tape could not be loaded with more than 50 μl formulation in the extraction efficiency experiments), whereas the MALDI-MS experiments involved tissue being treated with 500 μl Nizoral. One would therefore expect the MALDI-MS experiments to have demonstrated up to a ten-fold increase in drug concentration. The result obtained may therefore be explained by poor tissue blotting efficiency. Alternatively, it is possible that both concentrations fully saturated the diffusion capacity of the stratum corneum. The equilibrium constant of ketoconazole across the skin barrier would have to be calculated in order to answer this question. This could be done using Fick's second law of diffusion, but would require data on relative depth which was not obtained in this phase of work.

Tape stripping-tissue blotting-MALDI-MS experiments should be repeated with a tissue treatment of 50 μl Nizoral. Comparison of HPLC vs. MALDI profiles obtained may then allow calculation of the blotting efficiency.

It should also be noted that the MALDI concentration profiles presented in this chapter and Chapter 5, are calculated from a calibration of ketoconazole in solution, determined by spot analysis of samples prepared on stainless steel targets. It is expected that the ionisation properties of both the drug and matrix in the cellulose membrane may be different as compared to conventional spot analysis. Calibrations should be repeated by blotting tissue with a variety of known drug

concentrations and plotting the response of matrix:analyte against original concentration. A comparison of this data with the original calibration and a calibration of drug concentrations spotted into a matrix coated cellulose membrane would enable assessment of the following parameters:

1. The difference in ionisation efficiency of compounds prepared on stainless steel vs. cellulose;

2. The blotting, or transfer efficiency of drug from tissue to membrane.

Future work should also determine the relative depth associated with skin removed by each tape strip. This may enable tape stripping MALDI data to be used as a means of validating the profile prepared by imaging MALDI-MS, presented in Chapter 5 (Figure 5.6). This may also be achieved by sectioning treated skin to known depths by microtoming, removing for example 200 μm, 400 μm, 600 μm etc., and blotting the remaining tissue onto matrix-coated membranes. A drug concentration at each depth may be calculated from the TIC file and compared to the 'vertical' profile presented in Chapter 5.

6.4 Conclusions

An HPLC method was developed for the determination of ketoconazole recovered from tape used to strip porcine epidermal tissue. The optimal method demonstrated separation of both the analyte and internal standard from Sellotape matter. A calibration showing good linearity and precision (y =0·0104x+0·0185, r^2 =0·9974) was prepared for the quantitative determination of ketoconazole. The calibration was used to construct a quantitative profile of drug in skin, by plotting drug concentration against strip number. The profile demonstrated the expected trend of diminishing drug concentration with increasing strip number.

Tape-stripping methods were then employed in conjunction with tissue blotting/ MALDI-MS to construct a similar profile. Tissue imprints were created on matrix-coated membranes after every 5 tape strips. The concentration of ketoconazole on each membrane was estimated by relating the ratio of matrix:analye extracted from the TIC file to a calibration prepared from ketoconazole in solution.

Profiles obtained by the two methods exhibited similar trends of drug distribution, and similar concentration ranges. However, considerably larger errors were evident in the MALDI experiments. This is thought to have been due to variations in the blotting procedure and issues arising from ionisation of matrix and drug in the presence of excess formulation.

Profiles constructed by the two methods were not directly comparable due to variations in the tissue treatment. MALDI experiments involved a ten-fold increase in drug administered to the tissue surface, which was not reflected in the resulting profiles. It is predicted that only a fraction of drug present in tissue will be transferred to the membrane, which may account for a drug excess not being observed. However it is also possible that an equilibrium constant of drug in skin was achieved with both methods, due to an excess of shampoo being administered in each case.

An estimate of the amount of skin removed with each strip should be calculated to allow analysis of the change in concentration with relative depth. This in turn would permit comparison of the profiles with the that obtained by imaging MALDI-MS as presented in Chapter 5.

The tape stripping/ MALDI-MS experiments presented in this chapter should be repeated with a tissue treatment of 50 μl Nizoral, so that data may be compared to the HPLC methods developed in this phase of work.

Calibrations for the quantitative determination of ketoconazole should be repeated, so that concentrations are calculated from the MALDI response of drug:matrix from cellulose, rather than being related to the concentration of ketoconazole in solution.

In summary, while a successful and useful method of tape stripping/HPLC has been developed for permeation depth profiling ketoconazole in skin, further work is required in order to use this method to validate the MALDI-MS profiles presented in this thesis.

Chapter 7

Conclusions and Further Work

Methods for the analysis of drugs in skin by imaging MALDI-TOF-MS have been investigated in the work described in this thesis. Different approaches were evaluated in order to address key issues in imaging MALDI experiments, such as: direct vs. indirect analysis; substrates for indirect analysis; choice of matrix: layer homogeneity and application methods; analyte spreading and quantification. Tape stripping methods were developed as a strategy for the comparison of the optimised MALDI-TOF-MS method with HPLC analysis.

Initial work was conducted using a linear TOF mass spectrometer (Laser TOF 1500, SAI, Manchester), and involved selection of a suitable test analyte and a comparison of direct tissue analysis with the indirect analysis of tissue imprints created on a variety of substrates. Determination of aciclovir and piroxicam was unsuccessful, because poor mass accuracy and resolution made it diffucult to differentiate these compounds from interfering substances from the sample and matrix in the spectral region of interest. Similar problems were encountered by Reyzer *et al.* [100], where conventional MALDI-TOF methods failed to differentiate drug molecules in brain tissue from endogenous tissue molecules.

Ketoconazole was selected as a suitable analyte for the development of methods for the analysis of drugs in skin by imaging MALDI-MS. α-CHCA was found to be the most suitable matrix for the determination of ketoconazole, and deposition by electrospray.

Direct tissue analysis was unsuccessful due to problems associated with matrix crystallisation. The presence of an abundant and uniform matrix layer is essential in imaging methodology. The MALDI process is dependent on the formation of matrix

crystals, and the acquisition of useful MALDI images is dependent on the matrix layer being both abundant and homogeneous across the entire sample. An uneven matrix distribution may lead to ambiguous determination of the analyte within the samples: areas in an image or chromatogram indicating an absence of analyte must arise from true absence of analyte, rather than an insufficient matrix layer.

Chromatograms and spectra presented in Chapter 2 show that in the majority of samples no matrix was detected across the skin surface, and in these circumstances the drug molecule could not be detected. This is contrary to the findings of Caprioli *et al.* [101, 102], who presented successful determination of peptides and proteins in brain tissue coated in α-CHCA by electrospray. It is postulated in this thesis that the composition of different tissue types has a major effect on matrix crystallisation. The formation of matrix crystals, and the inclusion of analyte within crystals, is well documented to be adversely affected by salts [185]. Epidermal tissue is likely to contain a higher concentration of salts than brain tissue, which may explain the failure of this approach for this application.

Recent reports have demonstrated that sinapinic acid may be a more useful matrix material in imaging experiments, exhibiting superior crystalisation upon tissue surfaces as compared to a-CHCA [100, 113, 168]. In view of this, the direct analysis of drug treated skin was re-investigated in Chapter 3, employing sinapinic acid as the matrix material. Unfortunately the results obtained demonstrated a total absence of matrix material on the skin surface. This again implies that tissue type has a major effect on matrix crystallisation. It is therefore evident that the tissue type has a major effect on the suitability of different approaches in imaging applications. It is concluded that while direct tissue analysis has proved useful for the examination of brain tissue [100–103, 113, 168], it is not a desirable strategy for MALDI-MS imaging analysis of epidermal tissue.

A range of materials was evaluated as tissue blotting substrates for the indirect analysis of drug treated tissue. Tissue imprints were created upon C18 beads and C18 Envidisc, nitrocellulose, PVDF, cellulose and polyethylene-filled carbon conductive membranes. Tissue treatment was confined within a plastic ring adherent to the tissue surface in order to assess the usefulness of the techniques in retaining the expected spatial distribution of the analyte. There were problems blotting onto C18 beads because the beads became stuck to the tissue and were removed from

the MALDI target during the blotting procedure. It was also directly observed that matrix deposition caused movement of the beads around the target, resulting in determination of the analyte at erroneous locations. In addition, the matrix layer was found to be inhomogeneous, though this may have been due to the movement of matrix coated beads. Given the poor tissue imprint, movement of beads and poor matrix layer, C18 beads were not considered an appropriate substrate for this application. Similar problems were encountered with the C18 envidiscs, where C18 beads were observed on the tissue after the blotting procedure, implying creation of a poor tissue imprint. In addition the membranes were too thick to be mounted within the recess of the specialized MALDI targets, and it was therefore concluded that these were not suitable substrates.

The PVDF and nitrocellulose membranes behaved similarly. High analyte intensities were obtained, indicating that the membranes were ideal blotting substrates. However, chromatograms and spectra acquired demonstrated both an inhomogeneous matrix layer and evidence of analyte spreading. It was concluded that the waxy surface nature of these membranes resulted in matrix pooling due to hydrophobic repulsion of the matrix solvents, resulting in an uneven layer. Matrix movement across the membrane surface prior to solvent evaporation appeared to cause analyte speading.

More promising results were obtained with cellulose and carbon membranes. Spectra and chromatograms demonstrated sufficient matrix coverage of both substrates. Strong analyte intensities were achieved with both membranes, showing usefulness as blotting substrates. Some analyte spreading was evident upon carbon membranes, while chromatograms obtained from analysis of tissue imprinted cellulose revealed the expected distribution of the analyte molecule.

Scanning electron microspcopy of matrix coated membranes confirmed results obtained by MALDI-MS: matrix crystals appeared sparse on C18 envidiscs, nitrocellulose and PVDF membranes, while abundant matrix crystals could be formed on carbon and cellulose membranes.

These initial investigations demonstrated that there are three major issues that must be addressed in the design of a suitable approach for indirect tissue analysis by MALDI-MS. First, a successful tissue imprint must be created upon the substrate; second, a homogeneous matrix layer must be achieved; and finally, the method of

matrix application must avoid analyte spreading which would result in an incorrect display of the spatial distribution. Formation of a sufficient matrix layer appears to be greatly affected by the choice blotting substrate. Cellulose was found to be successful due to its absorbent nature, resulting in matrix drying in an even layer. Conversely the hydrophobicity of pvdf and nitrocellulose resulted in areas of matrix density, but also areas exhibiting a complete absence of crystals. The success of the carbon membranes is thought to be attributed to their conductive nature, resulting in superior electrospray performance, giving rise to an impressive crystal layer.

Initial work was hampered by poor mass accuracy and resolution of the linear TOF instrument, which was therefore deemed unsuitable for imaging. Work presented in Chapter 2 demonstrated that poor resolution resulted in failure to determine two out of three initial test compounds in the presence of interfering substances. In addition, fluctuations were observed in the mass determination of both ketoconazole and the matrix, which might have proved detrimental in an imaging experiment. Mass spectrometric images are simply a display of the distribution of a selected ion or range of ions; thus a poor image for the isotopic envelope of ketoconazole (m/z 531:533) would be obtained if ketoconazole was detected at m/z 530. Increasing the mass range displayed, e.g., m/z 529 – 534 to account for this would result in an image of poorer quality, as in the majority of cases m/z 529, 530 and 534 may not contribute many counts. Ambiguous mass determination may be partially explained by the axial geometry design of the instrument. Irregularities in sample topography result in differing flight times, resulting in erroneous mass determination. In addition the linear TOF employed only permitted analysis of a single 'row'. The sample plate could not be moved in x and y dimensions under the laser, thus no true images could be acquired. Consequently, despite having proved useful for initial method development, it was concluded that this instrument was not suitable for imaging analysis.

All subsequent MALDI-MS investigations were conducted on a hybrid quadrupole time of flight instrument (Qstar pulsar i, Applied Biosystems, Foster City, USA). Such an instrument configuration offered vast improvements in mass accuracy, resolution and sensitivity. In addition, the ion source was orthogonal to the detector. This decoupled arrangement is ideally suited to surface analysis as irregularities in sample topography have no effect on the length of flight, and thus no effect

on the calculated mass. Free movement of the sample plate in x and y locations meant that data could be acquired from whole membranes. The instrument was fitted with beta test ion imaging software (MDS Sciex, Ontario, Canada).

The first version of the software did not permit the images created to be saved, manipulated, or imported into commonly-used applications. The necessary data could however be exported from the total ion chromatogram. A computer algorithm was designed to convert spot numbers into x and y locations, permitting construction of images in alternative software. Images of the distribution of ketoconazole and α-CHCA on tissue imprinted cellulose membranes were constructed. Images revealed areas where analyte was not detected. Given that similar patterns were observed in images of matrix ions, this was concluded to be as a result of failures in the electrospray procedure. The images acquired highlighted the aforementioned importance of a homogeneous matrix layer. It was found that altering the intensity (z) scale of the images resulted in very different displays: it was difficult to display both qualitative and quantitative information in the same image. Thus it is important that the intensity of ions is always taken into account when assessing the presence and distribution of compounds of interest. There is an imporatnt caveat however: MALDI is not quantitative without some form of data normalisation. In Chapter 3, images were acquired demonstrating the superiority of matrix layer and analyte inclusion in electrospray sample deposition compared with the dried droplet method. Similar findings were presented by Garden *et al.* [126], who presented images of matrix heterogeneity in dried droplet samples.

The analysis of piroxicam and acyclovir was repeated using the Qstar pulsar i. The superior mass resolution of the hybrid instrument was demonstrated by the successful determination of both compounds. Ions associated with tape and matrix that proved problematic when employing the Linear TOF instrument were clearly resolved from the protonated analyte molecules. Comparison of the determination of ketoconazole with both instruments clearly demonstrated the improvements in mass accuracy and resolution offered by the Qstar pulsar i.

The mass determination of ketoconazole was evaluated across a membrane surface. The results obtained demonstrated that the mass did not vary significantly at different locations (as was observed using the LaserTOF 1500), demonstrating the advantages of an orthogonal ion source (as compared to an axial arrangement). The

hybrid instrumentation offered the possibility of tandem mass spectrometry, which was not employed in work presented in this thesis, but may be highly beneficial in further work, where an analyte may be imaged by mapping the dissociation of the compound, as demonstrated by Reyzer *et al.* [100]. In conclusion the results demonstrated the suitability of the Qstar pulsar *i* in imaging applications.

Ion imaging software updates (oMALDI 4.0, 2003) permitted free manipulation of the mass spectrometric images (e.g. image rotation, colour display and 3D representations). In addition all images created could be saved as picture files. The software employed in work presented in this thesis was released at the American Society for Mass Spectrometry annual conference (ASMS, Nashville, May 2004). Data and methods presented in this thesis were released as a technical applications note with the software. The technical note is included in Appendix 2 of this thesis.

MALDI-MS imaging was employed in work presented in Chapter 4 to assess the success of different methods of matrix application. Results presented in Chapters 2 and 3 suggested that blotting tissue onto cellulose and carbon membranes may be useful as an indirect method of imaging drugs in skin. The membranes were investigated further in work presented in Chapter 4. Membranes were coated in matrix by electrospray and airspray methodologies. Airspray was found to be the superior method, demonstrating a superior matrix layer on both membrane surfaces. This approach was also found to be considerably quicker and easier to perform. Aispray deposition has been presented as a method of matrix application in several recent reports [100, 113, 168].

The application of matrix to tissue imprinted membranes clearly resulted in undesirable analyte spreading. This again does not concur with the findings of Caprioli *et al.* , who presented images of the expected distribution of peptides on carbon conductive membranes (matrix was applied by electrospray deposition). The success of their experiments may be attributed to the electrostatic properties of the membrane, resulting in the proteins being 'anchored' to the substrate. This was not evident in the analysis of ketoconazole.

The novel method of precoating membranes in matrix prior to the blotting procedure was investigated. This approach was not found to be suitable for the analysis of carbon membranes, as matrix was removed from the substrate during the blotting procedure. The method was found to be ideal for the analysis of tissue imprinted

cellulose membranes. Images depicting the expected distribution of the analyte molecule were obtained. The author is not aware of any other reports of blotting tissue onto matrix-coated substrates in imaging MALDI.

The quantitative determination of ketoconazole ($0-0.4\,mg{\cdot}ml^{-1}$), employing the sodium adduct matrix ion as an internal standard was presented in Chapter 5. Relatively good linearity and precision was obtained. The use of matrix peaks as internal standards in MALDI experiments was first presented by Dally *et al.* [181]. This has enormous benefits in imaging experiments, making it unnecessary to incorporate additional compounds as internal standards. All quantitative determinations of ketoconazole by MALDI-TOF-MS presented in this thesis are equivalent to concentrations of ketoconazole in solution, as measured from analysis of the drug on a stainless steel target. Further work must be conducted in order to relate this to a true concentration of drug in skin. The blotting efficiency (transfer of drug from tissue to membrane) and a calibration of the determination of ketoconazole from cellulose must be determined in further work.

A cross sectional imprint of drug treated skin was made upon a matrix coated cellulose membrane. A 'quantitative' profile of ketoconazole in porcine epidermal tissue was prepared from the data obtained. Images demonstrating the spatial distribution of the drug molecule were obtained. These images were enlarged to reveal individual pixels. Data obtained from spectra relating to individual pixels permitted a calculation of the relative drug concentration at each location. This permitted construction of a profile indicating drug permeation up to 0.8 mm in the skin. Histological images of porcine ear epidermal tissue were prepared by conventional haemotoxylin and eosin staining methods. The histological image was superimposed upon the mass spectrometric image, demonstrating drug permeation up to and including the dermal skin layer. These experiments show the potential of MALDI imaging as a method of drug permeation depth profiling. Further work should be undertaken to investigate the permeation depth of the drug at different time points. In addition the absorption of different drugs must be explored.

A tape stripping method was developed in order to permit a comparison of tissue blotting/MALDI-MS methods with HPLC determination of ketoconazole. Corneum tape stripping with analysis by HPLC is a well-documented method and it was hoped that this phase of work would enable validation of the imaging strategies presented.

Drug profiles obtained by the two methods exhibited similar patterns of distribution and similar concentration ranges over 20 tape strips. Unfortunately there were limitations with the data collected that prevented a direct comparison of the two methods. Tissue was not treated with the same amount of drug in the two experiments. It is essential therefore that the tape stripping MALDI-MS experiments are repeated, with the same tissue treatment as administered in the HPLC experiments, in order to assess the utility and validity of the methods developed. As previously discussed, it is important that true drug concentrations on the cellulose membranes be determined and tissue blotting efficiency assessed. This would enable data collected by imaging MALDI-MS analysis of tissue imprinted cellulose membranes to be related to a true concentration of drug at different tissue depths.

Work presented in this thesis reveals that there are a variety of factors that influence the design and success of a MALDI imaging experiment. The tissue type under investigation determines whether direct or indirect analysis is the optimal approach. This is due to the ability to form a matrix layer on the sample. As discussed, formation of matrix crystals differs on different tissue types, which is possibly associated with their different salt contents. The choice of substrate for indirect analysis is governed by the feasibility of achieving a homogeneous matrix layer, which is probably the most important step in any imaging experiment. While some membranes are ideal blotting substrates and enhance mass spectral data quality [123–125], the failure to create an even layer of matrix upon them may result in unsuitability for imaging applications. The surface property of a membrane clearly has great effect upon matrix layer homogeneity. In addition other physical properties, such as electrical conductivity, affect the choice of matrix application method.

The method of matrix application depends upon both the substrate, and the analyte. For example, application of matrix onto peptide-imprinted carbon membranes did not induce analyte spreading [101,102]. This was not true for the analysis of drugs. Thus the solubility of the analyte in matrix solvents, and adherence of the analyte on substrate, should both affect experimental design. Whether the matrix is applied before or after the blotting procedure is dependent upon the substrate, and the matrix layer upon it. Blotting onto a matrix coated carbon membrane was not found to be successful. Conversely blotting onto a matrix coated cellulose membrane was found to be the optimum approach. Full impregnation of the membrane

with matrix was thought to be the reason for success of this strategy. Thus the matrix layer was not residual upon the membrane surface, and was therefore not removed during tissue blotting. In conclusion, matrix layer homogeneity and analyte speading caused by matrix deposition are the major issues in MALDI imaging.

Successful ionisation of an analyte in the absence of matrix material may therefore be the key to the greater success of the technique. Desorption/ionisation following a pulsed laser has been demonstrated on porous silicon (desorption/ionization on porous silicon, DIOS) [186,187]. Porous silicon is a UV-absorbing semiconductor with a large surface area and is produced through electrochemical anodization or chemical etching of crystalline silicon [188]. The structure of porous silicon provides a scaffold for retaining solvent and analyte molecules, and the UV absorptivity permits transfer of the laser energy to the analyte. The technique has demonstrated widespread use for the analysis of low molecular weight compounds, where interference from matrix ions in MALDI has often proved problematic. Further work is suggested to investigate the utility of such a substrate in imaging-MS. For this to be useful a successful tissue imprint must be achieved upon the silicon and the analyte must be ionized from the structure.

Anchoring or adhering the analyte to a substrate in imaging MALDI may also prove useful in preventing problems of migration associated with matrix application. Use of substrates or 'chips' with affinity for proteins is gaining widespread use in disease state profiling and analysis of proteins in complex mixtures. The technique, so called surface enhanced laser desorption ionization (SELDI), is described as combining sample clean up or enrichment with MALDI-TOF-MS [189–191]. A major advantage of such an approach is the elimination of possibly interfering compounds prior to mass spectral analysis. Following application of the complex sample to the target (which is coated with an active chemical surface (e.g. hydrophobic, hydrophilic, anionic or cationic), non-specifically bound matter is washed away prior to matrix application. Surfaces may also be prepared with antibodies to the analyte of interest offering enhanced sensitivity or specificity. It is postulated that blotting treated tissue onto such a surface may provide a means of reducing analyte spreading in imaging MALDI.

Appendix A: Other Applications

Methods presented in this thesis have been applied to the study of potato tuber and leaf sections, in collaboration with Professor Mike Burrell, University of Sheffield. The primary aim of this work was to acquire MALDI images of the distribution of endogenous molecules associated with primary metabolism in plants.

Materials

Trifluoroacetic acid (AR grade) and α-CHCA were purchased from Sigma-Aldrich (Dorset, UK). Methanol was HPLC grade, purchased from Fisher Scientific (Loughborough, UK). Cellulose membrane spacers were obtained from Goodfellow (Huntingdon, UK). The potato tuber and leaf sections were supplied and prepared by Professor Mike Burrell, at the University of Sheffield.

Instrumentation

Matrix application was conducted using a suction feed airspray device (Badger 150 Suction Feed air brush (The Air Brush Company, Lancing, West Sussex, UK)). Mass spectrometric analyses were performed on an Applied Biosystem Qstar pulsar i hybrid quadropole time of flight mass spectrometer, fitted with an orthogonal MALDI source and ion imaging software, as discussed in Chapter 3 of this thesis.

Methods

A cross section of potato tuber was prepared with a scalpel. A photo of the section is presented in Figure 7.1. The potato section was subsequently blotted onto a cellulose membrane, pre-coated in 25mg-ml_1 ct-CHCA (prepared in methanol containing 0.1% TFA) matrix material by airspray deposition. Methods for membrane preparation are given in Chapter 4 of this thesis.

Figure 7.1: Digital photograph of the potato tuber section that was blotted onto matrix coated cellulose membranes.

A cross section of potato leaf was also blotted onto a matrix coated cellulose membrane. The membranes were mounted in the recess of a specialised MALDI target (VoyagerDE, Sciex, Ontario) and analysed by imaging mass spectrometry in the Qstar pulsar *i*. Mass spectra were aquired every 0.25 mm. The laser was fired for 2 seconds at 14 *fi*J and a repetition rate of 20 Hz at all locations.

Results

MALDI images of the distribution of ions relating to the protonated molecules and sodium and potassium adducts of glucose,and glucose-6-phosphate were inconclusive. Images acquired indicated that the molecules were not present, or not successfully ionised. Standards of these molecules were analysed by conventional MALDI-TOF-MS on stainless steel spot targets, with α-CHCA. Analyses were performed on the Qstar pulsar *i*. No ions relating to the protonated molecules and sodium and potassium adducts of glucose or glucose-6-phosphate were detected. These results show that neither glucose nor glucose-6-phosphate can be determined by MALDI-TOF-MS with α-CHCA matrix material.

An image of the sodium adduct of sucrose in an imprint of potato tuber section (m/z 381) was obtained, presented in Figure 7.2. The image demonstrates that the distribution of sucrose was confined around the edge of the section, the outer cortex. The apparent 'outline' in the image showed good similarity to the shape of the section (Figure 7.1).

Examination of mass spectra corresponding to pixels in the image showed the presence of a peak at m/z 852. The range m/z 851–853 was processed in the ion imaging software. Images were created showing the distribution of this ion in imprints of potato leaf (Figure 7.3) and tuber (Figure 7.4) section. In both cases the images are a good anatomical fit of the original sections. The ion detected at m/z 852 ion is thought to be the sodium adduct of acetoacetyl-CoA, an intermediate in flavanoid biosyntheis and terpenoid metabolism. Further experiments should be conducted in order to permit confirmation of this identification. Product ion spectra from the precursor ion, m/z 852 by tandem mass spectrometry should be acquired.

Conclusions

Methods developed for the analysis of drugs in skin by imaging MALDI-TOF-MS have been successfully transferred to the study of endogenous small molecules in plant tissue.

Potato tuber and leaf sections were blotted onto cellulose membranes precoated in α-CHCA by airspray deposition. MALDI images showing the distribution of

Figure 7.2: MALDI image of the distribution of an ion observed at m/z 381. This is thought to be the potassium adduct of sucrose. A cross section of a potato tuber was blotted onto a cellulose membrane pre-coated in a-CHCA.

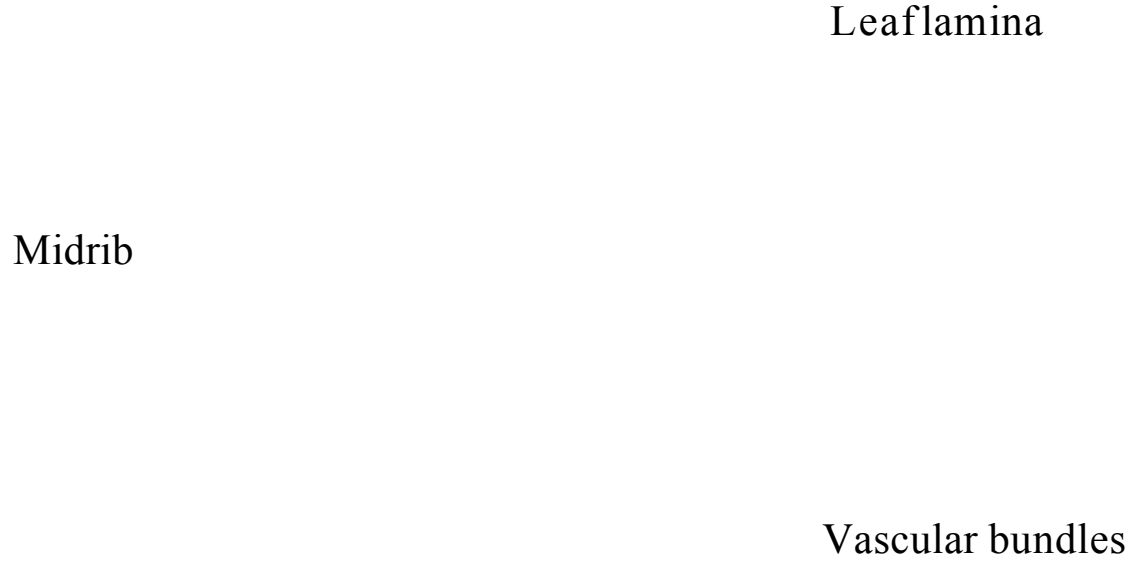

Figure 7.3: MALDI image of the distribution of an ion observed at m/z 852. This is thought to be the sodium adduct of aceto-acetyl-CoA. A cross section of a potato leaf was blotted onto a cellulose membrane pre-coated in a-CHCA.

Figure 7.4: MALDI image of the distribution of an ion observed at m/z 852. This is thought to be the sodium adduct of acetoacetyl-CoA. A cross section of a potato tuber was blotted onto a cellulose membrane pre-coated in a-CHCA.

sucrose and acetoacetyl-CoA (by mapping the potassium or sodium adducts respectively) were successfully acquired by this method. The images presented show good anatomical homology to the original tissue sections. Both molecules appear to be more dominant in the outer cortex of potato tubers. Acetoacetyl-CoA is observed most dominantly in the outer cortex of the tuber section, and in the vascular bundles of the leaf section.

Further work is recommended to explore the use of alternative matrices for the analysis of glucose and glucose-6-phosphate. Preliminary results obtained at Sheffield Hallam University indicate that THAP (containing 10% ammonium citrate) may be a useful matrix for the analysis of glucose-6-phosphate. This matrix has shown success for the analysis of other phosphate containing molecules, e.g., oligonucleotides. This should be investigated further and methods should be developed for imaging MALDI employing THAP (10% ammonium citrate).

Tandem mass spectrometry should be used to permit identification of the molecule detected at m/z 852.

This work shows that the methods developed in this thesis have widespread potential, showing success in mapping both drugs in skin, and molecules involved in primary metabolism in potato sections. Thus the technique may be useful in the study of both animal and plant tissues, with potential applications in many fields of research.

Appendix B

Presentations

Some of the work in this thesis has been published or presented as posters or talks at various conferences.

Publications

Bunch J, Clench MR, Richards DS. (2004) Determination of pharmaceutical compounds in skin by imaging matrix-assisted laser desorption ionisation mass spectrometry. *Rapid Communications in Mass Spectrometry*, 18: 3051–3060.

Oral presentations

The Analysis of Pharmaceutical Compounds in Skin by Imaging MALDI-TOF-MS. Royal Society of Chemistry Analytical Research Forum, University of Central Lancashire, 2004.

The Analysis of Low Molecular Weight Compounds in Animal and Plant Tissue by Imaging MALDI-TOF-MS. Applied Biosystems invited talk, American Society of Mass Spectrometry, Nashville, USA, 2004.

MALDI-MS Imaging to Reveal Metabolite Profiles in Potato Tubers. Society for Experimental Biology, Heriot Watt University, Edinburgh, 2004.

The Analysis of Low Molecular Weight Compounds in Biological Tissue by MALDI-TOF-MS. Royal Society of Chemistry Analytical Research Forum, University of

Sunderland, 2003.

Posters

The Analysis of Pharmaceutical Compounds in Biological Tissue was presented at:

The International Conference of Mass Spectrometry, Edinburgh, 2003

The American Society of Mass Spectrometry, Montreal, Canada, 2003

The British Society of Mass Spectrometry, Loughborough, 2002

Royal Society of Chemistry Analytical Research Forum, Kingston University, 2002.

Bibliography

[1] H.-D. Beckey. *Principles of field ionization and field desorption mass spectroscopy*, volume 61 of *International Series of Monographs in Analytical chemistry*. Pergamon Press, Oxford, 1977.

[2] M Barber, R.S. Bordoli, R.D. Sedgwick, and A.N. Tyler. Fast atom bombardment of solids as an ion source in mass spectroscopy. *Nature*, 293:270–275, 1981.

[3] R. D. Macfarlane and D. F. Torgerson. Californium-252 plasma desorption mass spectroscopy. *Science*, 191(4230):920–5, 1976.

[4] A. Benninghoven and W. K. Sichtermann. Detection, identification and structural investigation of biologically important compounds by secondary ion mass spectrometry. *Analytical Chemistry*, 50(8):1180–4, 1978.

[5] R. J. Cotter. Laser mass spectrometry: an overview of techniques, instruments and applications. *Analytica Chimica Acta*, 195:45–59, 1987.

[6] F. Hillenkamp, M. Karas, R. C. Beavis, and B. T. Chait. Matrix-assisted laser desorption/ionization mass spectrometry of biopolymers. *Analytical Chemistry*, 63(24):1193A–1203A, 1991.

[7] K. Tanaka, H. Waki, Y. Ido, S. Akita, Y. Yoshida, and T. Yoshida. Protein and polymer analyses up to m/z 100,000 by laser ionization time-of-flight mass spectrometry. *Rapid Communications in Mass Spectrometry*, 2(8):151–153, 1988.

[8] R. Zenobi and R. Knochenmuss. Ion formation in maldi mass spectrometry. *Mass Spectrometry Reviews*, 17(5):337–366, 1998.

[9] M. Karas and F. Hillenkamp. Laser desorption ionization of proteins with molecular masses exceeding 10,000 daltons. *Analytical Chemistry*, 60(20):2299–301, 1988.

[10] R. C. Beavis and B. T. Chait. Cinnamic acid derivatives as matrices for ultraviolet laser desorption mass spectrometry of proteins. *Rapid Communications in Mass Spectrometry*, 3:432–435, 1989.

[11] C. Eckerskorn, K. Strupat, D. Schleuder, D. Hochstrasser, J. C. Sanchez, F. Lottspeich, and F. Hillenkamp. Analysis of proteins by direct-scanning infrared-MALDI mass spectrometry after 2D-PAGE separation and electroblotting. *Analytical Chemistry*, 69(15):2888–92, 1997.

[12] A. Overberg, M. Karas, U. Bahr, R. Kaufmann, and F. Hillenkamp. Matrix-assisted infrared-laser (2.94 μm) desorption/ionization mass spectrometry of large biomolecules. *Rapid Communications in Mass Spectrometry*, 4:293–296, 1990.

[13] M. Baltz-Knorr, D. R. Ermer, K. E. Schriver, and Jr. Haglund, R. F. Infrared laser desorption and ionization of polypeptides from a polyacrylamide gel. *Journal of Mass Spectrometry*, 37(3):254–8, 2002.

[14] S.H. Bhattacharya, T.J. Raiford, and K. K. Murray. Infrared laser desorption/ionization on silicon. *Analytical Chemistry*, 74(9):2228–2231, 2002.

[15] J. Kim, K. Paek, and W. Kang. Visible surface-assisted laser desorption/ionization mass spectrometry of small macromolecules deposited on the graphite plate. *Bulletin of the Korean Chemical Society*, 23:315–319, 2002.

[16] S. Berkenkamp, C. Menzel, M. Karas, and F. Hillenkamp. Performance of infrared matrix-assisted laser desorption/ionization mass spectrometry with lasers emitting in the 3 μm wavelength range. *Rapid Communications in Mass Spectrometry*, 11(13):1399–1406, 1997.

[17] V. L. Talrose, M. D. Person, R. M. Whittal, F. C. Walls, A. L. Burlingame, and M. A. Baldwin. Insight into absorption of radiation/energy transfer in infrared matrix-assisted laser desorption/ionization: the roles of matrices, water and metal substrates. *Rapid Communications in Mass Spectrometry*, 13(21):2191–8, 1999.

[18] F. Kirpekar, S. Berkenkamp, and F. Hillenkamp. Detection of double-stranded DNA by IR- and UV-MALDI mass spectrometry. *Analytical Chemistry*, 71(13):2334–9, 1999.

[19] K. Strupat, J. Kampmeier, and V. Horneffer. Investigations of 2,5-DHB and succinic acid as matrices for UV and IR MALDI. Part II: Crystallographic and mass spectrometric analysis. *International Journal of Mass Spectrometry and Ion Processes*, 169-170:43–50, 1997.

[20] C.E. Costello, E. Nordhoff, and F. Hillenkamp. Matrix-assisted UV and IR laser desorption-ionization time-of-flight mass spectrometry of diamminoplatinum (II) Oligodeoxyribonucleotide adducts and their unplatinated analogs. *International Journal of Mass Spectrometry and Ion Processes*, 132:239–249, 1994.

[21] S. Niu, W. Zhang, and B. T. Chait. Direct comparison of infrared and ultraviolet wavelength matrix-assisted laser desorption/ionization mass spectrometry of proteins. *Journal of the American Society for Mass Spectrometry*, 9(1):1–7, 1998.

[22] B. Spengler, D. Kirsch, R. Kaufmann, and E. Jaeger. Peptide sequencing by matrix-assisted laser-desorption mass spectrometry. *Rapid Communications in Mass Spectrometry*, 6(2):105–8, 1992.

[23] R. C. Beavis, T. Chaudhary, and B. T. Chait. α-cyano-4-hydroxycinnamic acid as a matrix for matrix-assisted laser desorption mass spectrometry. *Organic Mass Spectrometry*, 27:156–158, 1992.

[24] K. Strupat, M. Karas, and F. Hillenkamp. 2,5-dihydroxybenzoic acid: a new matrix for laser desorption-ionization mass spectrometry. *International Journal of Mass Spectrometry and Ion Processes*, 111:89–102, 1991.

[25] T.M. Billeci and J.T. Stults. Tryptic mapping of recombinant proteins by matrix-assisted laser-desorption ionization mass-spectrometry. *Analytical Chemistry*, 65:1709–1716, 1992.

[26] M. Karas, H. Ehring, E. Nordhoff, B. Stahl, K. Strupat, F. Hillenkamp, M. Grehl, and B. Krebs. Matrix-assisted laser desorption/ionization mass spectrometry with additives to 2,5-dihydroxybenzoic acid. *Organic Mass Spectrometry*, 28:1476–1481, 1993.

[27] A. I. Gusev, W.R. Wilkinson, A. Proctor, and D.M. Hercules. Improvement of ion signal reproducibility and matrix/comatrix effects in MALDI analysis. *Analytical Chemistry*, 67:1034–1041, 1995.

[28] P. Juhasz, C. E. Costello, and K. Biemann. Matrix-assisted laser desorption ionization mass spectrometry with 2-(4- hydroxyphenylazo)benzoic acid matrix. *Journal of the American Society for Mass Spectrometry*, 4:399–409, 1993.

[29] F. Xiang and R. C. Beavis. In *Proceedings of The 42nd ASMS Conference on Mass Spectrometry and Allied Topics*, Chicago, IL, 1994.

[30] R. C. Beavis and B. T. Chait. Factors affecting the ultraviolet laser desorption of proteins. *Rapid Communications in Mass Spectrometry*, 3:233, 1989.

[31] K.J. Wu, Steding A., and Becker C.H. Matrix-assisted laser desorption time-of-flight mass spectrometry of oligonucleotides using 3-hydroxypicolinic acid as an ultraviolet-sensitive matrix. *Rapid Communications in Mass Spectrometry*, 7:142–146, 1993.

[32] U Pieles, W Zurcher, M Schar, and HE Moser. Matrix-assisted laser desorption ionization time-of-flight mass spectrometry: a powerful tool for the mass and sequence analysis of natural and modified oligonucleotides. *Nucleic Acids Research*, 21(14):3191–3196, 1993.

[33] P. Lecchi, H.M. Le, and L.K. Pannell. 6-aza-2-thiothymine: a matrix for MALDI spectra of oligonucleotides. *Nucleic Acids Research*, 23:1276–1277, 1995.

[34] F. Song. Quinaldic acid as a new matrix for matrix-assisted laser desorption/ionization of nucleic acids. *Rapid Communications in Mass Spectrometry*, 17(15):1802–7, 2003.

[35] R.A. Dwek, C.J. Edge, D. J. Harvey, M.R. Wormald, and R.B. Parekh. Analysis of glycoprotein-associated oligosaccharides. *Annual Review of Biochemistry*, 62:65–100, 1993.

[36] P. O. Danis and D. E. A. Karr. Facile sample preparation for the analysis of synthetic polymers by matrix-assisted laser desorption/ionization. *Organic Mass Spectrometry*, 28:923–925, 1992.

[37] M. Mank, B. Stahl, and G. Boehm. 2,5-dihydroxybenzoic acid butylamine and other ionic liquid matrixes for enhanced maldi-ms analysis of biomolecules. *Analytical Chemistry*, 76(10):2938–50, 2004.

[38] E. Nordhoff, R. Cramer, M. Karas, F. Hillenkamp, F. Kirpekar, K. Kristiansen, and P. Roepstorff. Ion stability of nucleic acids in infrared matrix-assisted laser desorption/ionization mass spectrometry. *Nucleic Acids Research*, 21(15):3347–57, 1993.

[39] Y. Dai, R. M. Whittal, and L. Li. Confocal fluorescence microscopic imaging for investigating the analyte distribution in MALDI matrices. *Analytical Chemistry*, 68:2494–2500, 1996.

[40] M. P. Balogh. Debating resolution and mass accuracy in mass spectrometry. *Spectroscopy*, 19(10):34–40, 2004.

[41] S.R. Weinberger, K.O. Boernsen, J.W. Finchy, V. Roberstson, and B.D. Musselman. An evaluation of crystallization for matrix-assisted, laser desorption/ionization of proteins. In *Proceedings of the 41st Annual ASMS Conference on Mass Spectrometry and Allied Topics*, volume 41, page 775a, San Francisco, 1993.

[42] F. Xiang and R. C. Beavis. A method to increase contaminant tolerance in protein MALDI by the fabrication of thin protein-doped polycrystalline films. *Rapid Communications in Mass Spectrometry*, 8:199–204, 1994.

[43] Y. Dai, R. M. Whittal, L. Li, and S. R. Weinberger. Accurate mass measurement of oligonucleotides using a time-lag focusing matrix-assisted laser desorption/ionization time-of-flight mass spectrometer. *Rapid Communications in Mass Spectrometry*, 10(14):1792–6, 1996.

[44] O. Vorm and M. Mann. Improved mass accuracy in matrix-assisted laser desorption/ionization time-of-flight mass spectrometry of peptides. *Journal of the American Society for Mass Spectrometry*, 5:955–958, 1994.

[45] Y. Dai, R. M. Whittal, and L. Li. Two-layer sample preparation: a method for maldi-ms analysis of complex peptide and protein mixtures. *Analytical Chemistry*, 71(5):1087–91, 1999.

[46] A. J. Nicola, A. I. Gusev, A. Proctor, E. K. Jackson, and D. M. Hercules. Application of the fast-evaporation sample preparation method for improving quantification of angiotensin ii by matrix-assisted laser desorption/ionization. *Rapid Communications in Mass Spectrometry*, 9(12):1164–71, 1995.

[47] R.D. Edmonson and D. H. Russell. Evaluation of MALDI-TOF mass measurement accuracy by using delayed extraction. *Journal of the American Society for Mass Spectrometry*, 7:995, 1996.

[48] P. Onnerfjord, S. Ekstrom, J. Bergquist, J. Nilsson, T. Laurell, and G. Marko-Varga. Homogeneous sample preparation for automated high throughput analysis with matrix-assisted laser desorption/ionisation time-of-flight mass spectrometry. *Rapid Communications in Mass Spectrometry*, 13(5):315–22, 1999.

[49] L. Li, R.E. Golding, and R. M. Whittal. Analysis of single mammalian cell lysates by mass spectrometry. *Journal of the American Chemical Society*, 118(11662-11663), 1996.

[50] I.K. Perera, J. Perkins, and S Kantartzogoulou. Spin-coated samples for high resolution matrix assisted laser desorption/ionization time-of-flight mass spectrometry of large proteins. *Rapid Communications in Mass Spectrometry*, 9:180–187, 1995.

[51] R. Skelton, F. Dubois, and R. Zenobi. A maldi sample preparation method suitable for insoluble polymers. *Analytical Chemistry*, 72(7):1707–10, 2000.

[52] S. Zhao, K.V. Somayajula, A. G. Sharkey, D. M. Hercules, F. Hillenkamp, M. Karas, and A. Ingendoh. Novel method for matrix-assisted laser mass-spectrometry of proteins. *Analytical Chemistry*, 63:450–453, 1991.

[53] T-W. Chan, A.W. Colburn, and P.J. Derrick. Suppression of matrix-ions in ultraviolet laser desorption: Scanning electron microscopy and raman spectroscopy of the solid sample. *Organic Mass Spectrometry*, 27:53–56, 1992.

[54] M. Dale, R. Knochenmuss, and R. Zenobi. Graphite/liquid mixed matrices for laser desorption/ionization mass spectrometry. *Analytical Chemistry*, 68:3321, 1996.

[55] J. Sunner, E. Dratz, and Y. C. Chen. Graphite surface-assisted laser desorption/ionization time-of-flight mass spectrometry of peptides and proteins from liquid solutions. *Analytical Chemistry*, 67(23):4335–42, 1995.

[56] M. Schurenberg, K. Dreisewerd, and F. Hillenkamp. Laser desorption/ionization mass spectrometry of peptides and proteins with particle suspension matrices. *Analytical Chemistry*, 71:221–229, 1999.

[57] T.P. Eric, T.W. Sze, D. Chan, and G. Wang. Formulation of matrix solutions for use in MALDI of biomolecules. *Journal of the American Society for Mass Spectrometry*, 9:166–174, 1998.

[58] R. R. Hensel, R. C. King, and K. G. Owens. Electrospray sample preparation for improved quantitation in matrix-assisted laser desorption/ionization time-of-flight mass spectrometry. *Rapid Communications in Mass Spectrometry*, 11(16):1785–93, 1997.

[59] S. Hanton, P. Clark, and K Owens. Investigations of MALDI sample preparation by TOF SIMS. *Journal of The American Society for Mass Spectrometry*, 10:104–111, 1999.

[60] J. Axelsson, A-M. Hoberg, C. Waterson, P. Myatt, G.L. Chield, J. Varney, D.M. Haddleton, and J. Derrick. Improved reproducibility and increased signal intensity in maldi as a result of electrospray sample preparation. *Rapid Communications in Mass Spectrometry*, 11:209–213, 1997.

[61] D.M. Haddleton, C. Waterson, and P.J. Derrick. Comment: A simple low-cost method of sample preparation for improved quantitative matrix-assisted laser desorption/ionisation mass spectrometry: Air-spray sample deposition for matrix-assisted laser desorption/ionisation mass spectrometry of derivatised poly(ethylene glycol). *European Mass Spectrometry*, 4:203–207, 1998.

[62] J. Yao, J. R. Scott, M. K. Young, and C. L. Wilkins. Importance of matrix:analyte ratio for buffer tolerance using 2,5-dihydroxybenzoic acid as a matrix in matrix-assisted laser desorption/ionization-fourier transform mass spectrometry and matrix-assisted laser desorption/ionization-time of flight. *Journal of the American Society for Mass Spectrometry*, 9(8):805–13, 1998.

[63] R. Knochenmuss, A. Stortelder, K. Breuker, and R. Zenobi. Secondary ion-molecule reactions in matrix-assisted laser desorption/ionization. *Journal of Mass Spectrometry*, 35(11):1237–45, 2000.

[64] K. Breuker and F. W. McLafferty. Native electron capture dissociation for the structural characterization of noncovalent interactions in native cytochrome c. *Angewandte Chemie, International Edition in English*, 42(40):4900–4, 2003.

[65] E. Lehmann, R. Knochenmuss, and R. Zenobi. Ionization mechanisms in matrix-assisted laser desorption/ionization mass spectrometry: contribution of pre-formed ions. *Rapid Communications in Mass Spectrometry*, 11(14):1483–1492, 1997.

[66] P.-C. Liao and J. Allison. Ionization processes in matrix-assisted laser desorption/ionization mass spectrometry: matrix-dependent formation of $[M+H]^+$ and $[M+Na]^+$ ions of small peptides and some mechanistic comments. *Journal of Mass Spectrometry*, 30:408–423, 1995.

[67] S. Bourcier, S. Bouchonnet, and Y. Hoppilliard. Ionization of 2,5–dihydroxybenzoic acid (DHB) matrix-assisted laser desorption ionization experiments and theoretical study. *International Journal of Mass Spectrometry*, 211:59–69, 2001.

[68] D.A. Allwood, P.E. Dyer, and R.W. Dreyfus. Ionization modelling of matrix molecules in ultraviolet matrix-assisted laser desorption/ionization. *Rapid Communications in Mass Spectrometry*, 11(5):499–503, 1997.

[69] V. Karbach and R. Knochenmuss. Do single matrix molecules generate primary ions in ultraviolet matrix-assisted laser desorption/ionization. *Rapid Communications in Mass Spectrometry*, 12(14):968–974, 1998.

[70] K.L. Busch. Desorption-ionization mass spectrometry. *Journal of Mass Spectrometry*, 30:230–240, 1995.

[71] K. Breuker, R. Knochenmuss, and R. Zenobi. Gas-phase basicities of deprotonated matrix-assisted laser desorption/ionization matrix molecules. *International Journal of Mass Spectrometry*, 184(1):25–38, 1999.

[72] R. Knochenmuss, V. Karbach, U Wiesli, K. Breuker, and R. Zenobi. The matrix suppression effect in matrix-assisted laser desorption/ionization: application to negative ions and further characteristics. *Rapid Communications in Mass Spectrometry*, 12(9):529–534, 1998.

[73] H. Ehring, M. Karas, and F. Hillenkamp. Role of photoionization and photochemistry in ionization processes of organic-molecules and relevance for matrix-assisted laser desorption ionization mass-spectrometry. *Organic Mass Spectrometry*, 27:472, 1992.

[74] R. Lidgard and M.W. Duncan. Utility of MALDI-TOF mass spectrometry for the analysis of low molecular weight compounds. *Rapid Communications in Mass Spectrometry*, 9:128–132, 1995.

[75] M. Karas, M. Gluckmann, and J. Schafer. Ionization in matrix-assisted laser desorption/ionization: singly charged molecular ions are the lucky survivors. *Journal of Mass Spectrometry*, 35(1):1–12, 2000.

[76] A Vertes and R.D. Levine. Sublimation vs. fragmentation in matrix assisted laser desorption. *Chemical Physics Letters*, 171:284–290, 1990.

[77] R.E. Johnson and B.U.R. Sundquist. Laser-pulse ejection of organic molecules from a matrix—lessons from fast-ion-induced ejection. *Rapid Communications in Mass Spectrometry*, 5:574–578, 1991.

[78] K. Dreisewerd, M. Schurenberg, M. Karas, and F. Hillenkamp. Influence of the laser intensity and spot size on the desorption of molecules and ions in matrix-assisted laser desorption/ionization with a uniform beam profile. *International Journal of Mass Spectrometry and Ion Processes*, 14:127–148, 1995.

[79] M. Schurenberg, K. Dreiswerd, S. Kamanabrou, and F. Hillenkamp. Influence of the sample temperature on the desorption of matrix molecules and ions in matrix-assisted laser desorption ionization. *International Journal of Mass Spectrometry and Ion Processes*, 172(1):89–94, 1998.

[80] W.C. Wiley and I.H. McLaren. Time-of-flight mass spectrometer with improved resolution. *Review of Scientific Instruments*, 26:1150–1157, 1955.

[81] S. Alves, M. Kalberer, and R. Zenobi. Direct detection of particles formed by laser ablation of matrices during matrix-assisted laser desorption/ionization. *Rapid Communications in Mass Spectrometry*, 17(18):2034–8, 2003.

[82] R. S. Brown and J. J. Lennon. Mass resolution improvement by incorporation of pulsed ion extraction in a matrix-assisted laser desorption/ionization linear time-of-flight mass spectrometer. *Analytical Chemistry*, 67(13):1998–2003, 1995.

[83] M.L. Vestal, P. Juhasz, and S.A. Martin. Delayed extraction matrix assisted laser desorption time of flight mass spectrometry. *Rapid Communications in Mass Spectrometry*, 9:1044–1050, 1995.

[84] A. N. Krutchinsky, W. Zhang, and B. T. Chait. Rapidly switchable matrix-assisted laser desorption/ionization and electrospray quadrupole-time-of-flight mass spectrometry for protein identification. *Journal of the American Society for Mass Spectrometry*, 11(6):493–504, 2000.

[85] K. F. Medzihradszky, J. M. Campbell, M. A. Baldwin, A. M. Falick, P. Juhasz, M. L. Vestal, and A. L. Burlingame. The characteristics of peptide collision-induced dissociation using a high-performance MALDI-TOF/TOF tandem mass spectrometer. *Analytical Chemistry*, 72(3):552–8, 2000.

[86] L. Pasa-Tolic, P.K. Jensen, G.A. Anderson, M.S. Lipton, K.K. Peden, S. Martinovic, N. Tolic, J.E. Bruce, and R.D. Smith. High throughput proteome-wide precision measurements of protein expression using mass spectrometry. *Journal of the American Chemical Society*, 121:7949–7950, 1999.

[87] D. R. Goodlett, J. E. Bruce, G. A. Anderson, B. Rist, L. Pasa-Tolic, O. Fiehn, R. D. Smith, and R. Aebersold. Protein identification with a single accurate mass of a cysteine-containing peptide and constrained database searching. *Analytical Chemistry*, 72(6):1112–8, 2000.

[88] M. Guilhaus, D. Selby, and V. Mlynski. Orthogonal acceleration time-of-flight mass spectrometry. *Mass Spectrometry Reviews*, 19(2):65–107, 2000.

[89] J. A. Loo, J. Brown, G. Critchley, C. Mitchell, P. C. Andrews, and R. R. Ogorzalek Loo. High sensitivity mass spectrometric methods for obtaining intact molecular weights from gel-separated proteins. *Electrophoresis*, 20(4-5):743–8, 1999.

[90] Y. Oda, K. Huang, F. R. Cross, D. Cowburn, and B. T. Chait. Accurate quantitation of protein expression and site-specific phosphorylation. *Proceedings of the National Academy of Sciences of the United States of America*, 96(12):6591–6, 1999.

[91] D. B. Wall, M. T. Kachman, S. Gong, R. Hinderer, S. Parus, D. E. Misek, S. M. Hanash, and D. M. Lubman. Isoelectric focusing nonporous RP HPLC: a two-dimensional liquid-phase separation method for mapping of cellular proteins with identification using MALDI-TOF mass spectrometry. *Analytical Chemistry*, 72(6):1099–111, 2000.

[92] M.L. Pachowlski and N. Winograd. Imaging with mass spectrometry. *Chemical Reviews*, 99(10):2977–3055, 1999.

[93] T. L. Colliver, C. L. Brummel, M. L. Pacholski, F. D. Swanek, A. G. Ewing, and N. Winograd. Atomic and molecular imaging at the single-cell level with TOF-SIMS. *Analytical Chemistry*, 69(13):2225–31, 1997.

[94] R. Zenobi. In situ analysis of surfaces and mixtures by laser desorption mass spectrometry. *International Journal of Mass Spectrometry and Ion Processes*, 145(1-2):51–77, 1995.

[95] F. Hillenkamp and H. Ehring. Laser desorption mass spectrometry. Part I: Basic mechanisms and techniques. In M.L. Gross, editor, *Mass Spectrometry in the Biological Sciences: A Tutorial*, NATO Science Series: C: Mathematical and Physical Sciences (continued within NATO Science Series II: Mathematics, Physics and Chemistry). Kluwer Academic, Dordrecht, 1991.

[96] L. van Vaeck, H. Struyf, W. van Roy, and F. Adams. Organic and inorganic analysis with laser microprobe mass spectrometry. Part 1: Instrumentation and methodology. *Mass Spectrometry Reviews*, 13:189–209, 1994.

[97] L. van Vaeck, H. Struyf, W. van Roy, and F. Adams. Organic and inorganic analysis with laser microprobe mass spectrometry. Part 2: Applications. *Mass Spectrometry Reviews*, 13:209–232, 1994.

[98] P. J. Todd, T. G. Schaaff, P. Chaurand, and R. M. Caprioli. Organic ion imaging of biological tissue with secondary ion mass spectrometry and matrix-assisted laser desorption/ionization. *Journal of Mass Spectrometry*, 36(4):355–69, 2001.

[99] F. J. Troendle, C.D. Reddick, and R.A. Yost. Detection of pharmaceutical compounds in tissue by matrix-assisted laser desorption/ionization and laser desorption/chemical ionization tandem mass spectrometry with a quadrupole ion trap. *Journal of the American Society for Mass Spectrometry*, 10(12):1315–1321, 1999.

[100] M. L. Reyzer, Y. Hsieh, K. Ng, W. A. Korfmacher, and R. M. Caprioli. Direct analysis of drug candidates in tissue by matrix-assisted laser desorption/ionization mass spectrometry. *Journal of Mass Spectrometry*, 38(10):1081–92, 2003.

[101] R. M. Caprioli, T. B. Farmer, and J. Gile. Molecular imaging of biological samples: localization of peptides and proteins using MALDI-TOF MS. *Analytical Chemistry*, 69(23):4751–60, 1997.

[102] P. Chaurand, M. Stoeckli, and R. M. Caprioli. Direct profiling of proteins in biological tissue sections by MALDI mass spectrometry. *Analytical Chemistry*, 71(23):5263–70, 1999.

[103] M. Stoeckli, P. Chaurand, D. E. Hallahan, and R. M. Caprioli. Imaging mass spectrometry: a new technology for the analysis of protein expression in mammalian tissues. *Nature Medicine*, 7(4):493–6, 2001.

[104] M. Stoeckli, D. Staab, M. Staufenbiel, K. H. Wiederhold, and L. Signor. Molecular imaging of amyloid beta peptides in mouse brain sections using mass spectrometry. *Analytical Biochemistry*, 311(1):33–9, 2002.

[105] L. Signor, G. Rovelli, D. Stauffer, M. Abramowski, M. Stauffenbiel, and M. Stoeckli. Profling, quantitation and imaging of amyloid-beta (Aβ) peptides in biological samples by MALDI mass spectrometry. In *Proceedings of the 16th International Mass Spectrometry Conference*, Edinburgh, U.K., 2003.

[106] A. Nilsson, J. L. Norris, H. R. Aerni, P. Svenningsson, R. M. Caprioli, and P. E. Andrén. Analyzing differential protein expression in experimental Parkinson's Disease using imaging MALDI MS. In *Proceedings of the 52nd Annual ASMS Conference on Mass Spectrometry and Allied Topics, Nashville, TN.*, page 71, 2004.

[107] J. Pierson, J. L. Norris, H. R. Aerni, P. Svenningsson, R. M. Caprioli, and P. E. Andren. Molecular profiling of experimental Parkinson's disease: direct analysis of peptides and proteins on brain tissue sections by MALDI mass spectrometry. *Journal of Proteome Research*, 3(2):289–95, 2004.

[108] P. Chaurand, B. B. DaGue, R. S. Pearsall, D. W. Threadgill, and R. M. Caprioli. Profiling proteins from azoxymethane-induced colon tumors at the molecular level by matrix-assisted laser desorption/ionization mass spectrometry. *Proteomics*, 1(10):1320–6, 2001.

[109] S. A. Schwartz, R. J. Weil, M. D. Johnson, S. A. Toms, and R. M. Caprioli. Protein profiling in brain tumors using mass spectrometry: feasibility of a new technique for the analysis of protein expression. *Clinical Cancer Research*, 10(3):981–7, 2004.

[110] A. C. Crecelius, B. Williams, L. Xia, D. S. Cornett, B. Dawant, R. Bodenheimer, M. Lepage, K. J. Niermann, and R. M. Caprioli. Reconstructing and visualizing protein distributions in 3D by imaging MALDI MS. In *Proceedings of the 52nd Annual ASMS Conference on Mass Spectrometry and Allied Topics, Nashville, TN.*, page 71, 2004.

[111] R. Kruse and J. V. Sweedler. Spatial profiling invertebrate ganglia using MALDI MS. *Journal of the American Society for Mass Spectrometry*, 14(7):752–9, 2003.

[112] B. J. Xu, R. M. Caprioli, M. E. Sanders, and R. A. Jensen. Direct analysis of laser capture microdissected cells by MALDI mass spectrometry. *Journal of the American Society for Mass Spectrometry*, 13(11):1292–7, 2002.

[113] S. A. Schwartz, M. L. Reyzer, and R. M. Caprioli. Direct tissue analysis using matrix-assisted laser desorption/ionization mass spectrometry: practical aspects of sample preparation. *Journal of Mass Spectrometry*, 38(7):699–708, 2003.

[114] A. I. Gusev, A. Proctor, Y.I. Rabinovich, and D. M. Hercules. Thin-layer chromatography combined with matrix-assisted laser desorption/ionization mass spectrometry. *Analytical Chemistry*, 67:1805, 1995.

[115] A. I. Gusev. Imaging of thin-layer chromatograms using matrix-assisted laser desorption/ionization mass specrometry. *Analytical Chemistry*, 67(24):4565–4570, 1995.

[116] S. Mowthorpe, M. Clench, A. Cricelius, D. Richards, V. Parr, and L.W. Tetler. Matrix-assisted laser desorption/ionisation time-of-flight/thin layer chromatography/mass spectrometry— a rapid method for impurity testing. *Rapid Communications in Mass Spectrometry*, 13(4):264–270, 1999.

[117] J. Guittard, X.L. Hronowski, and C.E. Costello. Direct matrix-assisted laser desorption/ionization mass spectrometric analysis of glycosphingolipids on thin layer chromatographic plates and transfer membranes. *Rapid Communications in Mass Spectrometry*, 13(18):1838–1849, 1999.

[118] A . Crecelius, M.R. Clench, D.S. Richards, and V. Parr. Quantitative determination of piroxicam by TLC-MALDI TOF ms. *Journal of Pharmaceutical and Biomedical Analysis*, 35:31–39, 2004.

[119] J. Bunch, M. Burrell, and M.R. Clench. Maldi imaging to reveal metabolite profiles in potato tubers. *Comparative Biochemistry and Physiology Part A*, 137:S149, 2004.

[120] H. R. Aerni, D. S. Cornett, P. Chaurand, K. Suzuki, M. C. Orgebin-Crist, T. Daikoku, S. K. Dey, and R. M. Caprioli. Automated sample preparation for MALDI imaging MS. In *Proceedings of the 52nd Annual ASMS Conference on Mass Spectrometry and Allied Topics*, Nashville, TN., 2004.

[121] E.J. Zaluzec, D.A. Gage, J. Allison, and J.T. Watson. Direct matrix-assisted laser desorption ionization mass spectrometric analysis of proteins immobilized on nylon-based membranes. *Journal of The American Society for Mass Spectrometry*, 5:230–237, 1994.

[122] D. Schleuder, F. Hillenkamp, and K. Strupat. IR-MALDI-mass analysis of electroblotted proteins directly from the membrane: comparison of different membranes, application to on-membrane digestion, and protein identification by database searching. *Analytical Chemistry*, 71(15):3238–47, 1999.

[123] L. M. Preston, K. K. Murray, and D. H. Russell. Reproducibility and quantitation of matrix-assisted laser desorption ionization mass spectrometry: effects of nitrocellulose on peptide ion yields. *Biological Mass Spectrometry*, 22(9):544–50, 1993.

[124] J. A. Blackledge and A. J. Alexander. Polyethylene membrane as a sample support for direct matrix-assisted laser desorption/ionization mass spectrometric analysis of high mass proteins. *Analytical Chemistry*, 67(5):843–8, 1995.

[125] M.M. Vestling and C. Fenselau. Surfaces for interfacing protein gel electrophoresis directly with mass spectrometry. *Mass Spectrometry Reviews*, 14(3):169–178, 1995.

[126] R. W. Garden and J. V. Sweedler. Heterogeneity within maldi samples as revealed by mass spectrometric imaging. *Analytical Chemistry*, 72(1):30–6, 2000.

[127] B. Spengler and M. Hubert. Scanning microprobe matrix-assisted laser desorption ionization (SMALDI) mass spectrometry: instrumentation for sub-micrometer resolved LDI and MALDI surface analysis. *Journal of the American Society for Mass Spectrometry*, 13(6):735–48, 2002.

[128] L. Sherwood. *Human Physiology: From Cells to Systems.* West Publishing Company, 2 edition, 1993.

[129] G.J Tortora and S.R. Grabowski. *Introduction to the Human Body.* John Wiley, 5 edition, 2001.

[130] R. J. Scheuplein and I. H. Blank. Permeability of the skin. *Physiological Reviews*, 51(4):702–47, 1971.

[131] G. Grubauer, K. R. Feingold, R. M. Harris, and P. M. Elias. Lipid content and lipid type as determinants of the epidermal permeability barrier. *Journal of Lipid Research*, 30(1):89–96, 1989.

[132] R. O. Potts and M. L. Francoeur. The influence of stratum corneum morphology on water permeability. *Journal of Investigative Dermatology*, 96(4):495–9, 1991.

[133] P. M. Elias. Epidermal lipids, barrier function, and desquamation. *Journal of Investigative Dermatology*, 80 Suppl:44s–49s, 1983.

[134] M. L. Williams and P. M. Elias. From basket weave to barrier. unifying concepts for the pathogenesis of the disorders of cornification. *Archives of Dermatology*, 129(5):626–9, 1993.

[135] P. M. Elias. Epidermal lipids, membranes, and keratinization. *International Journal of Dermatology*, 20:1–19, 1981.

[136] J. A. Bouwstra, P. L. Honeywell-Nguyen, G. S. Gooris, and M. Ponec. Structure of the skin barrier and its modulation by vesicular formulations. *Progress in Lipid Research*, 42(1):1–36, 2003.

[137] G. K. Menon. New insights into skin structure: scratching the surface. *Advanced Drug Delivery Reviews*, 54 Suppl 1:S3–17, 2002.

[138] G. K. Menon and P. M. Elias. Morphologic basis for a pore-pathway in mammalian stratum corneum. *Skin Pharmacology*, 10(5-6):235–46, 1997.

[139] P.W. Wertz and D.T. Downing. Stratum corneum: biological and biochemical considerations. In R. H. Guy and J. Hadgraft, editors, *Transdermal Drug Delivery: Developmental Issues and Research Initiatives*, pages 1–22. Marcel Dekker, New York, 1989.

[140] R. C. Wester, J. Christoffel, T. Hartway, N. Poblete, H. I. Maibach, and J. Forsell. Human cadaver skin viability for *in vitro* percutaneous absorption: storage and detrimental effects of heat-separation and freezing. *Pharmaceutical Research*, 15(1):82–4, 1998.

[141] H. Schaeffer, J. Watts, and B. Illel. Follicular penetration. In R. C. Scott, R. H. Guy, and J. Hadgraft, editors, *Prediction of Percutaneous Penetration: Methods, Measurements, and Modelling*, pages 163–173. IBC Technical Services, London, 1990.

[142] M. Heisig, R. Lieckfeldt, G. Wittum, G. Mazurkevich, and G. Lee. Non steady-state descriptions of drug permeation through stratum corneum. 1. The biphasic brick-and-mortar model. *Pharmacological Research*, 13(3):421–6, 1996.

[143] A.J. Lee, J.R. King, and D.A. Barret. Percutaneous absorption: a multiple pathway model. *Journal of Controlled Release*, 45:141–151, 1997.

[144] P. M. Elias, E. R. Cooper, A. Korc, and B. E. Brown. Percutaneous transport in relation to stratum corneum structure and lipid composition. *Journal of Investigative Dermatology*, 76(4):297–301, 1981.

[145] R. L. Bronaugh, R. F. Stewart, and E. R. Congdon. Methods for *in vitro* percutaneous absorption studies. II. Animal models for human skin. *Toxicology and Applied Pharmacology*, 62(3):481–8, 1982.

[146] R. L. Bronaugh and H. I. Maibach. Percutaneous absorption of nitroaromatic compounds: *in vivo* and *in vitro* studies in the human and monkey. *Journal of Investigative Dermatology*, 84(3):180–3, 1985.

[147] R. C. Scott and J. D. Ramsey. Comparison of the in vivo and in vitro percutaneous absorption of a lipophilic molecule (cypermethrin, a pyrethroid insecticide). *Journal of Investigative Dermatology*, 89(2):142–6, 1987.

[148] R. C. Wester and H. I. Maibach. *in vivo* methods for percutaneous absorption. In R. L. Bronaugh and H. I. Maibach, editors, *Percutaneous Absorption: Drugs-CosmeticsMechanisms-Methodology*, pages 215–227. Marcel Dekker, New York, 1999.

[149] A. Naik, Y.N. Kalia, F. Pirot, and R. H. Guy. Characterisation of molecular transport across human stratum corneum *in vivo* . In R. L. Bronaugh and H. I. Maibach, editors, *Percutaneous Absorption: Drugs-CosmeticsMechanisms-Methodology*, pages 148–175. Marcel Dekker, New York, 1999.

[150] J. Crank. *The Mathematics of Diffusion, 2nd Edition.* Oxford University Press, Oxford, 1979.

[151] R. O. Potts and M. L. Francoeur. Infared spectroscopy of stratum corneum lipids. In K.A. Walters and J. Hadgraft, editors, *Pharmaceutical Skin Penetration Enhancement.* Marcel Dekker, New York, 1997.

[152] B. Sennhenn, K. Giese, K. Plamann, N. Harendt, and K Kolmel. *in vivo* evaluation of the penetration of topically applied drugs into human skin by spectroscopic methods. *Skin Pharmacology*, 6:152–160, 1993.

[153] L.M. Lieb, C. Ramachandran, K. Egbaria, and N. Weiner. Topical delivery enhancement with multilamellar liposomes into pilosebaceous units: 1. *In vitro* evaluation using fluorescent techniques with the hamster ear model. *Journal of Investigative Dermatology*, 99:108–113, 1992.

[154] B. Fabin and E. Touitou. Localization of lipophilic molecules penetrating rat skin *in vivo* by quantitative autoradiography. *International Journal of Pharmaceutics*, 74(1):59–65, 1991.

[155] K Kolmel, B. Sennhenn, and K. Giese. Evaluation of drug penetration into the skin by photoacoustic measurement. *Journal of the Society of Cosmetic Chemists*, 37:375–385, 1986.

[156] Elka Touitou, Victor M. Meidan, and Ehud Horwitz. Methods for quantitative determination of drug localized in the skin. *Journal of Controlled Release*, 56(1-3):7–21, 1998.

[157] C Surber, E.W. Smith, F.P. Schwarb, and H.I. Maibach. Drug concentration in the skin. In R.L. Bronaugh and H.I. Maibach, editors, *Percutaneous Absorption: Drugs-CosmeticsMechanisms-Methodology*, pages 347–373. Marcel Dekker, New York, 3 edition, 1999.

[158] K. Fujuyama. Autoradiography. In D. Skerrow and C.J. Skerrow, editors, *Methods in Skin Research*, pages 71–89. John Wiley, London, 1985.

[159] K. Moser, K. Kriwet, A. Naik, Y.N. Kalia, and R.H. Guy. Passive skin penetration enhancement and its quantification *in vitro* . *European Journal of Pharmaceutics and Biopharmaceutics*, 52(2):103–112, 2001.

[160] W. Meyer and R. Schwarz. The skin of domestic mammals as a model for the human skin, with special reference to the domestic pig. *Current Problems in Dermatology*, 7:39–52, 1978.

[161] U. Hoeck, O. Jacobsen, and B. Kreilgard. Comparison of pig skin and human skin for *in vitro* percutaneous study of morphine prodrug. *Proceedings of the International Symposium on Controlled Release of Bioactive Materials*, 21:425–426, 1994.

[162] N. Sekkat, Y.N. Kalia, and R.H. Guy. Biophysical study of porcine ear skin *in vitro* and its comparison to human skin *in vivo* . *Journal of Pharmaceutical Science*, 91(11):2376–2381, 2002.

[163] I.P. Dick and R.C. Scott. Pig ear skin as an *in vitro* model for human skin permeability. *Journal of Pharmacy and Pharmacology*, 44(8):640–645, 1992.

[164] S.M. Harrison, B.W. Barry, and P.H. Dugard. Effects of freezing on human skin permeability. *Journal of Pharmacy and Pharmacology*, 36:261–262, 1984.

[165] G. S. Hawkins and W. G. Reifenrath. Development of an *in vitro* model for determining the fate of chemicals applied to the skin. *Fundamental and Applied Toxicology*, 4:S133–S144, 1984.

[166] M.A. Pellet, M.S. Roberts, and J. Hadgraft. Supersaturated solutions evaluated with an in vitro stratum corneum tape stripping technique. *International Journal of Pharmaceutics*, 151:91–98, 1997.

[167] J. Gobom, K. O. Kraeuter, R. Persson, H. Steen, P. Roepstorff, and R. Ekman. Detection and quantification of neurotensin in human brain tissue by matrix-assisted laser desorption/ionization time-of-flight mass spectrometry. *Analytical Chemistry*, 72(14):3320–6, 2000.

[168] J. Y. Zhao, A. Dindyal-Popescu, G. Scott, M. Ang, and J. E. Wingate. MALDI molecular imaging: evaluation of experimental techniques and application to drug metabolism distribution studies. In *Proceedings of the 52nd Annual ASMS Conference on Mass Spectrometry and Allied Topics*, page 71, Nashville, TN., 2004.

[169] Y. C. Ling, L. Lin, and Y. T. Chen. Quantitative analysis of antibiotics by matrix-assisted laser desorption/ionization time-of-flight mass spectrometry. *Rapid Communications in Mass Spectrometry*, 12(6):317–27, 1998.

[170] D. Mims and D. Hercules. Quantification of bile acids directly from urine by MALDI-TOF-MS. *Analytical and Bioanalytical Chemistry*, 375(5):609–16, 2003.

[171] D. C. Muddiman, A. I. Gusev, A. Proctor, D. M. Hercules, R. Venkataramanan, and W. Diven. Quantitative measurement of cyclosporin A in blood by time-of-flight mass spectrometry. *Analytical Chemistry*, 66(14):2362–8, 1994.

[172] J. Wu, K. Chatman, K Harris, and G Siuzdak. An automated MALDI mass spectrometry approach for optimizing cyclosporin extraction and quantitation. *Analytical Chemistry*, 69(18):3767–3771, 1997.

[173] P. Hatsis, S. Brombacher, J. Corr, P. Kovarik, and D. A. Volmer. Quantitative analysis of small pharmaceutical drugs using a high repetition rate laser matrix-assisted laser/desorption ionization source. *Rapid Communications in Mass Spectrometry*, 17(20):2303–9, 2003.

[174] C Wittman and E Heinzle. Maldi-tof ms for quantification of substrates and products in cultivations of *Corynebacterium glutamicum*. *Biotechnology and Bioengineering*, 72(6):642–647, 2001.

[175] C. T. Houston, W. P. Taylor, T. S. Widlanski, and J. P. Reilly. Investigation of enzyme kinetics using quench-flow techniques with MALDI-TOF mass spectrometry. *Analytical Chemistry*, 72(14):3311–9, 2000.

[176] M. J. Kang, A. Tholey, and E. Heinzle. Application of automated matrix-assisted laser desorption/ionization time-of-flight mass spectrometry for the measurement of enzyme activities. *Rapid Communications in Mass Spectrometry*, 15(15):1327–33, 2001.

[177] D. Bungert, E. Heinzle, and A. Tholey. Quantitative matrix-assisted laser desorption/ionization mass spectrometry for the determination of enzyme activities. *Analytical Biochemistry*, 326(2):167–75, 2004.

[178] M. W. Duncan, G. Matanovic, and A. Cerpa-Poljak. Quantitative analysis of low molecular weight compounds of biological interest by matrix-assisted laser desorption ionization. *Rapid Communications in Mass Spectrometry*, 7(12):1090–4, 1993.

[179] S. M. Helmke, C. Y. Yen, K. J. Cios, K. Nunley, M. R. Bristow, M. W. Duncan, and M. B. Perryman. Simultaneous quantification of human cardiac alpha-

and beta-myosin heavy chain proteins by MALDI-TOF mass spectrometry. *Analytical Chemistry*, 76(6):1683–9, 2004.

[180] M. Petkovic, J. Schiller, J. Muller, M. Muller, K. Arnold, and J. Arnhold. The signal-to-noise ratio as the measure for the quantification of lysophospholipids by matrix-assisted laser desorption/ionisation time-of-flight mass spectrometry. *Analyst*, 126(7):1042–50, 2001.

[181] J. E. Dally, J. Gorniak, R. Bowie, and C. M. Bentzley. Quantitation of underivatized free amino acids in mammalian cell culture media using matrix assisted laser desorption ionization time-of-flight mass spectrometry. *Analytical Chemistry*, 75(19):5046–53, 2003.

[182] Y.C. Chao and L.A. Nylander-French. Determination of keratin protein in a tape-stripped skin sample from jet fuel exposed skin. *Annals of Occupational Hygiene*, 48(1):65–73, 2004.

[183] Y. Vander Heyden, A. Nguyen Minh Nguyet, M. R. Detaevernier, D. L. Massart, and J. Plaizier-Vercammen. Simultaneous determination of ketoconazole and formaldehyde in a shampoo: Liquid chromatography method development and validation. *Journal of Chromatography A*, 958:191–201, 2002.

[184] I. Alberti, Y. N. Kalia, A. Maik, J. D. Bonny, and R. H. Guy. In vivo assessment of enhanced topical delivery of terbinafine to human stratum corneum. *Journal of Controlled Release*, 71:319–327, 2001.

[185] Y. Xu, M.L. Bruening, and J.T. Watson. Non-specific, on-probe cleanup methods for MALDI-MS samples. *Mass Spectrometry Reviews*, 22(6):429–440, 2003.

[186] J. Wei, J. Buriak, and G. Siuzdak. Desorption/ionization mass spectrometry on porous silicon. *Nature*, 399(6733):243–246, 1999.

[187] W. Lewis, Z. Shen, M.G. Finn, and Siuzdak G. Desorption/ionization on silicon (DIOS) mass spectrometry: background and applications. *International Journal of Mass Spectrometry*, 226:107–116, 2003.

[188] Z. Shen, J.J. Thomas, C. Averbuj, Broo K.M., M. Engelhard, J.E. Crowell, M.G. Finn, and G. Siuzdak. Porous silicon as a versatile platform for laser desorption/ionization mass spectrometry. *Analytical Chemistry*, 33:179–187, 2001.

[189] T.W. Hutchens and T.-T. Yip. New desorption strategies for the mass spectrometric analysis of macromolecules. *Rapid Communications in Mass Spectrometry*, 7:576–580, 1993.

[190] M. Merchant and S.R. Weinberger. Recent advancements in surface-enhanced laser desorption/ionization-time of flight-mass spectrometry. *Electrophoresis*, 21:1164–1177, 2000.

[191] N. Tang, P. Tornatore, and S.R. Weinberger. Current developments in seldi affinity technology. *Mass Spectrometry Reviews*, 23:34–44, 2004.

The Analysis of Pharmaceutical Compounds In Skin by Matrix Assisted Laser Desorption Ionisation - Time Of Flight - Mass Spectrometry (MALDI-TOF-MS)

Josephine Bunch[1], Malcolm R. Clench[1] and Don S. Richards[2]

1Biomedical Research Centre, School of Science and Mathematics, Sheffield Hallam University, Pond Street, Sheffield, S1 1WB, UK
2Pfizer Global R&D, Ramsgate Road, Sandwich, Kent CT13 9NJ, UK

Introduction

Mass Spectrometric techniques have been developed recently for the examination of biological tissue samples. Tandem mass spectrometry has been employed for the detection of pharmaceutical compounds[1] and also mass spectrometric 'images' have been produced that show the spatial distribution of peptides[2], proteins[2] and drugs[3,4] in tissue. We present here methods for the detection of a topically applied pharmaceutical formulation in porcine epidermal tissue by MALDI-TOF-MS. Figure 1 shows the structure of Ketoconazole, the active ingredient in Nizarol® shampoo.

Ketoconazole ($C_{26}H_{28}Cl_2N_4O_4$) FW 531.44

Figure 1. Ketoconazole is a widely used anti-fungal agent available in a variety ol formulations. *All work presented in this poster has been conducted using the form sold as Nizoral6 shampoo which is also prescribed for treatment for certain fungal conditions in skin.*

Method

Porcine epidermal tissue was treated with "Nizoral", a medicated shampoo containing ketoconazole as active ingredient. Following a one-hour incubation at 37°, all excess formulation was washed from the surface. A cross-section of the drug-treated tissue was then blotted onto a cellulose membrane that had been precoated in matrix (a-CHCA) using airspray deposition. Alternatively, the tissue surface was treated with Nizoral within a triangular former, and subsequently blotted onto a matrix-coated membrane. Sample membranes were then mounted into the recess of specialised MALDI targets with adhesive tape. All samples were analysed by MALDI-TOF-MS using an Applied Biosystems/MDS Sciex QSTAR® Pulsar i hybrid quadrupole time of flight mass spectrometer fitted with an oMALDI™ ion source and MALDI imaging software.

Principles of Imaging Mass Spectrometry

The initial step in MALDI imaging involves application of a thin layer of matrix to the sample. The chemistry of the sample can then be imaged by rastering the laser beam across the sample surface and acquiring mass spectra from each point. Three-dimensional images may be obtained by plotting the spatial dimensions of x and *y* versus absolute ion intensity, which is considered proportional to analyte concentration. In addition, quantification can be achieved by incorporation of an internal standard.

Results

Detection of the protonated molecule was readily achievable by this MALDI imaging technique. Figure 2 shows tissue after Nizoral shampoo was applied within a triangular former. After treatment, the skin was blotted onto a membrane precoated in a-CHCA by airspray deposition. The image demonstrates that spatial information is retained when the blotting technique is employed.

Figure 2 *MALDI image of the distribution of the protonated molecule [M+Hf at m/z 532 on cellulose membrane.*

Mass spectra shown in Figures 3 and 4 show detection of the drug within the dimensions of the triangular former, and not outside it.

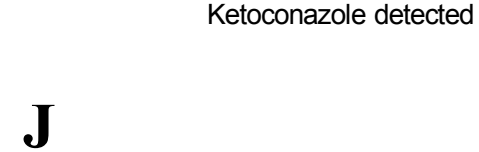

Figure 3. *Mass Spectrum Acquired Within the Triangular Former*

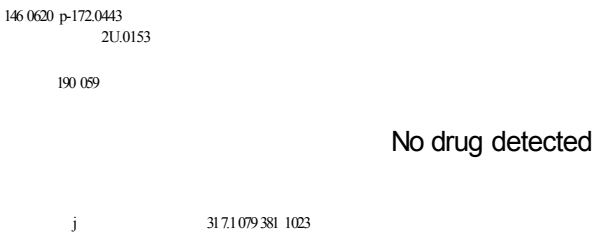

Figure 4. *Mass Spectrum Acquired Outside the Triangular Former*

Ion images demonstrating the permeation of the applied compound into the skin have been achieved by imaging a cross sectional imprint of treated tissue. Figure 5 shows an image of tissue after treatment with Ketoconazole. The treated tissue cross-section was blotted onto cellulose membrane, precoated in a-CHCA by airspray deposition. The image shows the 'vertical' distribution of the protonated drug molecule. Figure 6 shows the same data as presented in Figure 5, after rotation through 90°, giving a clear picture of the apparent change in drug concentration with depth. This provides a usefulsemi-quantitative display of the drug in skin.

Figure 5. *MALDI image of the distribution of the protonated molecule [M+HJ* at m/z532 of Ketoconazole in a vertical section of porcine skin*

Figure 6. *MALDI image of the distribution ot the protonated molecule [M+Hf at m/z532 ot Ketoconazole in a vertical section of porcine skin, after rotation by 90°*

Figure 7 shows a calibration graph for the determination of ketoconazole (0-0.4 mgmM). This graph was constructed using the intensity of the Na adduct of a-CHCA ion at m/z 212 as an "internal standard".

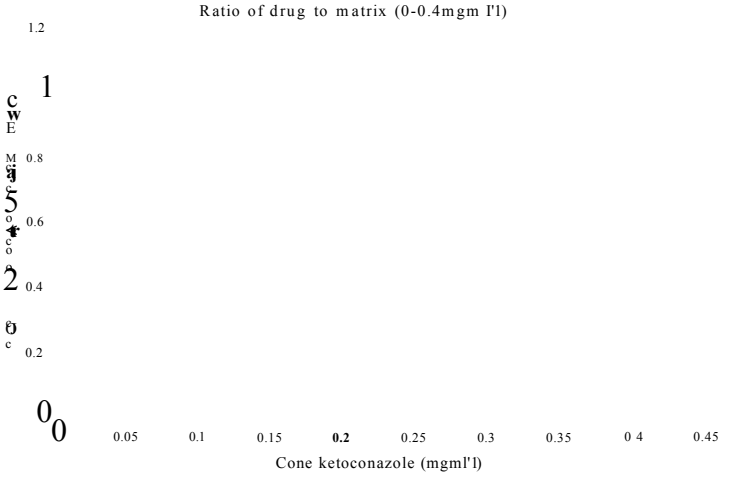

Figure *7. Calibration Plot for the Determination Ketoconazole*

The straight-line equation was used to produce a quantitative profile of drug concentration against tissue depth (Figure 8) by examination of an enlarged two-dimensional display of Figure 4 and spectra acquired during the imaging run (as demonstrated in Figure 9).

Figure 8. A Quantitative Profile of Ketoconazole in Porcine Epidermal Tissue. *Constructed from examination of selected spectra acquired during an imaging run, knowledge of vertical spacing between spectra, and the straight line equation from the calibration plot.*

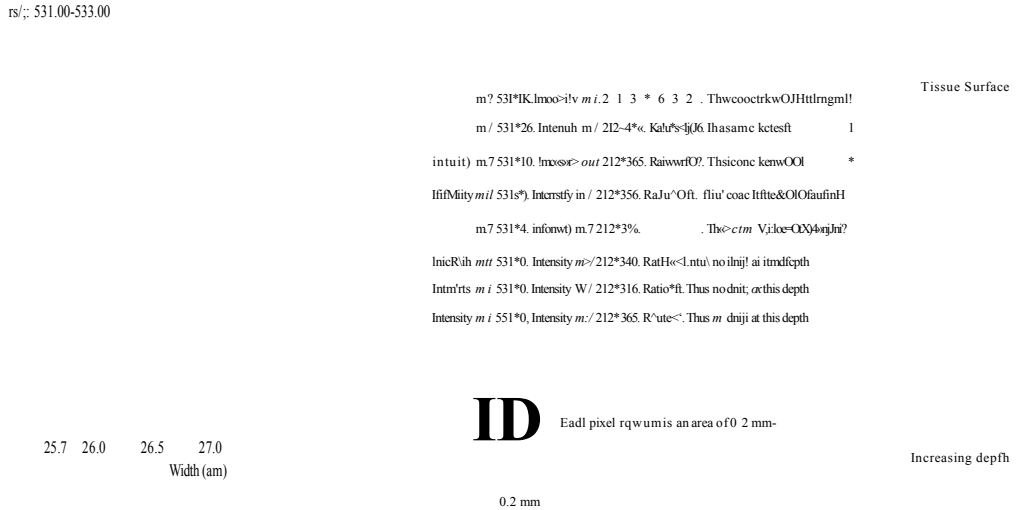

Figure 9. *Enlarging the image reveals pixels, each of which corresponds to an individual mass spectrum. The ratio of drug to matrix in these spectra can be used to calculate the concentration of drug at each location by rearranging the straight line equation obtained from the calibration plot.*

Conventional Haematoxylin and Eosin staining and microscopy methods were employed to obtain a histological image of the porcine epidermal tissue, shown in Figure 10. Thus the drug profile obtained indicates permeation into the dermal skin layer.

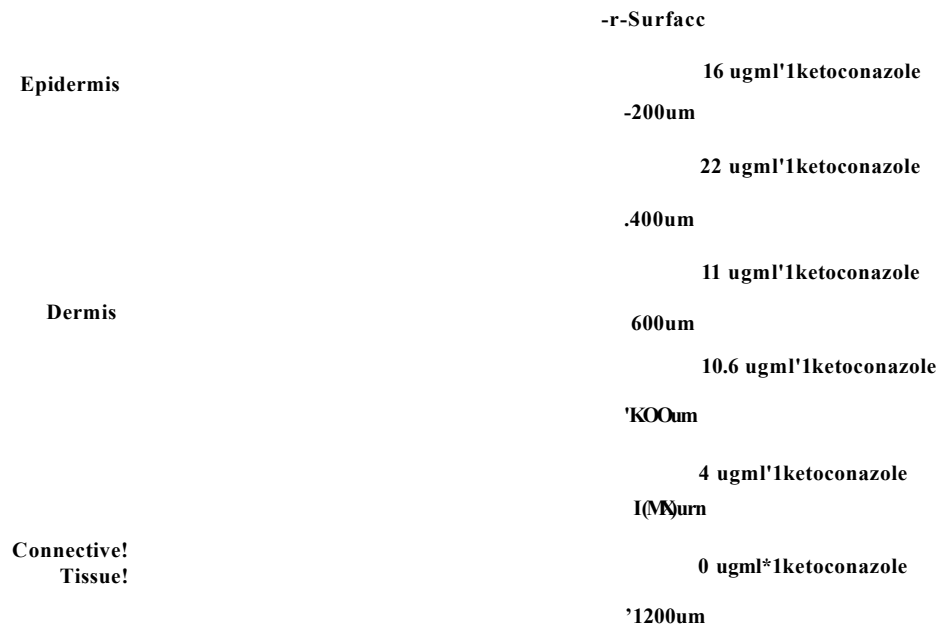

Figure 10. *Superimposing the mass spectrometric image over a histological image reveals that the drug is absorbed into the dermal skin layer*

Conclusion

These preliminary investigations indicate that this novel approach may be used to obtain qualitative and quantitative information on the absorption of topically applied pharmaceutical compounds. Images have been produced showing the dermal uptake of ketoconazole in porcine epidermal tissue, and the methods employed have been proven to retain the spatial distribution of the analyte molecule. Use of the sodium adduct of the matrix ion as an internal standard yields a calibration graph with a relatively good degree of precision and linearity. The calibration graph, combined with examination of individual image pixels and their corresponding spectra, has permitted construction of a quantitative profile of ketoconazole concentration against skin depth. Histological images reveal that this equates to drug permeation up to and including the dermal skin layer.

References

[1]Troend!e, F. J., Reddick, C. D., and Yost, R. A., Detection of Pharmaceutical Compounds in Tissue by Matrix-Assisted Laser Desorption/Ionisation and Laser Desorption/Chemical Ionization Tandem Mass Spectrometry with a Quadrupole Ion Trap. *J. Am. Soc. Mass Spectrom.* 1999, 10, 1315-1321.

[2] Chaurand, P., Stoeckli, M. and Caprioli, R. M. Direct Profiling of Proteins in Biological Tissue Sections by MALDI Mass Spectrometry. *Anal Chem.* 1999, 71, 5263-5270.

[3] Reyzer, M. L., Hsieh, Y., Ng, K., Korfmacher, W., and Caprioli, R. M. Direct Analysis of Drug Candidates in Tissue by matrix Assisted Laser Desorption Ionisation Mass Spectrometry. J. Mass Spectrom. 2003, 38, 1081-1092

[4] Bunch, J., Clench, M. R., and Richards, D.S. The analysis of Low Molecular Weight Compounds in Biological Tissue by Matrix Assisted Laser Desorption Ionisation Time of Flight Mass Spectrometry. In *Proceedings of the 51st ASMS Conference on Mass Spectrometry and Allied Topics, Montreal, Canada 2003.*

Trademarks/Licensing

Rapid Commun. Mass Spectrom. 2004; 18: 3051–3060
Published online 15 November 2004 in Wiley InterScience (www.interscience.wiley.com). DOI: 10.1002/rcm.1725

Determination of pharmaceutical compounds in skin by imaging matrix-assisted laser desorption/ionisation mass spectrometry

Josephine Bunch[1], Malcolm R. Clench[1]* and Don S. Richards[2]

[1]Biomedical Research Centre, Sheffield Hallam University, Howard Street, Sheffield S1 1WB, UK
[2]Pfizer Global R&D, Ramsgate Road, Sandwich CT13 9NJ, UK

Received 27 July 2004; Revised 18 October 2004; Accepted 18 October 2004

Matrix-assisted laser desorption/ionisation (MALDI) quadrupole time-of-flight mass spectrometry (Q-TOFMS) has been used to detect and image the distribution of a xenobiotic substance in skin. Porcine epidermal tissue was treated with 'Nizoral', a medicated shampoo containing ketoconazole ((±)-1-acetyl-4-[*p*-[[(2*R*,4*S*)-2-(2,4-dichlorophenyl)-2-(imidazol-1-ylmethyl)-1,3-dioxolan-4-yl]methoxy] phenyl]piperazine) as active ingredient. Following incubation for 1 h at 37°C all excess formulation was washed from the surface. A cross-section of the drug-treated tissue was then blotted onto a cellulose membrane, precoated in matrix (α-cyano-4-hydroxycinnamic acid (CHCA)), by airspray deposition. In separate experiments the tissue surface was treated with Nizoral within a triangular former, and subsequently blotted onto a matrix-coated membrane. Sample membranes were then mounted into the recess of specialised MALDI targets with adhesive tape. All samples were analysed by MALDI-TOFMS using an Applied Biosystem 'Q-star Pulsar i' hybrid Q-TOF mass spectrometer fitted with an orthagonal MALDI ion source and imaging software. Detection of the protonated molecule was readily achievable by this technique. Treatment of the tissue within a template gave rise to images depicting the expected distribution of the drug, demonstrating that this technique is capable of producing spatially useful data. Ion images demonstrating the permeation of the applied compound into the skin were achieved by imaging a cross-sectional imprint of treated tissue. A calibration graph for the determination of ketoconazole was prepared using the sodium adduct of the matrix ion as an internal standard. This enabled construction of a quantitative profile of drug in skin. Conventional haematoxylin and eosin staining and microscopy methods were employed to obtain a histological image of the porcine epidermal tissue. Superimposing the mass spectrometric and histological images appeared to indicate drug permeation into the dermal tissue layer. Copyright © 2004 John Wiley & Sons, Ltd.

A percutaneously delivered therapeutic agent, whether directed at the systemic circulation or the local tissues, must traverse the *stratum corneum* (the upper layer of the epidermis (which is itself the upper layer of skin)). Despite an insufficient knowledge of the precise mechanism of skin penetration it is clear that both the physiochemical and structural properties of the penetrating molecules and the internal structure and composition of the skin membrane are involved in the process. Absorption across the *stratum corneum* is a passive process of diffusion, with the *stratum corneum* behaving as a semi-permeable membrane. In principle there are three routes of diffusion: intercellular diffusion through the lipid matrix; transcellular diffusion through the corneocytes; and pilosebaceous diffusion along the sweat pores and hair follicles that 'pierce' the *stratum corneum*.[1]

Methods for analysing dermal xenobiotic absorption include skin extraction measurements,[2] horizontal sectioning (corneum tape stripping),[3] quantitative skin autoradiography,[4,5] and spectroscopic methods such as ATR-FTIR,[6,9] fluorescence,[7,8] remittance[9] and photothermal.[2,10] However, inherent problems such as the requirement of a labelled compound and issues such as sensitivity or the loss of spatial information limit the usefulness of these techniques for the permeation depth profiling of drug compounds in skin.

The use of mass spectrometry to obtain images started 30 years ago with the advent of imaging secondary ion mass spectrometry (SIMS). In imaging SIMS the surface of the

**Correspondence to*: M. R. Clench, Biomedical Research Centre, Sheffield Hallam University, Howard Street, Sheffield S1 1WB, UK.
E-mail: m.r.clench@shu.ac.uk
Contract/grant sponsors: Pfizer Global R&D; The British Mass Spectrometry Society.

sample is bombarded with high energy ions—this leads to the ejection (or sputtering) of neutral and charged (+/−) species from the surface. The ejected species may include atoms, clusters of atoms and molecular fragments. In traditional SIMS it is only the positive ions that are mass-analysed. Since the technique utilises a beam of atomic ions (i.e. charged particles) as the probe, it is a relatively easy matter to focus the incident beam and then to scan it across the surface. Thus the detector response for a selected mass at each raster spot becomes a pixel in the image. The use of an ion beam results in sub-micron spatial resolution. Imaging SIMS has been used in a range of pharmaceutical applications including monitoring drugs at the cellular and sub-cellular level. New developments apply SIMS to organic compounds and metabolites of low mass (<500 u) in biological samples.[11] However, a major limitation is the mass range that may be analysed by this technique.

Recently, imaging using matrix-assisted laser desorption/ionisation mass spectrometry (MALDI-MS) has become a subject of interest. The initial step in MALDI-MS imaging involves application of a thin layer of matrix to the sample. The chemistry of the sample is then imaged by moving the sample under a stationary laser and acquiring mass spectra from each point. Three-dimensional images may be obtained by plotting the spatial dimensions of x and y versus absolute ion abundance, which is considered to be proportional to analyte concentration.

MALDI has been used for the imaging both of biological samples[12–18] and of thin layer chromatography (TLC) plates,[19,20] with the method of matrix application to such samples additionally requiring that the spatial distribution of the analyte in the sample be maintained. A number of methods of matrix application have been assessed to fulfil these criteria, including indirect matrix deposition,[19] brushing of the sample with a supersaturated matrix solution,[20] and electrospraying.[12,20]

Caprioli and co-workers developed MALDI imaging techniques to identify and profile peptides and proteins in biological tissue.[12] Methods of direct tissue analysis and indirect analysis (blotting onto a layer of C18 beads or a cellulose membrane) were compared. Analysis of C18 blots was found to be the superior method.

Optimum results were achieved by electrospraying the matrix onto the samples. In agreement with the findings of Mowthorpe *et al.*,[20] this approach minimised analyte spreading and allowed the mapping and localisation of specific compounds within tissue sections.

In a subsequent study the Caprioli group investigated the use of a carbon-filled polyethylene membrane for tissue blotting prior to MALDI analysis.[13] This type of membrane was selected because of its electrical conductivity and protein adhesion properties. The method produced unique protein profiles. This group has reported improvements in the rate of image acquisition, indicating that such a technique may lend itself to automated high-throughput analysis.[14]

The use of a range of membranes for matrix support in MALDI, e.g. nylon,[21] poly(vinylidine difluoride),[22] nitrocellulose[23] and polyethylene,[24] has been reported. The use of such membranes to enhance the MS analysis of proteins has been reviewed by Vestling *et al.*[25]

Troendle and colleagues[26] have demonstrated the detection of pharmaceutical compounds in animal tissue. Matrix was applied to the tissue surface by pipetting and electrospraying. In these experiments MALDI quadrupole ion trap mass spectrometry was employed to detect the anti-cancer drug paclitaxel in a human ovarian tumour. The anti-psychotic drug spiperone was also detected in spiked sections of rat liver tissue.

Images of pharmaceutical compounds in tissue have previously been acquired.[19] An anti-tumour drug was detected and imaged in mouse tumour tissue by monitoring the dissociation of the protonated drug. A second drug was detected in rat brain following oral administration. Matrix was applied to intact tissue by either spotting small volumes of the matrix in selected areas, or by coating the entire surface by airspraying.

Methods of tissue preparation and matrix application for the direct analysis of tissue samples by MALDI-TOFMS have been reviewed by Schwartz *et al.*[27] MALDI imaging has also been used as a general method for assessing matrix application in MALDI.[28]

The detection[25] and imaging[18] of low molecular weight compounds in tissue, together with the imaging of drugs on TLC plates[20,21] and of proteins in tissue, by MALDI-MS[12–17] shows promise that these methods may be used as a means of mapping drugs in biological systems. Thus imaging with MALDI-MS may have widespread application in future pharmaceutical and medical research.

The work presented in this paper demonstrates novel sample preparation for imaging MALDI-MS, involving precoating cellulose membranes in matrix prior to tissue blotting. Methods for the semi-quantitative analysis and imaging of a topically applied anti-fungal agent (ketoconazole RMM 531.44) in porcine epidermal tissue by MALDI-TOFMS are presented.

EXPERIMENTAL

Materials

Trifluoroacetic acid (AR grade) and α-cyano-4-hydroxycinnamic acid (CHCA) were purchased from Sigma-Aldrich (Poole, UK). Methanol was HPLC grade, purchased from Fisher Scientific (Loughborough, UK). Porcine ears, Nizoral shampoo (20 mg/g ketoconazole, ((±)-1-acetyl-4-[*p*-[[(2*R*,4*S*)-2-(2,4-dichlorophenyl)-2-(imidazol-1-ylmethyl)-1,3-dioxolan-4-yl]methoxy]phenyl]piperazine); manufactured by Janssen Cilag, High Wycombe, UK), and cellulose membranes were obtained commercially.

Instrumentation

All mass spectrometric analysis was performed using an Applied Biosystems (Foster City, CA, USA) hybrid quadrupole time-of-flight instrument (QStar) fitted with an orthogonal MALDI ion source and beta test imaging software supplied by MDS Sciex (Concord, Ontario, Canada). The nitrogen laser used has an elliptical spot size of 100 × 150 μm and an available power range of 0–58.4 μJ.

Confocal microscopy was performed on a Zeiss 510 CSLM, equipped with an argon laser. Phase contrast images were acquired with an objective lens (×20).

Scanning electron microscopy (SEM) was performed using a Phillips XL40 scanning electron microscope, fitted with a tungsten wire filament. The working distance (from the bottom of the column to the sample surface) was 10 mm. An electron gun potential of 15 kV was employed in all experiments.

Matrix investigation

Initial experiments were undertaken to assess the suitability of various matrices for the analysis of ketoconazole.

Matrix assessment was based on solubility in methanol (in order to facilitate the spraying of the matrix), and the behaviour of a pre-mixed matrix/analyte solution during MALDI-TOFMS analysis on a conventional stainless steel target. Assessment was made according to the following criteria:

- The absence of interfering peaks in the spectral region of interest;
- The reproducibility of analyte signal intensity from laser spot to spot over the target;
- High analyte signal intensity for the pharmaceutical analyte.

A range of common organic acid matrices was investigated. It was found that CHCA provided the best spectral results, analyte signal intensity and reproducibility for the detection of ketoconazole, and it was therefore selected for use in these investigations.

Tissue treatment

A 'confined treatment area' was created on the tissue surface by protecting the skin around the application site with adhesive tape sealed with barrier cream to give a 'triangular' treatment area. The tissue was treated with 500 µL Nizoral shampoo (2% ketoconazole) inside the area of the former and incubated for 1 h at 37°C. These experiments were used to assess the success of the technique in displaying spatially relevant information. Alternatively, 500 µL of Nizoral were applied to the centre of a 2 cm^2 piece of tissue, which was then incubated as before.

After incubation the tissue surface was rinsed with deionised water to remove any excess formulation.

Membrane preparation and tissue blotting

Conventional cellulose membranes were coated in CHCA matrix material by airspray deposition. The methodology adopted involved the use of a Badger 150 suction-feed air brush (The Air Brush Company, Lancing, UK). Matrix solution (25 mg/mL) was applied to the membrane using five cycles of the air brush, where one cycle comprises five passes of the air brush over the sample, giving an estimated total matrix usage of approximately 375 mg per sample. The membranes were dried under a heat lamp for 5 min between each cycle.

The epidermal surfaces of tissue samples treated within a former were subsequently blotted (pressed) onto the matrix-coated cellulose membrane. Samples treated without the former were bisected and a 'cross-sectional' imprint created upon the membrane. All membranes were mounted in the recess of a specialised MALDI target prior to MS analysis.

Sample preparation for optical and electron microscopy

Optical microscopy

Samples for optical micrcoscopy were prepared by micotoming to an approximately 15 µm thick section. They were subsequently mounted onto a polylysine-coated microscope slide (BDH, Poole, UK) and stained using a conventional Harris haematoxylin and eosin (H&E) staining protocol.[29]

Electron microscopy

Samples for SEM were sputter-coated with a thin layer of gold prior to examination using standard procedures. In

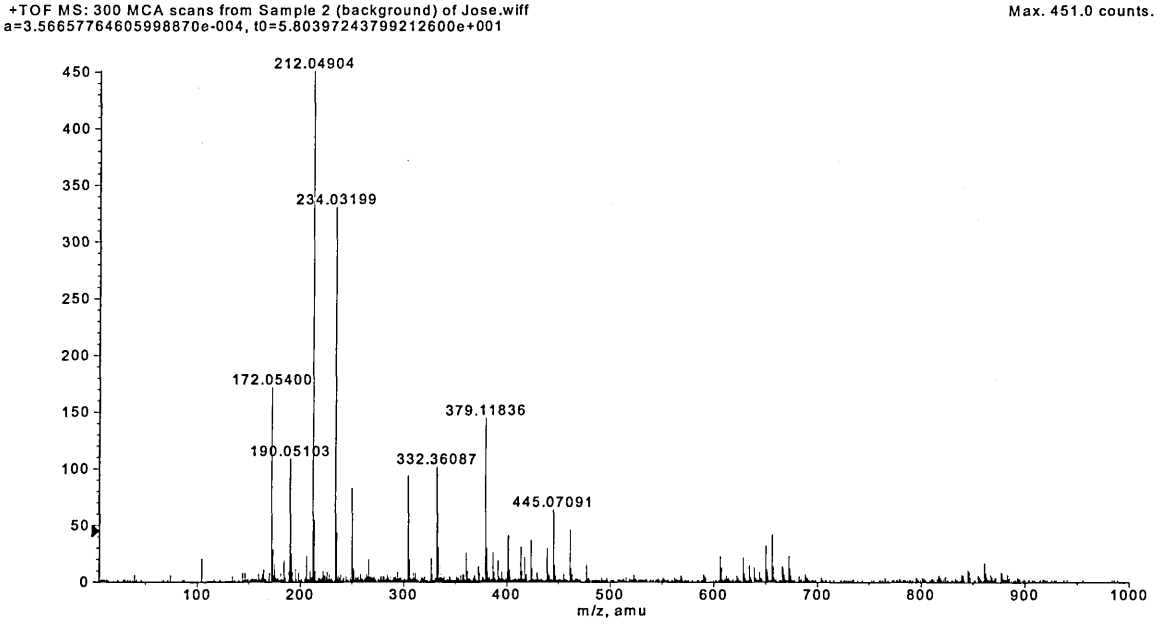

Figure 1. Mass spectrum acquired at a position on the membrane where no drug was blotted. No interfering peaks were observed.

order to maintain electrical contact between the surface of the membrane and the sample holder (to minimise surface charging) a thin line of silver-conducting paint was applied from one corner of the membrane to the underlying sample stage.

Imaging the membrane

The area on the target where the membrane was mounted was selected within the software and then imaged as follows: The target was moved in x and y dimensions at set increments of 0.2 mm while firing the laser for 2 s at each location, at a laser repetition rate of 20 Hz. Thus mass spectra were acquired at sequential increments in a 'snake-like' pattern over the entire two-dimensional area. This created a data set of several thousand mass spectra. The software capabilities enabled ion images to be created by selecting appropriate mass ranges (i.e. *m/z* 531–533); thus the distribution, and

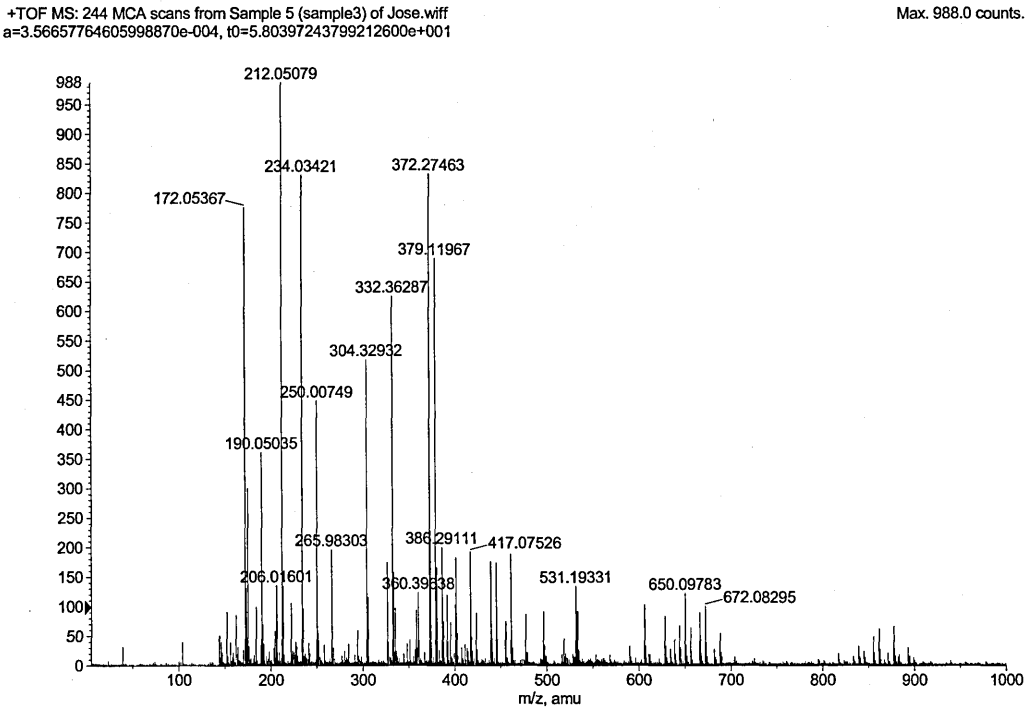

Figure 2. Mass spectrum acquired at a position on the membrane where drug-treated tissue was blotted. Ketoconazole was detected at *m/z* 531.19.

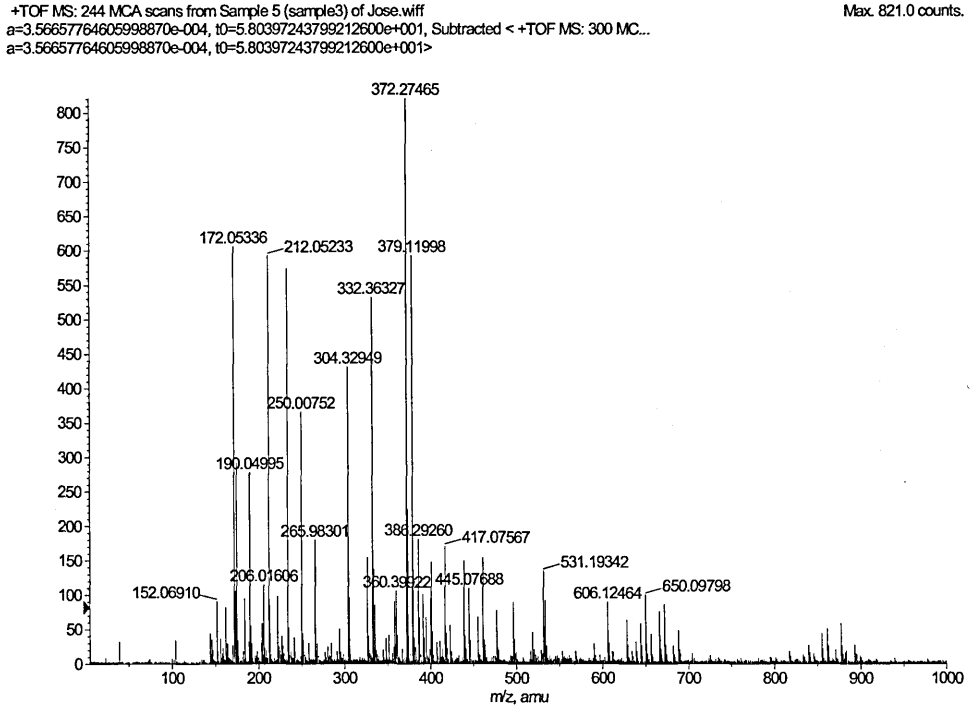

Figure 3. The background spectra can be subtracted from the sample spectra to emphasise the presence of the drug.

relative ion abundances, were displayed as two- and three-dimensional colour images, hence creating x, y, z plots of location vs. abundance of the selected ion/ions.

RESULTS AND DISCUSSION

MALDI-Q-TOF analysis of membranes

Mass spectra were acquired from a variety of positions on the blotted membrane. Areas corresponding to regions outside the treated tissue imprint showed an absence of interfering peaks in the mass region of interest (Fig. 1). Mass spectra acquired within the region of the tissue imprint showed detection of the analyte with high ion abundances (Fig. 2). 'Background' spectra (obtained from a co-ordinate where no drug was present) (Fig. 1) were subtracted from the sample spectra (obtained from a co-ordinate where treated tissue was blotted) (Fig. 2) and the resultant spectra (Fig. 3) show drug-associated peaks in better detail. These mass spectra demonstrate that the most abundant matrix ion observed is the sodium adduct (*m/z* 212), which is concurrent with the images obtained.

Assessment of matrix coverage

The success of matrix coverage on cellulose membranes by airspray deposition was assessed by the degree of homogeneity of matrix material over the membrane, and the abundance, size and distribution of matrix crystals at various locations.

MALDI images for the protonated matrix ion at *m/z* 190, the sodium and potassium adducts at *m/z* 212 and 228, respectively, and the matrix dimer at *m/z* 379, were obtained (Fig. 4). The images reveal that the matrix coverage is relatively dense and uniform in comparison with previously reported methodologies for matrix application.[28] The sodium adduct appears to be the most abundant ion, and shows the highest ion abundances over the imaged area.

Scanning electron microscopy (SEM) was performed at a range of magnifications in order to obtain images showing density of coverage and images depicting individual matrix crystals. At 500× magnification (Fig. 5) it is observed that the

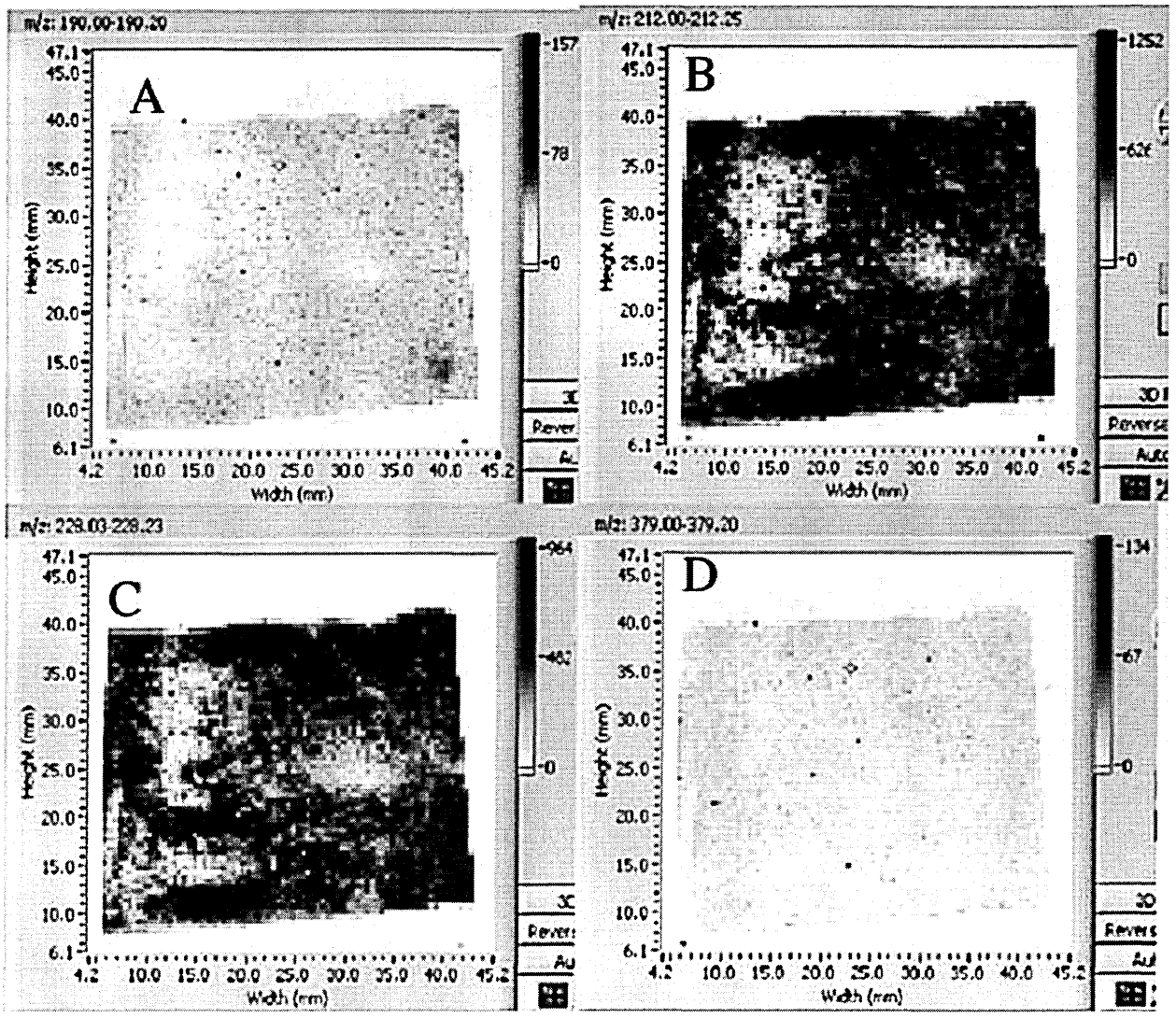

Figure 4. MALDI images of CHCA on a cellulose membrane. (a) The protonated molecule (*m/z* 190); (b) the sodium adduct (*m/z* 212); (c) the potassium adduct (*m/z* 228); and (d) the protonated matrix dimer (*m/z* 379).

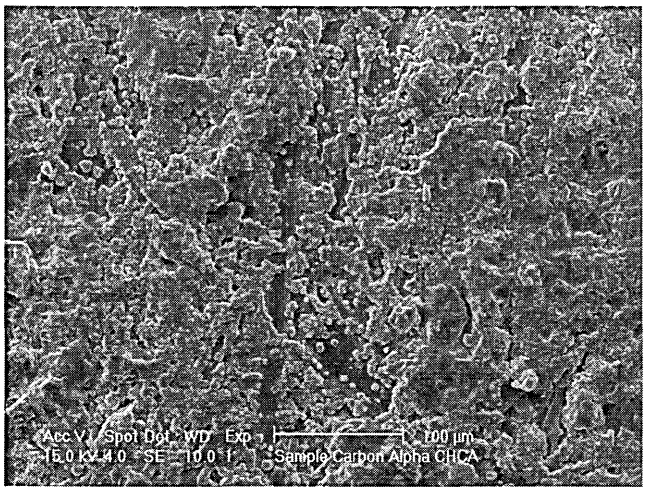

Figure 5. SEM image of matrix-coated cellulose membrane acquired at a magnification of 500×. Coverage appears to be dense and relatively even.

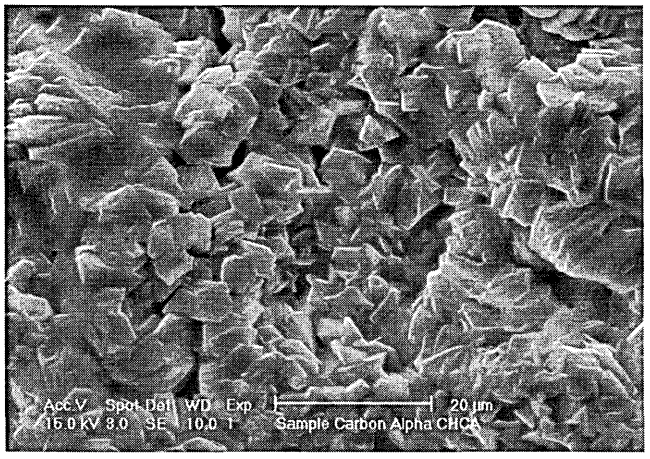

Figure 6. SEM image of matrix-coated cellulose membrane acquired at a magnification of 3000×. Matrix crystals are abundant and exhibit characteristic rosette shapes associated with CHCA crystals.

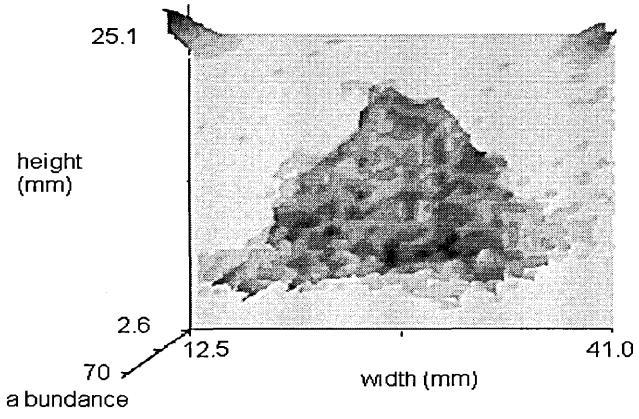

Figure 7. MALDI image of the distribution of the isotopic envelope of the protonated molecule $[M+H]^+$ (*m/z* 531–533) of ketoconazole. Tissue was treated with Nizoral within a triangular former. The skin was blotted onto a cellulose membrane, precoated in CHCA by airspray deposition. Image demonstrates retention of spatial information when the blotting technique is employed.

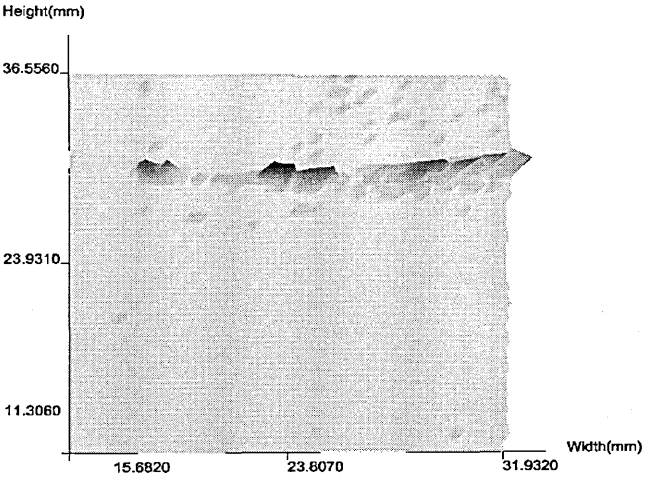

Figure 8. MALDI image of the distribution of the isotopic envelope of the protonated molecule $[M+H]^+$ (*m/z* 531–533) of ketoconazole in a vertical section of porcine epidermal tissue. In this case the treated tissue was bisected and a cross-section was blotted onto cellulose membrane, precoated in CHCA by airspray deposition. Image shows 'vertical' distribution of the protonated drug molecule.

matrix coverage is abundant and homogeneous. At 3000× magnification (Fig. 6) typical rosette-shaped crystals are seen. Thus it was concluded that both the methodology adopted for matrix deposition and the membrane material were suitable for this application.

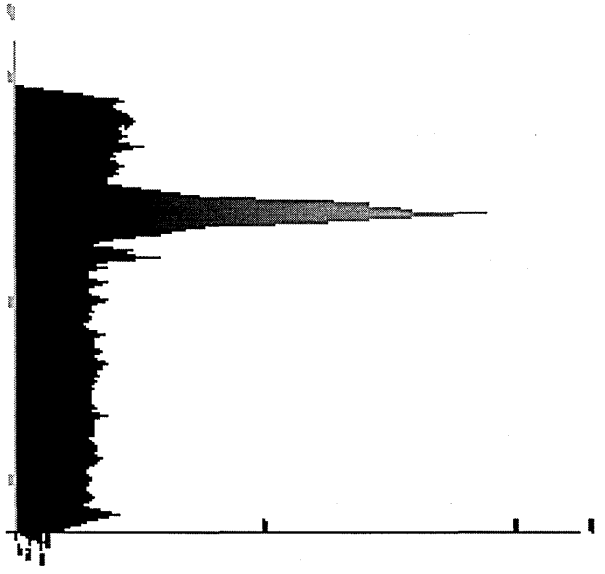

Figure 9. MALDI image of the distribution of the isotopic envelope of the protonated molecule $[M+H]^+$ (*m/z* 531–533) of ketoconazole in a vertical section of porcine epidermal tissue. In this case the treated tissue was bisected and a cross-section was blotted onto cellulose membrane, precoated in CHCA by airspray deposition. Image shows 'vertical' distribution of the protonated drug molecule. This is the same data as shown in Fig. 8 and the image has been rotated through 90°, giving a clear picture of the apparent change in drug concentration with depth.

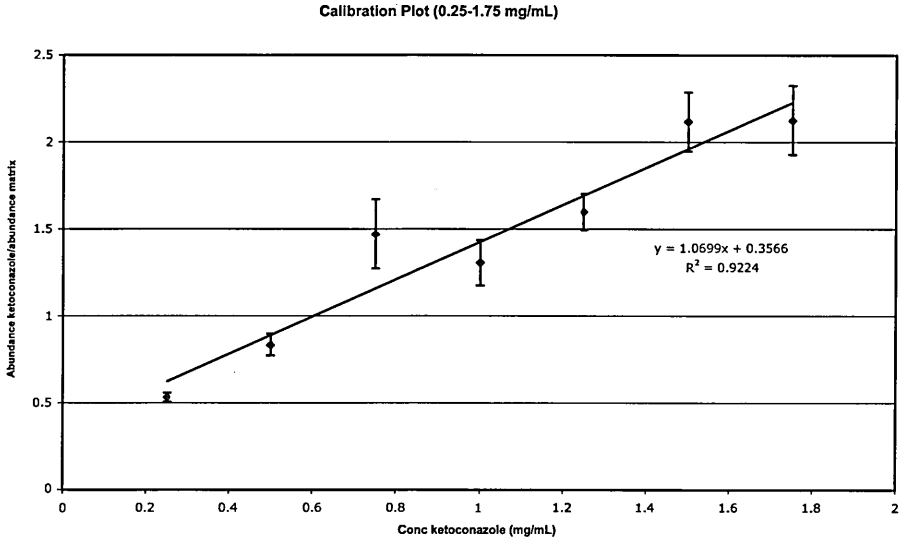

Figure 10. Calibration plot for the determination of ketoconazole (0.25–1.75 mg/mL) constructed using the abundance of the Na adduct of CHCA at *m/z* 212 as an 'internal standard' ($y = 1.0699x + 0.3566$, $r^2 = 0.9224$).

MALDI images of membranes

Experiments involving treatment within a triangular former were used to assess whether or not spatial resolution is maintained when pre-coated membranes are employed. Figure 7 shows an image produced by plotting the abundance of the ion for the protonated molecule of ketoconazole following application to porcine skin through a triangular former. As can be seen, the triangular shape is maintained and this was taken as evidence of the validity of the proposed methodology.

Figure 8 shows an image generated of ketoconazole distribution in a 'vertical' skin section following blotting of the bisected tissue cross-section onto a precoated cellulose membrane. The apparent localisation of the drug in the uppermost layers of the skin is clearly observable.

In order to clearly see the apparent depth of penetration the image shown in Fig. 8 can be rotated via 90° using the supplied software. This is shown in Fig. 9. This form of presentation allows a quantitative assessment of the data.

Quantification of drugs in skin

The use of matrix peaks as an 'internal standard' for the normalisation of ketoconazole signals has been investigated. This procedure was used in order to compensate for variations in matrix coverage. Examination of spectra obtained from analysis of (pre-coated) tissue-imprinted cellulose membranes reveals that the most abundant and consistent matrix peak observed is the sodium adduct of CHCA (*m/z* 212) (Figs. 4, 5 and 6).

An initial calibration graph for the concentration range 0.25–1.75 mg/mL ketoconazole was prepared by plotting the ratio of *m/z* 531–533:212 against drug concentration (Fig. 10). The calibration represents the mean value of 20 samples and

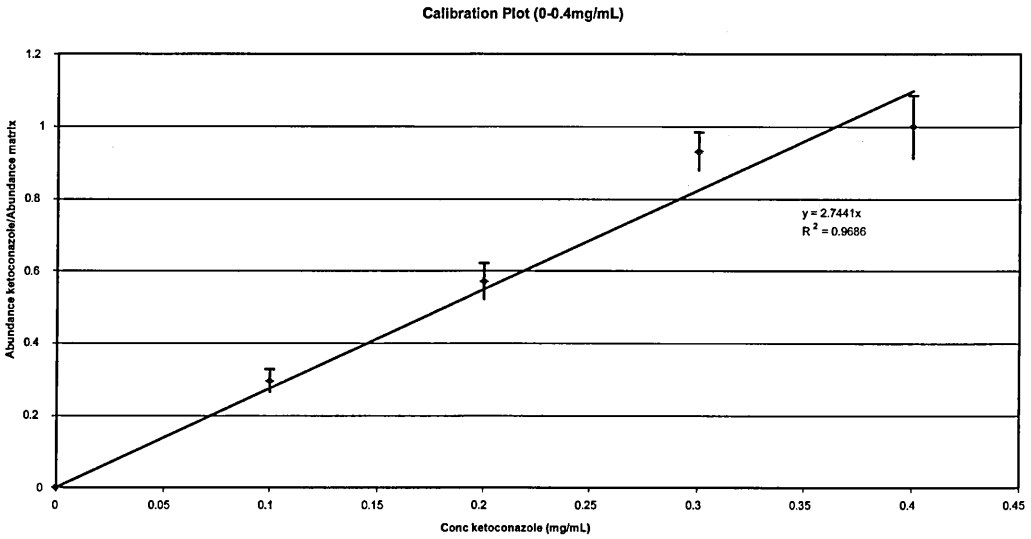

Figure 11. Calibration plot for the determination of ketoconazole (0–0.4 mg/mL) constructed using the abundance of the Na adduct of CHCA at *m/z* 212 as an 'internal standard' ($y = 2.7441x$, $r^2 = 0.9686$).

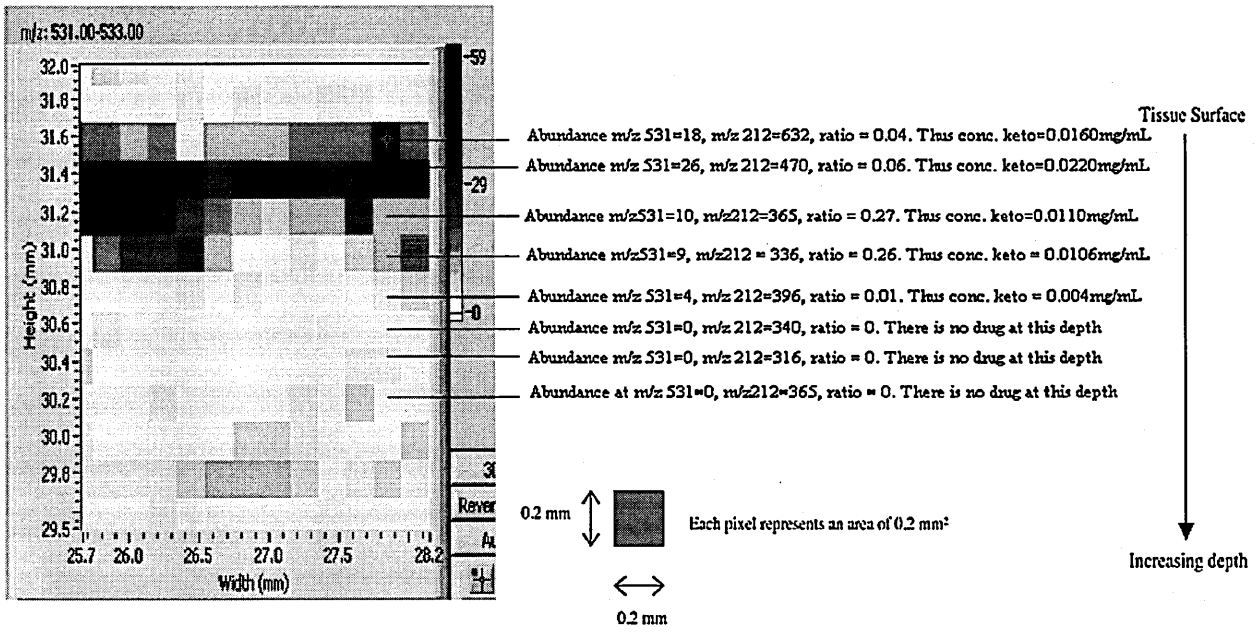

Figure 12. A 2D representation of the data presented in Fig. 8 was enlarged within the software to reveal pixels. Each pixel within the image corresponds to an individual mass spectrum. The ratio of drug to matrix in these spectra was used to calculate the concentration of drug at each location by rearranging the straight line equation obtained from the calibration plot shown in Fig. 11.

their associated error. All analyses were performed using an automated search pattern to acquire data from within the sample spots.

The ratio of drug to matrix observed on tissue-imprinted membranes is consistently under 0.5, indicating that a more effective calibration range would be 0–0.4 mg/mL. The calibration was repeated for this range to ensure a more accurate interpretation of results (Fig. 11). Good linearity ($r^2 = 0.9686$) and precision (average standard deviation = 0.055 (n = 20)) were achieved.

The straight line equation from Fig. 11 was then used to calculate the concentration of ketoconazole in a vertical profile as follows: The data set used to construct the 3D images was displayed in two dimensions and magnified in the software in order to observe individual pixels. Each pixel in the image corresponds to a spectrum acquired in the imaging run. Thus the abundances of the protonated analyte and sodium matrix adduct ions were extracted from spectra acquired in a sequential, vertical fashion, as illustrated in Fig. 12. The ratio of the peaks was calculated and the straight line equation from the calibration was used to calculate the concentration of drug at each location.

Knowledge of the degree of vertical spacing between spectra enables the data to be presented as a profile of drug concentration against increasing depth, as shown in Fig. 13. The drug is detected up to 0.8 mm into the skin.

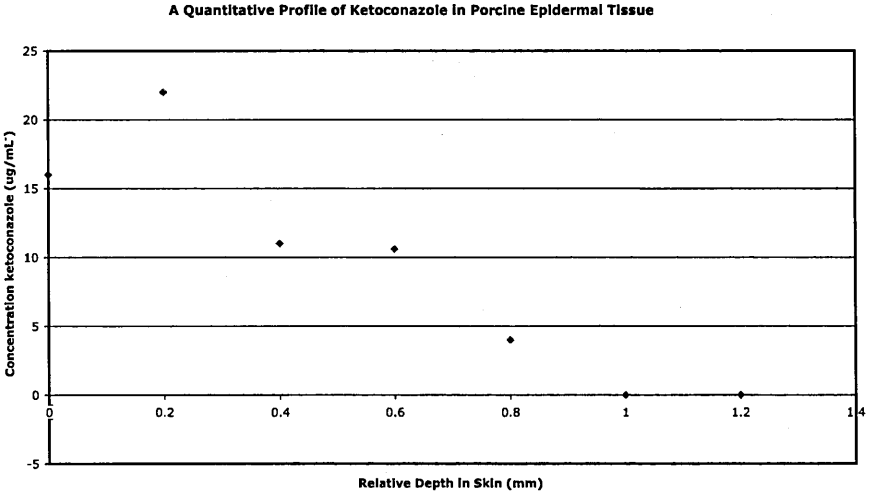

Figure 13. A quantitative profile of drug in skin constructed from examination of selected spectra acquired during an imaging run.

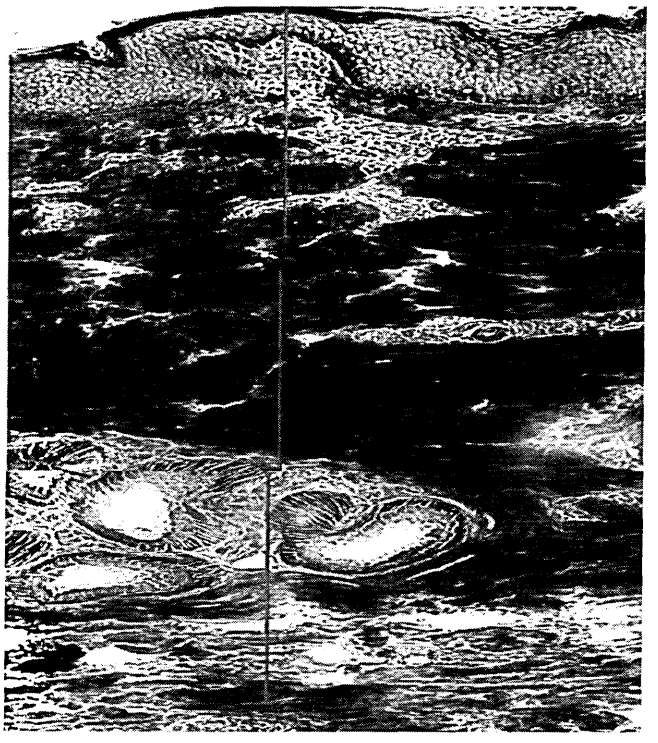

Figure 14. Confocal microscope image of a cross-section of porcine skin. Sample prepared by conventional H&E staining methods.

In order to relate the profile to skin structure, conventional H&E staining was performed on a cross-section of porcine epidermal tissue. The section was imaged by confocal microscopy and the histological image obtained is demonstrated in Fig. 14. The original MALDI image (Fig. 8) was enlarged to reveal individual pixels (each representing a 0.2 mm^2 area) and this was superimposed upon the histological image, as shown in Fig. 15. This demonstrates drug permeation up to and including the dermal skin layer. No drug is detected in the underlying connective tissue. All labelled concentrations are equivalent to the concentration of ketoconazole in solution. Thus further work must be undertaken in order to calculate a true concentration in skin. This may be achieved by preparing calibrations of different drug concentrations on cellulose membranes, calibrations of different drug concentrations applied to the skin surface and blotted onto a membrane, and hence determining the blotting efficiency itself.

There may be concern over the possibility of smudging during the blotting procedure resulting in a loss in quality of spatial information. It is therefore essential to optimise methods for this blotting procedure, so that they are normalised or automated to ensure reproducibility. However, the data shown here appear to confirm that, at our current spatial resolution of 100 μm, smudging is not significant.

CONCLUSIONS

This programme of work has demonstrated that imaging MALDI-MS is a potentially powerful tool for studying pharmaceutical compounds in biological systems.

To date there has been limited exploration of the use of imaging MALDI in biomedical applications. Ion beam

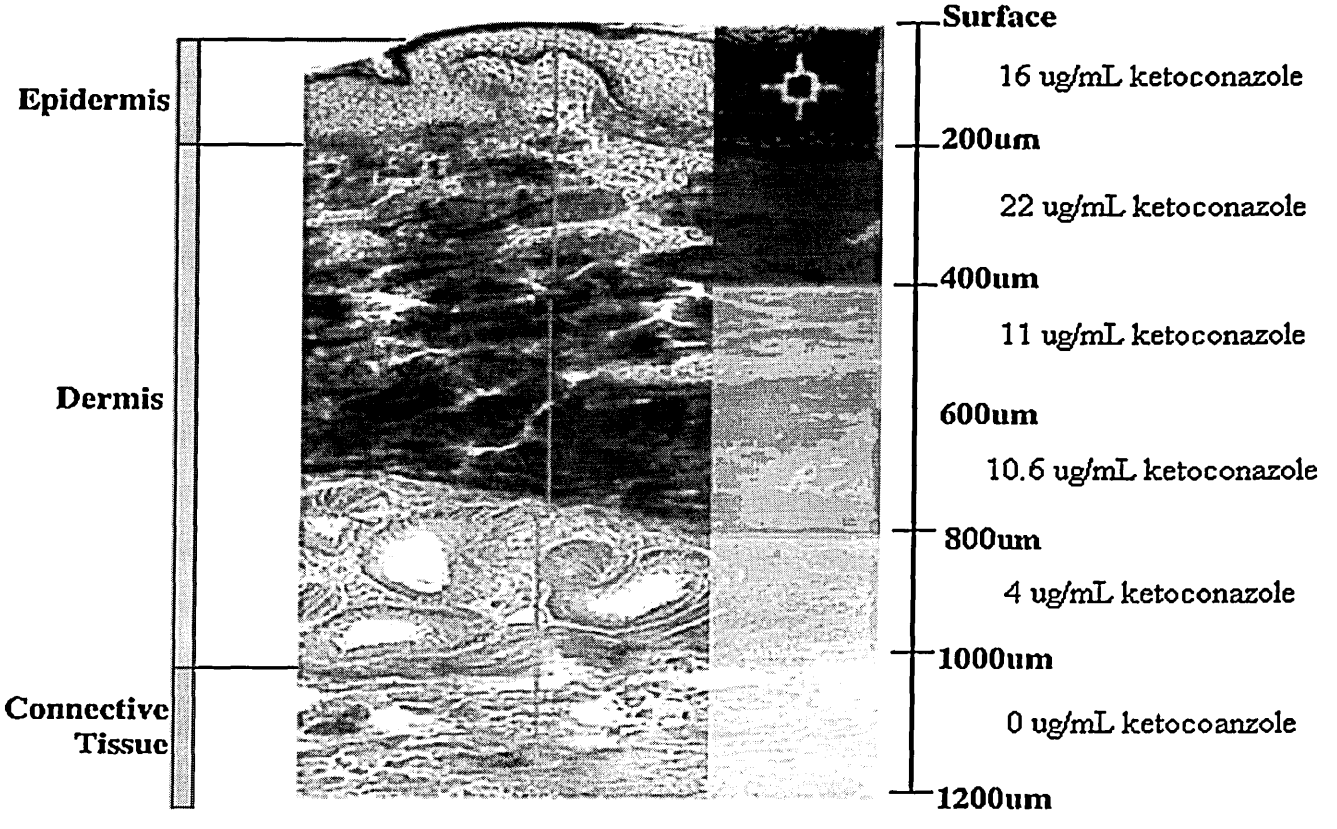

Figure 15. The mass spectrometric image is superimposed upon a histological image to reveal that the drug is absorbed into the dermal skin layer.

approaches such as SIMS have been utilised in similar applications, but suffer limitations such as mass range and sensitivity. Caprioli and co-workers have introduced the use of imaging MALDI for studying peptides, proteins, and drugs in tissues. The authors are unaware of any other research utilising imaging MS in percutaneous depth profiling. The work presented in this paper introduces the possibilities of this technique in such an application.

The use of lasers in imaging MS has several advantages over using ion beams alone, such as high sensitivity, selective ionisation, and quantification. However, while imaging MALDI experiments have yielded better quality spectra and can detect a higher mass range than SIMS, the lateral resolution needs to be greatly improved.

Successful detection and imaging of drug compounds on and under the skin surface have been achieved by the indirect analysis of tissue-imprinted cellulose membranes by MALDI-TOFMS. The methods developed have yielded high-quality spectra and images of the drug molecule. The method of pre-coating cellulose membranes in matrix by airspray deposition gives rise to a relatively abundant and homogeneous layer of matrix crystals compared with other methodologies investigated. Treatment through a triangular former shows that the method is capable of maintaining the spatial distribution of the analyte. Images have been generated showing the dermal uptake of the drug molecule in skin, and show the expected trend of diminishing drug concentration over increasing depth.

Calibration graphs for the determination of ketoconazole have been prepared using the sodium matrix adduct ion as an internal standard. A relatively good degree of linearity and precision has been achieved. The linear relationship obtained has permitted calculation of the concentration of ketoconazole at different skin depths by examination of individual spectra acquired during an imaging run. Histological images reveal that this equates to drug permeation up to and including the dermal skin layer.

Acknowledgements

This work was supported by grants from Pfizer Global R&D and The British Mass Spectrometry Society. The assistance of Mr Jonnie Plumb, Biomedical Research Centre, Sheffield Hallam University, and Mr Stuart Creasy, Materials and Engineering Research Institute, Sheffield Hallam University, in obtaining the confocal and SEM images is gratefully acknowledged. The technical support for the imaging software provided by Dr Julie Wingate, Applied Biosystems/MDS Sciex, is also gratefully acknowledged.

REFERENCES

1. Elias PM. *Int. J. Dermatol.* 1981; **20**: 1.
2. Touitou E, Meidan VM, Horwitz E. *J. Control. Release* 1998; **56**: 7.
3. Rougier A, Lotte C, Maibach HI. *J. Pharm. Sci.* 1987; **76**: 451.
4. Wester RC, Maibach HI. In *Percutaneous Absorption: Drugs-Cosmetics Mechanisms-Methodology* (3rd edn), Bronaugh RL, Maibach HI (eds). Marcel Dekker: New York, 1999; 215–227.
5. Fabin B, Touitou E. *Int. J. Pharm.* 1991; **74**: 59.
6. Naik A, Kalia YN, Pirot F, Guy RH. In *Percutaneous Absorption: Drugs-Cosmetics Mechanisms-Methodology* (3rd edn), Bronaugh RL, Maibach HI (eds). Marcel Dekker: New York, 1999; 148–175.
7. Lieb LM, Ramachandran C, Egbaria K, Weiner N. *J. Invest. Dermatol.* 1992; **99**: 108.
8. Fabin B, Touitou E. *Int. J. Pharm.* 1991; **74**: 59.
9. Sennhenn B, Giese K, Plamann K, Harendt N, Kolmel K. *Skin Pharmacol.* 1993; **6**: 152.
10. Kolmel K, Sennhen B, Giese K. *J. Soc. Cosmet.* 1986; **37**: 375.
11. Colliver TL, Brummel CL, Pacholski ML, Swanek FD, Ewing AG, Winograd N. *Anal. Chem.* 1997; **69**: 2225.
12. Caprioli RM, Farmer TB, Gile J. *Anal. Chem.* 1997; **69**: 4751.
13. Chaurand P, Stoeckli M, Caprioli RM. *Anal. Chem.* 1999; **71**: 5263.
14. Stoeckli M, Chaurand P, Hallahan DE, Caprioli RM. *Nat. Med.* 2001; **7**: 493.
15. Chaurand P, DaGue BB, Pearsall RS, Threadgill DW, Caprioli RM. *Proteomics* 2001; **10**: 1320.
16. Farmer TB, Caprioli RM. *J. Mass Spectrom.* 1998; **33**: 697.
17. Todd PJ, Schaaff TG, Chaurand P, Caprioli RM. *J. Mass Spectrom.* 2001; **36**: 355.
18. Reyzner ML, Hsieh Y, Ng K, Korfmacher WA, Caprioloi RM. *J. Mass Spectrom.* 2003; **38**: 1081.
19. Gusev AI, Vasseur OJ, Proctor A, Sharkey AG, Hercules AM. *Anal. Chem.* 1995; **67**: 4565.
20. Mowthorpe S, Clench MR, Crecelius A, Richards DS, Parr V, Tetler LW. *Rapid Commun. Mass Spectrom.* 1999; **13**: 264.
21. Zaluzec EJ, Gage DA, Allison J, Watson JT. *J. Am. Soc. Mass Spectrom.* 1994; **5**: 230.
22. Schleuder D, Hillenkamp F, Strupat K. *Anal. Chem.* 1999; **71**: 3238.
23. Preston LM, Murray KK, Russell DH. *Biol. Mass Spectrom.* 1993; **22**: 544.
24. Blackledge JA, Alexander AJ. *Anal Chem.* 1995; **67**: 843.
25. Vestling MM, Fenselau C. *Mass Spectrom. Rev.* 1995; **4**: 169.
26. Troendle FJ, Reddick CD, Yost RA. *J. Am. Soc. Mass Spectrom.* 1999; **10**: 1315.
27. Schwartz SA, Reyzer ML, Caprioli RM. *J. Mass Spectrom.* 2003; **38**: 699.
28. Garden RW, Sweedler JV. *Anal. Chem.* 2000; **72**: 30.
29. Disbrey BD, Rack JH. *Histological Laboratory Methods.* E&S Livingstone: Edinburgh, London, 1970.